Technical Report Documentation Page

1. Report No. FHWA/TX-13/0-6648-1	2. Government Accession No.	3. Recipient's Catalog No.
4. Title and Subtitle Characterizing Fly Ash		5. Report Date November 2012; Published August 2013
		6. Performing Organization Code
7. Author(s) Karla Kruse, Andres Jasso, Dr. Kevin Folliard, Dr. Raissa Ferron, Dr. Maria Juenger, Dr. Thanos Drimalas		8. Performing Organization Report No. 0-6648-1
9. Performing Organization Name and Address Center for Transportation Research The University of Texas at Austin 1616 Guadalupe, Suite 4.202 Austin, TX 78701		10. Work Unit No. (TRAIS) 11. Contract or Grant No. 0-6648
12. Sponsoring Agency Name and Address Texas Department of Transportation Research and Technology Implementation Office P.O. Box 5080 Austin, TX 78763-5080		13. Type of Report and Period Covered Technical Report September 2010–August 2012 14. Sponsoring Agency Code
15. Supplementary Notes Project performed in cooperation with the Texas Department of Transportation and the Federal Highway Administration.		
16. Abstract Although fly ash can and typically does impart all of the above benefits to concrete, several technical and practical issues must still be addressed. First, all fly ashes are not created equally. The chemical/mineralogical/ physical properties can vary significantly from one source to another, based on differences in fuel sources (coal), combustion conditions, and cooling regimes. Furthermore, the fly ash industry is quite dynamic and is rapidly changing due to recently imposed environmental regulations. As such, fly ash produced from a given power plant may be considerably different than fly ash produced from the same plant just a few years ago. Therefore, it is becoming increasingly important to be able to characterize fly ash in a way that best predicts how it will perform in concrete, and this is the primary focus of this project		
17. Key Words Fly ash	18. Distribution Statement No restrictions. This document is available to the public through the National Technical Information Service, Springfield, Virginia 22161; www.ntis.gov.	

19. Security Classif. (of report)	20. Security Classif. (of this page)	21. No. of pages	22. Price
Unclassified	Unclassified	172	

Form DOT F 1700.7 (8-72) Reproduction of completed page authorized

Characterizing Fly Ash

K. Kruse
A. Jasso
K. Folliard
R. Ferron
M. Juenger
T. Drimalas

CTR Technical Report:	0-6648-1
Report Date:	November 2012
Project:	0-6648
Project Title:	Characterizing Class C Fly Ashes for Alkali Silica Reaction Mitigation Effectiveness
Sponsoring Agency:	Texas Department of Transportation
Performing Agency:	Center for Transportation Research at The University of Texas at Austin

Project performed in cooperation with the Texas Department of Transportation and the Federal Highway Administration.

Center for Transportation Research
The University of Texas at Austin
1616 Guadalupe, Suite 4.202
Austin, TX 78701

www.utexas.edu/research/ctr

Disclaimers

Author's Disclaimer: The contents of this report reflect the views of the authors, who are responsible for the facts and the accuracy of the data presented herein. The contents do not necessarily reflect the official view or policies of the Federal Highway Administration or the Texas Department of Transportation (TxDOT). This report does not constitute a standard, specification, or regulation.

Patent Disclaimer: There was no invention or discovery conceived or first actually reduced to practice in the course of or under this contract, including any art, method, process, machine manufacture, design or composition of matter, or any new useful improvement thereof, or any variety of plant, which is or may be patentable under the patent laws of the United States of America or any foreign country.

Engineering Disclaimer

NOT INTENDED FOR CONSTRUCTION, BIDDING, OR PERMIT PURPOSES.

Project Engineer: Dr. David W. Fowler
Professional Engineer License State and Number: Texas No. 27859
P. E. Designation: Researcher

Acknowledgments

The authors express appreciation to the TxDOT Project Director, members of the Project Monitoring Committee, and the staff at the Concrete Durability Center.

Table of Contents

List of Figures

List of Tables

Chapter 1. Introduction and Scope

Fly ash is a by-product material produced from coal-combustion power plants and is one of the most commonly used supplementary cementing materials (SCMs) in the world. Prudent use of fly ash as a replacement for portland cement can have several major technical benefits, including reduced heat of hydration, reduced permeability, and improved resistance to alkali-silica reaction (ASR), sulfate attack, delayed ettringite formation (DEF), and external sulfate attack. Fly ash also enhances the sustainability of concrete as a building material—for every ton of portland cement replaced by fly ash, CO_2 emissions are reduced by approximately 0.9 tons.

Although fly ash can and typically does impart all of the above benefits to concrete, several technical and practical issues must still be addressed. First, all fly ashes are not created equally. The chemical/mineralogical/physical properties can vary significantly from one source to another, based on differences in fuel sources (coal), combustion conditions, and cooling regimes. Furthermore, the fly ash industry is quite dynamic and is rapidly changing due to recently imposed environmental regulations. As such, fly ash produced from a given power plant may be considerably different than fly ash produced from the same plant just a few years ago. Therefore, it is becoming increasingly important to be able to characterize fly ash in a way that best predicts how it will perform in concrete, and this is the primary focus of this project.

1.1 Report Organization and Outline

This report summarizes the main findings from TxDOT Project 6648, *Characterizing Class C Fly Ashes for Alkali Silica Reaction Mitigation Effectiveness*, a two-year laboratory-based project that focused primarily on the characterization of fly ash as it relates to ASR and external sulfate attack. The research focusing on fly ash characteristics/properties and their relation to ASR is presented first (Chapters 2 through 8), followed by Chapters 9 through 12, which focus specifically on the characterization of fly ash and its relation to external sulfate attack.

Chapter 2. Sulfate Attack: The Basics

This chapter presents a concise literature review of the mechanisms of sulfate attack and methods aimed at preventing sulfate attack, with particular emphasis on the use of fly ash. Various methods by which fly ash has been characterized and its properties linked to sulfate resistance will be presented.

2.1 Sulfate Attack

Sulfate attack is a durability concern for concrete members. It involves the reaction of sulfate ions and concrete constituents. This concrete deterioration is due to two types of sulfate action: internal sulfate attack and external sulfate attack. The classical type of attack is external where the source of sulfate ions is from an external source, such as groundwater or seawater. External sulfate attack also involves thaumasite formation. Internal sulfate attack involves the role of sulfates internally present in cement needed for portland cement hydration. Internal attack also involves the phenomena of delayed ettringite formation (DEF). The two mechanisms that cause sulfate deterioration are the formation of ettringite and the formation of gypsum (ACI201.2R-01, 2001). The formation of ettringite leads to expansion and cracking in the hardened paste due to the absorption of water and internal pressure. When gypsum is formed, there is a loss of mass due to the water soluble nature of gypsum and resulting loss of cohesion of the cement paste (Folliard, 2010). Expansion from ettringite formation is more likely than gypsum formation due to ettringite's low solubility (Skalny, Marchand, & Odler, 2002). Sulfate attack can lead to spalling, delamination, cracking, and loss of strength.

2.1.1 External Sulfate Attack

External sulfate attack may be either physical or chemical. Physical sulfate attack is referred to as salt crystallization due to sulfate salts that penetrate into the concrete and cause deterioration on the concrete exterior (Skalny, Marchand, & Odler, 2002). However, sulfates can also penetrate the concrete and react with constituents to form ettringite and gypsum, which can be detrimental to the concrete. According to ACI 201.2R-01, sodium, potassium, calcium, and magnesium sulfates are responsible for this concrete deterioration. Concrete in contact with gypsum rich sources exhibit sulfate attack in Texas, while sodium and magnesium sulfate sources tend to show even greater durability issues elsewhere in the United States (Drimalas, 2007).

Physical External Sulfate Attack

Salt crystallization sulfate attack, or physical external sulfate attack, involves the formation of salt crystals near the concrete surface that leads to surface scaling. Most commonly, concrete is in contact with sulfates in soils from groundwater, but sulfates are also introduced from industrial waste and fertilizers. These sulfates wick up the concrete via capillary action and can penetrate the concrete due to its porous nature. The resulting distress is due to a conversion from a low to a higher hydrate phase and a resulting volume increase due to crystallization pressure. This refers to the transition from thenardite to mirabilite with sodium sulfate and a resulting 314% volume increase (Haynes & Bassuoni, 2011). These phase transitions occur due

to a change in temperature and/or humidity. See Figure 2.1 for the optimum conditions for the transition from mirabilite to thenardite or vice versa.

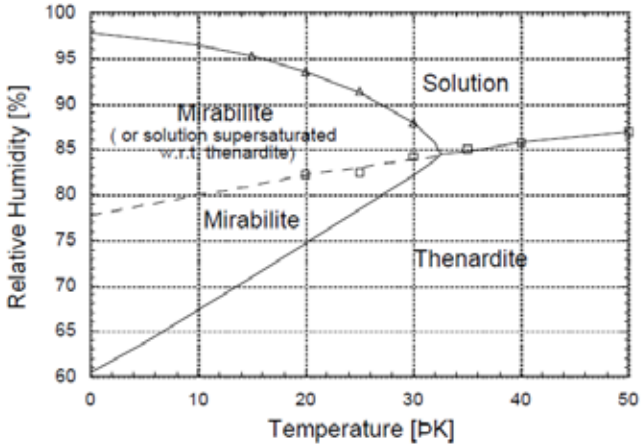

Figure 2.1: Mirabilite-Thenardite Transition (Flatt & Scherer, 2002)

Chemical External Sulfate Attack

The deterioration in this type of sulfate attack is due to the formation of ettringite and gypsum. This is a consequential attack due to a series of actions. Sodium sulfate solution reactions are presented below due to their frequency in nature and literature.

Firstly, in normal portland cement hydration, calcium silicates, C_3S and C_2S, react with water to form calcium silicate hydrate (C-S-H) and calcium hydroxide (CH). The C-S-H is responsible for binding the concrete together for strength gain. In the presence of a pozzolan, such as fly ash, the pozzolan will react with the CH to form more beneficial C-S-H. Any leftover CH is available for reaction with sulfate ions.

Sulfate ions can penetrate the concrete due to the porosity of the mix, type of ions, and the sulfate concentration. These sulfate ions are usually found in the groundwater. These ions, sulfate shown below, react with remaining CH to form gypsum, shown in Equation 2.1 (Folliard, 2010).

$$CH + N_2\bar{S}H_{10} \rightarrow C\bar{S}H_2 + 2NH + 8H$$

Calcium Hydroxide + Sodium Sulphate → Gypsum + Sodium Hydroxide + Water (2.1)

This gypsum can react with monosulfate, C_3A, and calcium aluminates to produce ettringite. See the reaction between gypsum and monosulfate in Equation 2.2 (Folliard, 2010). Monosulfate is present due to the reaction of C_3A, water, and ettringite during cement hydration. Ettringite can also be formed due to the reaction between calcium aluminate hydrates and sodium sulfate, shown in Equation 2.3, and due to the reaction between calcium aluminate sulfates and gypsum.

$$C_3A(C\bar{S})H_{12} + 2C\bar{S}H_2 + 16H \rightarrow C_3A(C\bar{S})_3H_{32}$$

Calcium Monosulphoaluminate + Gypsum + Water → **Ettringite** (2.2)

$$2C_3AH_{12} + 3N_2\bar{S}H_{10} \rightarrow C_3A(C\bar{S})_3H_{32} + 2AH_3 + 6NH + 17H$$

Tri-Calcium Aluminate Hydrate + Sodium Sulphate → **Ettringite** + Aluminum Hydroxide + Sodium Hydroxide + Water (2.3)

Through the above processes, gypsum and ettringite are formed. The formation of gypsum leads to a loss of mass and paste cohesion due to gypsum's solubility. The formation of ettringite is accompanied by a large volume expansion. Ettringite formed from monosulfate, shown in Equation 2.2, occupies twice the initial volume (Neville, 1996).

Thaumasite Attack

Thaumasite is a naturally occurring mineral similar in appearance to ettringite. The destruction of concrete is due to the transition from C-S-H into thaumasite, a non-binder that destroys cement paste. Thaumasite forms at low temperatures, especially 0–5°C, in the presence of calcium, carbonate, silica, sulfate, and water. Thaumasite is generally more of an issue when limestone fillers are used in the concrete mix design due to the introduction of calcium carbonate. This is a slow reaction that takes 6 months to 1 year, but it can be even slower at slightly higher temperatures up to 15°C (Bensted, 1999).

2.1.2 Internal Sulfate Attack

To fully understand internal sulfate attack, a look into portland cement hydration is essential. Calcium sulfates are added to the clinker in the cement production process. Gypsum is often the form of this added sulfate, but alkali sulfates are present in the clinker due to the cement manufacturing process. The addition of gypsum controls setting time and increases strength. The gypsum reacts with water and C_3A from the cement to form ettringite, shown in Equation 2.4.

$$C_3A + 3C\bar{S}H_2 + 26H \rightarrow C_3A(C\bar{S})_3H_{32}$$

Tri-Calcium Aluminate + Gypsum + Water → **Ettringite** (2.4)

This ettringite is referred to as blocking ettringite because it coats the C_3A grains to slow down the hydration reaction. This reaction will continue until all of the C_3A or gypsum reacts. If there is an excess of C_3A, it becomes available for reaction with ettringite and water to form monosulfate. If there is even more C_3A present, it hydrates and forms calcium aluminate hydrate (C-A-H). Sulfate attack and expansion occur as the monosulfate reacts with gypsum and water

and converts back to ettringite. See Equation 2.5 for the chemical equation for this reaction (Skalny, Marchand, & Odler, 2002).

$$\underset{\text{Monosulfate}}{C_4A\bar{S}H_{12}} + \underset{\text{Gypsum}}{2C\bar{S}H_2} + \underset{\text{Water}}{16H} \rightarrow \underset{\text{Ettringite}}{C_6A\bar{S}_3H_{32}} \quad (2.5)$$

When ettringite is accompanied by the absorption of water, expansion occurs. It is important to note that if ettringite forms early during hydration, the concrete can accommodate the expansion. However, if ettringite continues to form after hardening, expansion and cracking will result (Tishmack, Olek, & Diamond, 1999).

Delayed Ettringite Formation

Delayed ettringite formation (DEF) is a type of concrete distress due to the formation of ettringite in hardened concrete. This is known to be a result of high curing temperatures because ettringite dissolves at these higher temperatures. Sulfate and alumina get trapped in the inner C-S-H layer. The sulfate and alumina are slowly released, leading to the formation of ettringite at later ages (Folliard, 2010). When this ettringite is accompanied by water absorption, it leads to detrimental expansion.

2.2 Sulfate Attack Mitigation

ACI recommends using low permeability concrete and concrete components appropriate for mitigating sulfate resistance as the best defense to sulfate attack (ACI201.2R-01, 2001).

For both types of sulfate attack, the permeability of the concrete is a very important factor to limit the ingress of sulfate ions. This is achieved by lowering the water to cementitious ratio (w/cm). See Table 1 for w/cm requirements. ACI recommends using air entraining and a reduction in w/cm ratio to minimize shrinkage cracking (ACI201.2R-01, 2001). Proper curing of the concrete is also essential to the permeability of the concrete. Vapor barriers and other membranes can be utilized to prevent the ingress of sulfates as well.

Table 2.1: Sulfate Attack Mitigation Requirements (ACI201.2R-01, 2001)

Severity of potential exposure	Water-soluble soluble sulfate (SO_4)*	Sulfate (SO_4)* in water, ppm	*w/cm* by mass, max.†‡	Cementitious material requirements
Class 0 exposure	0.00 to 0.10	0 to 150	No special requirements for sulfate resistance	No special requirements for sulfate resistance
Class 1 exposure	> 0.10 and < 0.20	> 150 and < 1500	0.50‡	C 150 Type II or equivalent§
Class 2 exposure	0.20 to < 2.0	1500 to < 10,000	0.45‡	C 150 Type V or equivalent§
Class 3 exposure	2.0 or greater	10,000 or greater	0.40‡	C 150 Type V plus pozzolan or slag§
Seawater exposure	—	—	See Section 2.4	See Section 2.4

Using sulfate resistant cement is another mitigation technique. Decreasing the C_3A content of the cement will decrease the amount of ettringite formed. Type II and V cements are permitted for this use per ASTM C 150 due to their low C_3A content, 5% and 8% respectively.

Type V cements should not be used in excess of 25% due to the involvement of the alumina in aluminoferrite phase of C_4AF with sulfate attack (Bhatty & Taylor, 2006). See the relationship between C_3A content and amount of cement added with sulfate resistance in Figure 2.2.

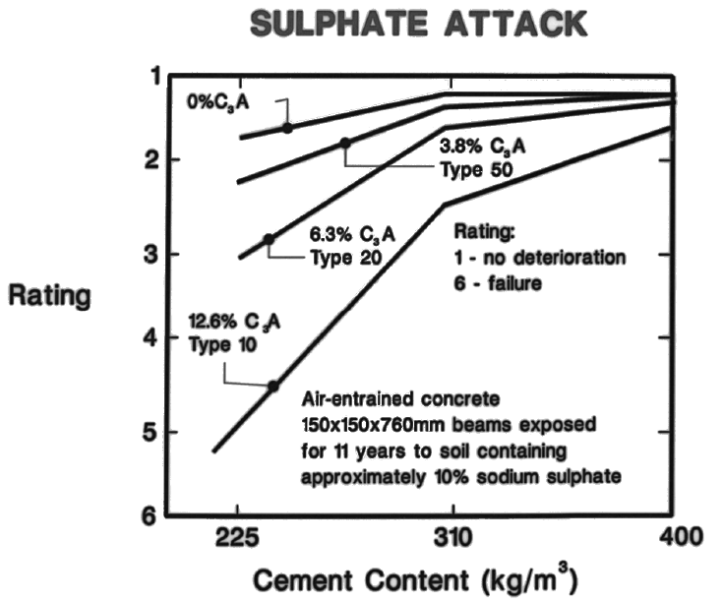

Figure 2.2: Sulfate Attack and Cement Content (Kosmatka & Panarese, 1194)

Using supplementary cementitious materials (SCMs) is another way to increase sulfate resistance. The use of SCMs is dictated by a one year long test as required by ACI 201 to ensure enhanced sulfate resistance. Specific mixtures are to be evaluated based on their sulfate exposure class, see Table 2.2 for criteria. Preventing the occurrence of CH will improve sulfate resistance. This is achieved by adding pozzolans to convert CH into C-S-H, a beneficial component in cement hydration. By replacing cement with SCMs, the amount of C_3A is reduced in the mixture as well; however, high calcium fly ashes contain C_3A. See the relationship between cement content and sulfate attack in Table 2.2.

Table 2.2: Exposure Classification Expansion Limits (ACI201.2R-01, 2001)

Severity of Potential Exposure	Cementitious Material Requirements	Expansion Limits
Class I	C150 Type II	≤ 0.10% at 6 months
Class II	C150 Type V	≤ 0.10% at 1 year
Class III	C150 Type V plus pozzolan or slag	≤ 0.10% at 18 months

Overall, sulfate attack depends on where the sulfates originate the concentration of the sulfates, and the types of sulfates. The temperature and relative humidity can play an important role as well especially for DEF and thaumasite formation. The constituents in the concrete, such

as the type of cement, SCMs, and w/cm ratio, are the most important factors that can impact sulfate resistance. This report will only focus on the effects and mechanisms of the addition of fly ash to the concrete mix to control sulfate attack.

2.3 Fly Ash

2.3.1 Fly Ash Background

Fly ash is a by-product of coal combustion power plants which is often used in concrete. Fifty million tons of fly ash is produced annually in the United States with 10–12% being used in concrete (ACI 232.R-96, 1996). Fly ash enhances the properties of concrete when used effectively. With typical replacement percentages of 15–25%, less cement is used resulting in fewer CO_2 emissions from cement manufacturing plants and a lower overall cost of concrete. Fly ash reduces the heat of hydration, reduces permeability, and improves concrete resistance to durability issues such as alkali silica reaction (ASR), sulfate attack, and DEF.

Fly ash particles are heterogeneous, fine particles carried away by flue gas and caught by mechanical or electrostatic precipitators in coal combustion power plants. With temperatures in excess of 2700°F, non-organic matter in the coal forms molten droplets which are quenched. This process forms glassy spheres, mostly solid but some hollow, with a smooth surface. These particles range in size from 0.5–200 μm with a range of densities from 123 lb/ft^3 to 187 lb/ft^3 (ACI 232.R-96, 1996).

Figure 2.3: Cementitious Materials Ternary Diagram (Scrivener & Nonat, 2011)

The composition of the fly ash changes drastically with the parent coal burned in the power plant, the combustion conditions, and cooling regimes. Due to the wide variety of fly ash compositions, it is difficult to characterize this material. In the United States, there are two main classification groups for fly ash, shown in Table 2.3. ASTM identifies these groups as Class F and Class C ashes. Class F ashes are produced from the burning of anthracite or bituminous coal. The total silica, alumina, and iron oxide content must be greater than 70%. This classification usually refers to the lower calcium ashes. Class C ashes are produced from the burning of lignite or sub-bituminous coal. The total silica, alumina, and iron oxide content must be greater than 50% for this classification (ASTM C 618, 2008). Class C ashes are the higher calcium ashes, refer to Table 2.3. Although not recognized as an identifier by ASTM, ashes greater than 20%

calcium oxide content are referred to as Class C ashes in the United States. However, in Canada, a mid-level of fly ash is referred to as Class CH. Based on past research, Canada may begin classifying fly ash in terms of calcium oxide content. The United States, Canada, and the United Kingdom all have different criteria for the classification of fly ash, although bulk oxide content is the basis for most characterizations.

Table 2.3: ASTM C 618 Fly Ash Classification (ASTM C 618, 2008)

Class	Description	Requirements
F	-Anthracite or bituminous coals -Pozzolanic	$SiO_2 + Al_2O_3 + Fe_2O_3 \geq 70\%$
C	-Lignite or sub-bituminous coals -Pozzolanic and cementitious	$SiO_2 + Al_2O_3 + Fe_2O_3 \geq 50\%$

Fly ash is a pozzolanic material. ASTM defines a pozzolan as "a siliceous or siliceous and aluminous material that in itself possesses little or no cementitious value but will, in finely divided form and in the presence of moisture, chemically react with calcium hydroxide at ordinary temperatures to form compounds possessing cementitious properties" (ASTM International, 2011). This pozzolanic reaction results in greater strength gain and reduced permeability attributed to SiO_2 and Al_2O_3 components. Class F and C ashes are pozzolanic; however, Class C ashes also exhibit cementitious properties, meaning they can harden and gain strength when mixed only with water and not cement. This reaction is due to the reactive crystalline phases found in higher-calcium ashes reacting with water.

2.3.2 Fly Ash Changes

The United States Congress passed the Clean Air Act in 1990 in an attempt to reduce the harmful emissions of the coal-burning power plants by controlling the SO_2 and NO_x emissions. This Act required the power plants to use low-NO_x burners. This increases the percentage of unburned carbon in the fly ash, which can significantly impact water demand and workability in a concrete mix. To control SO_x emissions, scrubbers, such as SO_3, were added due to the presence of pyrite and gypsum in the parent coals. A reaction with lime and alkalis resulted in sulfur scrubbing the fly ash particles (ACI 232.R-96, 1996). The main effect of this Act was the switch from using any locally available parent coal to coals from the Powder River Basin, an area in the western region of the United States. This region is now the largest coal producing region in the United States. The coal from this region is lignite or sub-bituminous coal, which creates a higher calcium oxide content of the output fly ash. These coals have lower amounts of SO_2 to help control the emissions due to the high cost of adding scrubbers. This coal is also close to the surface requiring fewer resources to mine the Powder River Basin. This increase in calcium in the output fly ash can lead to problems including increased heat of hydration, increase in set time, and decreased resistance to sulfate attack.

2.3.3 Fly Ash Mineralogy

Fly ash composition has three components: inorganic material comprised of crystalline and amorphous phases, organic material, and fluid material found in the organic and inorganic material. Each part of the fly ash can be classified according to time of formation. Primary

phases undergo no phase transformations. Secondary phases are formed during coal combustion and include the silicates and oxides. The tertiary phases were formed during fly ash transport and include portlandite and gypsum. The main elements of the fly ash are O, Si, Al, Ca, Fe, C, K, Mg, H, Na, Ti, N, P, Ba, and other trace elements (Vassilev & Vassileva, 2007).

When the fly ash particles are cooling, the rate of cooling affects the formation of the inorganic matter. A slow cooling results in larger, crystalline particles whereas a fast cooling results in smaller, 1–5 μm glassy particles (Hemmings & Berry, 1988). The crystalline and amorphous phases make up the fly ash.

Fly ash currently is classified by its bulk oxide content. Refer to Table 2.4 for typical bulk fly ash compositions. The CaO, SiO_2, Al_2O_3, and Fe_2O_3 make up the majority of the fly ash. As the CaO increases, the other three oxides listed above decrease. As CaO increases, the SO_3 and alkalis (Na_2O and K_2O) increase as well. The more iron in the fly ash, the greater the density; the greater the carbon in the fly ash, the lower the density (ACI 232.R-96, 1996). The loss on ignition (LOI) is related to the carbon content in the fly ash, which effects water demand and workability. LOI is higher for Class F ashes than Class C because of the presence of more unburnt carbon.

Table 2.4: Typical Fly Ash Bulk Composition (ACI 232.R-96, 1996)

	Bituminous	Subbituminous	Northern Lignite	Southern Lignite
SiO_2, percent	45.9	31.3	44.6	52.9
Al_2O_3, percent	24.2	22.5	15.5	17.9
Fe_2O_3, percent	4.7	5.0	7.7	9.0
CaO, percent	3.7	28.0	20.9	9.6
SO_3, percent	0.4	2.3	1.5	0.9
MgO, percent	0.0	4.3	6.1	1.7
Alkalies,* percent	0.2	1.6	0.9	0.6
LOI, percent	3	0.3	0.4	0.4
Air permeability fineness, m^2/kg	403	393	329	256
45 μm sieve retention, percent	18.2	17.0	21.6	23.8
Density, Mg/m^3	2.28	2.70	2.54	2.43

* Available alkalies expressed as Na_2O equivalent.

Crystalline Phases

Crystalline phases account for 5–50% by mass of the fly ash (Hemmings & Berry, 1988). Following are the ten main crystalline phases (McCarthy, Solem, Manz, & Hassett, 1190):

- Anhydrite ($CaSO_4$) – found in most Class C ashes and is a result of the Cao, SO_2 and O_2 in the furnace, it increases with an increase in SO_3 and is involved with ettringite formation
- Mullite(A_3S_2) – found more in Class F ashes, not reactive
- Quartz – in all fly ash
- Melite – a solid solution of akermanite and gehlenite found in Class C ashes and related to MgO content
- Merwinite – found in Class C ashes and related to MgO content

- Periclase (crystalline MgO) – ASTM C 618 limits MgO to ≤ 5% due to soundness issues, found in Class C ash
- C3A – in all Class C ashes, forms ettringite responsible for sulfate expansions
- Magnetite (Fe3O4) – known as spinel
- Hematite (Fe2O3) – common in F ash
- Lime (crystalline CaO) –found in all Class C ashes and some Class F ashes, free lime participates in hydration reactions and dissolves to increase the pH greater than 12, usually at 2–5% because if all of the free lime doesn't react initially then it'll react with portlandite and result in soundness issues (Roy, Luke, & Diamond, 1985)

The crystalline phases are identified through x-ray diffraction (XRD), specifically identifying which phases are reactive and which are stable. The reactive phases most vulnerable to sulfate attack are C_3A, gehlenite, periclase, and anhydrite (Carrasquillo & Tikalsky, 1993). The reactive C_3A component is responsible for ettringite formation and associated expansion, but it is not in large enough quantities to solely cause full deterioration (Carrasquillo & Tikalsky, 1992). The stable phases do not participate in hydration reactions or reactions with sulfates.

Amorphous Phases

Amorphous particles are the circular particles 1–5 μm in diameter. These particles are formed due to quenching of particles, resulting in disordered, lack of crystal structures, making them harder to characterize. This lack of crystal structure is due to "rapid cooling, network isomorphic substitution, and cation modification" (Hemmings & Berry, 1988). Parent coal with a low calcium results in aluminosilicate glass. Parent coal with higher levels of calcium result in calcium aluminosilicate glass, a known reactive phase in Class C ashes (ACI 232.R-96, 1996). The presence of the calcium aluminosilicate glass makes Class C ashes more reactive than Class F ashes.

The amount of amorphous phases is found by subtracting the amount of crystalline phases from the total bulk mass. This is discussed in the testing methods section, Section 3.3.

2.3.4 Fly Ash and Sulfate Attack

Fly ash is used as a supplementary cementitious material in concrete to enhance strength properties, reduce permeability, and reduce heat of hydration to name a few technical benefits. Adding fly ash into a concrete mixture can also improve the resistance of sulfate attack.

It is generally understood that Class F ashes improve the sulfate resistance, but Class C ashes decrease the sulfate resistance. Class C ashes contain C_3A, which is responsible for ettringite formation and resulting expansions. See Figure 2.4 for the relationship of cement C_3A with expansions. As the calcium oxide content increases past 20%, the percent C_3A begins to increase rapidly (Folliard, 2010). Class C ashes have a reduced pozzolanity compared to Class F ashes as well. Therefore, Class C ashes are not as effective at consuming CH and converting it into C-S-H. Class C ashes also contain reactive glassy calcium-aluminate phases (Folliard, 2010).

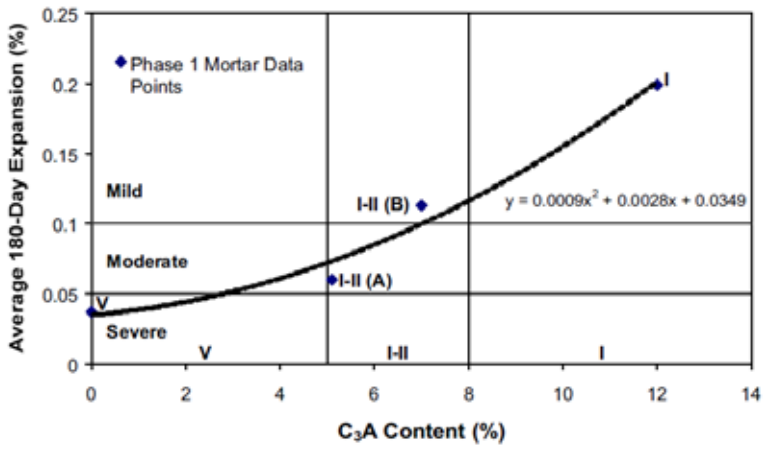

Figure 2.4: Average Expansions versus C_3A Content for Portland Cement Mortar (Stephens & Carrasquillo, 2000)

In addition, Class C ashes increase the amount of expansion and decrease the time to failure as the fly ash replacement levels increase (Tikalsky & Carrasquillo, 1992). Refer to Figure 2.5 to see this relationship. This relationship is due to more reactive crystalline phases of anhydrite, lime, periclase, sodalite, and C_3A present in high calcium fly ashes. Class F ashes do not contain these reactive phases and only the inert crystalline phases of mullite, quartz, ferrite spinel, and hematite (Carrasquillo & Tikalsky, 1992).

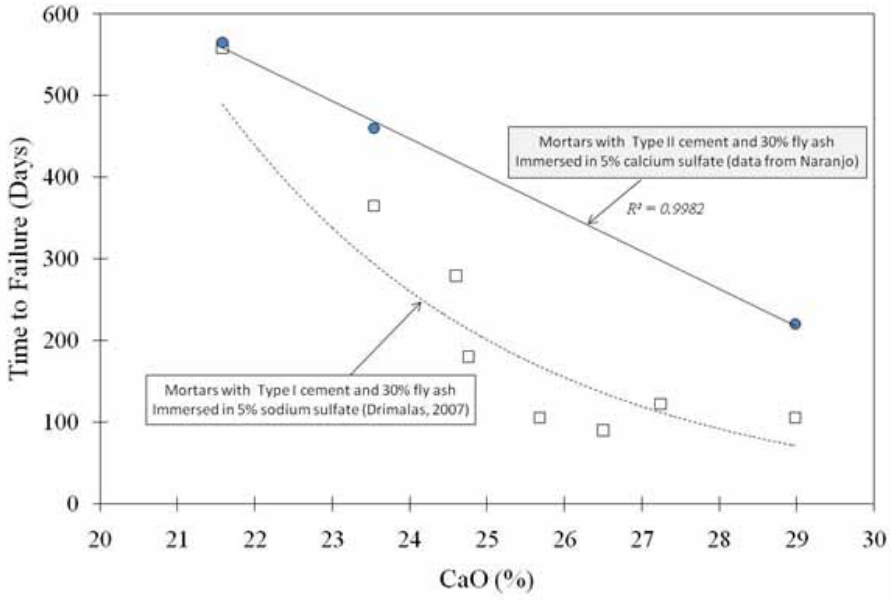

Figure 2.5: Relationship between CaO content and Time to Failure (Folliard, 2010)

Dunstan acknowledged that C_3A content was related to sulfate durability because it is the reactive aluminate compound responsible for ettringite formation. He argued that C_3A in combination with alumina and C_4AF was the contributing factor to sulfate resistance though. Alumina itself is introduced from mullite (A_3S_2) as a non-reactive crystalline phase. However, in

high calcium ashes, other crystalline phases do contain alumina. The glassy alumina in calcium-alumina-silicate glass is more reactive with sulfates because of the formation of monosulfate and calcium alumina hydrates (Tishmack, Olek, & Diamond, 1999) and lies in the gehlenite region (C_2AS) on the CaO-SiO_2-Al_2O_3 ternary diagram. As calcium content increases, the glass turns into calcium aluminosilicate glass and reactivity increases. Refer to Figure 2.6 to see this transition to reactive glass phase with an increase in calcium content, left to right on x-axis.

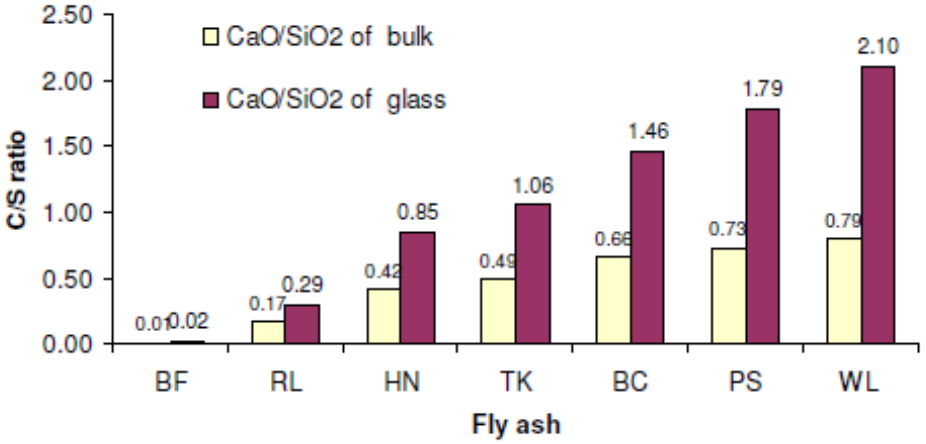

Figure 2.6: C /S Ratio of Fly Ash Compositions (Folliard, 2010)

Therefore, plotting fly ash on the ternary diagram may be useful to indicating sulfate resistance. Refer to Figure 2.7 for these regions on the ternary diagram. If the fly ash falls within the mullite region, it has good sulfate resistance. If the fly ash falls within the gehlenite region, the ash has reduced sulfate resistance (Dunstan, 1980). Watt and Thorne continued this theory to say that the amount of iron oxide (Fe_2O_3) could be used to determine sulfate durability for Class F ashes. It is stated that ettringite can be iron-rich or iron-poor, and the iron-rich ettringite particles will not cause expansion (Kalousek & Benton, 1970). Iron found in fly ash may be related to the type of ettringite, and the theory stated that an increase in iron oxide reduced sulfate expansion (Watt & Thorne, 1965–66). Later research conducted at The University of Texas at Austin found no linear relationship between iron oxide content and sulfate resistance as proposed (Carrasquillo & Tikalsky, 1992).

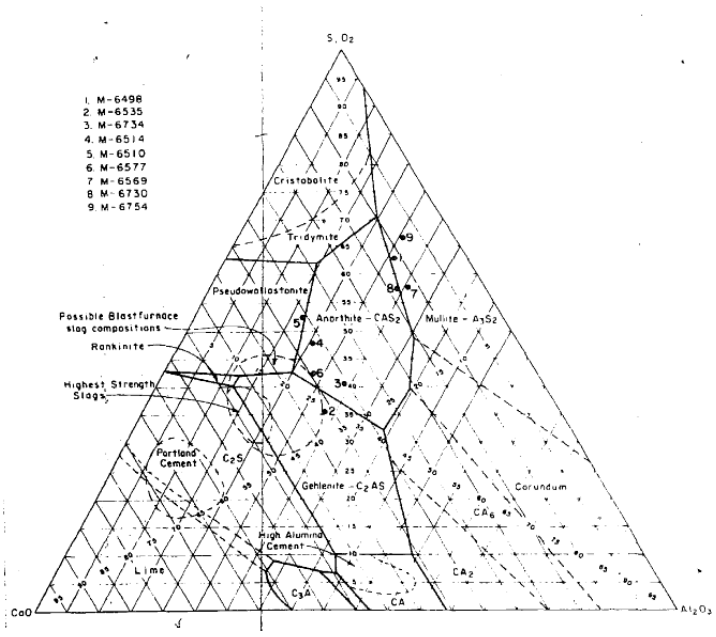

Figure 2.7: CaO-SiO_2-Al_2O_3 Ternary Diagram (Dunstan, 1980)

Dunstan proposed a resistance factor that related calcium and iron content. Sulfate resistance is proportional to calcium oxide content greater than 5% and inversely related to the amount of iron oxide. This R-factor is found by the following Equation 2.6 where C is CaO and F is Fe_2O_3 in percentages.

$$R = (C - 5)/F \tag{2.6}$$

If the R value is less than 1.5, the fly ash had good resistance to sulfate attack, but if the value exceeds 3.0, the ash has poor resistance (Dunstan, 1980).

Critics say that this R-factor does not account for the sources of ettringite formation. Manz proposed a revised model that included fly ash reactive crystalline components. This model was based on two parameters, the calcium aluminate potential (CAP) and the calculated sulfate equivalent (CSE). CAP is calculated using bulk oxide contents identified in XRF analysis and subtracting inert crystalline compounds identified through XRD and Rietveld analysis. The CAP equation is presented below in Equation 2.7 and CSE formula in Equation 2.8 (Bhatty & Taylor, 2006).

$$CAP = (C^* + A^* + F^*) / S^* \tag{2.7}$$

C* = Bulk CaO – Reactive crystalline CaO (lime, anhydrite, C_2S) – inert crystalline CaO (melillite, merwinite)
A* = Bulk Al2O3 – inert Al_2O_3 (mullite)
F* = Bulk Fe2O3 – inert crystalline Fe_2O_3 (hematite, spinel)
S* = Bulk SiO2 – inert crystalline SiO_2 (quartz, mullite)

$$CSE = \text{Anhydrite} + 1.7\$ \tag{2.8}$$

This relationship is plotted on an x-y graph shown in Figure 2.8. As the CSE parameter increases, the fly ash becomes more sulfate resistant. The problem with this proposed model is that it neglects the combined role of cement and fly ash reaction products.

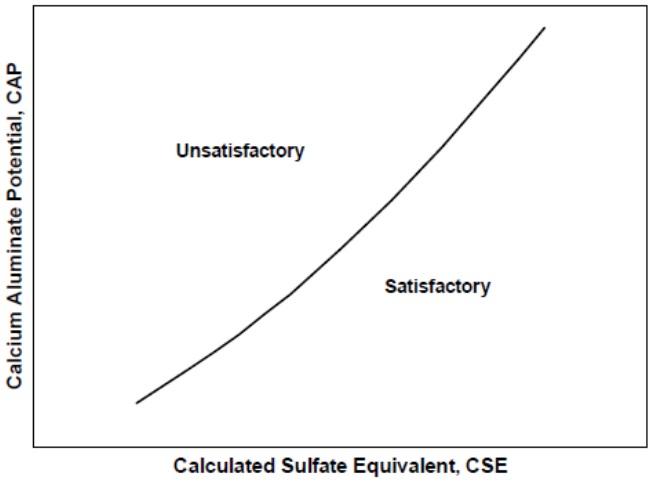

Figure 2.8: Relationship between CAP and CSE and Sulfate Resistance (Bhatty & Taylor, 2006)

Another proposed model based on Dunstan's original model was created by Hartmann and Mangotich. This model introduced an oxide durability factor (ODF) to predict sulfate resistance. See Equation 2.9 for this calculation (Bhatty & Taylor, 2006). As the ODF value decreases, the sulfate resistance of the concrete increases.

$$ODF = (\text{Bulk CaO in fly ash and cement}) * \text{Free lime} / (\text{Bulk } SiO_2 \text{ in fly ash and cement}) + (\text{Bulk } Al_2O_3 \text{ in fly ash and cement}) + (\text{Bulk } Fe_2O_3 \text{ in fly ash and cement}) \quad (2.9)$$

This equation was important because it took into consideration the composition of the fly ash and of the cement since both constituents add reactive components to the concrete. However, the cement and fly ash hydration products are more important than their individual contributions. This equation also emphasizes the importance of alumina in the concrete.

The three proposed models highlighted the role of crystalline phases, but later research proposed the glassy phase as a more important factor for sulfate resistance. Fly ashes that have high-calcium glass discharge calcium aluminates that when mixed with sulfates form expansive products. Through a study conducted at The University of Texas at Austin, the composition of the glassy portion was important in determining the sulfate resistance of fly ash. The type of cement used, presence of entrained air, slump, and different curing length had little effects on the sulfate resistance of fly ash mixtures. It was concluded that even using sulfate-resistant cement, with little or no C_3A, did not affect sulfate resistance if a poor fly ash was used in the concrete mix. It was recommended to use fly ash in a sulfate environment if calcium oxide is less than 10% but not acceptable for use if calcium oxide is greater than 25%. For those ashes whose calcium oxide falls within this range, it is recommended to perform testing and observe the

sulfate resistance in addition to noting where the ash falls on the ternary diagram shown in Figure 2.7 (Tikalsky & Carrasquillo, 1993). The effects of calcium oxide and sulfate resistance were tested by Tikalsky, but he did not observe the trend of poor resistance with increasing calcium content for all ashes studied. However, he still did not advocate the use of high calcium ashes in sulfate environments due to their potential to expand (Tikalsky P. J., 1989).

As for the effect of fly ash on delayed ettringite formation, it is believed that the alumina oxide (Al_2O_3) content is the contributing factor because of its role in ettringite stability. Class F and C ashes can be used to control DEF; however, more Class C replacement is needed to control the expansion (Folliard, 2006).

There is still not a full understanding of the mechanism(s) contributing to sulfate resistance. A general acceptance that Class F ashes are suitable and Class C is not suitable for use holds true. This project aims to better understand the mechanism of Class C ash in sulfate environments.

Chapter 3. Testing Methods

Chapter 3 provides background on the testing methods and machines used in this report.

3.1 XRF

All of the fly ashes were analyzed with x-ray fluorescence (XRF) to evaluate the bulk oxide contents. High energy x-rays excite the fly ash, which emit fluorescent, or secondary, x-rays. These secondary x-rays are used to qualitatively and quantitatively identify the oxides in the sample. XRF can be used to determine amorphous content by subtracting the crystalline amount by the total bulk oxide amount found with XRF.

3.2 Particle Size

Particle size in this report was measured by two different methods: laser diffraction and No. 325 sieving. A laser diffraction machine uses a laser to plot the particle size distribution of a fly ash, or any material. An electron in the electron cloud removes light from the light beam due to interaction of the light beam and the material and then re-emits that light causing light scattering. This scattering is due to reflection, refraction and diffraction of the light due to this interaction (Webb, 2000). The light can also be absorbed. The machine analyzes the interaction of the material particles and the light based on the diffraction pattern and matches the analyzed pattern to a mathematically calculated model. This mathematical model is estimated using the Mie or Fraunhofer theory. The diffraction pattern is created due to the beam shot through the particles suspended in a dispersive agent and being diffracted, deviation due to a light ray traveling close to a particle. A Fourier transform lens focuses the diffracted light beam to convert incident energy into electric signals. The angle between the incident and diffracted light is related to the particle size (Cyr & Tagnit-Hamou, 2001). The dispersive agent recommended by NIST is isopropyl alcohol due to its high viscosity and increased reproducibility (Ferraris, Bullard, & Hackley). The broader the particle size distribution, the greater the packing density of the mixture and resulting greater workability.

Particle size distribution was also performed with a No. 325 wet sieve analysis as required and outlined in ASTM C 618 and C 311/430 respectively. The code requires that no more than 34% of the material can be retained on the No. 325 sieve. Coarser materials contain more unburnt carbon, affecting LOI, and larger particles affect the material's reactivity. The coarser the fly ash, the decrease in the pozzolanic activity index (PAI). As particle size increases, quartz (crystalline SiO_2) increases and calcium containing products decreases. As the particle size increases, the number of spherical particles decreased. Most crystalline material was found to be larger than No. 325 sieve (Joshi, Natt, Day, & Tillerman, 1985).

3.3 X-Ray Diffraction

X-ray diffraction (XRD) qualitatively identifies the crystalline phases of the fly ash sample. In this machine, electrons hit a solid sample and x-rays are emitted. When the x-rays hit a crystal structure, some x-rays diffract based on this crystal structure but other x-rays penetrate further into the sample until colliding into a crystal. The machine reads all of the angles of diffracted, scattered x-rays and their intensities to create a pattern. These patterns are plotted, creating a diffractogram as seen in Figure 3.1 relating diffracted intensity to diffraction angle.

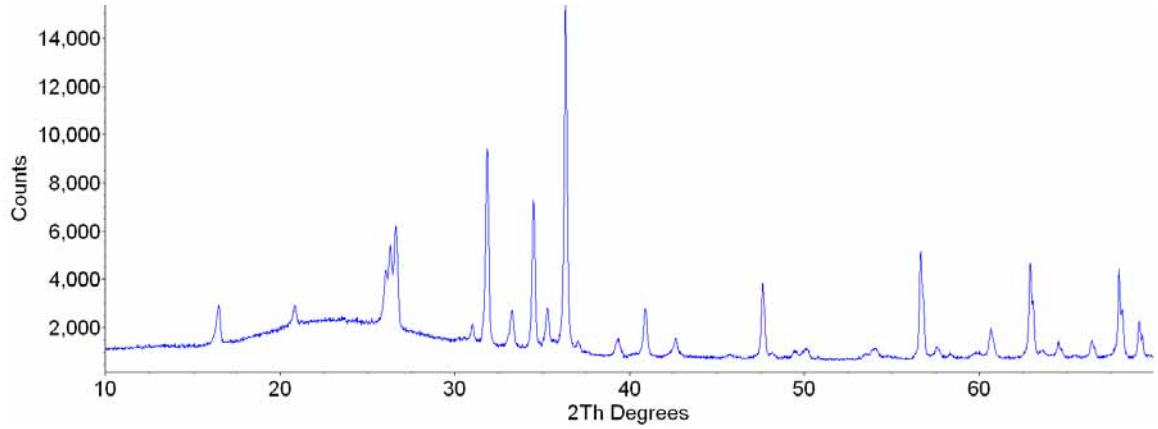

Figure 3.1: XRD Pattern of a Fly Ash

With a high intensity scan, major and minor crystalline phases can be identified. A major match involves the match of 3 peaks of that phase. For a very detailed analysis, a quantitative analysis called Rietveld QXRD (RQXRD) is possible. Rietveld uses an internal standard, zincite in this project, with a computer program called Topas manufactured by Bruker-AXS. This program uses a curve-fitting algorithm to match crystal structures to the peaks identified in the XRD scan. Refining each crystal structure enables the user to more accurately fit the peak and/or intensities identified. During sample preparation, the fly ash powder is packed with a flat, glass surface. This alters the orientation of the crystals but is corrected with refining the preferred orientation, the tendency for crystals to be oriented in a specific way. Refining is continued until the residual is small. R values less than 10 were deemed acceptable in this analysis. The output crystalline percentages were then adjusted to the known amount of added internal standard, 10% was used for these analyses, and values were back calculated to remove this known addition. It is these numbers that will be presented in the results of this report. The amount of amorphous phases can also be calculated by subtracting the total crystalline percentage without the internal standard from 100%.

Zincite, ZnO, was chosen as the internal standard based on previous research. One study examining different internal standards compared rutile, zincite, and alumina. Internal standard selection should be based on grain size due to smaller sizes obtaining more accurate intensities due to sufficient particle diffraction. Based on a five-phase mixture, rutile had the lowest weighted relative error at 5.3%. Zincite and alumina had almost double the error at 10% and 11% respectively (Winburn, Lerach, Jarabek, Widsom, Grier, & McCarthy, 2000). In another test, rutile was found to have a large refined March-Dollase coefficient, which deals with preferred orientation and is a problematic issue for using Rietveld for amorphous content analysis (De La Torre, Bruque, & Arand, 2001). A third research project compared alumina and zincite and found alumina was a better choice for cement Rietveld analysis (Wei, Yao, & Wang, 2012). Rutile, zincite, and alumina are all suitable choices as an internal standard; however, due to the desire to use Rietveld to identify the total amorphous content, rutile was deemed an unsuitable choice. Due to the significant cost increase of alumina over zincite, zincite was deemed the most cost-effective internal standard for this project.

3.4 SEM

To identify the composition of the amorphous phases of the fly ashes, samples were analyzed with a scanning electron microscope (SEM). This machine employs an electron beam to penetrate about 1 μm deep into a sample. This beam focuses on a point and detectors read signals and convert them into intensities on the attached computer to create an image.

One image of interest is the secondary electron signal. These signals produce information about the surface topography. These are created due to a beam hitting valence electrons, which resultantly are emitted from the atom. These valence electrons are attracted to a detector, which produces a signal proportional to the number of electrons it has attracted (Chancey, 2008). See Figure 3.2 for a secondary electron image.

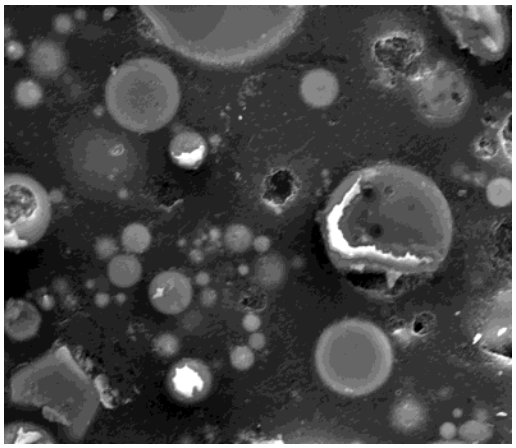

Figure 3.2: Secondary Electron Image of Fly Ash

Another image of interest is the backscattered electron image. This image is created due to electrons from the electron beam being reflected from the specimen. A detector identifies the amount of electrons reflected. As the atomic number increases, the more reflected electrons present. Therefore, brighter spots in an image mean a higher atomic number than the darker spots. See Figure 3.3 for a backscattered electron image.

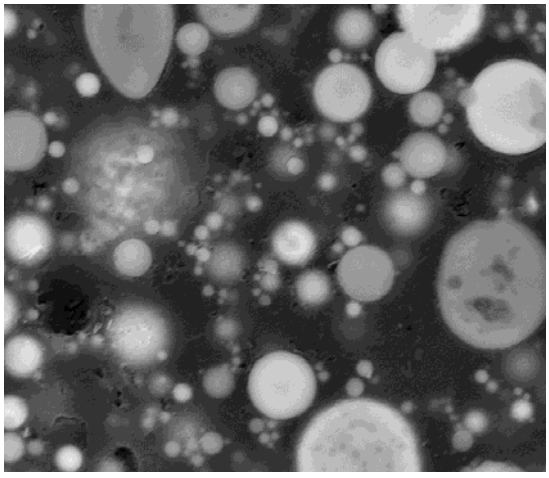

Figure 3.3: Backscattered Electron Image of Fly Ash

An energy-dispersive x-ray analyzer (EDXA) was used to point count amorphous particles. This was performed in the computer program Espirit. As the beam hits the specimen surface, x-rays are emitted that are characteristic of the specimen's elemental composition. Therefore, this technique is used to identify the elemental make-up of the amorphous particles. As mentioned in the literature review, the amorphous particles are the spherical particles of 1–5 μm in diameter. These amorphous particles were identified by measuring circular particles with a built-in measuring tool. Only those particles 1–5 μm in diameter were selected for the point analysis. Analysis of 150–200 amorphous particles constituted a comprehensive analysis of the fly ash specimen. These particles were quantitatively investigated for eight elements: calcium, aluminum, iron, sodium, potassium, silicon, oxygen, and carbon. These elements were converted into oxides, and each point was plotted on a ternary diagram for further analysis. For more information on ternary diagrams, refer to the literature review background and Section 5.3.2 for these results.

3.5 Reactivity

A patent was issued to Dodson in 1980 for a simple test to identify reactive fly ashes. This test was initially created to identify early strength characteristics of fly ashes, but there appears to be a correlation between high early strength and poor sulfate resistance found in TxDOT Project 4889. This test involves the mixing fly ash with tartaric acid solution, boiling the solution, and cooling covered for 3 hours. After this waiting period, the height of the mixture is measured. If the product exceeds 20 mm in height, the fly ash is considered reactive (Dodson & Roberts, 1980). See Figure 3.4 for differences in height of the gel product formed as a result of this procedure.

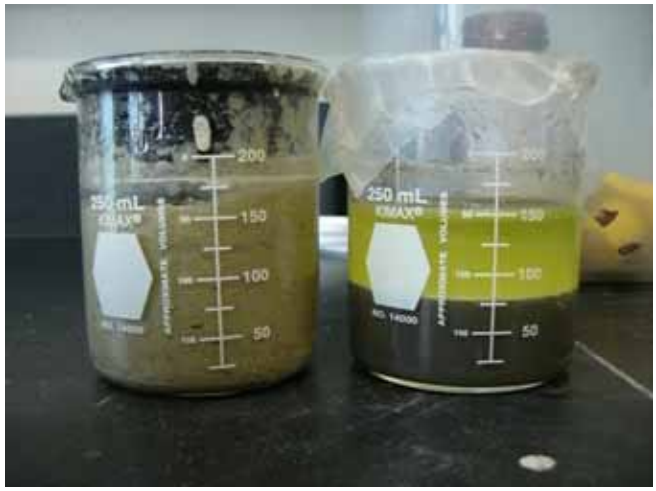

Figure 3.4: Reactivity Gel Product

3.6 Calorimetry

Heat of hydration is the heat produced from the reaction of portland cement and water. This heat is greatly influenced by C_3A and C_3S content of the cement, but also the w/c ratio, fineness of the particles, and the curing temperature. The five stages of hydration are shown in Figure 3.5.

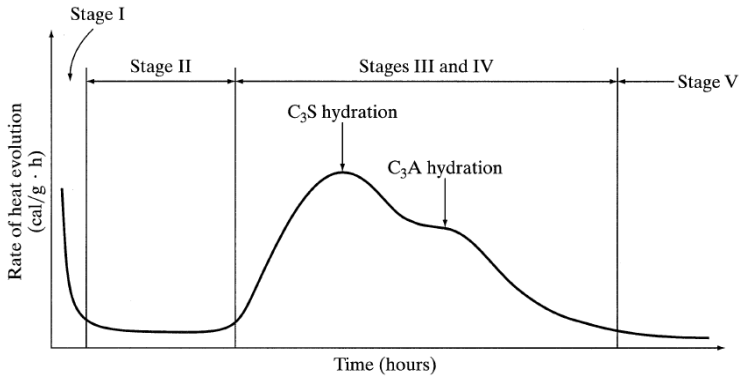

Figure 3.5: Portland Cement Hydration (Mindess & Young, 1981)

Stage I is the dissolution of solids phase where water is introduced into the mixture. Stage II is the induction period and involves the slow dissolution of C_3S. The acceleration period occurs in Stage III where CH crystallizes and C-S-H forms on the surface of grains. The mixture begins to harden here. This C-S-H layer thickens and controls the rate of reaction in Stage IV. Hydration here is controlled by diffusion. In Stage V, hydration products continue to fill empty space and continue until full hydration. These stages hold true with the introduction of SCMs, especially fly ash, in the mixture.

Heat of hydration curves are generated by the use of an isothermal calorimeter. This report aimed to plot the heat of hydration of all fly ash studied with different cement replacement percentages and at different temperatures, following protocol outlined in ASTM C1679, using an isothermal calorimeter ADIACAL TC produced by Grace. Also, by removing the mixtures at predetermined times from the calorimeter, stopping hydration, and scanning in XRD, it is possible to observe crystalline phase formation as a product of hydration time. For those samples identifying hydration products, a scan range of 5° to 70° 2θ degrees, step 0.02, and 4 sec dwell was employed for an average scan of 3.5 hours. This timed calorimetry was performed on a select number of fly ashes to observe microstructural development.

The isothermal calorimetry curves were used to observe the heat flow during hydration, the cumulative heat release, and the activation energy. By observing heat flow graphs, one can compare the hydration differences between the fly ashes, between different replacement percentages, and between the different mixing temperatures. Identifying the length of the dormant period, the time and height of C_3A and C_3S peaks, and the slopes of the acceleration and deceleration time will allow for a quantitative comparison of all the mixtures. The cumulative heat release is another interesting plot. It is calculated by Simpson's Rule of integration of the heat flow curve. This plot shows the strength development of the mixture. The third interesting heat of hydration parameter is activation energy, the energy required to start a reaction. This calculation is based on Arrhenius equation, shown in Equation 3.1.

$$k = Ae^{-E_a/RT} \tag{3.1}$$

The variable k is the reaction rate coefficient, A the proportionality constant, Ea the activation energy, R the ideal gas constant 8.314 J/mol-K, and T the temperature in Kelvin. The

constant Ea is often called the "apparent" activation energy because Ea is a representative average over a range of temperatures. Activation energy is a function of temperature and the degree of hydration. In general, Ea decreases with the increase of Class F replacement. Ea increases with increasing Class C replacement of a low C_3A, low equivalent alkali (Na_2O_e) cement but does not change when Class C replaces a high C_3A, high N_a2O_e cement. In a study looking at the fly ash oxide values, CaO content was the only oxide found to correlate with activation energy (Riding, Poole, Folliard, Juenger, & Schindler, 2011).

Previous research indicates that fly ash with higher CaO and C_3A content exhibit more heat release early in the hydration process and also show poor sulfate resistance. The fly ash that forms monosulfate rather than ettringite in the early hydration stages show poor sulfate resistance as well due to the transformation of monosulfate to ettringite and associated cracking. The higher calcium ashes are more reactive. The fly ashes that delay hydration, or an elongated Stage II, show improved sulfate resistance (Folliard, 2010).

3.7 Sulfate Immersion

The testing to observe the sulfate exposure on hydration products was repeated as performed at the University of New Brunswick with Rajaram Dhole and Dr. Michael Thomas (Dhole, 2008). Fly ash was mixed with calcium hydroxide and an alkaline solution to create a paste with a w/c of 0.45. These pastes were cured over water at 38°C for 28 days. At the end of curing, samples were crushed and a small amount was run in XRD to identify hydration products and the remainder was immersed in sodium and calcium sulfate solutions for 90 days. At the end of sulfate immersion, the samples were run in XRD again to re-identify and re-quantify hydration products. An investigation in the impact of the sulfate solution on the hydration products was conducted and linked to the sulfate resistance of the fly ashes.

Mehta's research proposed that the formation of hydration products at the time of sulfate immersion is the most important factor in determining sulfate resistance. If monosulfate and C-A-H is formed initially, then these products will convert to ettringite over time and cause detrimental expansion. If ettringite formed initially, it would remain as a stable product and the mixture would exhibit good sulfate resistance. Mehta's work directly refuted Dunstan's R factor, outlined in Section 2.3.4, finding some ashes that failed according to Dunstan's equation but performed satisfactorily (Mehta, 1986). This observation that Class C ashes initially produced monosulfate was also observed in work performed by Tishmack. This was a result of more alumina and less SO_3 in the mixture (Tishmack, Olek, & Diamond, 1999).

Other work investigated the hydration product formation of high lime fly ashes. The Class C ashes formed calcium hydroxide from free lime and formed gypsum from anhydrite; however, calcium hydroxide and gypsum were converted into ettringite. This formation was due to the reactive glassy phases in the higher calcium ashes. The Class F ashes formed no ettringite but rather only gypsum from the anhydrite (Tokyay & Hubbard, 1992).

Chapter 4. Concrete Durability Results

4.1 Introduction

Chapter 4 contains information about the selected materials used for this report. This chapter also presents the sulfate attack testing results conducted in a previous testing program at The University of Texas at Austin under TxDOT Project 0-4889.

4.2 Materials

4.2.1 Fly Ash

Eighteen different fly ashes were used in this research. These fly ashes were selected based on completed sulfate attack testing results at UT-Austin and to obtain a wide variety of fly ashes used. The bulk oxide contents presented in Table 4.1 are based on testing performed by TxDOT Materials Lab in Cedar Park, Texas. The fly ash identification numbers were generated based on increasing calcium oxide content of the fly ashes under investigation due to the established relationship between calcium content and sulfate resistance.

Table 4.1: Fly Ashes Tested XRF Results

Fly Ash	Chemical Composition										
ID	SiO_2	Al_2O_3	Fe_2O_3	Sum of Oxides	CaO	MgO	SO_3	Na_2O	K_20	Na_2O_e	LOI
FA-1	53.8	29.5	4.6	87.9	1.1	0.7	0.1	0.4	2.2	1.9	1.8
FA-2	51.4	20.7	7.1	79.2	10.2	3.0	0.3	0.4	1.3	1.3	
FA-3	55.3	17.8	7.6	80.7	10.6	2.3	0.4	0.3	1.1	1.0	0.2
FA-4	51.6	22.8	3.8	78.2	11.9	2.0	0.5	0.2	0.8	0.7	1.1
FA-5	42.9	21.6	4.3	68.8	13.6	2.5	0.9	8.1	0.4	8.4	0.4
FA-6	49.9	18.1	7.8	75.8	14.5	2.8	0.7	0.3	0.9	0.9	0.4
FA-7	45.7	21.0	5.1	71.9	15.3	3.6	0.5	0.8	0.8	1.3	0.5
FA-8	34.9	19.2	5.5	59.6	17.2	3.5	2.8	8.4	0.4	8.6	0.7
FA-9	37.4	18.9	6.5	62.9	21.0	4.3	1.1	1.2	0.4	1.4	0.1
FA-10	33.9	19.3	6.4	59.5	22.9	4.6	0.8	1.2	0.3	1.4	0.2
FA-11	34.4	18.4	6.6	59.4	23.1	4.6	1.3	1.2	0.4	1.4	0.3
FA-12	33.5	19.4	6.0	58.9	24.3	5.4	1.1	1.2	0.3	1.4	
FA-13	31.8	18.6	6.4	56.8	24.7	4.4	2.4	1.1	0.3	1.3	0.3
FA-14	32.5	19.3	6.0	57.7	25.4	4.4	1.2	1.1	0.2	1.2	0.5
FA-15	30.8	19.5	5.6	56.0	25.5	4.5	1.4	1.2	0.3	1.4	0.3
FA-16	32.0	17.2	5.8	55.0	25.8	6.1	1.9	1.3	0.3	1.4	
FA-17	30.9	17.3	5.8	53.9	26.6	7.8	2.3	1.4	0.2	1.5	
FA-18	27.1	17.1	5.8	50.0	29.2	6.2	3.5	1.1	0.2	1.2	0.6

The fly ash background is as follows:

- FA-1: a low CaO, fly ashes this low are not available in Texas, imported from NC
- FA-2: from Texas
- FA-3: large quantities used in central Texas, from Texas
- FA-4: large quantities used in central Texas, from Texas
- FA-5: high-alkali from Michigan, produced from Powder River Basin Coal

- FA-6: from Texas
- FA-7: produced in Texas, low CaO fly ash previous to plant changes compared to FA-10
- FA-8: high-alkali from Southern Canada, produced from Powder River Basin Coal
- FA-9: produced in Texas
- FA-10: produced in Texas, higher CaO compared to FA-7 fly ash after plant changes that is currently produced
- FA-11: produced in Texas
- FA-12: from Arkansas
- FA-13: produced in Texas, used in precast concrete applications
- FA-14: from Texas
- FA-15: produced in Texas, most commonly used in central Texas
- FA-16: from Texas
- FA-17: from Oklahoma
- FA-18: known very poor sulfate resistance, produced in Texas

According to the criteria presented in Table 4.1, FA-1 thru FA-7, with the exception of FA-5, are Class F fly ashes. FA-5 has low calcium content for a Class C ash. The remaining ashes are Class C ashes based on the sum of oxide content.

See Appendix A for the relationship between oxide contents from the XRF results. Because of the debate about classifying ashes based on calcium oxide content, especially in Canada, these figures plot the oxides generated by XRF testing versus calcium oxide content.

4.2.2 Cement

The cement used in testing is Type I-II cement commonly used in central Texas. The XRF data for the cement is shown in Table 4.2. The Bogue values were calculated using ASTM C150-07 calculations.

Table 4.2: Cement XRF Values

Cement ID	C-1	C-2
SiO_2	18.95	20.04
Al_2O_3	5.35	4.49
Fe_2O_3	2.57	3.63
CaO	63.87	63.8
MgO	1.14	0.72
SO_3	3.27	3.02
Na_2O	0.113	0.037
K_2O	0.9	0.62
TiO_2	0.23	0.21
Mn_2O_3	0.049	0.096
P_2O_5	0.34	0.305
Cl	0.007	0.0063
ZnO	0.0108	0.007
Cr_2O_3	0.0122	0.0149
LOI	2.99	2.75
CO_2	1.806	1.759
C_3S	58	54
C_2S	11	16
C_3A	10	6
C_4AF	8	11

C-1 is high alkali cement whereas C-2 has lower alkali content. C-1 was used in ASTM C1012 testing due to the requirement that cement C_3A content must be greater than 8%. C-2 was used in calorimetry and sulfate reactivity testing.

4.3 ASTM C1012 Tests

ASTM C1012 is a widely used test method to examine the external sulfate attack resistance of blended cements with SCMs. The test involves casting mortar bars, curing until they reach a specified strength, and placing the bars in a 5% sodium sulfate solution. Other sulfate solutions may be used; however, only the effect of sodium sulfate was studied in this research. Measurements are taken over a period of 18 months with a change of solution at each measurement. The expansion limits are listed in Table 4.3. The expansion in this test is directly a result of the formation of ettringite and resulting expansions.

Table 4.3: Fly Ash Expansion Limits for ASTM C1012 (ASTM C 618, 2008)

Sulfate resistance of blended cement	Expansion (maximum) at 6 months, %	Expansion (maximum) at 12 months, %
Moderate	0.10	—
High*	0.05	0.10
Very high	—	0.05

*If expansion at 6 months is >0.05% but expansion at 12 months is <0.10%, blended cement is considered to have high sulfate resistance.

This project utilized past data from previous University of Texas projects to minimize the number of ASTM C1012 samples cast. See Table 4.4 for the summary showing which ashes were tested as part of this report. The previous work was conducted by Dr. Thano Drimalas and John Christopher Clement at The University of Texas at Austin.

Table 4.4: ASTM C1012 Testing Summary

	Previous Results	Needed
FA-1	x	
FA-2		x
FA-3		x
FA-4	x	
FA-5		x
FA-6	x	
FA-7		x
FA-8		x
FA-9	x	
FA-10		x
FA-11	x	
FA-12		
FA-13	x	
FA-14	x	
FA-15	x	
FA-16	x	
FA-17		
FA-18	x	

FA-12 and FA-17 were not analyzed by the ASTM C1012 testing due to the material's late arrival.

4.4 Results

In general, high calcium ash offered poor resistance to sulfate attack as compared to low calcium ashes. Compared to the control of 100% cement, most of the Class C ashes failed at comparable measurements. See Figure 4.1 for a representative Class F ash performance and Figure 4.2 for a representative Class C ash performance compared to the control mixture. Graphs presenting ASTM C1012 expansions for each fly ash are presented in Appendix B.

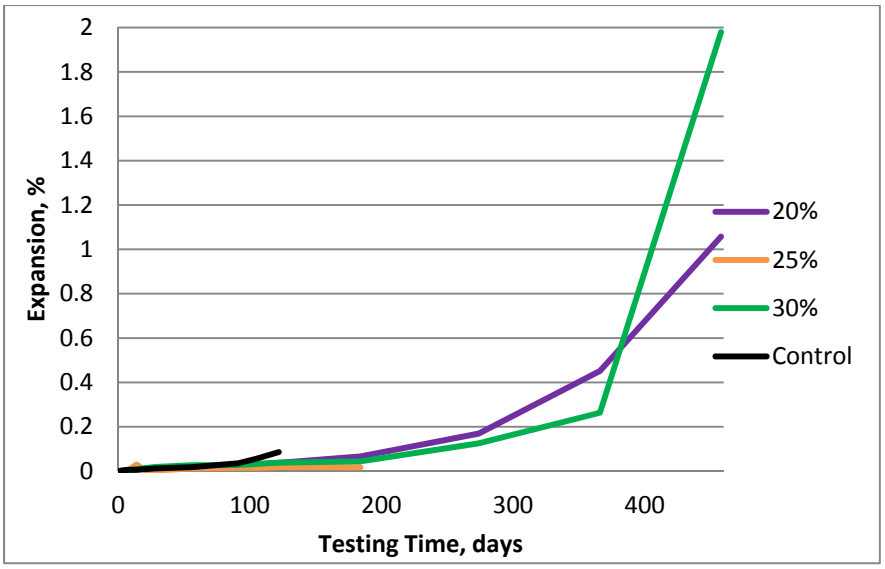

Figure 4.1: Typical Class F Fly Ash ASTM C1012 Data

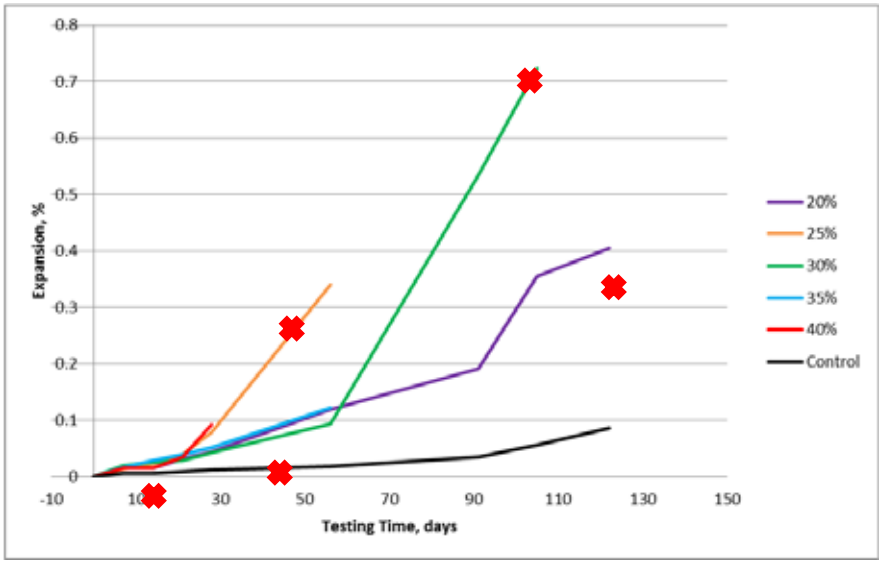

Figure 4.2: Typical Class C Fly Ash ASTM C1012 Data

Another way to observe this data was the time to failure. Failure occurs when the bars exceed 0.1% expansion at one year or when all of the bars became unreadable. See Figure 4.3 for the time to failure plot of all the fly ashes. Notice that for all replacement levels, the highest calcium Class C ashes failed much faster than the other ashes studied. High calcium fly ashes at 40% replacement had the highest linear correlation, meaning that as the calcium content increased, the expansion increased.

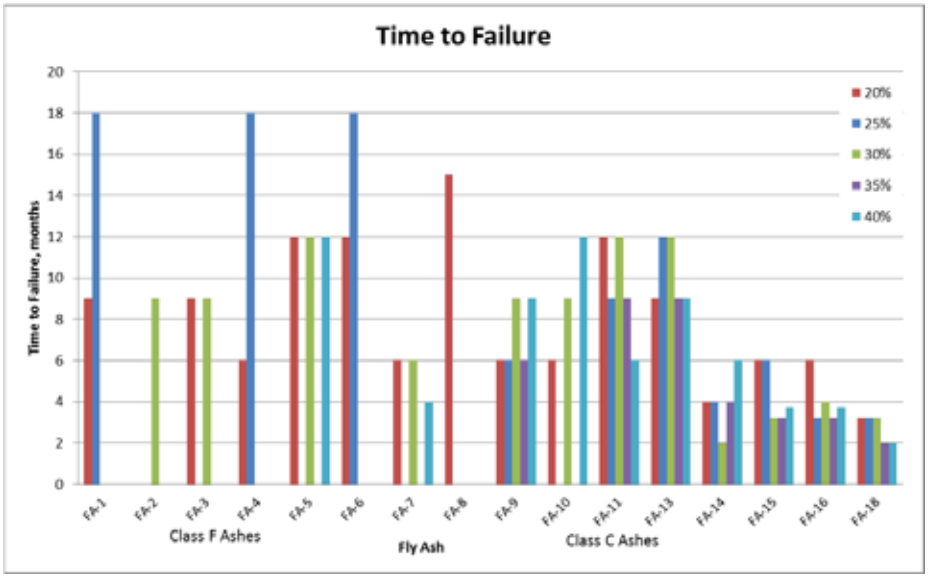

Figure 4.3: Time to Failure Data

The average time to failure values are plotted in Figure 4.4. Looking at this plot, the average time to failure for Class F ashes was much higher than that of the Class C ashes for the same replacement percentages. As the replacement percentage increased for a Class F ash, the sulfate resistance improved or the time to failure increased. There was a slight inverse relationship for time to failure and increasing Class C replacement percentage, meaning as replacement percentage increased, expansion increased. These correlations were very weak ones though.

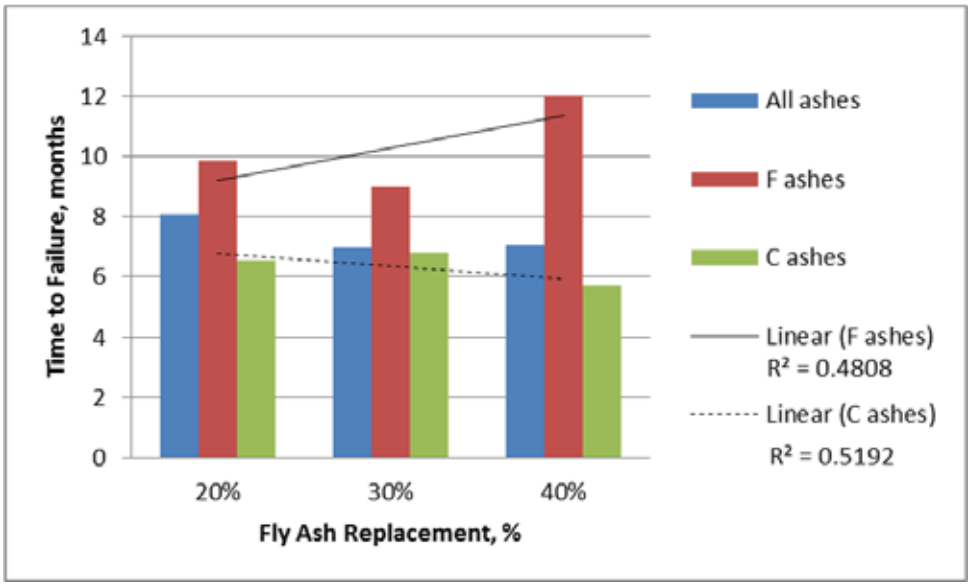

Figure 4.4: Average Time to Failure

4.5 Discussion

Previous work has showed that Class F ash improves the sulfate resistance of the mixture. In general, Class C ash had an increase in expansions compared to a control and had a decreased resistance. The results shown in Figure 4.4 confirm this finding. The effect of the replacement percentage of Class F ashes on expansion varied with the type of cement used. As replacement with Class C ashes increased, there was also an increase in expansions (Stephens & Carrasquillo, 2000). In this work, as the replacement percentage of Class F ashes increased, the expansion decreased. The testing results from this report and previous testing displayed in Figure 4.4 agreed with the findings on replacement percentages.

Comparing the time to failure results with the XRF data for the ashes seen in Table 2.5, there were a few interesting items to note. When the calcium oxide content is greater than 25%, it is not recommended to use the fly ash in sulfate environments stated in literature. FA-14 through FA-18 have calcium oxide content in excess of 25%, and as seen in Figure 4.5**.** these ashes had a significant drop in time to failure compared to the other ashes. The testing data confirms this statement.

In literature, if the alumina, iron, and silica oxide sum, which will be referred to as sum of oxides, is greater than 70% and the silicon dioxide value is greater than 40%, the fly ash will improve the sulfate resistance. The ashes with silicon dioxide values greater than 40%, which was all of the Class F ashes, had improved sulfate resistance. FA-6 had the longest average time to failure out of the ashes that have failed and interestingly the highest iron oxide content.

It is interesting to look at the performance of the two high alkali fly ashes, FA-5 and FA-8. These two ashes have the highest alkali content by a factor of around 6 compared to the other ashes. They are both classified as Class C ashes; however, FA-8 has greater calcium content. Refer to the XRF data presented in Table 4.5. One would expect FA-8 to have larger expansions, but this was not the case as shown in Figure 4.5. FA-5 specimens all failed at 12 months whereas most FA-8 specimens have not yet failed to date. FA-5 had significantly higher expansions at the 18 month reading for all replacement percentages. These two ashes have differing silica and sulfur oxide contents. This relationship will be analyzed more in depth in the later sections of this report.

Table 4.5: XRF Values for High Alkali Fly Ashes

Chemical Composition	Fly Ash	
	FA-5	FA-8
SiO_2	42.9	34.9
Al_2O_3	21.6	19.2
Fe_2O_3	4.3	5.5
Sum of Oxides	68.8	59.6
CaO	13.6	17.2
MgO	2.5	3.5
SO_3	0.9	2.8
Na_2O	8.1	8.4
K_20	0.4	0.4
Na_2O_e	8.4	8.6
LOI	0.4	0.7

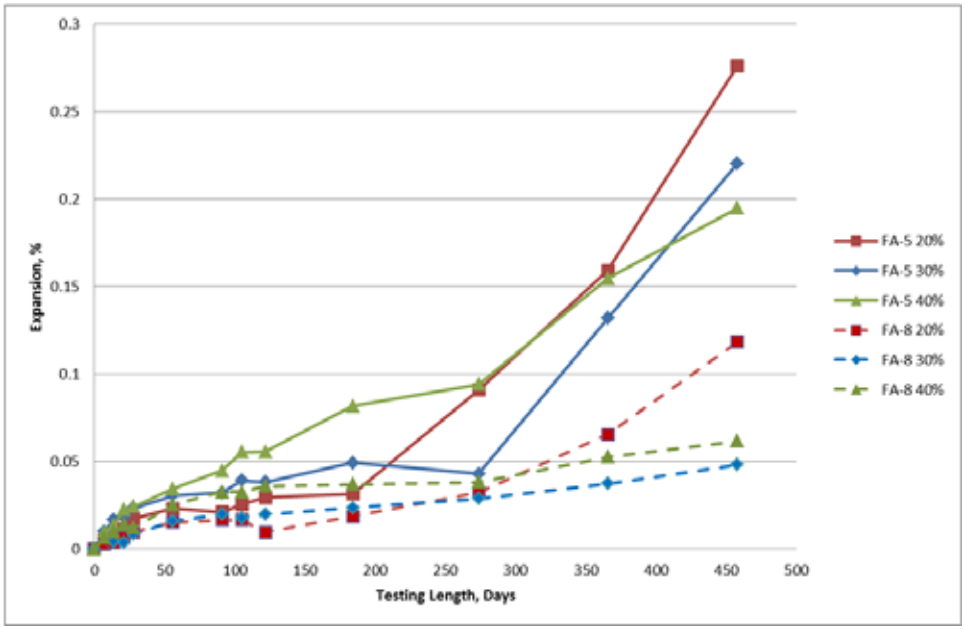

Figure 4.5: ASTM C1012 Results for the Two High-Alkali Fly Ashes

The following were trends found when analyzing the XRF data in Figure 4.6 with expansion data at 15 weeks and 9 months, plotted in Figure 4.6. The x-axis is increasing CaO content. The 15 week data was used for comparison purposes due to most every specimen under investigation having a valid reading at this length of time. The 15 week expansion data may not be indicative of true sulfate expansion performance due to the possibility of large expansions later in the testing regime. Therefore, trends looking at expansions at 9 months were observed in the same manner as the 15 week expansion data. On this plot, the bars for each fly ash are 20%, 25%, 30%, 35%, and 40% fly ash replacement. Not all replacement percentages were tested for every fly ash. Also, if there is a 15 week but no 9 month reading, the bars failed before this reading.

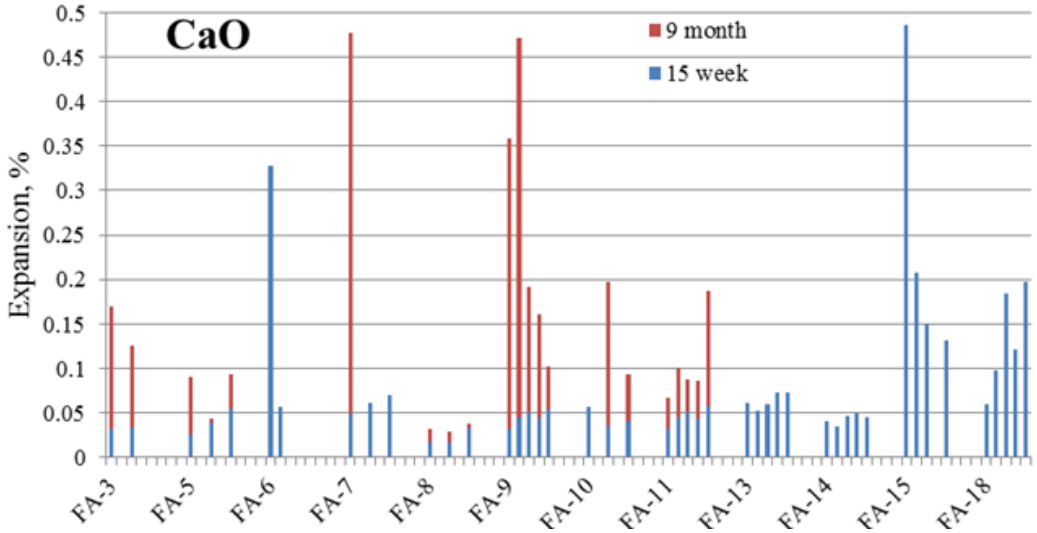

Figure 4.6: Comparison of XRF Calcium Oxide Contents with ASTM C1012 Expansions at 15 weeks and 9 months

FA-6, FA-15, and FA-18 had the largest 15 week expansions. The XRF data for these ashes is presented in Table 4.6. There seemed to be no similarities between all three ashes for any oxide value. This relationship will be observed in following testing chapters.

Table 4.6: XRF Data for FA-6, FA-15, and FA-18

Chemical Composition	Fly Ash		
	FA-6	FA-15	FA-18
SiO_2	49.9	30.8	27.1
Al_2O_3	18.1	19.5	17.1
Fe_2O_3	7.8	5.6	5.8
Sum of Oxides	75.8	56.0	50.0
CaO	14.5	25.5	29.2
MgO	2.8	4.5	6.2
SO_3	0.7	1.4	3.5
Na_2O	0.3	1.2	1.1
K_20	0.9	0.3	0.2
Na_2O_e	0.9	1.4	1.2
LOI	0.4	0.3	0.6

Plots comparing the expansions at 15 weeks and 9 months and XRF oxides were generated to see if any trends existed between oxides other than calcium, shown in Figure 4.6, and expansions. These plots are presented in Figure 4.7 where the x-axis ashes have increasing oxide contents.

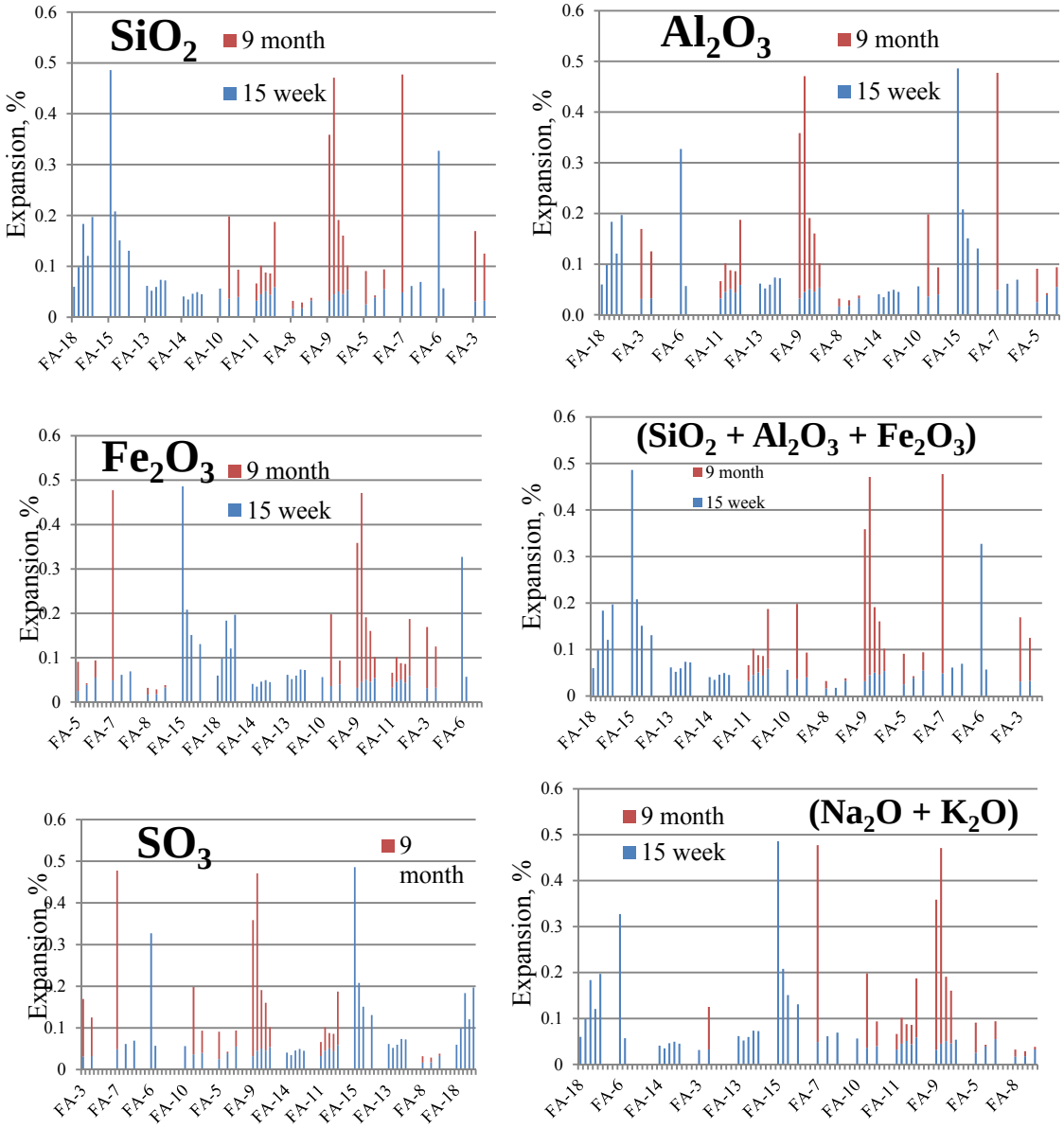

Figure 4.7: Comparisons between XRF Oxides and ASTM C1012 Expansion Data

Observing the general trends between 15 week and 9 month expansions and XRF data, the following relationships were observed:

- SiO_2: At 15 weeks, the lower the SiO_2 content, the greater the expansion. At longer testing periods, the lower SiO_2 contents had expansions large enough to break all specimens and render a 6 month reading unattainable. The higher the SiO_2 content, the lower the expansions.
- Al_2O_3: There does not appear to be a trend with Al_2O_3 at any testing age.
- Fe_2O_3: The highest expansions had Fe_2O_3 content around 6.0%, the mean of the XRF values. These specimens had the largest 15 week expansions and unreadable

bars at 9 months. The fly ashes with the lowest and highest Fe_2O_3 values had less expansion.

- Sum of oxides: The lower the sum of the oxides, the greater the expansion at 15 weeks. This correlated to the greatest expansions breaking all specimens at 9 months as well. For the ashes with largest sum of oxide values, the expansions were less. FA-6 is the only outlier to this conclusion.
- CaO: At 15 weeks, the fly ashes with the largest expansions had the highest CaO contents. This held true for the later testing ages. FA-6 is the only outlier again for this conclusion.
- SO_3: The higher the SO_3 content, the larger the expansions at 9 months. FA-6 is an outlier to this argument as well.
- $Na_2O + K_2O$: Note this is the sum of the alkalis, not Na_2O_e. The larger the sum of the alkalis, the less the expansions. FA-3 was an outlier to this finding.

4.6 Summary

In general, the ASTM C1012 results correlate with findings from other research studies. The lower calcium ashes had improved sulfate resistance while the greater the calcium, the lower the sulfate resistance. Also, as Class C ash replacement percentage increased, the expansion increased. No strong relationship was observed between Class F ash replacement and expansion.

Chapter 5. Fly Ash Characteristics

Chapter 5 contains the testing results that describe the nature of the fly ash, including its composition, and fly ash testing independent of its reaction with cement during hydration studies.

5.1 Composition and Particle Size Distribution

5.1.1 Testing

XRF

The XRF testing was performed at TxDOT's Materials Department in Cedar Park, Texas using a 1 kW Wavelength Dispersive S4 Explorer manufactured by Bruker-AXS. TxDOT utilized fusion pellets as the preferred XRF method over pressed pellets to obtain a truly homogeneous sample removing the particle size effect and to obtain a higher accuracy output.

Particle Size Distribution

Particle size distribution was evaluated using laser diffraction and wet sieving through No. 325 sieve. For laser diffraction, the instrument used was a Spraytec by Malvern Instruments, Inc. with Spraytec software. The material refractive index was 1.5 with an imaginary index of 0.1. This machine uses degassed isopropyl alcohol as the dispersive agent. The fly ash is added to the dispersant, and a stirrer suspends the particles and shoots them through a small separation between 2 glass plates. A laser shoots through the glass plates and measures the diameters of the particles traveling through the plates. The diameter of 10%, 50%, and 90% are numerically reported in addition to a particle size distribution plot. The wet sieving procedure was followed as outline in ASTM C430.

5.1.2 Results

XRF Results

The XRF results were presented in Section 4.2 in Table 4.1 and Table 4.2. The XRF values will continuously be used throughout the following results in an attempt to understand the presented results pertaining to sulfate attack.

Particle Size Distribution Results

Research conducted on fly ash particle size and sulfate resistance states that the coarser fly ash particles have increased expansion. In fine fly ash particles, the glass content increased over that of coarser particles, enhancing reactivity. The finer particles lead to a denser cement matrix, though, due to the fine particles decreasing the pore volume. Due to the enhanced reactivity and reduced permeability, the finer fly ash particles had good sulfate resistance (Chindaprasirt, Homwuttiwong, & Sirivivatnanon, 2004). This research was conducted creating mortar of only the fine fly ash particles, mortar of the medium particles, and mortar of only the coarse particles. This work failed to characterize the effect of a range of sizes in a mortar matrix on sulfate resistance. Another research project aimed to characterize different fly ash sizes by

their mineralogy from XRD. As the size of the fly ash increased, the amount of calcium-bearing compounds decreased and the amount of quartz increased. McCarthy conducted a test that found the opposite results from fly ash size and mineralogy though. It was found that quartz did take part in the pozzolanic reaction and the amount of glass in all of the sizes was the same. Any material greater than 75 µm was found to be nonreactive (Joshi, Natt, Day, & Tillerman, 1985).

All fly ashes had good size gradation, displayed in Figure 5.1. This S-shape means even distribution of all sizes with no missing sizes present for all fly ashes. This range of sizes ensures good packing density to create less permeable concrete.

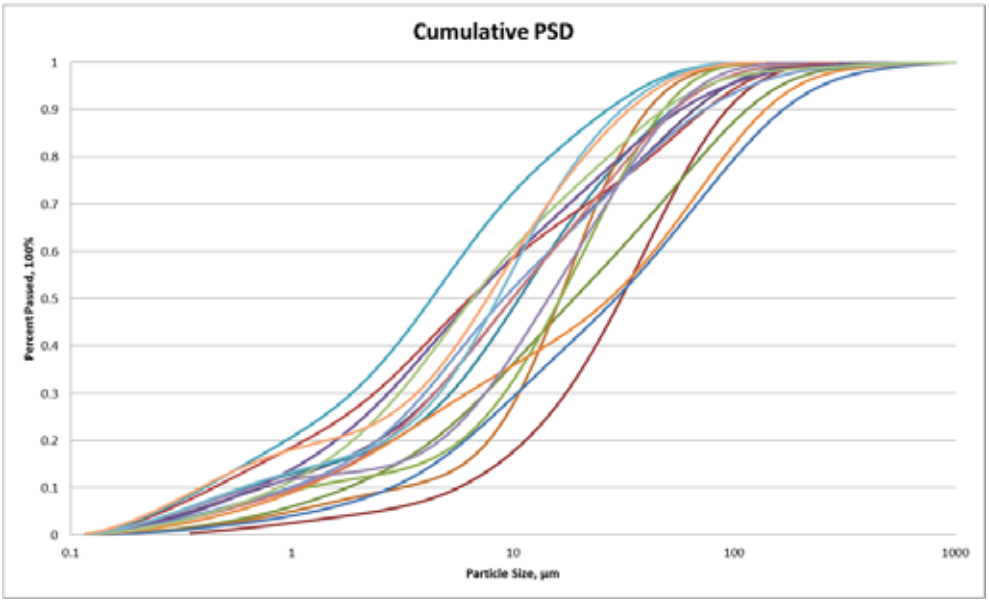

Figure 5.1: Fly Ash Particle Size Distribution

The particle size results are shown in Figure 5.2. In general, as the CaO content of the ashes increased, the particle size decreased. From the argument posed above that finer particles have better sulfate resistance due to their better packing density, the Class C ashes should have larger particle diameters. However, this result was not observed. It is proposed that these higher calcium ashes have poor sulfate resistance due to a finer, more reactive fly ash due to greater surface area of the particles. The argument of sizes on packing density and resulting impermeability was understood, but due to the ASTM C1012 sulfate testing method, permeability was not the primary mechanism under investigation. The research performed by Joshi stating larger particles contain more quartz used in pozzolanic reactions was confirmed by the testing results. The Class F ashes were larger particles and were more pozzolanic than the Class C ashes. Joshi also stated that particles greater than 75 µm were nonreactive. The lower calcium ashes had the greatest content of 75 µm and greater particles. If more of the ash is nonreactive, it will have better sulfate resistance due to sulfate ions attacking fewer reactive components. LOI is related to particle size. LOI is increased with increasing unburnt carbon content and is usually higher for Class F ashes. The greater the carbons content of the ash, the lower the density (ACI 232.R-96, 1996). This relationship was confirmed here, and a correlation established between LOI and D(50).

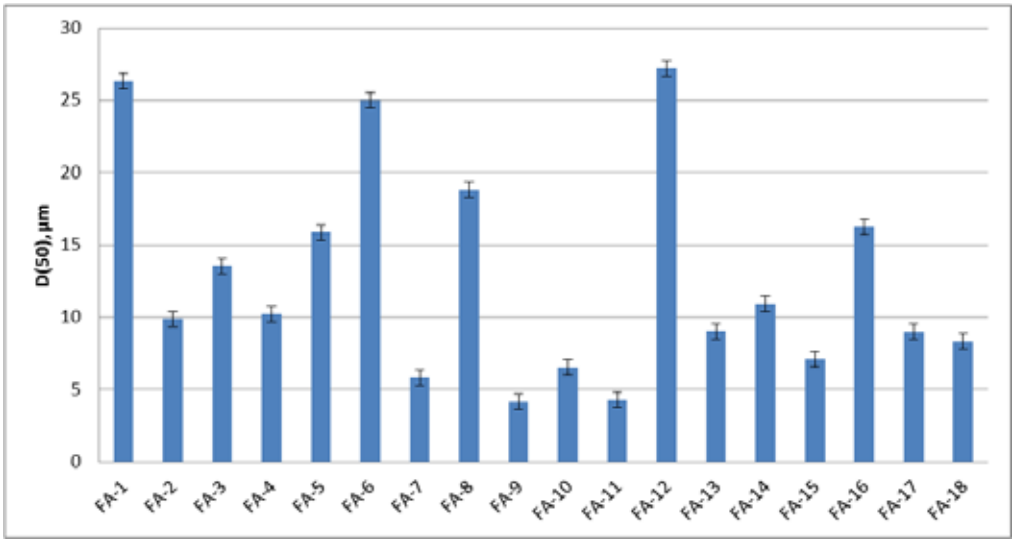

Figure 5.2: Average Particle Diameter by Mass

Out of the lower calcium ashes that performed well in sulfate environments, only FA-7 had a very short time to failure. This ash had the smallest particle size diameter compared to the other Class F ashes. FA-5 and FA-11 had similar time to failure data but drastically different particle diameters. FA-2, FA-4, and FA-14 had similar particle diameters but very different sulfate expansions. FA-9 and FA-11 had the smallest average particle diameter; however, these ashes did not have the worst sulfate performance. The worse sulfate resistant ashes, FA-14 thru FA-18, had moderate average particle diameters.

The results from the No. 325 wet sieve standard are presented in Figure 5.3. All of the ashes passed the requirement that no more than 34% of the material can be retained on the No. 325 sieve.

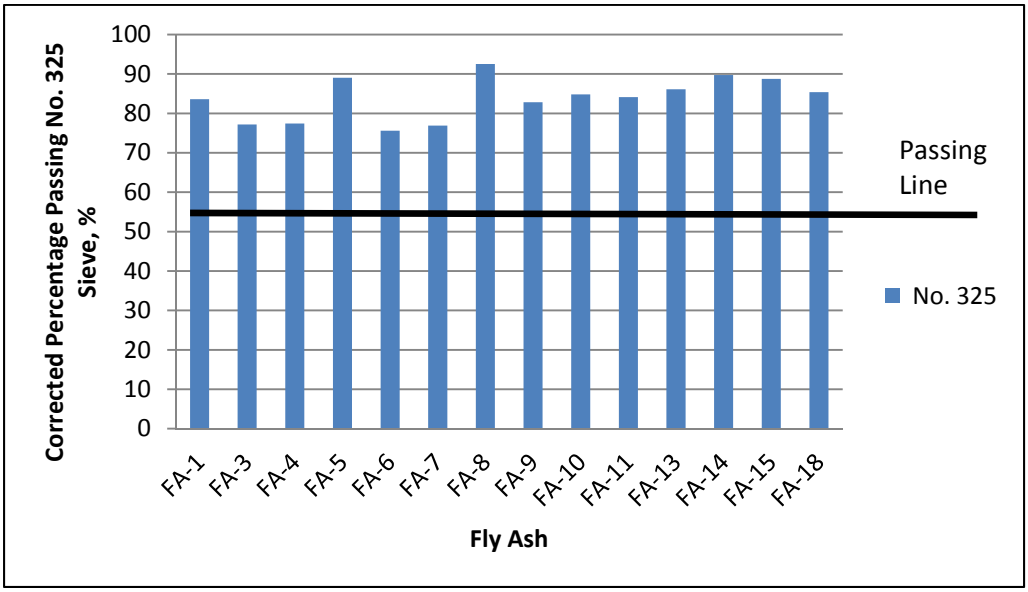

Figure 5.3: Fly Ash Fineness by the 45-µm (No. 325) Sieve

In general, there does not appear to be a definite correlation between particle size diameter and sulfate resistance. There was a general trend of increasing calcium content with decreasing average particle diameter and increasing expansion. No other oxide values correlated to particle size diameter. As average particle size decreased, sulfate resistance decreased in this study.

5.2 Crystalline Phase Composition

5.2.1 Testing

The pure powder fly ash samples were examined through XRD analysis. Tests were run on Siemens D500 diffractometer with scan parameters of 10° to 70° 2θ degrees, step 0.02, and 8 sec dwell. The average scan time was 6.75 hours per fly ash powder sample for a high intensity scan. Rietveld was performed on all scans to identify the major crystalline phases. The Rietveld analysis was adjusted until the best fit regression analysis had a correlation coefficient value under 10.

5.2.2 Results

Reactive vs. Non-Reactive

Based on previous research stating which crystalline phases are reactive and those that are not, the phases identified through Rietveld analysis were categorized based on their reactivity. The following were considered reactive phases: anhydrite, merwinite, periclase, sodalite, lime, C_3A, C_4AF, C_2AS, C_2S, and arcanite. These results are presented in Figure 5.4. The lower calcium ashes had a greater percentage of non-reactive crystalline phases whereas the higher calcium ashes had a greater percentage of reactive crystalline phases. This correlates with the poor sulfate resistance of higher calcium ashes. Note the large percentage of reactive phases in FA-17 and FA-18.

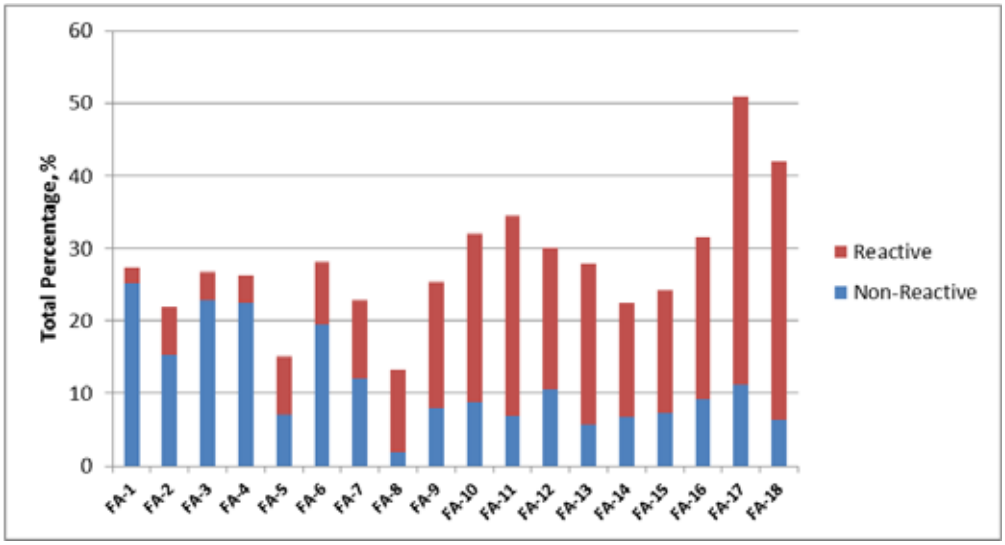

Figure 5.4: Breakup of Crystalline Phases of Power Fly Ash XRD

Trends were observed between XRF values and reactive content.

- SiO_2: The lower the SiO_2 content, the more reactive phases present. The observation also exists for the sum of the oxides. These two oxides are the opposite of the CaO results shown in Figure 5.4.
- Al_2O_3: The lower the Al_2O_3 content, the more reactive phases present. The exceptions are FA-3, FA-6, and FA-8.
- Fe_2O_3: The moderate Fe2O3 contents contain the most reactive phases.
- SO_3: The lower the SO_3 amounts, the more content of reactive phases. The exception is FA-8.
- Na_2O_e: The middle Na_2O_e values contain the most reactive phases. FA-17 and FA-18 are the exceptions.

Crystalline Phases

As for the main crystalline phases outlined in Section 2.3.3, a more in depth look follows. Anhydrite, a reactive phase involved in ettringite formation, was somewhat increased for the higher calcium ashes, but there was a large amount for FA-18. FA-18 had one of the shortest time to failures or the poorest sulfate resistance. In previous research, anhydrite was thought to be released at later stages of hydration to form ettringite. This phase is linked to DEF and resulting durability issues (Dhole, 2008). More mullite, a non-reactive phase, was found in Class F ashes. More merwinite was found in Class C ashes. This result matches what was expected and was related to MgO content. More quartz was observed in Class F ashes, supporting the PSD results that quartz was involved in the pozzolanic reaction and found in lower calcium ashes. See these relationships in Figure 5.5.

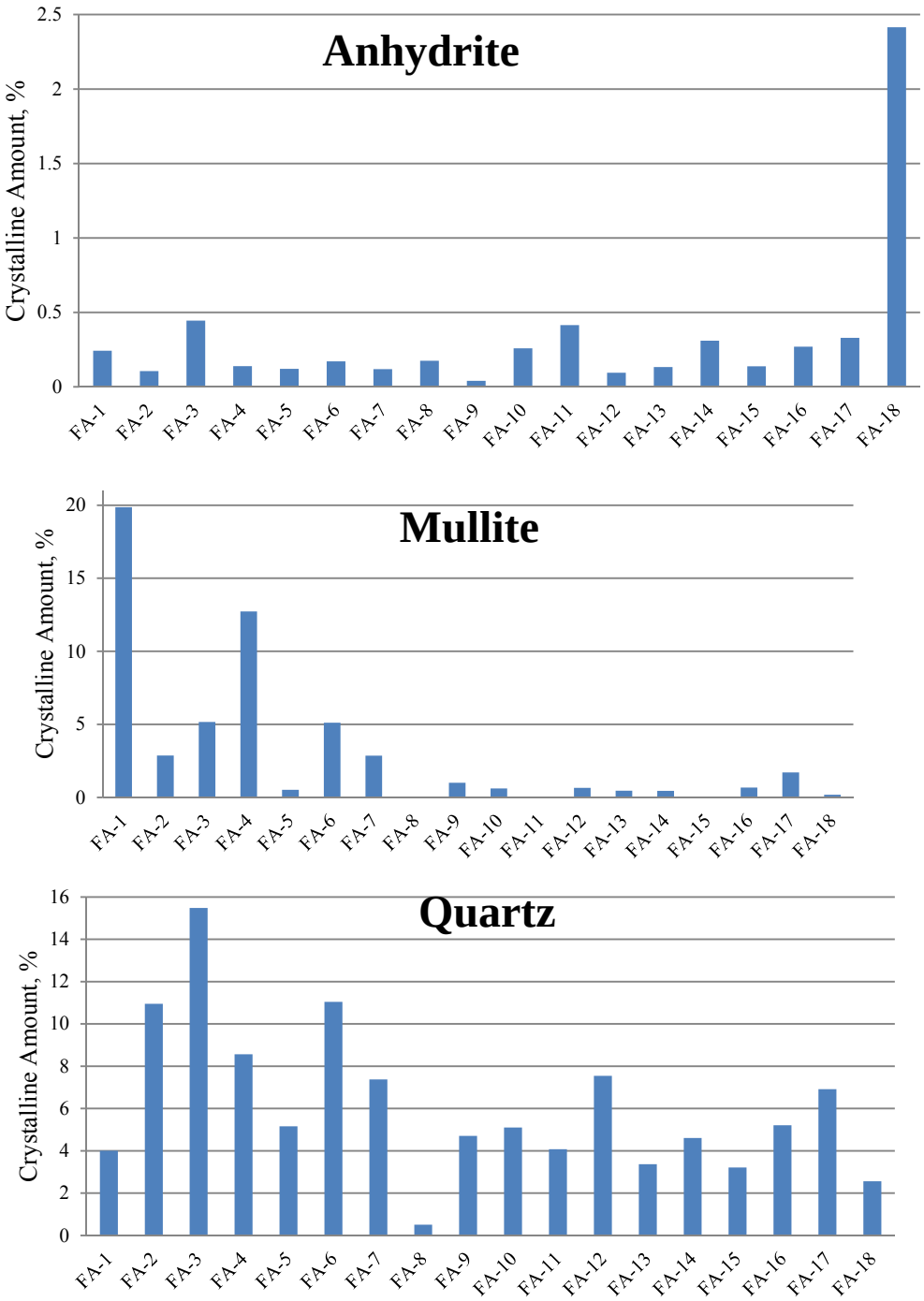

Figure 5.5: Select Crystalline Phase Amounts in Powder Fly Ash XRD

The C_3A content is a very reactive crystalline phase known to be related to sulfate performance. See the relationship with C_3A in Figure 5.6. The C_3A content increased with increasing calcium content which also correlated to poor sulfate performance. FA-16 had a very low percentage of C_3A but a very short time to failure. FA-16 had a very high percentage of

periclase though, which is another reactive crystalline phase. FA-6 had a large amount of C_3A, which could explain the large expansion at 15 weeks noted previously.

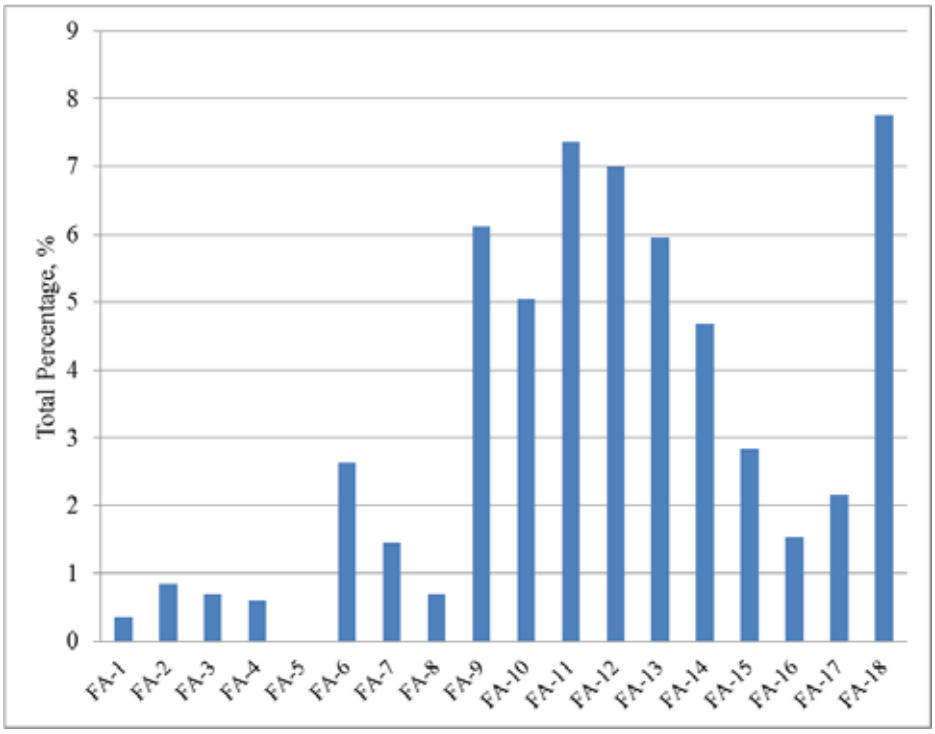

Figure 5.6: Crystalline C_3A Amount in Powder Fly Ash XRD

Dunstan also proposed that C_4AF along with C_3A contributed to the fly ashes sulfate resistance. C_4AF, also known as brownmillerite, forms ettringite when mixed with water and calcium sulfates. The amount of C_4AF increased with increasing calcium content, which correlated to poor sulfate performance. See this relationship in Figure 5.7.

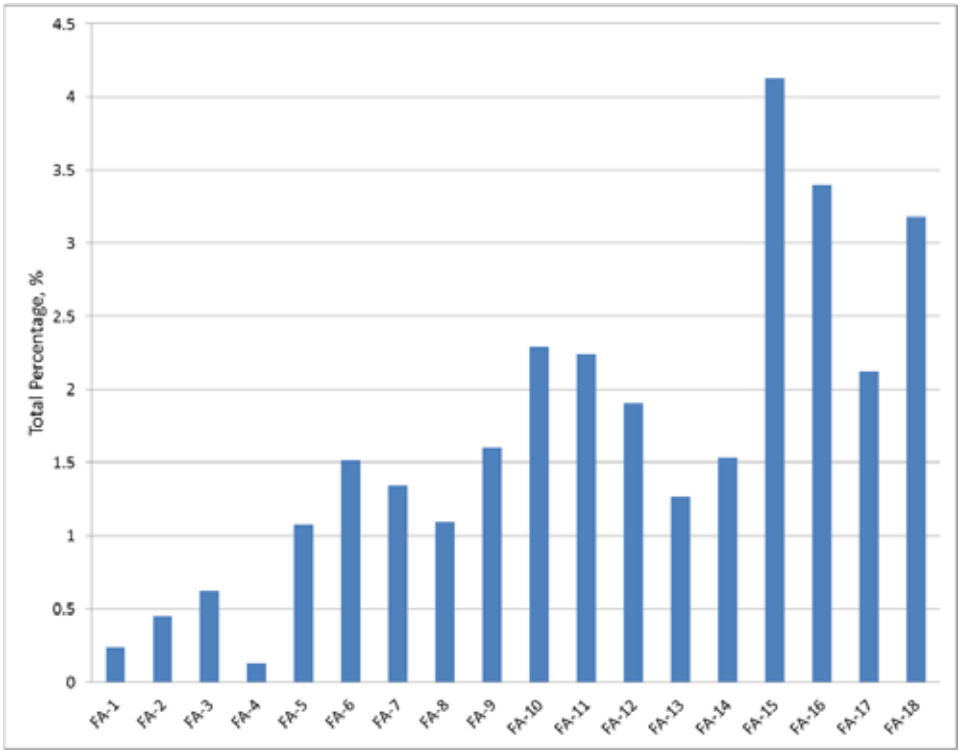

Figure 5.7: Crystalline Brownmillerite in Powder Fly Ash XRD

FA-11 and FA-13 had longer times to failure than FA-14 through FA-18. Analysis shows FA-11 and FA-13 had significantly lower amounts of periclase and lime, which are known reactive components. Periclase is limited to 5% due to potential soundness issues in fly ash. Periclase has a very small particle size, so if reactive periclase exists, it will hydrate early and not cause soundness issues (Tikalsky P. J., 1989). All of the fly ashes met this standard; however, the amount of periclase increased with increasing calcium content. See the periclase results in Figure 5.8.

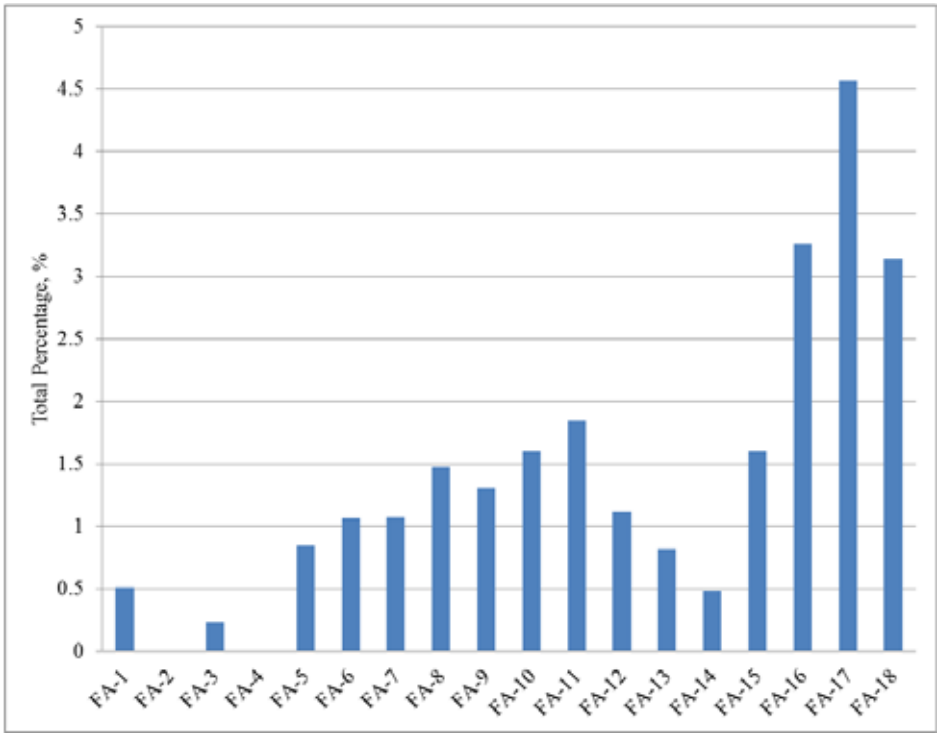

Figure 5.8: Crystalline Periclase Amount in Powder Fly Ash XRD

Lime is documented to be in all Class C ashes and some Class F ashes, which was observed in Figure 5.9. Lime is responsible for autoclave expansion, but depending on the form of the lime present it may or may not result in soundness issues. Free lime left over after the pozzolanic reaction is available for reaction with sulfates. The Class F lime percentages were mostly all consumed in this pozzolanic process and therefore not able to react with sulfates. Class C had a surplus of free lime, allowing for a reaction with sulfates and resulting poor sulfate performance.

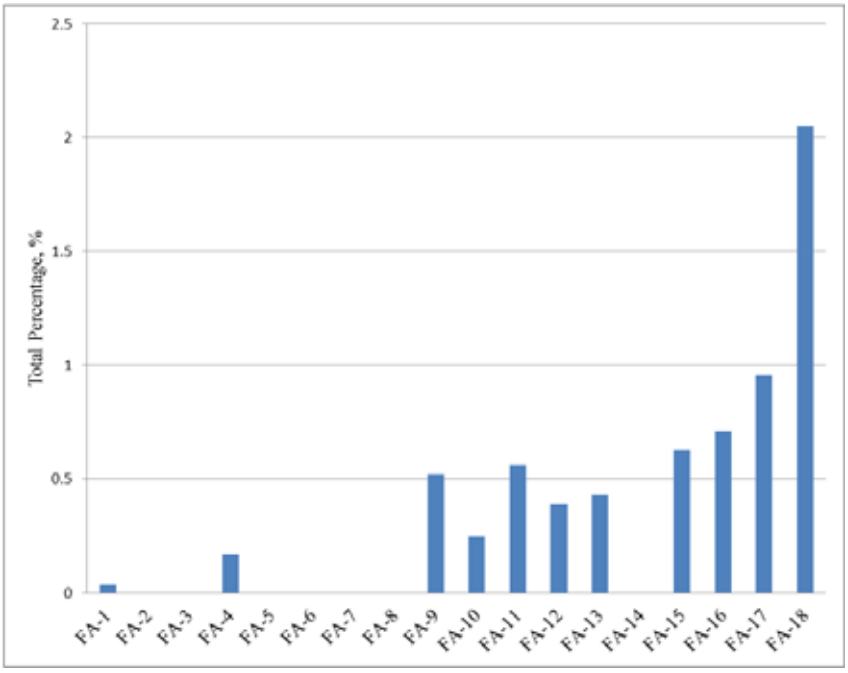

Figure 5.9: Crystalline Free Lime Amount in Powder Fly Ash XRD

Past Models

As for the model proposed by Dunstan, see Equation 2.6 in Section 2.3.4 for review, the results are presented in Figure 5.10. The correlation between the R-factor and sulfate resistance is indicated on the right side of the graph. As the calcium content of the ashes increased, the R-factor increased, which correlated to a decrease in sulfate resistance. FA-5 and FA-11had R-factors in the no change region, and these two ashes had similar time to failure performance. FA-6 did see reduced expansions when compared to FA-4 and FA-5. FA-12 thru FA-18 all had reduced resistance R-factors with FA-13 being right on the edge of the lower region. FA-13 had the longest time to failure of all of these higher calcium fly ashes. There did seem to be a correlation between the sulfate expansion data produced in this project and Dunstan's R-factor.

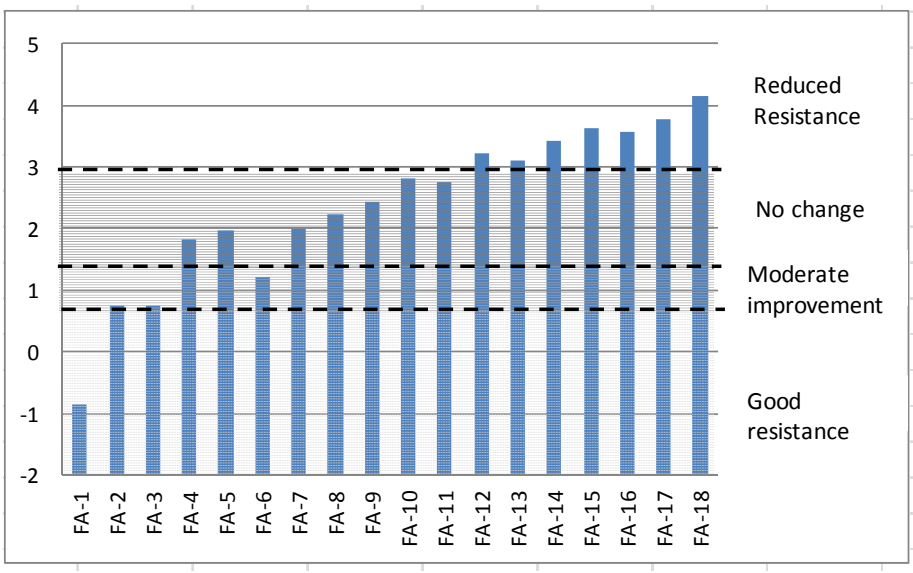

Figure 5.10: Dunstan's R-Factor

Manz also proposed a model correlating fly ash XRF oxide values and crystalline phases on sulfate resistance based on Dunstan's model. The results from these calculations are presented in Figure 5.11. The initial graph proposed plotted CSE on the x-axis and CAP on the y-axis, but this resulted in only FA-18 having acceptable performance, which is incorrect based on the time to failure and expansion data. However, when the regions of performance were flipped, the results were accurate with the expansions recorded. This flipped regions graph was presented below. The only incorrectly plotted point is FA-8, which has low expansions but would be deemed unsatisfactory with this revised model. Due to these findings, the model as proposed by Manz does not seem to accurately predict sulfate resistance, but the revised model with flipped regions accurately predicted performance with the observed expansions.

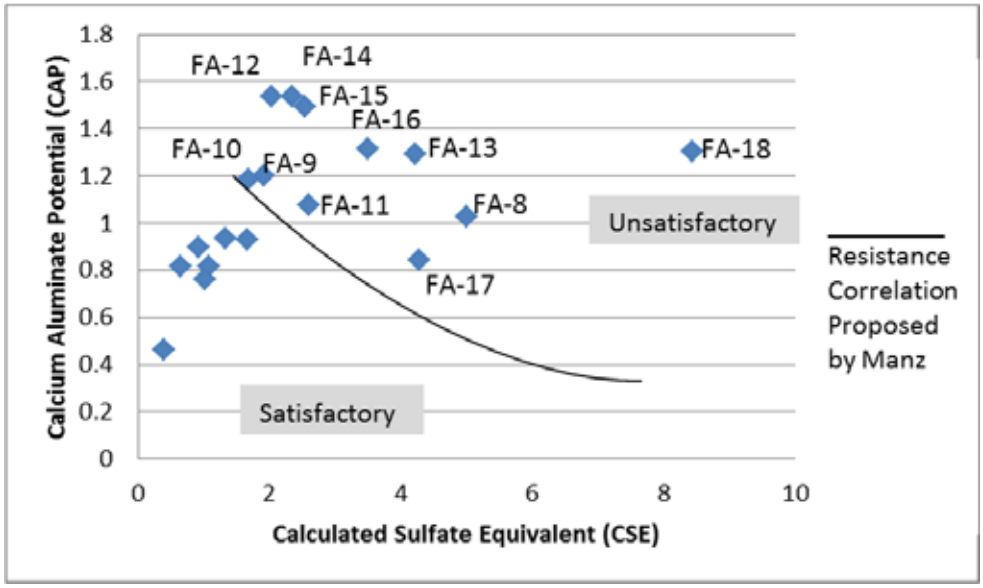

Figure 5.11: Manz Sulfate Resistance Parameters

Hartmann and Mangotich also presented a model for sulfate resistance based on Dunstan's original model. This calculation accounted for the composition of the fly ash and the cement used. The results from this model are presented in Figure 5.12, which also presents both cements used in this study. The blue bar is the fly ash mixed with C-1 and the red is missed with C-2. The cement lines refer to 100% cement. The lower ODF values correlate to greater sulfate resistance, but if the ODF is less than that of the cement then the sulfate resistance is improved. For the latter hypothesis, FA-18 was the only fly ash to decrease the sulfate resistance. From the time to failure data, FA-14 through FA-18 all had similar poor resistance, but the ODF values were significantly different for these ashes. The middle calcium ashes, FA-9 through FA-13, FA-1, and FA-4 should have had the greatest sulfate resistance based on the proposed ODF hypothesis. FA-1 and FA-4 had long times to failure, but FA-9 through FA-13 had moderate resistance. FA-6 had lower expansions than these moderate resistant ashes but a greater ODF. Due to these inconsistencies, this model did not correlate well with sulfate performance.

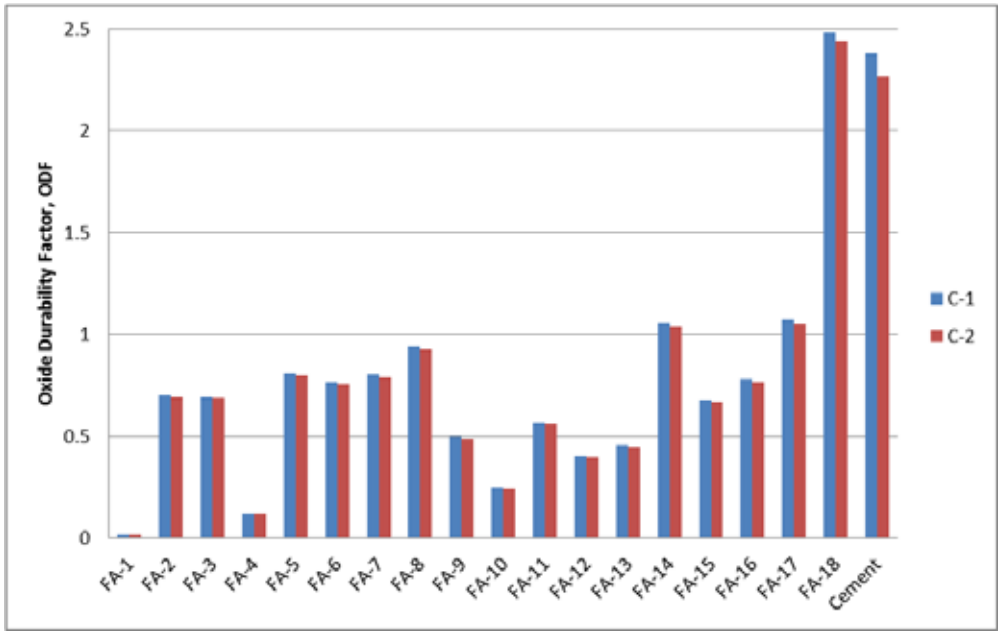

Figure 5.12: Hartmann and Mangotich Oxide Durability Factor

In general, the higher calcium ashes contained more reactive crystalline phases whereas the lower calcium ashes contained more non-reactive phases. The three models outlined in the literature review aim to correlate the effect of crystalline phases and XRF oxide values with sulfate resistance. Although the most scrutinized, Dunstan's R-factor appeared to be the most accurate with the testing results obtained from this report.

5.3 Amorphous Phase Composition

5.3.1 Testing

The amorphous content of the fly ashes were studied using a SEM. The machine used was a Quanta 650 SEM with a backscatter detector, 20 kV beam, 4.5 spot size and magnification around 5000x. Testing was performed on 14 of the 18 fly ashes under investigation. As mentioned previously, amorphous particles are 1–5 μm in diameter. In order to obtain a

representative sample for each fly ash, compositions of 150–200 amorphous particles were collected and analyzed. These compositions were converted into oxides based on conversion factors and molecular weights. The oxides for all data points were plotted on a series of conventional ternary diagrams by the use of a tri-plot spreadsheet (Graham & Midgley, 2000).

5.3.2 Results

CaO-Al_2O_3-Si_2O_3 Diagram

This ternary diagram is the most widely used diagram used to explain the glassy phases of fly ash as outlined in Section 2.3.3 This ternary diagram will be called diagram #1 in this report. On this diagram, mullite is alumina-silica oxide and anorthite and gehlenite are calcium alumina-silica oxides. Parent coal with higher levels of calcium resulted in fly ash with calcium aluminosilicate glass. Therefore, on this ternary diagram, one would have expected to see a shift from the mullite region to the gehlenite region when comparing low to high calcium oxide fly ashes. See this shift in a typical Class F ash in Figure 5.13 and with a typical Class C ash in Figure 5.14. The results confirmed that the higher calcium ashes contained more of the reactive calcium aluminosilicate glass. It is very important to note the regions discussed do not mean the amorphous content is gehlenite, but only that it performs like gehlenite or the other regions.

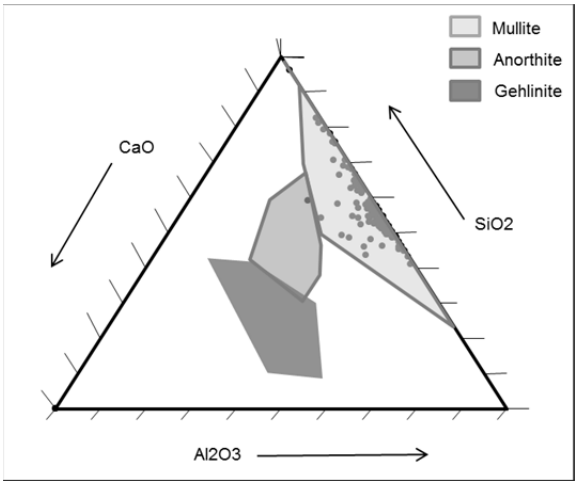

Figure 5.13: Typical Ternary Diagram #1 of Class F Fly Ash

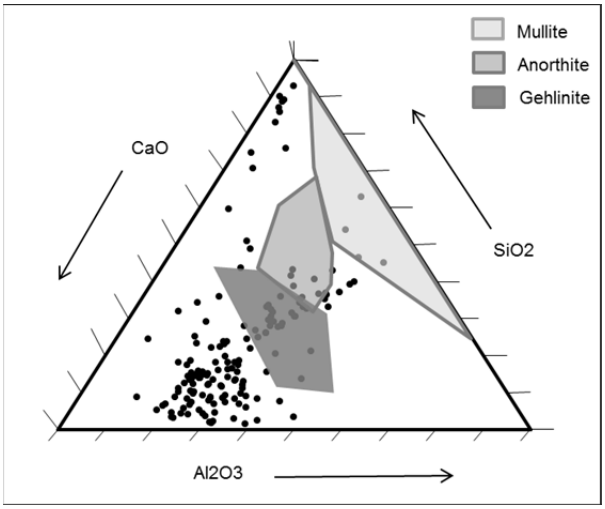

Figure 5.14: Typical Ternary Diagram #1 for Class C Fly Ash

The rest of these ternary diagrams are displayed in Appendix C. The numerical results of all the ternary diagrams are displayed in Figure 5.15. The relationship showing that higher calcium content ashes had less amorphous particles in the mullite region is shown here in the far right region of the graph. FA-9 and FA-13 had very different amounts of amorphous content in the gehlenite region; however, in the time to failure plot, the results were almost identical. It would be assumed that FA-13, which had more gehlenite amorphous content, would have more sulfate expansion. It is also interesting to note the behavior of FA-6. FA-6 had a very long time to failure, but it had mostly content in the gehlenite region. This contradicts what is expected. Looking at the XRF data for FA-6 though, this ash was classified as a Class F ash. This fly ash is an example of how plotting on the ternary diagram is not always accurate for individual fly ashes but seems to be accurate for the trend of a wide range of fly ashes. Looking at the high alkali ashes, FA-5 and FA-8, FA-8 had a greater percentage of amorphous content in the mullite region. This confirmed the sulfate expansion results presented previously that FA-8 had lower expansion than FA-5, which was not fully understood under examination of their XRF results. FA-1, FA-3, and FA-4 fully proved the argument that ashes falling in the mullite field have good sulfate resistance. These three ashes have the highest amorphous content in the mullite region and have not failed the ASTM C1012 sulfate testing to date or have the maximum time to failure of 18 months depending on the replacement percentage.

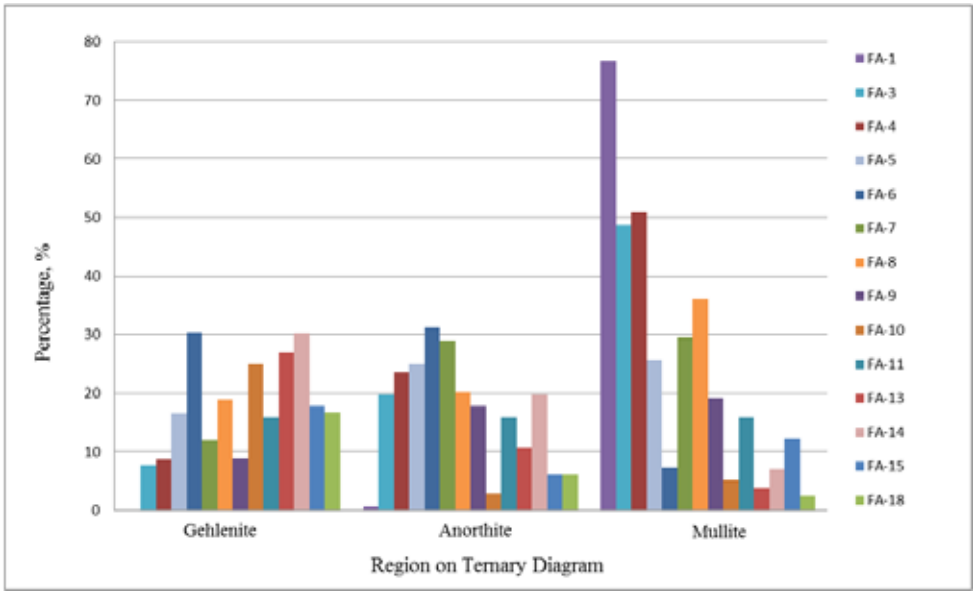

Figure 5.15: Amorphous Content on Ternary Diagram #1

FA-3 and FA-8 had a large cluster of points at the top point correlating to 100% SiO_2, shown in Figure 5.16. These ashes had a long time to failure or low expansions. Stated in literature, if the SiO_2 content is in excess of 40%, the ash will improve the sulfate resistance, and as CaO content increases, there is a shift decreasing the percentage of SiO_2 amorphous points. FA-9 and FA-11 had similar plots on diagram #1, except that FA-11 had a cluster at this 100% SiO2 apex and more content in the gehlenite region. See these diagrams in Figure 5.17. Due to this observation, FA-9 should have had better resistance; however, this was not the case. It appears this SiO_2 cluster is quite important. It seems for Class C ashes, sulfate resistance is improved if a cluster exists at 100% SiO_2.

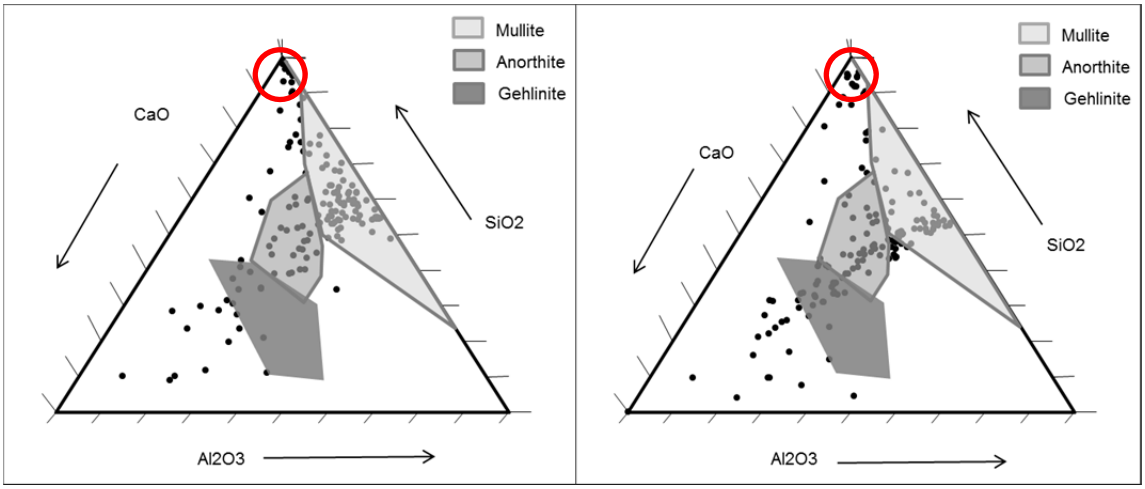

Figure 5.16: SiO_2 Clusters with FA-3 (left) and FA-8 (right)

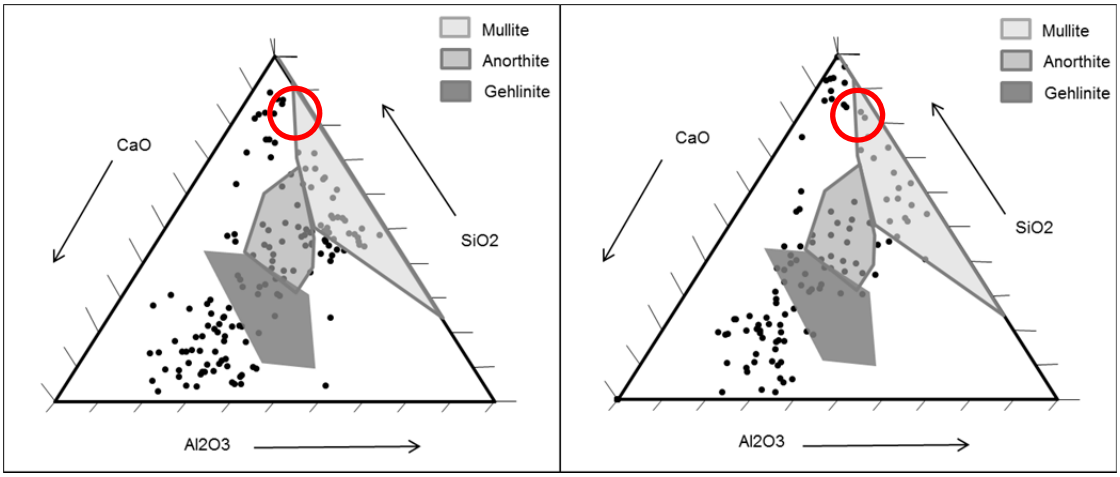

Figure 5.17: Difference in SiO_2 Clusters with FA-9 (left) and FA-11 (right)

$FeO{\cdot}Fe_2O_3$-Al_2O_3-SiO_2 Diagram

This ternary diagram was under investigation due to the argument that iron content plays a role in sulfate resistance as outlined in Section 2.3.4. An increase in iron relating to an increase in sulfate expansion was initially thought true; however, this was disproved in later research. This ternary diagram will be referred to as diagram #2. On this diagram, corundum is aluminum oxide, hematite is iron oxide, and spinel is magnetite or magnesium iron oxide with some aluminum substitutions. Again, the results presented are not the region they are plotted in but rather behave like that region.

The results of a typical Class F ash and typical Class C ash are presented in Figure 5.18 and Figure 5.19 respectively. The remaining ternary diagrams are presented in Appendix C. From solely observing this graph, there did not appear to be a trend involving iron. Analyzing the numerical results, there seemed to be a very slight linear relationship between increasing amorphous content in the spinel ss region and increasing calcium content, but this relationship did not have a high correlation coefficient. Ashes that had large amounts of spinel, such as FA-3 and FA-6, had good sulfate resistance. There existed a wider range of Al_2O_3 points plotted on this diagram; however, no correlation was found between this finding and sulfate expansion data.

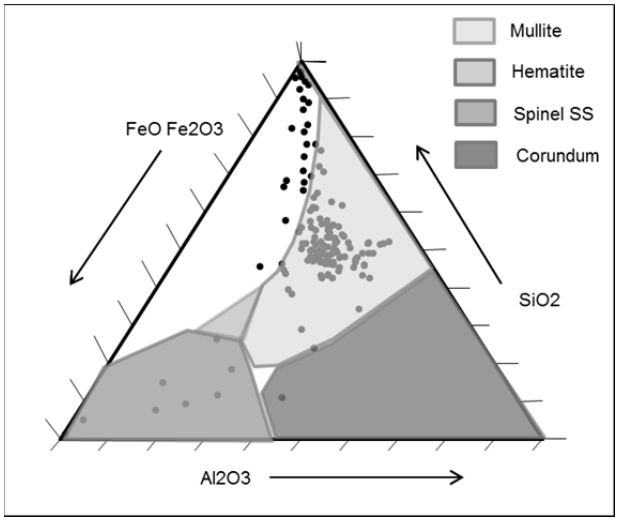

Figure 5.18: Typical Ternary Diagram #2 for Class F Fly Ash

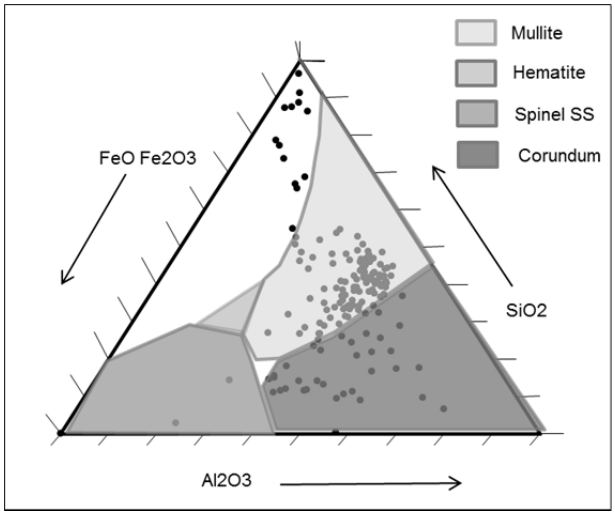

Figure 5.19: Typical Ternary Diagram #2 for Class C Fly Ash

The numerical results of the point count analysis are displayed in Figure 5.20. Again, there was a trend away from the mullite region as calcium content of the ashes increased as proved in ternary diagram #1. As for the iron content relating to sulfate performance, little amorphous content was observed even in the hematite region in this study. No correlation could be observed from the numerical analysis of hematite iron content of the glassy phases. There was an increase in corundum with increasing calcium content. This increase in corundum correlated to a decrease in silica oxide content in ternary diagram #2. A decrease in SiO_2 below 40% relates to poor resistance based on fly ash ASTM classification. This relationship between CaO and SiO_2 is also observed from XRF data shown in Appendix A in Figure A-1. FA-7 had a very high corundum content compared to the other Class F ashes, noting that FA-5 was a Class C ash because of its sum of oxide content. FA-7 also had the poorest sulfate resistance, observed by the shortest time to failure, of all of the Class F ashes as well.

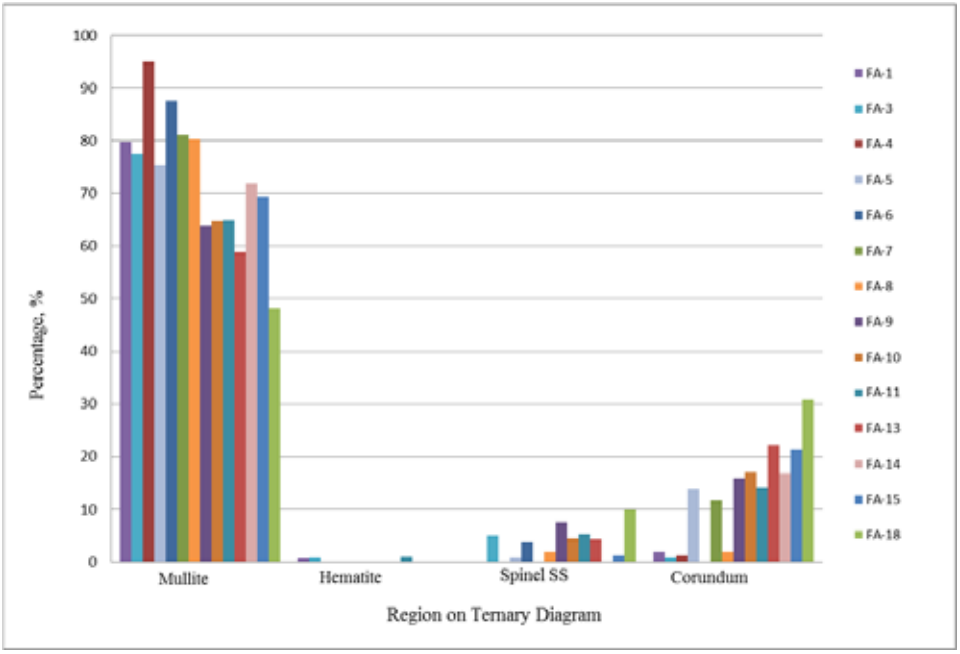

Figure 5.20: Amorphous Content on Ternary Diagram #2

FA-10 and FA-11 display the hypothesis that 100% amorphous SiO_2 helps sulfate resistance. FA-11 had a slight increase in SO_3 content, but otherwise these two ashes had very similar XRF data. FA-11 had a cluster at the 100% SiO_2 apex and improved resistance, shown in Figure 5.21. This result was more pronounced for diagram #1, however.

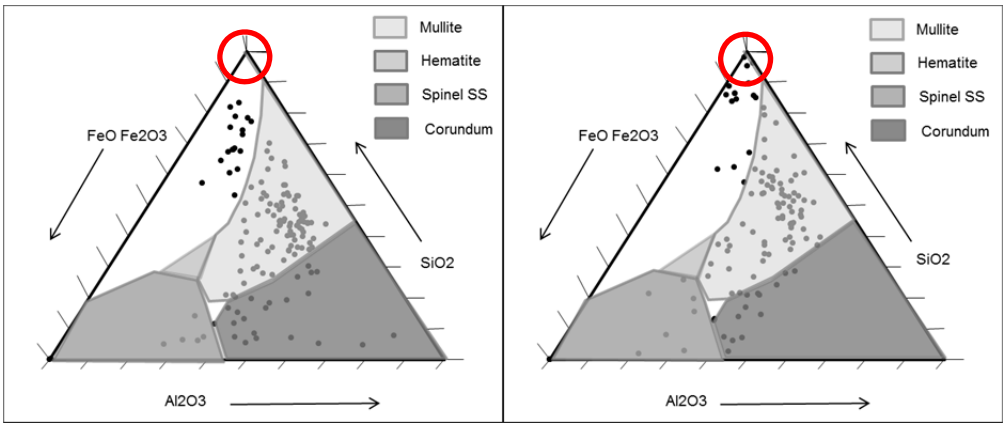

Figure 5.21: Difference in SiO_2 Clusters with FA-10 (left) and FA-11 (right)

5.4 Reactivity

5.4.1 Testing

This patent was discussed in Section 3.5, but the testing will be outlined more in depth in this section. The following procedure was performed for all 18 fly ashes under investigation. Approximately 20 g of fly ash was mixed with 250 mL of 5% tartaric acid solution. The mixture was placed over heat and boiled for 15 minutes with constant stirring. See the picture of the

boiling mixture in Figure 5.22. The container was covered and allowed to cool for 3 hours. After this cooling period, the height of gel was measured and recorded.

Figure 5.22: Boiling during Reactivity Procedure

If the fly ash was reactive, the gel height would exceed 20 mm. A reactive fly ash had high early strength, which was the purpose of identifying fly ashes for which this test was created.

5.4.2 Results

The height of gel of all fly ashes studied is presented in Figure 5.23. A control, cement C-1, was also tested and is presented in the graph. The dashed line is the limit imposed by the reactivity test patented in the 1980s; however, a new proposed limit was suggested based on the results. This proposed limit increased the gel height to 30 mm for a fly ash to be considered reactive. All of the Class C ashes were labeled as reactive if this 30 mm gel height limit was used. Therefore, if the gel height exceeded 30 mm, the ash was considered reactive and would have poor sulfate resistance.

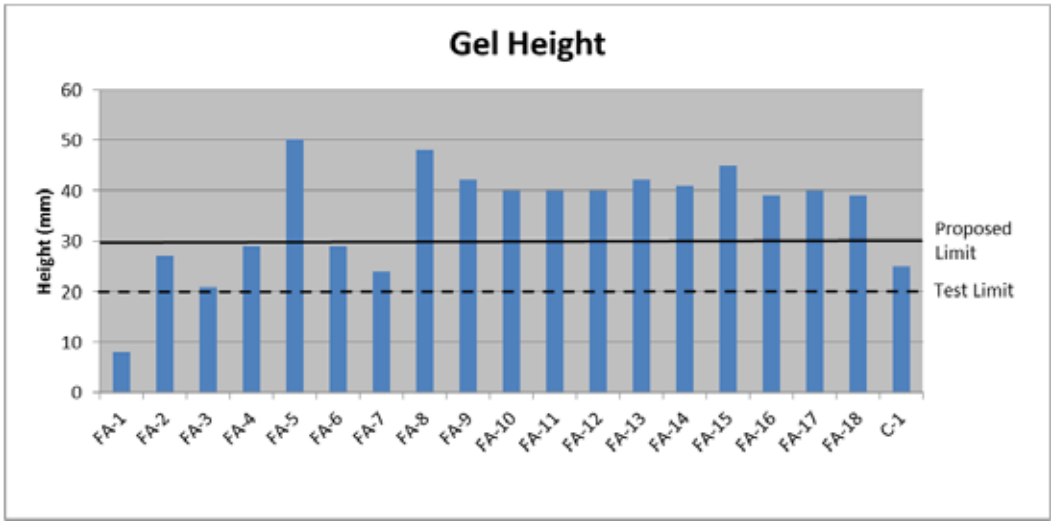

Figure 5.23: Reactivity Gel Heights

It is interesting to show the observed visual difference between gel products of the ashes. See Figure 5.24 for the relationship between a low, moderate, and a high calcium ash. FA-1 had the lowest gel height at 8.0 mm. This ash did fail but took a very long time to do so. FA-7 had the worst sulfate performance of all Class F ashes, but this fly ash did not have the highest gel height of Class F ashes.

Figure 5.24: Differences in Gel Heights of Low Calcium Ash (left), Moderate Calcium Ash (middle), and High Calcium Ash (right)

There did not appear to be a relationship between oxide values from XRF results and gel height except for SO_3 content and the alkali values. These relationships are presented in Figures 5.25 through 5.27, respectively, with increasing oxide contents on the x-axis. As SO_3 content increased, the gel height increased. Adding SO_3 will react and cause an expansion, which was observed here. As Na_2O content increased, the gel height increased greater than the proposed limit. As K_2O content increased though, the gel height decreased. When the equivalent alkali content was plotted though, not shown in this report, there did not appear to be a relationship. All of the ashes that had gel height under the proposed limit in these three figures, except for FA-6 and FA-7, had ASTM C1012 measurement bars that had not yet failed to date. All of these fly ashes were also classified as Class F ashes. Therefore this proposed height limit of 30 mm accurately predicted sulfate performance.

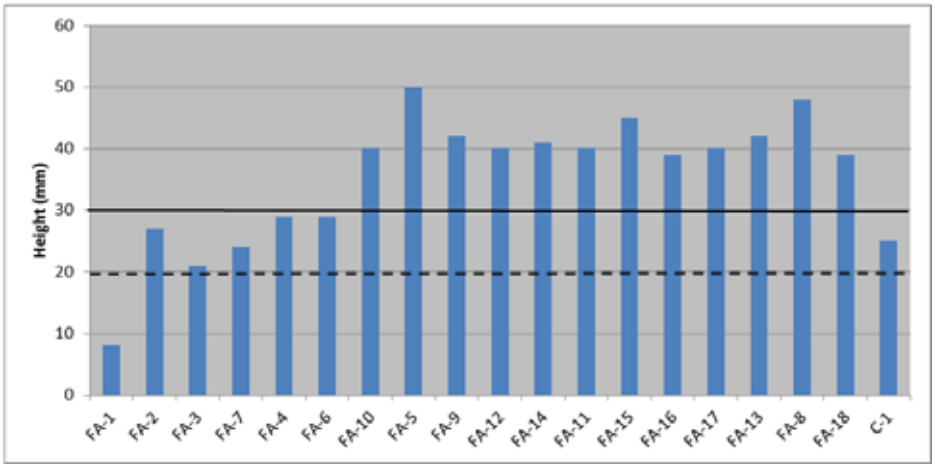

Figure 5.25: Relationship between SO_3 and Gel height

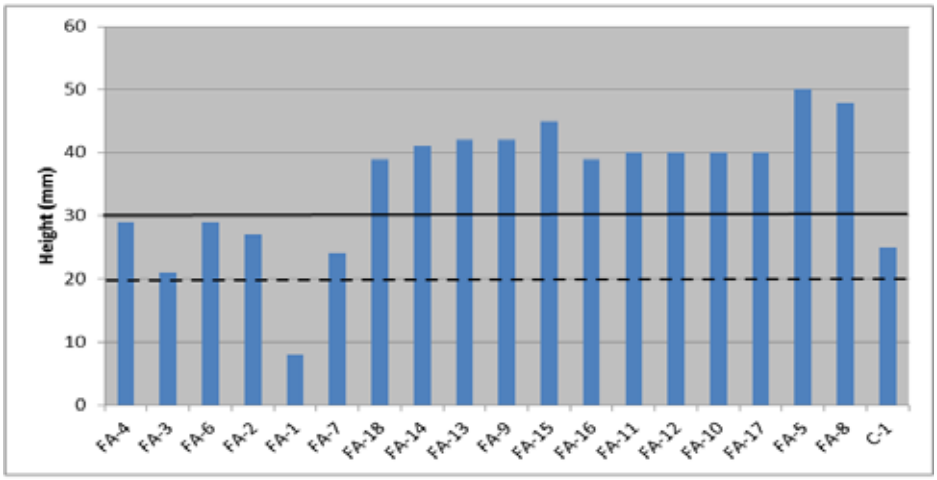

Figure 5.26: Relationship between Na_2O and Gel Height

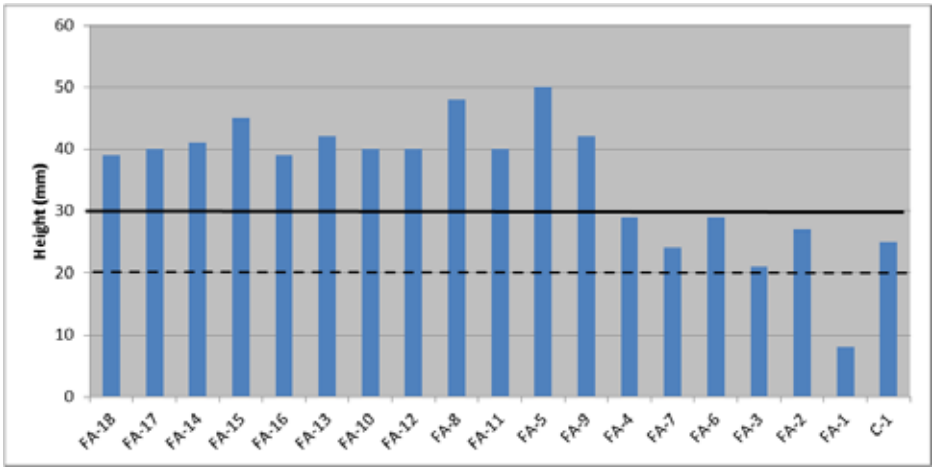

Figure 5.27: Relationship between K_2O and Gel Height

Chapter 6. Paste/Mortar Performance

Chapter 6 contains testing results that describe the interaction of fly ash with cement during hydration.

6.1 Heat of Hydration

6.1.1 Testing

As discussed in Section 3.6, the heat of hydration was measured using an isothermal calorimeter. All 18 fly ashes were analyzed at 20%, 30%, and 40% replacement percentages at temperatures of 5°C, 23°C, and 38°C. These three different temperatures were used to mimic field performance in cold, moderate, and hot environments.

Three key items were used from calorimeter studies: heat of hydration graphs, cumulative heat graphs, and activation energy. The information obtained from the heat of hydration graphs were time and heat at the maximum peak, slope of the ascending line, and total heat generated. A cumulative heat graph was also useful for strength development. Activation energy was calculated to determine the amount of heat needed to start the reaction.

6.1.2 Results

All of the fly ashes studied showed the same general behavior on heat flow graphs. A heat flow graph showing the relationship between fly ash replacement percentages is displayed in Figure 6.1. As the replacement percentage increased, the total heat released decreased and the peak became narrower. Figure 6.2 shows the relationship between temperature and heat flow. As the temperature increased, the reaction proceeded at a faster rate, and the curve shifted to the left. The colder temperatures delayed the hydration reaction.

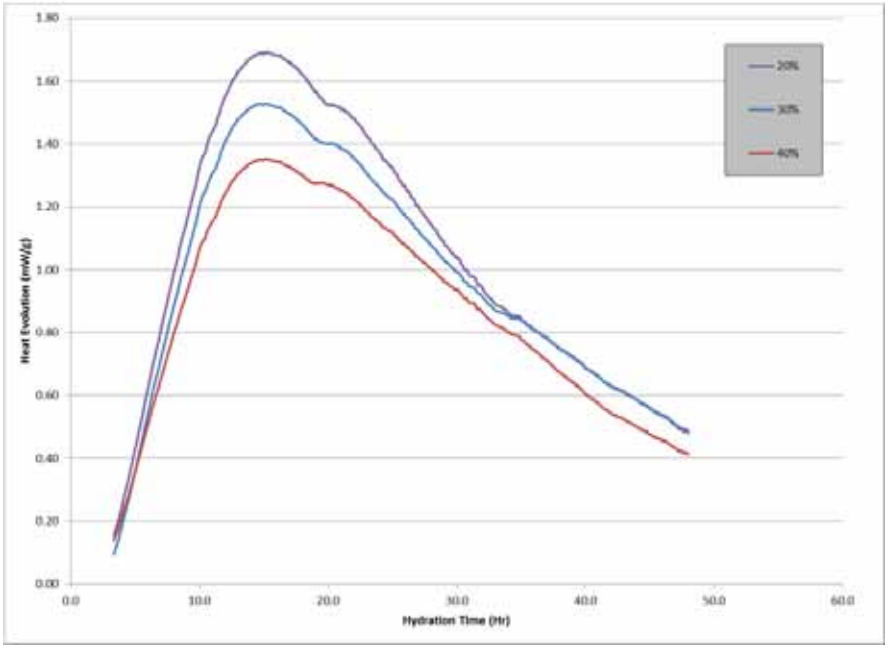

Figure 6.1: Typical Heat Flow Graph with Fly Ash Replacement Percentages

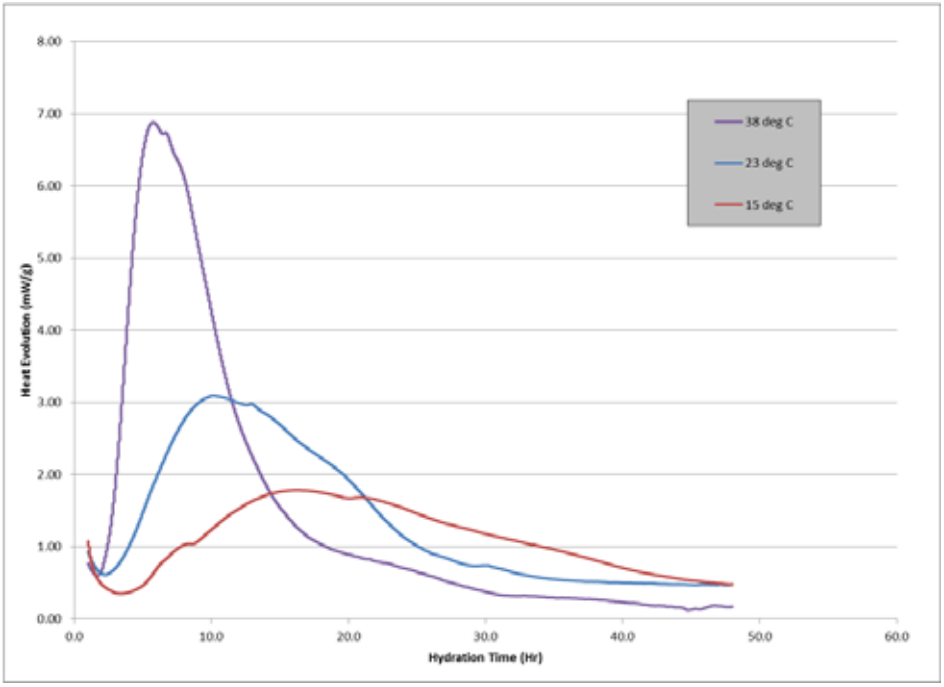

Figure 6.2: Typical Heat Flow Graph with Temperature Variations

The time of maximum peak was roughly the same for fly ash with similar calcium oxide contents at all replacement percentages for a given temperature. The results at 23°C are displayed in Figure 6.3. This time related to the length of the dormant period identified in Chapter 2. Note the Class C ashes had increased times over Class F ashes for lower temperatures. Past research demonstrated that a longer dormant period results in improved sulfate resistance, but this was not observed here. As the temperature increased, the time to the maximum peak decreased. See this relationship in Figure 6.4.

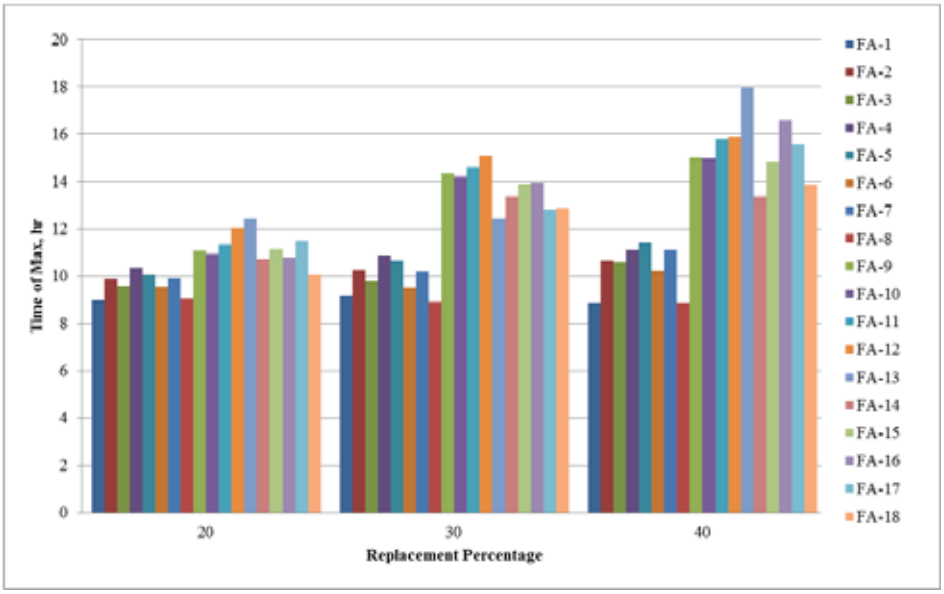

Figure 6.3: Time of Maximum Peak at 23°C

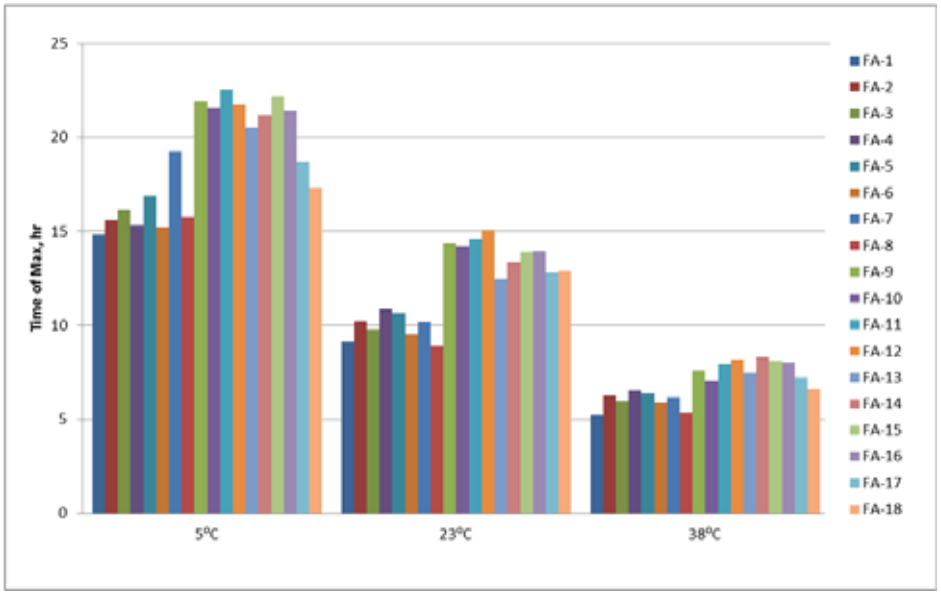

Figure 6.4: Time of Maximum Peak at 30% Fly Ash Replacement

The heat flow at this location of maximum peak was affected by the temperature. See this relationship in Figure 6.5. This graph was typical for all replacement percentages studied. The heat flow increased with rising temperature, but not with the class of the fly ash. FA-8 had the greatest heat flow at the maximum peak. FA-8 had good sulfate resistance due to ASTM C1012 specimens having either not yet failed or a long time to failure. This ash is one of high alkali; however, the other high alkali fly ash, FA-5, did not have high heat flow at the maximum peak. The heat flow at the maximum peak was greater for high calcium ashes than lower calcium ashes for ash replacement of 40%.

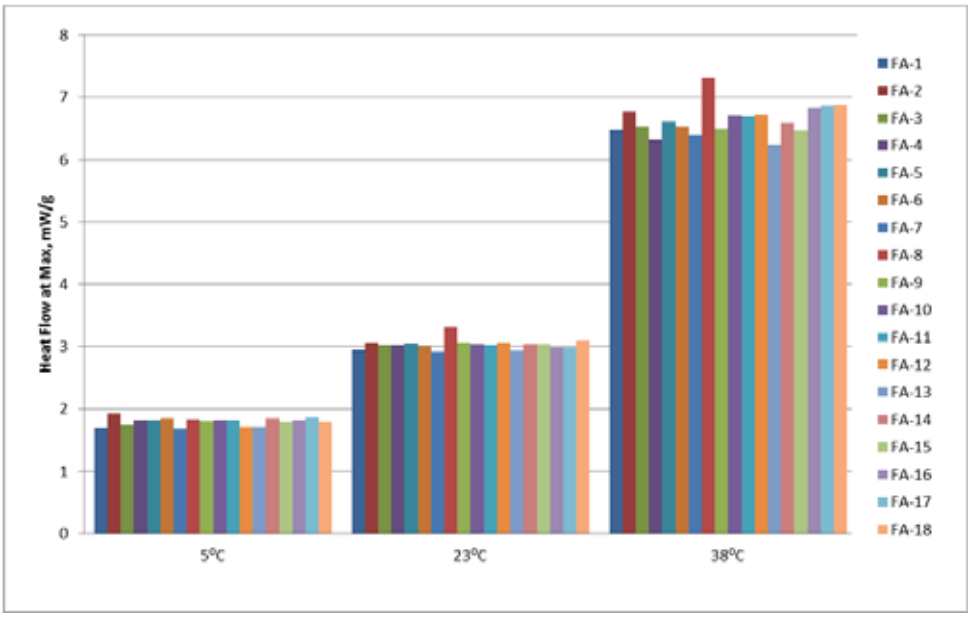

Figure 6.5: Heat Flow at Maximum Peak for 20% Fly Ash Replacement

The ascending slope of the heat flow plot, see Figure 6.2, was important in total heat generated during this reaction. As the slope increased, the peak became narrower, but the peak also increased as shown again in Figure 6.2. The slope increased with an increase in temperature but did not change with replacement percentage at equal temperatures. This narrowing but higher curve related in roughly equal total cumulative heat generated for all fly ashes at all replacement percentages. Refer to Figure 6.6 for this relationship. At higher temperatures, there seemed to be a slight increase in total generated heat for the higher calcium ashes.

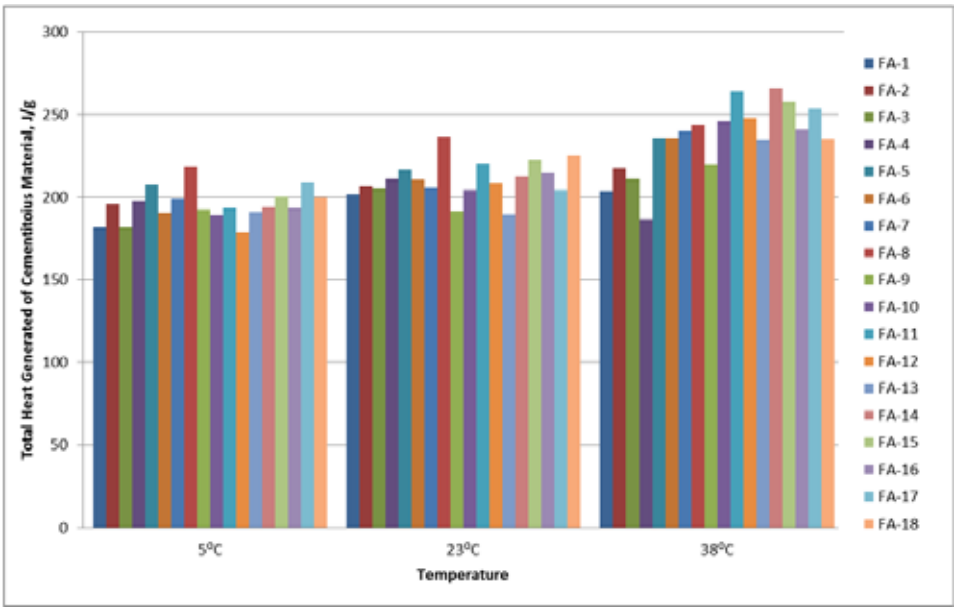

Figure 6.6: Total Heat Generated due to Cementitious Material

Activation energy did not seem to vary between all fly ashes under investigation until a later time of hydration, 48 hours for example. It is at this later hydration age that trends developed. Notice in Figure 6.7 the behavior of replacement percentage on a Class F fly ash. There was not a significant difference between the activation energies at the lower times of hydration; however, at the higher times, an increase in replacement percentage resulted in a lower activation energy. See the opposite effect for Class C ashes in Figure 6.8. The trend showing an increase in ash replacement percentage resulting in higher activation energies was not observed until later hydration ages. Activation energy values at early hydration ages were comparable for Class F and Class C ashes. Class C ashes had greater activation energy values than Class F ashes for the three replacement percentages at later stages of hydration. See this general trend in Figure 6.9.

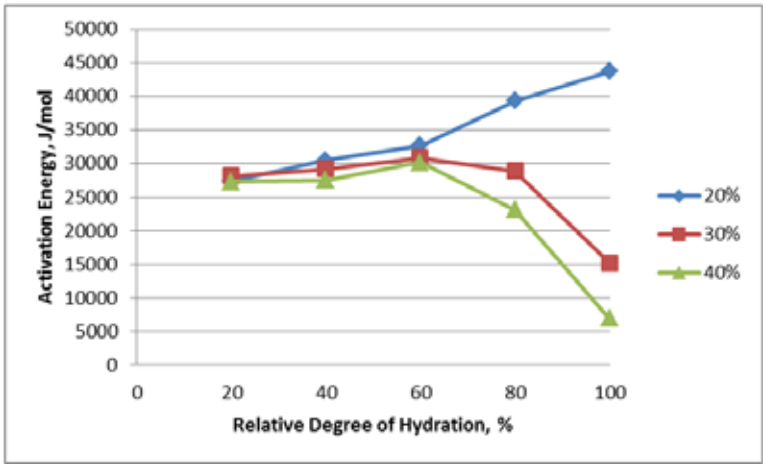

Figure 6.7: Typical Class F Ash Activation Energy vs. Time Plot

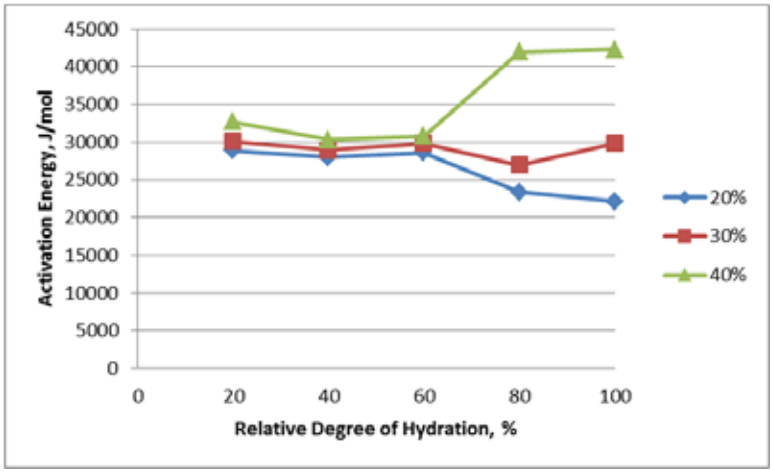

Figure 6.8: Typical Class C Ash Activation Energy vs. Time Plot

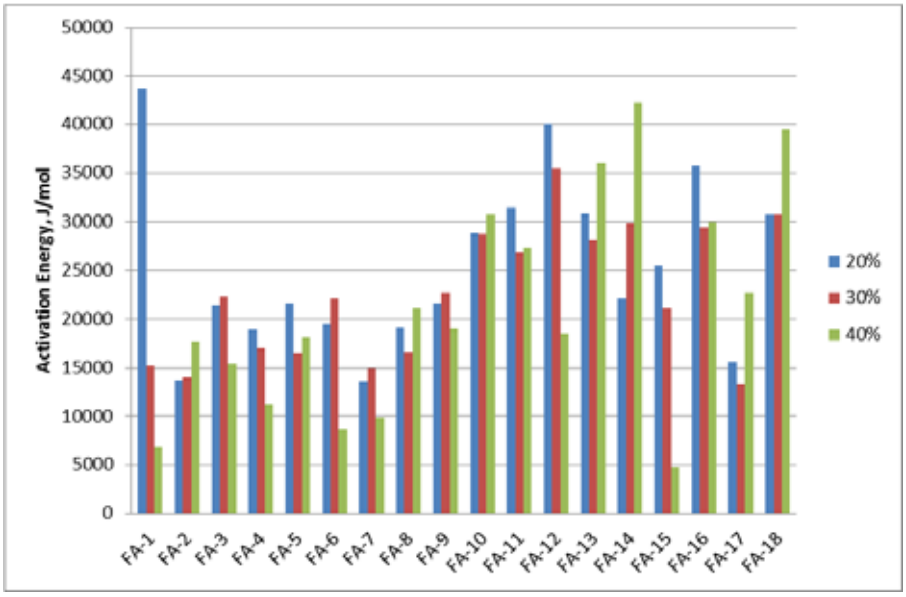

Figure 6.9: 48 Hour Hydration Activation Energy Values

The following graphs in Figure 6.10 show the relationship between XRF oxide values in ascending amounts on the x-axis with activation energies at 48 hours of hydration on the y-axis.

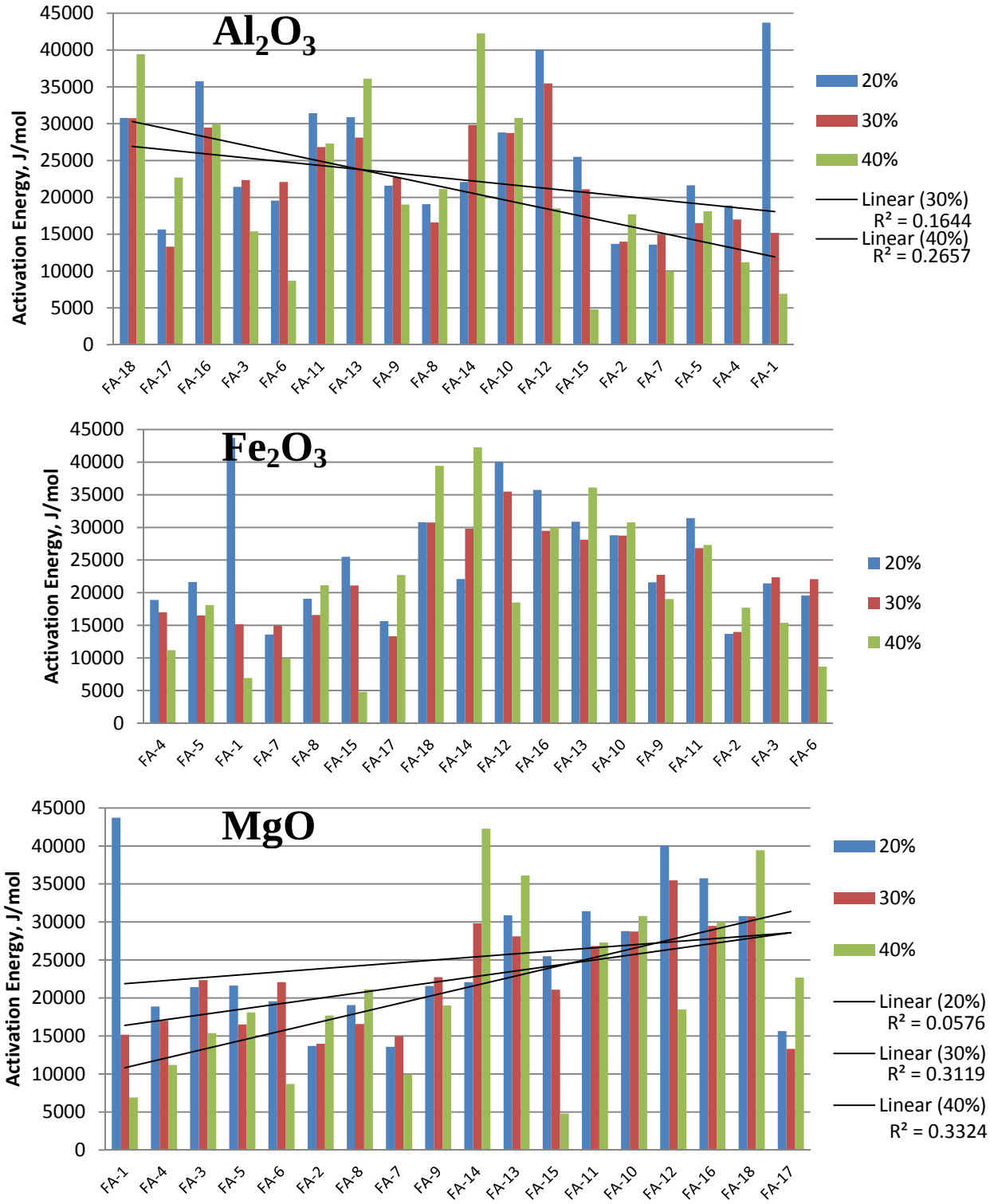

Figure 6.10: XRF Oxides versus Activation Energy at 48 hr Hydration Time

In comparing the activation energies of different replacement percentages of all fly ashes to XRF values in Figure 6.10, some trends were observed:

- Al_2O_3: An increase in Al_2O_3 corresponded with a decrease in activation energy, and this was more drastic as the replacement percentage increased. The ashes with lowest Al_2O_3 content did not have the greatest expansions.
- Fe_2O_3: The highest activation energies corresponded to the medium Fe_2O_3 values. Most of the mid-range Fe_3O_2 ashes had the highest sulfate expansions.
- CaO: The strongest correlation was the linear relationship between calcium content and activation energy shown in Figure 6.9. The highest calcium ashes had the poorest sulfate resistance.
- MgO: An increase in MgO content yielded a higher activation energy. This trend was better fit for the higher replacement percentages. This trend also held true for SO_3. Ashes with greater MgO and SO_3 contents did not necessarily have the greatest expansions.

Another interesting item noted included FA-1. This ash seemed to have very large values compared to the other Class F ashes, reference Figure 6.9. XRF values revealed this ash had the lowest calcium content and the highest sum of oxide percentage by a wide margin. From the sulfate testing results, this ash had the longest times to failure.

In general, for the factors of interest from heat flow graphs, the most important indicator of sulfate resistance seemed to be the time to the maximum peak. This correlated to the length of the dormant period or the reactivity of the ash. The more C_3A and calcium content of the ashes, the more reactive they were; this corresponded to the Class C ashes which had a shorter time to failure in sulfate environments. This finding is contradictory to the findings published in literature. The higher activation energies tended to correspond to poor sulfate resistance. Class C ashes had greater activation energies than Class F ashes and the worst sulfate performance. At the longer hydration ages, an increase in replacement percentage resulted in lower activation energies for Class F ashes; the opposite effect happened for Class C ashes.

6.2 Microstructural Development

6.2.1 Testing

This testing section aimed to characterize sulfate resistance with the formation of hydration products over time. This study was performed on two machines. A Grace isothermal calorimeter was used to measure heat flow until a predetermined hydration age was reached. The samples were then removed and placed in acetone to stop hydration for 48 hours and ground for analysis in the XRD machine. Rietveld analysis was performed on these samples to identify hydration products. All samples were run at 23°C, and the times of interest were 30 min, 1 hour, 2 hours, 4 hours, 8 hours, 24 hours, and 48 hours. Two replacement percentages of fly ash, 20% and 40%, were used. The XRD machine parameters used were a scan range of 5° to 70° 2θ degrees, step 0.02, and 4 sec dwell was employed for an average scan of 3.5 hours. The main products under investigation were portlandite, ettringite, monosulfate, and C_3A. This analysis was performed only on 7 of the 18 fly ashes. Cement C-2 was used in this testing regime.

6.2.2 Results

The same trends for the calorimeter heat flow data as presented in the previous section apply to this data. This section will only present the XRD data related to the hydration products.

Portlandite, or calcium hydroxide, was the primary phase attacked by sulfates. This phase was used during the pozzolanic reaction with fly ash to convert into beneficial calcium silica hydrate phases. The excess calcium was used in this reaction and led to ettringite formation. Portlandite was not detected at significant levels until 24 hours later for all ashes and continued to form at 48 hours. There were slightly higher amounts in the lower calcium ashes, especially at higher replacement percentages, see Figure 6.11. It was observed that the amount of portlandite formed would increase up to 28 days of hydration and then be used in the pozzolanic reaction, which would not be fully observed at normal fly ash replacement levels until around 90 days of hydration (Jozic, Zelic, & Janjatovic, 2010). The effect of portlandite on sulfate resistance could not be determined from this short hydration age.

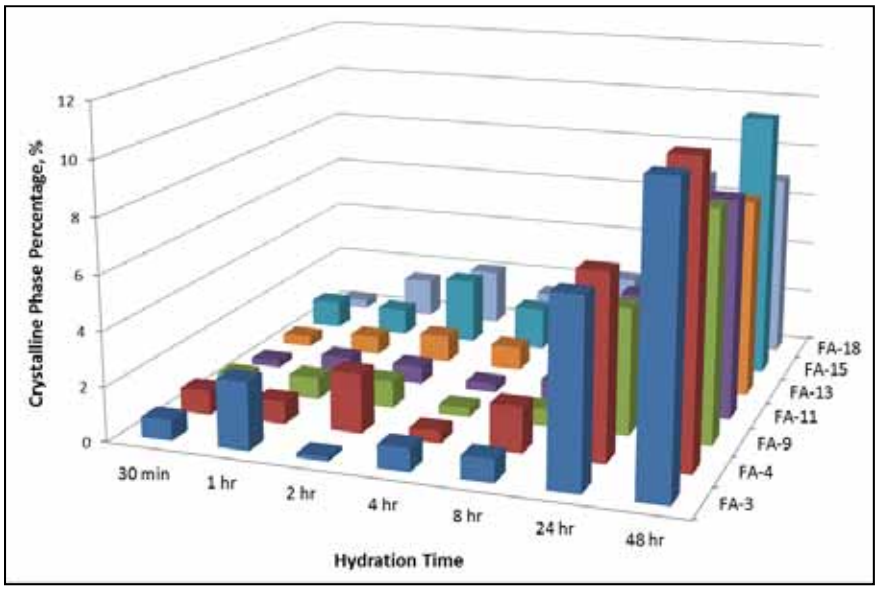

Figure 6.11: Portlandite Formation at 40% Fly Ash Replacement

The percentage of ettringite present increased with the hydration age. In general, as the calcium content increased, the amount of ettringite formed increased as well. There was also a decrease in ettringite as replacement percentage increased. See Figure 6.12 for the relationship between a Class F ash, FA-4, and a Class C ash, FA-18, and different replacement percentages. The higher calcium ash produced more ettringite at both replacement percentages for most of the hydration times under investigation. Figure 6.13 and Figure 6.14 show the ettringite formation over hydration time for all ashes studied. Note that most ettringite was formed from FA-15 and FA-18; however, FA-9 had a large amount at 20% replacement at 48 hours. FA-9 had a relatively short time to failure compared to FA-11 and FA-13, which had lower amounts of ettringite formation. It is interesting to note that at 40% ash replacement the amount of ettringite produced with FA-9 was 50% less, and the time to failure at 40% replacement lengthened by 3 months. There was a correlation between amount of ettringite produced and time to failure related to sulfate expansions: an increase in ettringite resulted in shorter time to failure.

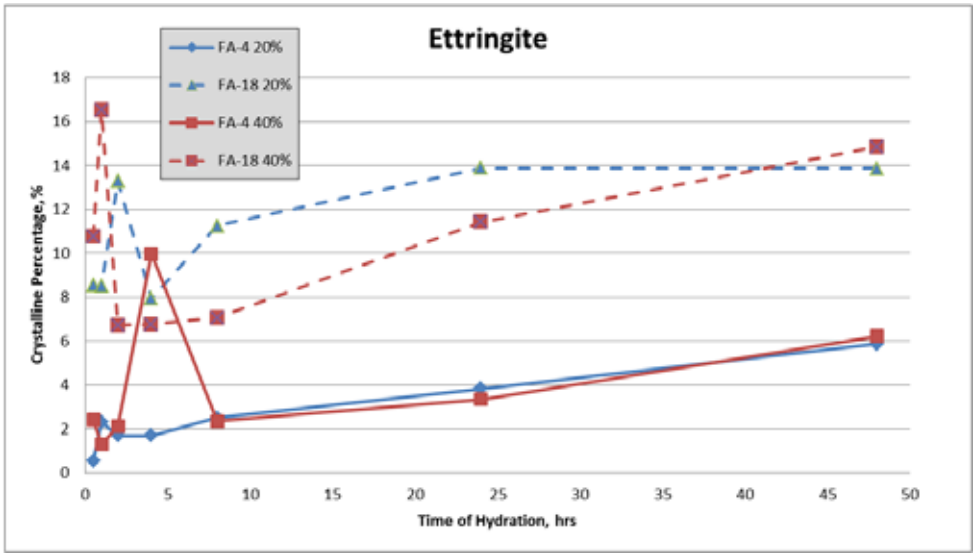

Figure 6.12: Ettringite Formation during Hydration of Two Fly Ashes

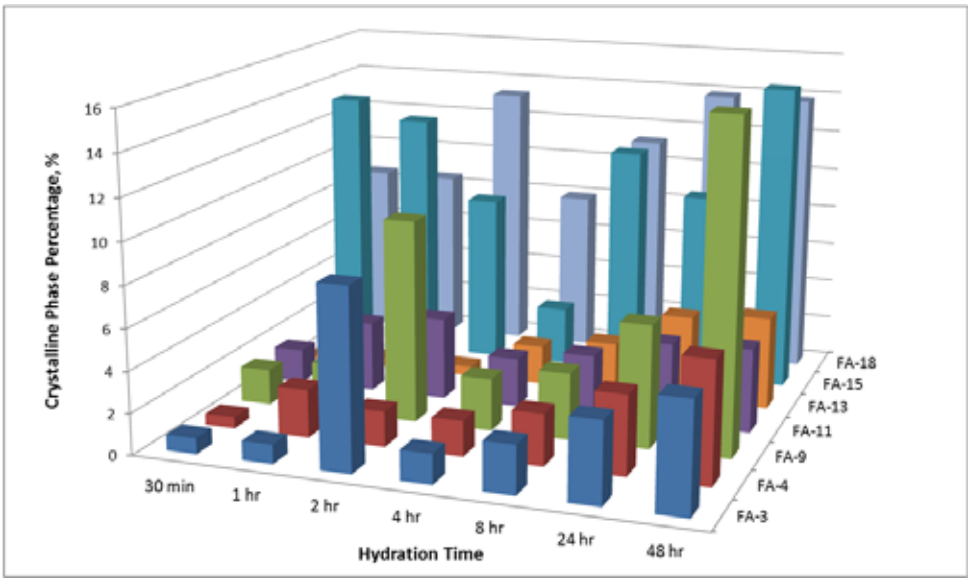

Figure 6.13: Ettringite Formation at 20% Fly Ash Replacement

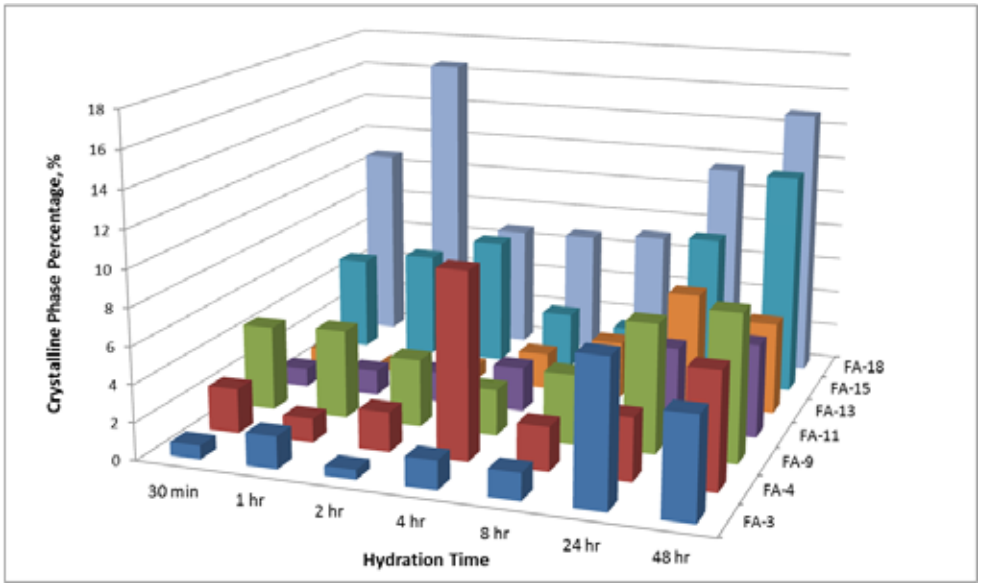

Figure 6.14: Ettringite Formation at 40% Fly Ash Replacement

Gypsum was another phase present during hydration. The formation of gypsum was another mechanism of sulfate attack; however, rather than causing expansion, it led to a loss of strength and cohesion. Anhydrite hydrated to gypsum as hydration continued; however, this process could take 30 days (Ubbriaco, Bruno, Traini, & Calabrese, 2001). In this study, the amount of gypsum identified was small, around 2-3% of crystalline phases. As hydration continued, the amount of gypsum decreased for both replacement percentages to almost negligible levels. See the higher levels at 48 hours for FA-3 and FA-13 in Figure 6.15. These two ashes had similar time to failure lengths, but ashes with lower amounts of gypsum at 48 hours had varying sulfate performance. Due to this finding, there did not appear to be a relationship between gypsum and sulfate expansion up to 48 hours of hydration evaluated in this study.

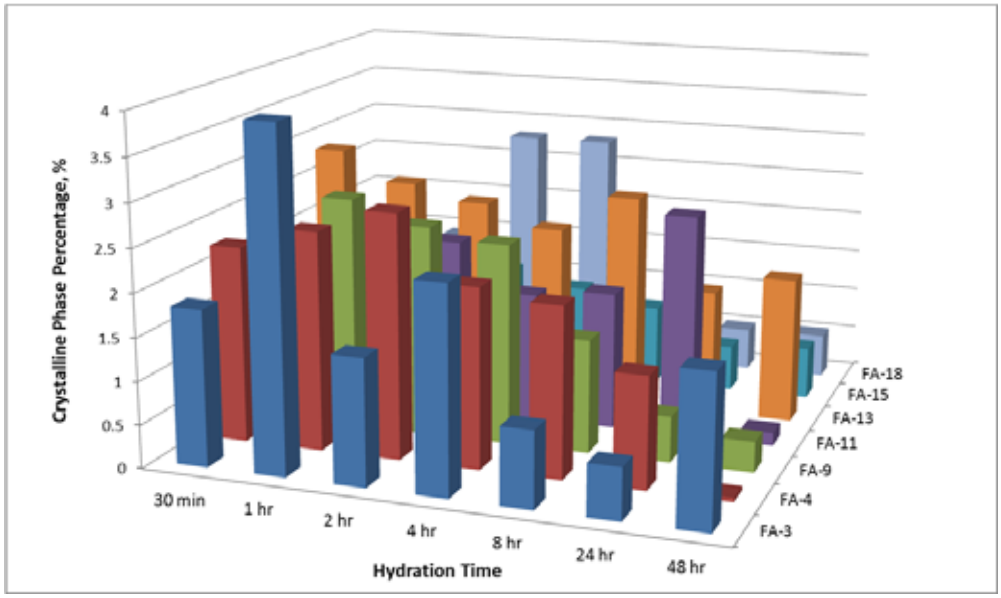

Figure 6.15: Gypsum Formation at 40% Fly Ash Replacement

Gypsum and ettringite formation is related due to setting and hardening of the fly ash-cement paste. Gypsum will form initially during hydration and then dissolve to form ettringite. This relationship is observed in the data previously presented. Gypsum content decreases as hydration continues, and ettringite content increases with aging hydration. The more ettringite that forms, the more strength gained. This is the mechanism responsible for higher calcium ashes having early strength gain than lower calcium fly ashes. This ettringite formation also leads to reduced sulfate resistance.

C_3A is the reactive aluminate component responsible for the expansions due to ettringite formation. C_3A content slightly decreased as hydration continued; however, the Class C ashes had much greater levels of C_3A at 48 hours than the Class F ashes. See Figure 6.16 for this relationship. The higher calcium ashes had worse sulfate resistance than Class F ashes, demonstrated by the C_3A formation during hydration.

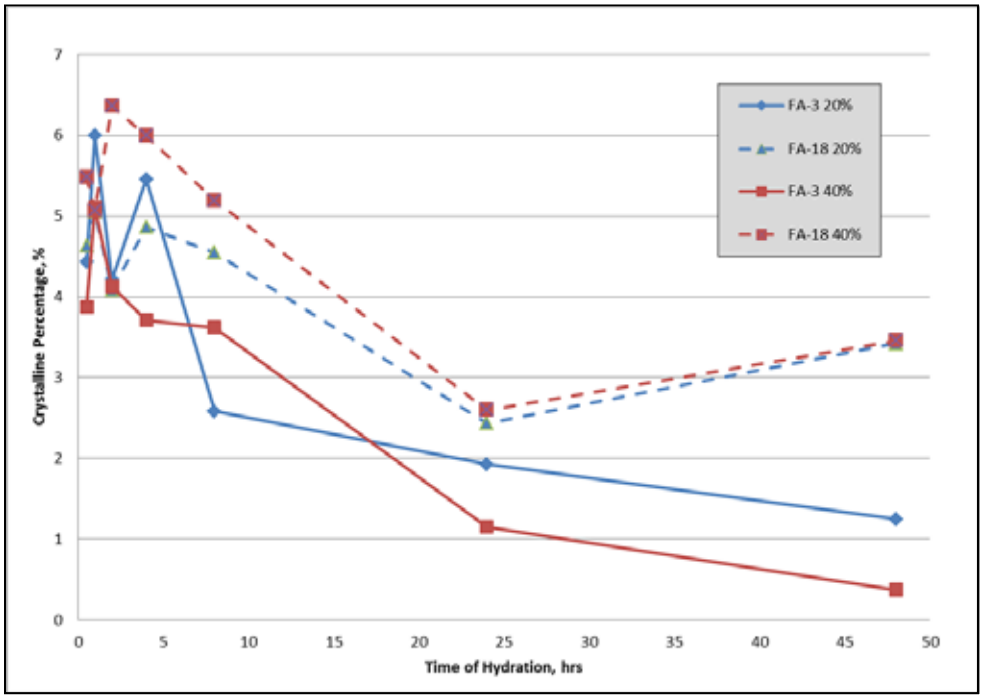

Figure 6.16: C_3A Formation at 40% Fly Ash Replacement

No monosulfate was observed in any fly ash up to 48 hours of hydration. The only trends observed were a function of calcium content of the ashes, which was also an inverse relationship with silica and potassium oxide values as well.

6.3 Sulfate Immersion

6.3.1 Testing

This testing was first conducted at the University of New Brunswick and will be repeated in this study in the same manner. A control of C-2 and 7 fly ashes were used in this study. The ashes used were FA-3, FA-4, FA-8, FA-11, FA-13, FA-15, and FA-18. A 150 g sample of fly ash was mixed with 100 g of calcium hydroxide. These dry materials were hand mixed until a uniform color was obtained. An alkaline solution was made consisting of 0.15 M NaOH and 0.35

M KOH, and 112.50 mL of this solution was added to the dry material mixture resulting in a w/c ratio of 0.45. This mixture was hand mixed for roughly 20 minutes when all materials were moved into a plastic container, sealed, and cured over water at 38°C for 28 days. After this part was complete, the samples were removed from the plastic container. Samples were crushed into pieces and further ground until 50–75 g passed a No. 200 sieve. About 2 g of this finely ground sample was set aside for XRD analysis, and the remaining finely ground sample was kept for sulfate immersion.

Of the finely ground remaining sample, 15 g was immersed in sulfate solution. Two different sulfate solutions of calcium and sodium sulfate each at 5% were used for this test. The 15 g sample was mixed with 300 mL of each sulfate solution in a plastic bottle and sealed. All of the samples were continuously rotated on a mechanical rolling machine for 15 days. During the first month, the sodium sulfate solutions were changed weekly and then every 2 weeks thereafter, measuring the pH of the solutions at these times. This was done to control the pH of the solution to reduce the possibility that the reaction could reach equilibrium. The calcium sulfate solutions were not changed. To change the solution, the paste was filtered out of the sulfate solution. Then 300 mL of the sodium sulfate solution was added to the paste in a plastic bottle and resealed. The samples were immersed in these two sulfate solutions for 90 days. At the end of immersion, the bottles were vigorously shaken and the paste was filtered, washed with ethanol, and dried until a constant mass was obtained. A few grams were used for XRD analysis. For the pre- and post-sulfate immersion XRD, zincite was used as the internal standard. The scan parameters were a range of 5° to 70° 2θ degrees, step 0.02, 4 sec dwell. The average scan time was 3.5 hours per sample.

The study at the University of New Brunswick included a SEM and point count EDS analysis of mortar bars used in ASTM C1012 solution to study the effects of exposure to sulfate solution on CaO and SiO_2 content. This analysis was not conducted in this study due to time constraints.

6.3.2 Results

Pre-Sulfate Immersion

The pre-sulfate immersion XRD results are presented in Table 6.1. The specimens had been curing for 28 days over water. The phases of interest were monosulfate, ettringite, and portlandite.

Table 6.1: Pre-Sulfate Immersion Phase Amounts

FA-ID	Monosulfate	Ettringite	Portlandite
C-2	0.500	2.584	47.450
FA-3	0.025	10.847	25.720
FA-4	0.292	4.589	22.393
FA-9	0.133	0.682	19.608
FA-11	0.786	1.445	16.415
FA-13	0.070	2.108	21.610
FA-15	0.011	2.580	20.670
FA-18	0.467	3.987	25.966

On average, the Class F ashes, FA-3 and FA-4 had less monosulfate than Class C ashes and more ettringite after 28 days of curing. According to Mehta, if ettringite was formed initially, the phase would be stable and not cause expansion. If monosulfate was formed, though, it would convert over time to form ettringite and would cause expansions (Mehta, 1986). These statements confirm the findings presented in Table 6.1. The Class C ashes, which had poor sulfate resistance, had more monosulfate formed prior to sulfate immersion, and the Class F ashes, which had good sulfate resistance, formed more ettringite initially.

The reference cement had a large amount of portlandite. The fly ash samples had significantly less portlandite after 28 days of curing. This suggests that the portlandite was consumed during fly ash reactions in this period of time, which was also observed by Raj Dhole in his work (Dhole, 2008). The Class F ashes in this study consumed more portlandite on average than the Class C ashes. The Class F ashes are more pozzolanic fly ashes and would consume portlandite (CH) in the pozzolanic reaction.

Post-Sulfate Immersion

The hydration product intensities formed during the sodium and calcium sulfate immersion were very different. See this relationship between FA-4 and FA-18 in Figure 6-17 and Figure 6-18, respectively. The numerical results from the post-sulfate immersion studies are presented in Table 6-2.

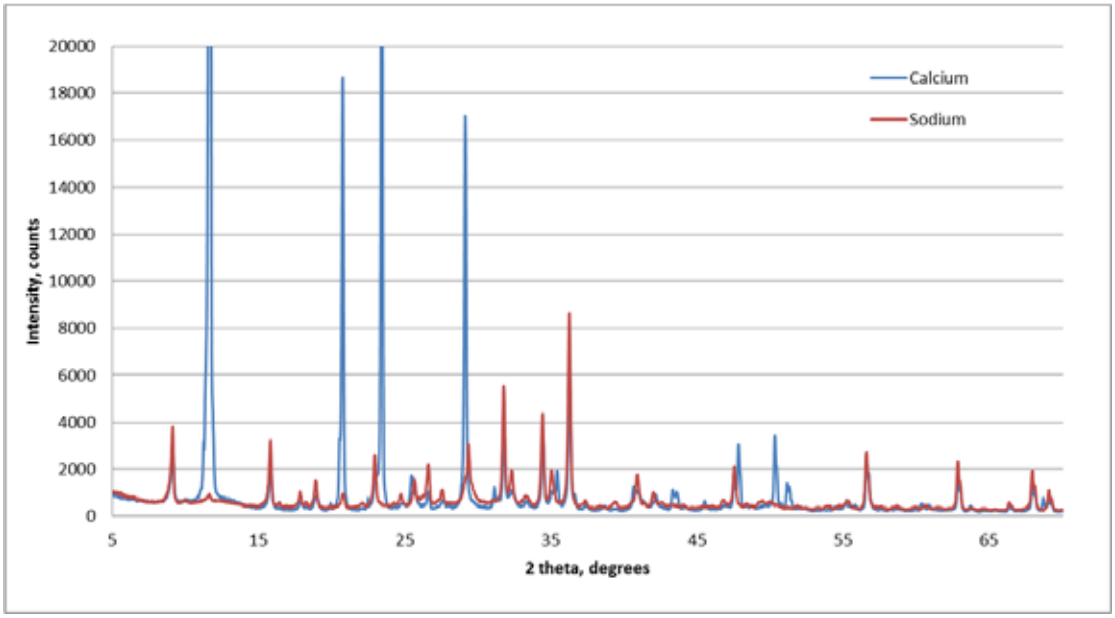

Figure 6.17: Comparison of Post-Sulfate Solution RQXRD of FA-4

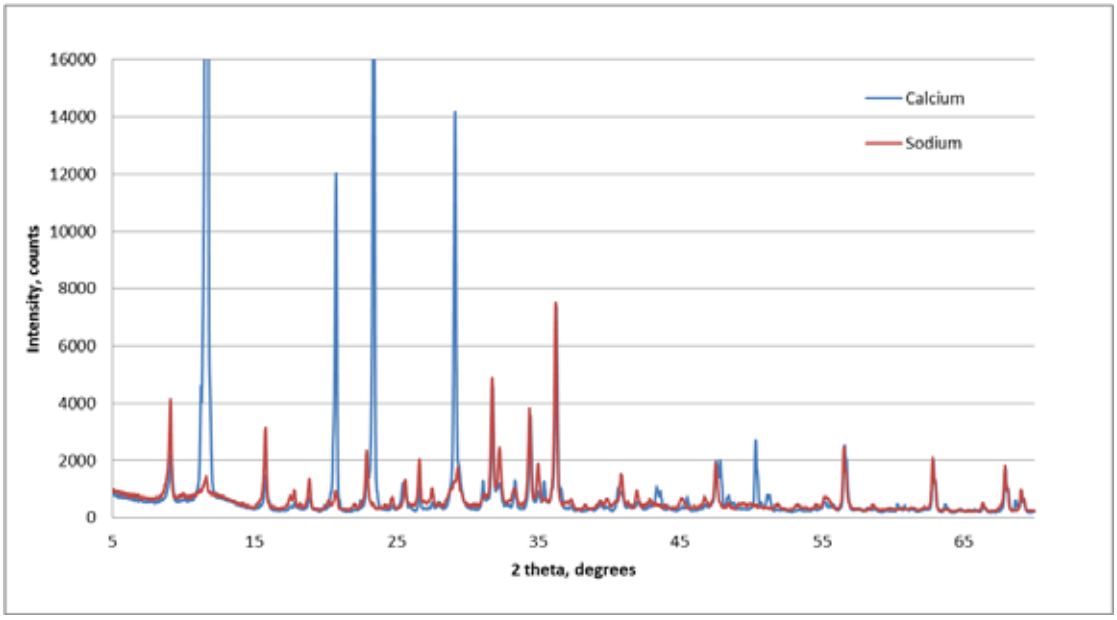

Figure 6.18: Comparison of Post-Sulfate Solution RQXRD of FA-18

Table 1: Post-Sulfate Immersion Phase Amounts

FA-ID	FA Source	Sulfate Solution	Gypsum	Ettringite	Portlandite
C-2	Alamo	5% Sodium	14.89	9.21	22.43
		5% Calcium	22.60	5.22	23.28
FA-3	LEGS	5% Sodium	25.51	25.59	0.42
		5% Calcium	67.23	17.03	0.73
FA-4	Rockdale	5% Sodium	19.11	28.30	0.59
		5% Calcium	71.72	24.11	0.07
FA-9	Harington	5% Sodium	9.53	27.38	0.61
		5% Calcium	68.58	17.15	0.73
FA-11	Tolk	5% Sodium	13.33	21.44	0.40
		5% Calcium	70.58	15.49	0.78
FA-13	Parish	5% Sodium	5.44	28.78	0.42
		5% Calcium	70.61	19.26	0.71
FA-15	Deely	5% Sodium	7.30	23.70	0.85
		5% Calcium	69.83	17.33	0.27
FA-18	Welsh	5% Sodium	8.11	25.37	0.26
		5% Calcium	73.25	15.00	0.27

The ashes immersed in the calcium sulfate solution formed substantialy more gypsum than those ashes immersed in the sodium sulfate soltuions. As noted in Dhole's dissertation, this gypsum formation was not solely from reactions with sulfate solutions (Dhole, 2008). More ettringite was produced for ashes submersed in sodium sulfate solutions. No monosulfate was identified in any of the samples for either solution.

The relationships between hydration product content and cakium oxide content of the ashes are presented in **Error! Reference source not found.**9 and **Error! Reference source not found.** for 5% calcium sulfate and 5% sodium sulfate soltuions. There did not appear to be a relationship between ettringite formation and calcium content of the ashes for either sulfate solution. This is contradictory to what would be assumed and Dhole's findings. A larger amount of ettringite at a later age, significantly after final set and curing, could potentially cause severe cracking and poor sulfate resistance. This expected result was confirmed in Dhole's disseration, so repeat testing is recommended for a comprehensive analysis. This relationship is highlighted in **Error! Reference source not found.**6-21. **Error! Reference source not found.**9 above shows an increase in gypsum formation for higher calcium ashes immersed in a calcium sulfate solution. This increase in gypsum may have been produced from the sulfate solution rather than the fly ashes (Dhole, 2008). The amount of portlandite identified was very small compared to the other products of interest. Most likely, the portlandite was consumed in the pozzolanic reactions. On average, the amount of portlandite identified was greater for Class C ashes than Class F ashes because they are less pozzolanic.

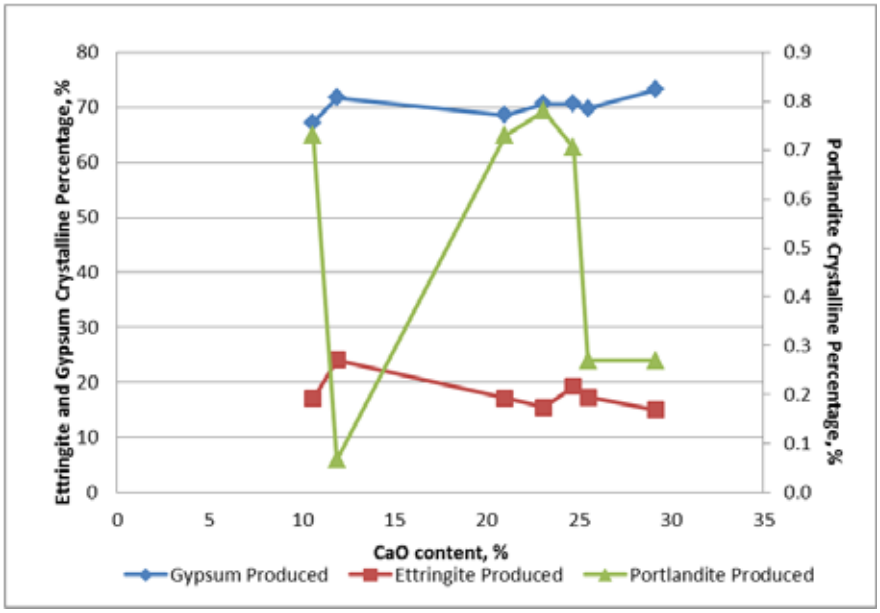

Figure 6.19: Hydration Products from 5% Calcium Sulfate Immersion

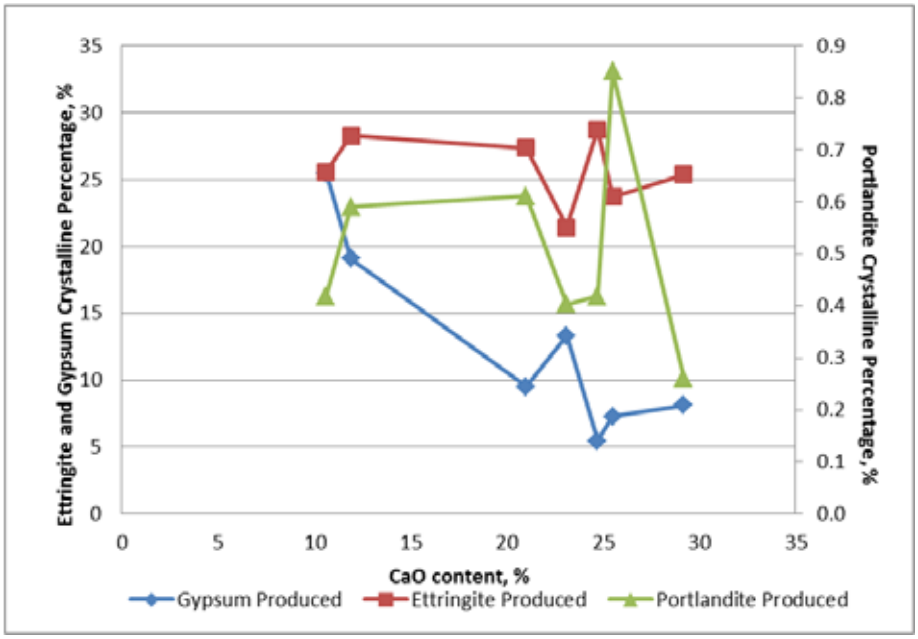

Figure 6.20: Hydration Products from 5% Sodium Sulfate Immersion

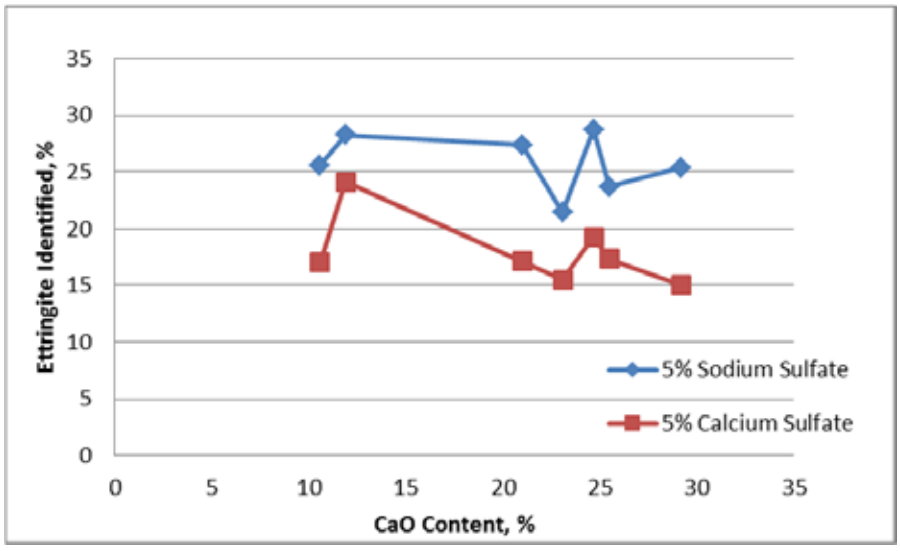

Figure 6.21: Comparison of Ettringite Formation in Different Sodium Solutions

In general, the results obtained in similar testing by Dhole did not agree with the testing results presented above. There appeared to be no correlation between the calcium content of fly ash and ettringite formation after sulfate immersion. One would have expected for the reactive calcium aluminosilica glass found in the higher calcium fly ashes to react with the sulfate solutions and formed more ettringite. No correlation was observed between time to failure and ettringite formation to explain the poor sulfate resistance by the higher calcium ashes. The pre-sulfate immersion results were agreeable with those found by Dhole and past literature. The better sulfate performing ashes formed more ettringite and less monosulfate early in the hydration process.

Chapter 7. Discussion

This chapter presents a summary of all testing results presented in the previous two chapters. This chapter aims to relate all findings to sulfate attack and present recommendations based on these findings.

The following tables identify a trend of sulfate results with probable reasons for these results. If a test is not listed, no strong correlations could be drawn from the data. Table 7.1 lists possible explanations for higher calcium ashes performing worse than lower calcium ashes in sulfate environments.

Table 7.1: Possible Explanations for Increased Expansions for Class C Ashes

Test	Findings
XRF	Increased CaO
	Decreased SiO_2
	Decreased sum of oxides
	Mid-range Fe_2O_3 (~6.0%)
	Increased SO_3
PSD	Smaller D(50)
XRD—more reactive phases	Decreased SiO_2
	Decreased Al_2O_3
	Mid-range Fe_2O_3 (~6.0%)
	Increased CaO
	Increased MgO
	Increased SO_3
	Mid-range Na_2O_e
XRD—more crystalline phases	Increased C_3A (~>2.7%)
	Increased brownmillerite (~>1.5%)
	Increased periclase
	Increased free lime
Previous Models	R-factor > 2.4 (Dunstan)
	Unacceptable region (revised Manz model)
SEM—diagram #1	Lack of 100% SiO_2 cluster for Class C ashes
	More points in gehlenite region
	Fewer points in mullite region
Reactivity	Gel height > 30mm
Activation Energy	AE>22500
Calorimetry	Longer time to maximum peak
Timed Calorimetry	Increased ettringite formation
	Increased C3A formation

Table 7.2 explains reasons that an increase in Class C replacement led to increased sulfate expansions, whereas an increase in Class F replacement led to decreased sulfate expansions. The primary reason for this finding was the increased amount of reactive phases introduced into the concrete mix.

Table 7.2: Possible Explanations for Increased Expansions with Increased Class C Replacement Percentage

Test	Findings
PSD	Increased amount of smaller, reactive particles
XRD	Increased amount of reactive phases, such as C_3A

Table 7.3 lists possible mechanisms to explain the behavior of the two high alkali fly ashes, FA-5 and FA-8. The behavior of the ashes is illustrated in the first row of the table. The results stated were from an analysis of testing from just these two ashes independent from the other ashes studied unless otherwise noted. The results stated also do not necessarily correlate to the other findings listed in the other tables in this chapter; they apply only to the high alkali ashes.

Table 7.3: Possible Explanations for Different High Alkali Fly Ash Sulfate Performance

Test	FA-5	FA-8
ASTM C1012 expansion	12 months to failure	Bars still readable
XRF of solely these two ashes	Increased SiO2	Increased Fe_2O_3
	Increased Al2O3	Increased CaO
	Increased sum of oxides	Increased MgO
	-	Increased LOI
	-	Increased SO_3
XRF of all the ashes	Second lowest Fe2O3	Third highest LOI
		Highest SO_3
PSD	-	Slightly larger D(50)
SEM—diagram #1	More points in gehlenite region	100% SiO_2 cluster
		More points in mullite region
Reactivity of all ashes	Highest gel height	Second highest gel height
Calorimetry	-	More total heat released for all replacement percentages

Table 7.4 lists possibilities for large 15-week expansions. These sulfate testing results did not seem to correlate to long-term performance, though, so these conclusions are stated merely to link to the conclusions drawn in Chapter 4 results section, and have no true merit.

Table 7.4: Possible Explanations for Large 15 week Expansions

Test	FA-6	FA-15	FA-18
XRF of these three ashes	Highest SiO_2	Highest Al_2O_3	Highest CaO
	Highest Fe_2O_3	Highest Na_2O_e	Highest MgO
	Highest sum of oxides	-	Highest SO_3
XRF of all the ashes	Highest Fe_2O_3	-	Lowest SiO_2
	Second lowest Na_2O	-	Lowest Al_2O_3
	Second lowest Na_2O_e	-	Lowest sum of oxides
	-	-	Lowest SO_3
	-	-	Lowest K_2O
	-	-	Second highest MgO
PSD	Very high D(50)	Small D(50)	Small D(50)
XRD	High C3A for Class F Ash	Roughly same C3A content as FA-6	Increase in reactive content
		Highest brownmillerite	Most C3A content

The following are a series of hypotheses created to help propose a model to identify a fly ash's sulfate resistance more accurately. The results are discussed in the following chapter.

Looking individually at 20%, 30%, 40% fly ash replacement, and an average of all replacement percentages, a chart was created to identify if the fly ash passed or failed a test. Criteria used were proposed in the literature review or specifically developed/refined for the data presented. The graphs used to correlate testing to time to failure are shown below in Figure 7.2, Figure 7.3, Figure 7.4, and Figure 7.5.

Looking through these charts with the time to failure data, tests were eliminated that produced an inaccurate outcome or were approved if a test accurately predicted sulfate performance. Based on this method, the following steps are proposed to identify a fly ash's acceptable or unacceptable use in a sulfate environment:

1. **Find the sum of the oxide (SiO_2 + Al_2O_3 + Fe_2O_3) content.** If this sum is greater than 70%, the ash will have good sulfate resistance. If the sum is less than 70%, the ash has poor sulfate resistance. This step essentially groups the ashes in the Class F or Class C groups.
2. **Of the remaining unacceptable ashes, calculate Dunstan's R-factor.** If the R-factor is greater than 2.3, the ash will have poor performance. If the R-factor is less than 2.3, it is acceptable for use in a sulfate performance. The total reactive percentage from Rietveld XRD can also be used in this step instead of Dunstan's R-factor. If the total reactive percentage is greater than 15%, the ash will have poor sulfate performance. If the reactive components are less than 15%, the ash will have good resistance to sulfate attack.
3. **For the remaining Class C ashes deemed unacceptable for use in a sulfate environment, plot the amorphous phases identified through SEM on ternary diagram #1.** If any Class C ashes have a cluster of amorphous particles at 100% SiO_2

apex, they will have good resistance. The remaining Class C ashes with no cluster at this location will have poor performance.

This combination of three tests most accurately covers the performance of a wide range of ashes. The sum of oxide step referenced above was included because it generally does an accurate job of combing through the majority of ashes and determining their acceptability in a sulfate environment. This test does not accurately predict the behavior of high alkali fly ashes though, so step two was introduced. Both Dunstan's R-factor with a revised limit of 2.3 (rather than the initially proposed 3) and the total crystalline reactive amount calculation limit predict the performance of high alkali ashes. These two tests had the exact same outcome for all ashes studied and for all replacement percentages. The third step was introduced because some Class C ashes in this study had acceptable expansion limits and a cluster of 100% SiO_2 amorphous particles. These three tests address the chemical make-up of the ash itself with XRF analysis, reactive crystalline phases in the fly ash through Rietveld XRD, and amorphous content of the ash. Dunstan's model was initially criticized for lacking phases responsible for ettringite formation, so this model includes the role of those reactive phases. Other critics stated the glassy phase was responsible for sulfate resistance, so amorphous content was included in this model as well.

The tests not included were the timed calorimeter microstructural development studies specifically related to ettringite formation at 48 hours. These results accurately predicted performance for 20% and 40% replacement; however, these tests were run only on a select number of samples and cannot be correlated with all of the sulfate data. In addition, the inclusions of XRD phase percentages alone as a screening tool were deemed unacceptable for use in these steps because the error in the Rietveld analysis, from 4–6%, was larger than most of the phase amounts identified. Dunstan's R-factor and the sum of total crystalline reactive percentage are calculated by using crystalline phase amounts, but many phases are included and error would be diminished.

Chapter 8. Conclusion

8.1 Summary of Project

The addition of some fly ashes is widely understood to improve the sulfate resistance of the concrete, but some fly ash additions actually reduce the sulfate resistance. This project aimed to understand this relationship between fly ash and sulfate resistance. Using sulfate testing results previously performed at The University of Texas at Austin, this project conducted a wide variety of physical and advanced chemical characterization techniques to understand the role of fly ash in the sulfate resistance of concrete.

8.2 Conclusions

Overall, the chemistry of the ash, the reactive crystalline phases, and the amorphous content must be considered to most accurately predict the sulfate resistance of a fly ash. A three-step process was proposed in the previous chapter, outlining the steps necessary to properly predict the performance of all ashes, including high alkali and Class C ashes. In general, Class F ashes will perform better in a sulfate environment though.

8.3 Future Work

The work performed in this report was limited to a year's duration, limiting the analysis needed for full understanding of fly ash and sulfate attack. The following work is proposed on this topic:

- Continue this analysis on more fly ashes with a wide range of compositions, including other high alkali ashes.
- Perform all of the testing for a sulfate solution other than sodium sulfate. Re-run ASTM C1012 expansions tests and compare the different sulfate solution results with the sodium sulfate results presented in this report.
- Perform more detailed SEM analysis, including elemental maps for multi-spectral image analysis (MSIA). This data can be used for better understanding of the glassy phases.
- Continue refining previously proposed models and the steps presented in this report to more accurately predict a fly ash's sulfate resistance.

Chapter 9. Alkali-Silica Reaction: The Basics

This chapter presents a concise summary of the alkali-silica reaction (ASR), with particular emphasis on the role of fly ash in preventing or minimizing expansion and cracking due to ASR.

9.1 Alkali-Aggregate Reaction

Alkali-aggregate reaction (AAR) is a chemical reaction that occurs in concrete and induces stress. The pores within concrete are filled with highly basic solutions that consist of many dissolved ions, mostly K^+, Na^+, and OH^-. Other ions include Ca^{2+} and SO_4^{-2} but these are not as important to AAR as the ions mentioned. Some fine and coarse aggregates contain chemically unstable mineral phases that can react deleteriously in the high pH environment in concrete. This then can cause internal expansion, cracking, and loss of serviceability that can lead to failure of the concrete element (Fournier, Berube, 2000). The two types of AAR, alkali-carbonate reaction (ACR) and alkali-silica reaction (ASR), will be discussed in the following two sections.

9.1.1 Alkali-Carbonate Reaction

ACR is similar to ASR but requires a different set of aggregates for reaction. ACR has been observed to occur with certain dolomitic rocks and the reaction with the high pH solution in the pores of the concrete. The first case of ACR was reported in the late 1950s in Canada and since then has been greatly studied (Swenson, 1957).

The alkali hydroxides of the concrete pore solution attack the dolomite crystals of the aggregate and begin the process of dedolomitization. It is believed that this process, the breakdown of dolomite, is responsible with expansion. Figure 9.1 shows the breakdown of dolomite with the alkali hydroxides to form brucite, calcite, and alkali carbonates.

$$\underset{\text{dolomite}}{CaMg(CO_3)_2} + \underset{\text{alkali hydroxides}}{2(Na,K)OH} \rightarrow \underset{\text{brucite}}{Mg(OH)_2} + \underset{\text{calcite}}{CaCO_3} + \underset{\text{alkali carbonates}}{(Na,K)_2CO_3}$$

Figure 9.1: Dedolomitization Process

This reaction then can possibly allow for channels to open in the concrete, thus allowing more ions from the pore solution to penetrate deeper to reactive aggregates (Fournier, Berube, 2000). The ACR mechanism occurs in the two steps in Figure 9.1 and Figure 9.2. In Figure 9.2, the alkali carbonates and portlandite reproduce more alkalis, which in turn will maintain a high pH and cause more reaction. This can mean that ACR could continue to proceed almost indefinitely.

$$\underset{\text{alkali carbonates}}{(Na,K)_2CO_3} + \underset{\text{portlandite}}{Ca(OH)_2} \rightarrow \underset{\text{calcite}}{CaCO_3} + \underset{\text{alkali hydroxides}}{2(Na,K)OH}$$

Figure 9.2: Regeneration of Alkalis

The deterioration caused by ACR and ASR are similar; the cracking and expansion of the concrete are very comparable. However, ACR is far less common than ASR because the type of aggregate needed for ACR is far rarer and sometimes not even allowed in concrete for other reasons. Because of this, occurrences of ACR in concrete structures are very limited.

9.1.2 Alkali-Silica Reaction

ASR is more much more common than ACR because of large abundance of reactive siliceous aggregate. This reaction occurs between the high pH pore solution in concrete and certain types of aggregates with poorly crystalline silica. The reaction causes the formation of a gel that expands when it absorbs water.

The mechanism of ASR and the chemistry behind it was studied greatly by Glasser and Kataoka (1981). They stated that when poorly crystalline hydrous silica is exposed to a strong alkaline solution, an acid-base reaction occurs. This reaction can be described in Figure 9.3. This figure shows the first step of the alkaline solution attacking the silica. The negatively charged oxygen terminal is then balanced by alkali cations (Na^+ and K^+) from the solution.

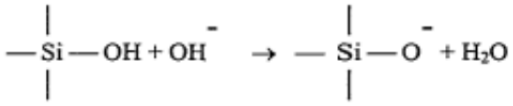

Figure 9.3: Reaction between Acidic Silanol and Hydroxyl Ions

When there continues to remain a strong alkaline solution and further hydroxide diffusion into reactive silica particles, siloxane linkages are also attacked as shown in Figure 9.4. If sufficient amounts of alkali hydroxides are still available, then the process continues to produce an alkaline silicate solution.

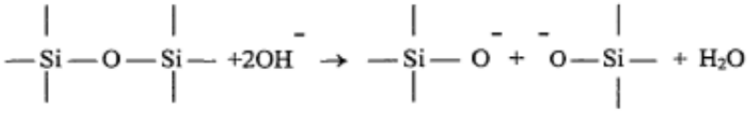

Figure 9.4: Reaction between Hydroxyl Ions and Siloxane Linkages

Thomas (2011) states that the extent or rate of dissolution is controlled by the alkalinity of the solution and the structure of the silica and the solubility of poorly crystalline or amorphous silica increase with pH. Glasser and Kataoka (1981) illustrated the formation of alkali-silicate gel that is accompanied by an increase of volume. This occurs from the dissolution of silica from reactive particles caused by hydroxide ions in solution.

Studies have been performed to determine the minimum hydroxide concentration in pore solution for ASR to occur in concrete. Researchers have concluded that concentrations within the range of 0.20 M to 0.30M can be the minimum threshold. Diamond et al. (1981), Kollek et al. (1986), and Thomas, Shehata (2006) have come with values within this range and a probable cause between the differences may be the type of reactive aggregate used. One could argue that a more reactive aggregate can still react with a lower threshold. An aggregate that's not too reactive might have a minimum threshold closer to 0.30 M.

Monteiro et al. (1997) conducted studies on ASR gel chemical composition on 30-day old mortar bars. The mortars were soaked in 1 M NaOH, and expansion measurements were taken in accordance with ASTM C1260. The mortar bars were mixed with different SCM dosages and cements. After 30 days, the mortar bars were examined with an SEM with BEI and EDS analysis. More specifically the chemical composition of the ASR gel found within the mortar bars was determined. Figure 9.5 shows the results from this analysis.

Sample	CaO%	SiO_2%	Na_2O_e%	Ca/Si	CaO/Na_2O_e	Expansion
OPC 1, Na_2O_e =1.37%	30.32	53.40	11.06	0.61	3.10	0.145%
OPC 1 + 25% Pozzolan	24.27	60.18	9.17	0.43	3.49	0.079%
OPC 1 + 25% FA	28.84	58.05	8.03	0.54	3.59	0.078%
OPC 2, Na_2O_e = 0.68%	20.52	51.51	9.89	0.43	2.16	0.155%
OPC 2 + 45% Slag	29.83	67.18	6.76	0.47	4.80	0.166%
OPC 2 + 55% Slag	37.92	51.07	3.7	0.79	12.15	0.032%

Figure 9.5: Chemical Composition for ASR Gel Formed (Monteiro et al., 1997)

The Ca/Si within the ASR gel plays a role in expansion. The highest ratio was 0.79 and is associated with the least amount of expansion of 0.032%. The mixture with the lowest ratio did not have the high expansion measurement. Generally speaking, the mixtures with lower Ca/Si ratios did have higher expansion. Monteiro et al. (1997) concluded that not all alkali silica gels are equally expansive. Alkali and calcium contents in ASR gel factor the expansion mechanism. Also, the higher the CaO/Na_2O_e ratio in the ASR gel, the less expansive the gel.

The amount of ASR induced expansion is dependent of several parameters. According to Thomas (2011), they include the availability of alkalis in the system, the nature and amount of reactive silica in the aggregate, exposure conditions (temperature and moisture availability), and the degree of internal and external restrain to movement (e.g., amount and distribution of reinforcing steel). Fly ash is only involved in one parameter—the availability of alkalis in the system.

9.2 Fly Ash

Fly ash is a by-product of the process of coal combustion in power generating stations. Coal is a complex and heterogeneous material used around the world as an energy source. When this coal is burnt to generate electrical power, large quantities of fly ash are produced and can be collected. Fly ash and bottom are produced but the fine grade fly ash is the important component for the concrete industry.

9.2.1 Background

Fly ash is a solid, fine-grained material collected from the combustion of coal in power station furnaces. The physical and chemical properties of fly ash can vary significantly and largely depend of the composition of the coal and the burning conditions in the furnace. Fly ashes that react with $Ca(OH)_2$ at room temperature can be classified as a pozzolan. These fly ashes act as pozzolan because of the higher amounts of SiO2 and Al2O3 in their amorphous form. Fly ashes can are divided into two groups by the American Standard for Testing and Materials (ASTM). Table 9.1 displays the classes and their chemical requirements. Class F fly

ashes are normally produced from burning anthracite or bituminous coal and are required to have the oxide percentage greater than or equal to 70% as shown in Table 9.1. Also, Class F fly ashes generally have pozzolanic properties. Class C ashes are normally produced from lignite or sub-bituminous coal and have both pozzolonic and cementious properties. The chemical requirement for the Class C fly ash is that their oxide percentage must sum up to or greater than 50%. These classifications are covered in ASTM C 618-08, Standard Specification for Coal Fly Ash and Raw or Calcined Natural Pozzolan for Use in Concrete.

Table 9.1: Fly Ash Classification

Class	Description	Chemical Requirements
F	Fly ash normally produced from burning anthracite or bituminous coal that meets the applicable requirements for this class as given herein. This class of fly ash has pozzolanic properties.	$SiO_2 + Al_2O_3 + Fe_2O_3 \geq 70\%$
C	Fly ash normally produced from lignite or sub-bituminous coal that meets the applicable requirements for this class as given herein. This class of fly ash, in addition to having pozzolanic properties, also has some cementious properties.	$SiO_2 + Al_2O_3 + Fe_2O_3 \geq 50\%$

The mineralogical composition of fly ash depends on the characteristics and composition of the coal burned at the power plant. The composition of the coal is largely dependent on the original location of the coal (Wesche, 1991). Because fly ash is rapidly cooled, it mostly consists of glassy particles (50–90%). A small amount of the fly ash is crystalline and a small amount of unburned carbon can remain. The most important minerals found in fly ashes from bituminous coal are magnetite, hematite, quartz, mullite, and free calcium oxide. Other minerals found in sub-bituminous coal are anhydrite, melilite, merwinite, periclase, and tricalcium aluminate. Several more minerals are found in fly ash in trace amounts. These minerals can be detected using X-ray diffraction because they are in crystalline phases.

9.2.2 Effects on Concrete

The proper use of fly ash improves the properties of concrete. It exhibits pozzolanic properties that react with $Ca(OH)_2$ resulting from the hydration of portland cement and form better hydration products. Calcium-silicate-hydrate (C-S-H) and calcium aluminate silicate hydrates (C-A-S-H) hydrations products are formed from this pozzolanic reaction. Fly ashes with high CaO contents also show hydraulic properties as well as pozzolanic properties.

The use of fly ash is known to reduce the expansion caused by ASR and this reduction is caused by the fact the hydration products tend to bind alkalis. The pozzolanic reaction when using fly ash produces C-S-H, which contains a lower Ca/Si ratio than that of just portland cement hydration. C-S-H with a low Ca/Si ratio has the potential to bind alkalis, thus removing them from the pore solution. Hong and Glasser (1999) claimed that the lower the Ca/Si ratio, the more negative the surface charge becomes, attracting the positive alkali cations from pore solution.

Table 9.2 shows the results of much research on the chemical composition of C-S-H using a variety of SCMs in their mixes. High CaO fly ash is less effective in reducing the Ca/Si ratio in C-S-H when compared to Class F fly ash. Also, notice how the alkali cation (K+, Na+) contents of C-S-H increase as the Ca/Si ratio decreases. The lower ratio has a higher capacity to bind these alkalis.

Table 9.2: C-S-H Composition

Author	sample	(Na_2O_e%) OPC	(Na_2O_e%) SCM	Curing	SCM Level	C-S-H Composition Ca/Si	Na	K
Rayment, 1982	Paste FA: F	1.07	0.75	8 days @ 20 C	0 %	1.71	**	0.58
					20%	1.55	**	0.76
Thomas et al., 1991	Conc. FA: F	1.07	3.40	7 years external	0 %	1.94	**	0.15
					20-30	1.57	**	0.68
Uchikawa et al., 1989	Paste FA: F	0.59	1.29	91 days @ 20 C	0 %	1.8	0.03	0.10
				91 days @ 20 C	25 %	1.7	0.05	0.12
				60 days @ 40 C	25 %	1.2	0.10	0.18
Thomas, 1994	Paste FA: F	0.80	2.16	28 days @ 80 C	0 %	1.78	0.12	0.54
	FA: CH		1.82		25 %	1.61	0.17	0.68
					25 %	1.84	0.25	0.36
Regourd et al., 1983	Mortar with SF	0.80	2.24	28 days @ 20 C	0 %	1.70	-	-
					5 %	1.43	-	-
Regourd et al., 1983	Conc. with SF	1.15	0.47	200 days	15%	1.3	-	0.40*
					20%	0.9	-	0.40*
Ushikawa et al., 1989	Conc. with SF	0.59	1.52	91days @ 20 C	0 %	1.8	0.03*	0.10*
					10%	1.3	0.10*	0.25*

Notes: FA: F is Type F fly ash; FA: CH is Type CH fly ash
**: Below detection limit
*: Expressed as Na_2O% or K_2O %
-: Not determined.

9.3 Effects of Fly Ash on Alkali-Silica Reaction

The use of fly ash and other SCMs is one of the most popular solutions to suppress ASR induced expansion. Some fly ashes behave differently than others and can be very effective against ASR while others can actually contribute to the problem. Several reasons are mentioned in articles proposing various mechanisms to explain fly ash effectiveness against ASR.

9.3.1 Fly Ash Effectiveness

Duchesne and Berube (1994a) listed four of the most common mechanisms to explain the effectiveness of fly ash against ASR:

- Lower permeability and consequent lower ion mobility
- Strength improvement and higher resistance to the expansive stress developed by ASR
- Alkali dilution resulting from cement replacement, (at least for admixtures with a lower available alkali content)
- Pozzolanic reaction producing secondary (pozzolanic) hydrates that entrap alkali ions and deplete portlandite in the cement paste, thus reducing the alkali ions and the pH in the pore solution.

Duchesne and Berube (1994a) performed concrete prism expansion tests similar to ASTM C 1293 that included the use of different fly ashes. Their studies included the use of three fly ashes (two Class F and one Class C with high alkali content). They found 40% replacement with the high alkali fly ash did reduce expansion over a 2-year period with respect to the control but 20% performed worse than the control. Of the other two fly ashes 20% were found to be enough to conform to the perform criterion. These results indicate that fly ash with higher alkali

content requires higher replacement dosages and excessive alkali contents can possibly render the fly ash totally ineffective.

Thomas (2011) wrote that alkalis in the binder are released in one of three ways: dissolved within the pore solution, bound by the hydration products, or incorporated in ASR gel. If there is no reactive aggregate, then the pore solution and hydration products will reach some sort of equilibrium and the amounts are dependent on the composition of the binder. Many researchers have found that the incorporation of fly ash leads to a reduction of the alkali concentration inside of the concrete pore solution and with higher dosages the concentrations decreases. Figure 9.6 shows how higher replacement levels of SCMs results in lower OH^- concentrations in the pore solution. Three fly ashes were tested (Class C, Class F, and high alkali). Notice how the high alkali fly ash had the highest concentration at all levels, followed by the Class C, and then the Class F. The Class F performed the best in the lowest OH^- concentrations. Also, notice how the concentration continues to decrease at higher replacements.

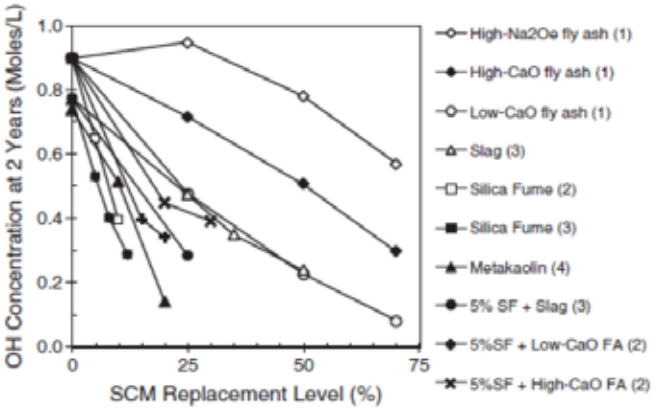

Figure 9.6: Effect of SCM and Replacement Level on the Pore Solution [OH-] (Thomas, 2011)

Also, Thomas (2011) shows not only how the OH^- concentration decreases at higher replacement levels but also how ASR induces expansion. Figure 9.7 displays similar results from Figure 9.6. Performance increases as fly ash replacement level increases. Expansion can drastically be reduced with the higher replacement levels, especially with a low CaO fly ash. Notice how even the higher replacement levels with high CaO and high alkali contents performed better.

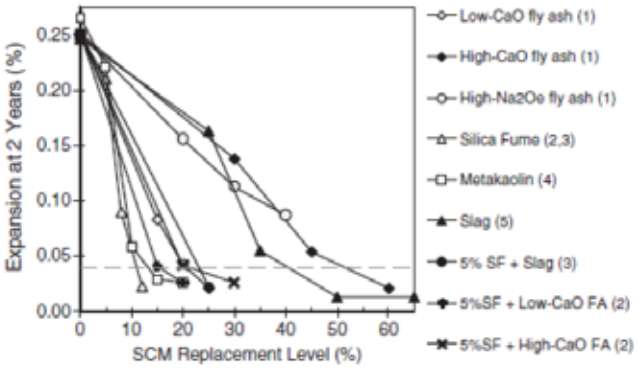

Figure 9.7: Effect of SCM Replacement on ASR Expansion (Thomas, 2011)

The dosage of fly ash needed to control ASR induced expansion is believed to be dependent on several variables, including the alkali content of cement and possible aggregate, the alkali content of fly ash, the CaO/SiO_2 of fly ash, and the reactivity of the aggregate. If any or all of these variables increase so does the need for higher fly ash dosages. Thomas has developed a relationship between the chemical composition of the binder, and pore solution concentration and ASR expansion. This index $[(Na_2O_e)^{0.33}xCaO]/(SiO_2)^2$ clearly shows which three chemical parameters affect ASR the most. As many researchers state, the alkalis of the binder contribute to ASR and so does the CaO/SiO_2. A combination of all three influences ASR expansion the most. This relationship will be used in the later sections will the research of this report to determine if trends can be discovered.

9.3.2 Available Alkalis

The term *available alkalis* refers to the amount of alkalis released by a fly ash into the concrete pore solution, enabling it to react with a reactive aggregate if available. Fly ash contains a percentage of alkalis just like cement but not all of it is available. Some of the alkalis are trapped in non-reactive crystalline phases while others are separated between hydration products and pore solution liquid (Thomas, Shehata, 2006).

In Section 10.2.4, the ASTM C311 method and procedure for determining the amount of available alkalis in fly ashes is described. This procedure is thought by many to be inaccurate in determining the amount of alkalis available for reaction with reactive aggregate. Thomas and Shehata (2006) state that the problem with this procedure is that the leaching medium is of neutral pH. The use of distilled water (not something similar to the high pH of concrete pore solution) will not correctly represent available alkalis. Many researchers have shown that most of the alkalis will be released under these conditions, especially if the curing period is extended past the 28 days required.

Duchesne and Berube (1994b) state that almost all alkalis in fly ash are released over a long period and will remain in the concrete pore solution at least for a short period. It states that once the alkalis are in solution, they are either entrapped in cement hydration or pozzolanic reactions, or remain available in solution for ASR. All fly ash alkalis are released into solution at some point but only a certain amount remains available.

Work by Lee et al. (1985) states that ASTM C 311 underestimates the amount of available alkalis, especially with only 28 days of curing. They tested not only at 28 days but at regular increments from 2 days to 6 months. They tested six different fly ashes and only one (a strong Class F) at 28 days had a good long term indication. The other fly ashes continued to release noticeable amounts of alkalis as time increased. Figure 9.8 shows a typical plot from their results. Notice how both curves continue to increase beyond the 28 days of curing. There is a significant increase beyond the normal curing amount and under ASTM C 311. These alkalis after 28 days would not be considered available because they would not have been detected. This test is not indicative of the total amount of alkalis released into pore solution in the long term.

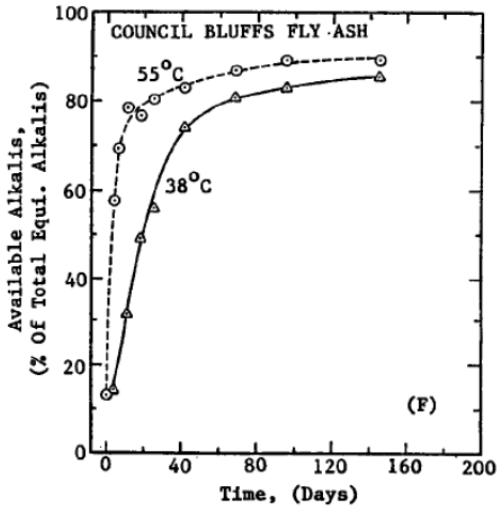

Figure 9.8: Long-Term Available Alkalis (Lee et al., 1985)

The experiments by Lee et al. (1985) also showed that the amount of available alkalis were about 50% of total equivalent alkalis for Class F fly ashes and 90% for Class C fly ashes after 5–6 months of curing. Although the percentages may be over- or underestimated because of the test method, a relative relationship can be noticed. Class C fly ashes will have plenty of more of their alkalis available for reaction than Class F fly ashes. The numbers may not be around 90% and 50% respectively, but in general Class C fly ashes have more available alkalis. Also, Lee et al. (1985) states that the test method may not be valid for high calcium fly ashes because its calcium may be reactive and interfere with the assigned fly ash to calcium hydroxide ratio (2.5:1) from ASTM C 311. Also their testing at higher temperatures to try and expedite the process resulted in the opposite—lower amounts of available alkalis.

Thomas and Shehata (2006) developed a method to determine the amounts of available alkalis from blended cements. The procedure involved mixing paste samples with different fly ashes and cements and allowing them to cure for a certain period for the pore solution to reach equilibrium. Then the paste samples were crushed and a certain amount was placed in different concentrations of OH^- with the same Na2O to K2O ratios of its binder. They were allowed to rest in the solution for a certain period and the concentrations before and after were taken. This method allowed for the determination of alkalis either released or bound by the paste when place into simulated pore solutions of different concentrations. This procedure was replicated during the research of this report and is discussed further in Sections 10.2.7 and 11.3.2. Thomas and Shehata (2006) found that the amount of available alkalis increases as the calcium and alkali contents of the blends increase and the silica content decreases. High CaO fly ashes had more available alkalis and confirm why these fly ashes perform worse at controlling ASR. Also, they stated that fly ashes with higher amount of alkalis also contributed more alkalis into the simulated pore solution. In Figure 9.9, one can notice how the replacement of more fly ash in the binder decreases the amount of available alkalis for reaction with reactive aggregate. Three different fly ashes of different chemistries showed that certain fly ashes are more efficient at higher replacement dosages in terms of ASR.

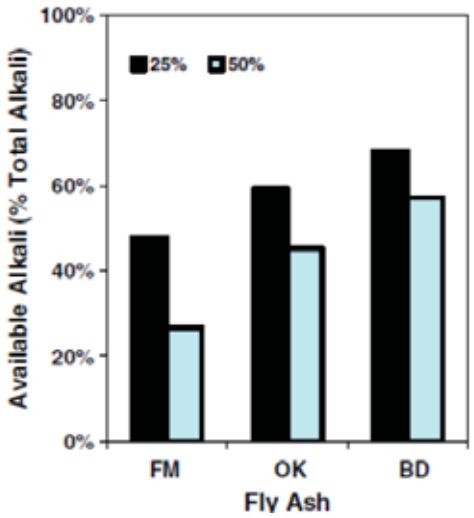

Figure 9.9: Effect of Fly Ash on Available Alkalis (Thomas, Shehata, 2006)

9.3.3 Pore Solution Chemistry

In hydrating paste cement paste, the concentration of the alkalis in the pore solution continuously changes. Many factors play a role in pore solution composition such as the cement, SCM, hydration products, aggregate, and potential ASR gel. Different levels and types of cement and SCMs can affect the composition as well. Figure 9.10 illustrates the possible sources of alkalis in the pore solution. It also shows how alkalis can be bound by hydration's products and consumed by ASR gel.

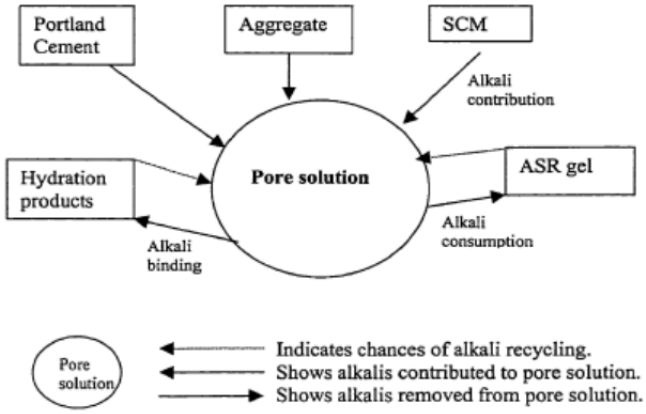

Figure 9.10: Sources of Alkalis in Pore Solution (Shehata, 2001)

Fly ash contains appreciable contents of potassium and sodium and a certain amount of them are available as described in the previous section. The concentration of alkalis in concrete pore solution is of importance when concerned about ASR. Certain fly ashes can reduce the alkali concentration by binding alkalis within hydration products. Other fly ashes have no effect or can increase the alkali concentration in the pore solution.

Class F fly ashes have been shown to reduce the concentration of alkali ions in the pore solution. Their effectiveness depends on the nature of the fly ash (e.g., fineness, glass content, and alkali availability), the level of replacement, the alkali content of the portland cement, and age (Shehata et al., 1999).

Diamond (1981) was one of the first to study the effects of fly ash on the alkali contents of pore solution. He studied the influence of two Danish fly ashes on the alkali content of cement paste pore solutions. The paste samples had up to 30% replacement and were allowed to hydrate for up to 6 months. Both fly ashes were low in CaO content and had moderate amount of alkalis (2.4–3.3% Na_2O_e). Figure 9.11 displays the pore solution concentrations at several time increments. Notice how the curves usually have a maximum concentration around 10 days and after 30 days the plot sort of evens off. The left figure has potassium ion concentrations and the right has sodium ion concentrations. In both cases, the pore solution concentrations were drastically reduced with the use of both fly ashes.

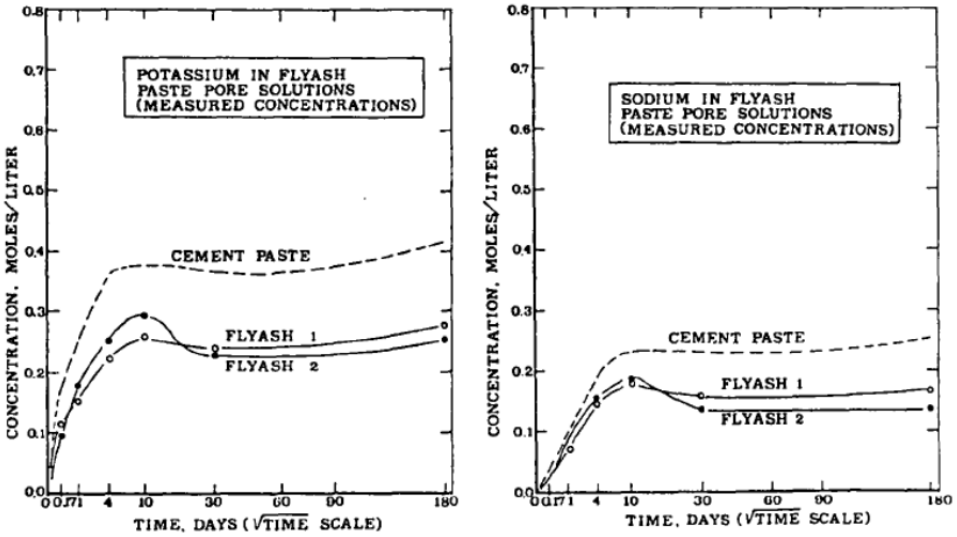

Figure 9.11: Pore Solution Concentrations (Diamond, 1981)

Diamond's (1981) studies concluded that both fly ashes acted in an inert manner with respect to alkali concentrations. They did not contribute or remove alkalis from solution but because it replaced 30% of the cement, the alkalis were reduced by the dilution effect. The second fly ash had a slightly higher alkali content but slightly lower CaO content and showed the effect of some removal of alkalis between 10 and 30 days.

Duchesne and Berube (1994) analyzed the pore solution chemistry of several cement pastes that contained a variety of SCMs at different time periods. Three of the SCMs were fly ashes (A, B, C) with different CaO and alkali contents. The CaO and alkali contents increased from A to C with C having significant higher values at 20.7 and 8.55 respectively.

Figure 9.12 illustrates the effectiveness of certain fly ashes in reducing alkalis in the pore solution. Fly ash A and B would be classified as Class F fly ashes with moderate amounts of alkalis (≈3%). Fly ash C is a Class C fly ash with 8% alkali content and performed worse than the control. This result indicates that not all fly ashes, even at high dosages, can be effective at

reducing alkalis. The Class F ashes performed better than the control and even better at replacement levels.

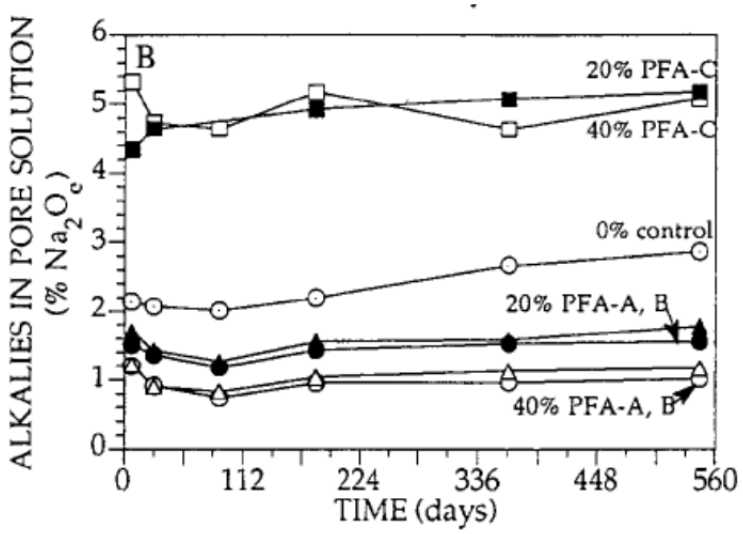

Figure 9.12: Alkalis in Pore Solution (Duchesne, Berube, 1994)

Hooton et al. (2009) showed similar results while they tested several fly ashes of different chemistry compositions. Figure 9.13 shows similar and more extensive results than Figure 9.12. At higher fly ash replacement levels, the OH- concentration in the pore solution decreases. The figure illustrates that this is true for both Class C and F ashes with low alkali contents. Even though the left plot contains an ash with a very high CaO content, all levels of replacement perform better than the control. Also, notice how the fly ash curves on the right plot are generally lower than the curves on the left plot. This shows that lower CaO fly ashes are more efficient at reducing alkalis in pore solution.

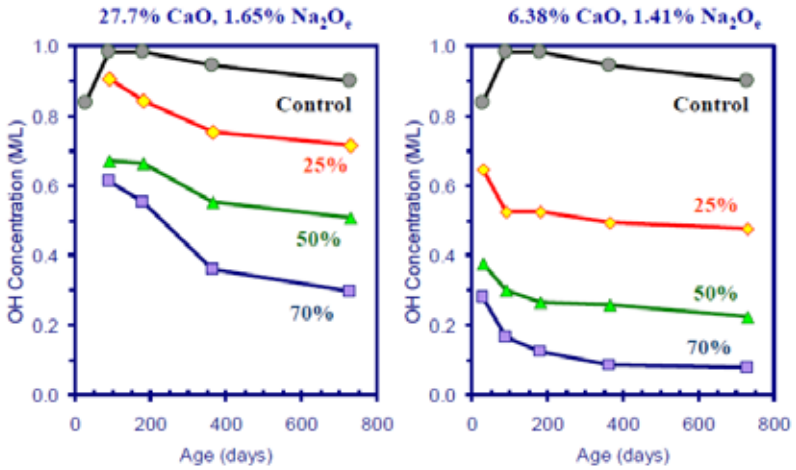

Figure 9.13: Effect of % Fly ash on Pore Solution (Hooton et al., 2009)

Figure 9.14 shows the effects of 25% fly ash with different chemistry compositions. Four fly ashes were used with low to high CaO contents and similar alkali contents. The results clearly

show the efficiency of lower CaO fly ashes; as CaO decreases, so does the OH^- concentration in the pore solution. As in Figure 9.14, even the high CaO fly ash was more efficient than the control.

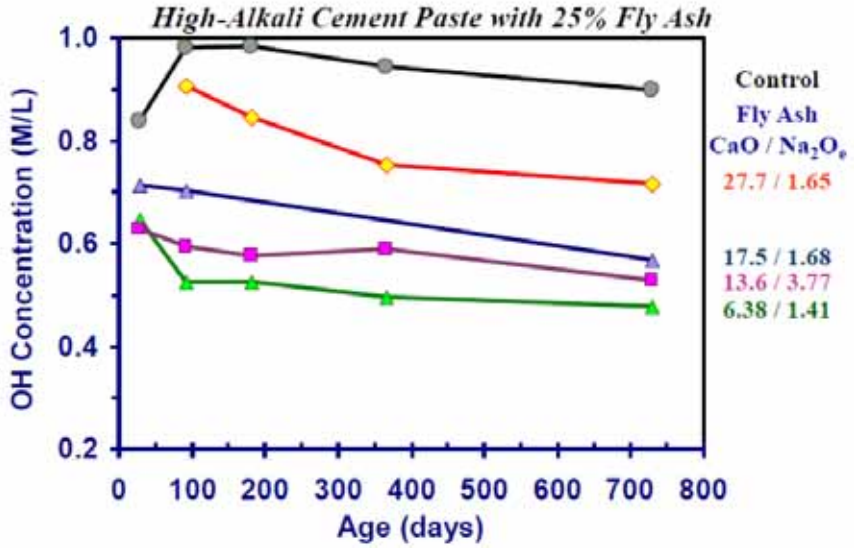

Figure 9.14: Effect of 25% Fly Ash on Pore Solution (Hooton et al., 2009)

9.4 Testing of Expansion due to Alkali-Silica Reaction

Many different expansion tests have been used to evaluate the efficiency of the addition of fly ash in suppressing ASR induced expansion. ASTM has two popular experiments (ASTM C 1260 & 1293) that test mortar bars and concrete prisms respectively. Other methods, such as the use of outdoor concrete block exposure sites, have also been implemented to provide more realistic results. The three methods have their advantages and disadvantages, and will be discussed in the following section.

9.4.1 ASTM C1260 and ASTM C1567

ASTM C 1260 is the accelerated ASR mortar bar test that measures expansion up 16 days while the specimen is placed in an 80°C 1M NaOH solution. The procedure and other matters are discussed in detail in Section 3.2.6. This test is for mortar only, so if a coarse aggregate must be tested, then it must be crushed and sieved to the appropriate size distribution. This can create different results from what would be achieved in realistic field conditions. Expansion measurements less than 0.10% at 16 days is considered indicative of innocuous behavior and expansions greater than 0.20% is indicative of potentially deleterious expansion. Expansion between 0.10% and 0.20% indicates that the aggregate may exhibit either innocuous or deleterious performance in the field (ASTM C1260, 2007). Similarly ASTM C1567 states that combinations of cements and SCMs that provide expansion less than 0.1% at 16 days are acceptable and anything greater indicative of potential deleterious expansion.

9.4.2 ASTM C 1293

In this test, concrete prisms are cast with square cross sections of 3.00 ± 0.03 in and are 11.25 in. long. Stainless steel gauge studs are cast in both ends of each prism to give an effective

gauge length of 10.00 ± 0.10 in. An ASTM C150/C150M Type I cement with a 0.9 ± 0.1% Na2Oeq is specified for this test method. A sodium hydroxide solution is added to the mixing water to raise the alkali content to 1.25 Na2Oeq. Prisms are demolded after 23.5 ± 0.5 hours and are measured for an initial reading. Prisms are then stored at 38.0°C ± 2.0°C for 1 year for concrete containing no SCMs. At The University of Texas at Austin measurements are usually taken up to 2 years regardless of whether SCMs are used or not. Prior to any length change measurements, prisms are brought to 23°C ± 2.0°C for 16 ± 4 hours. Length change measurements are performed at 1, 4, 8, and at 3, 6, 9, and 12 months. The optional additional readings are taken at 18 and 24 months for mixtures containing SCMs. An expansion of 0.04% at 1 year is considered potentially deleterious and the same for 2-year measurements when involving SCMs (ASTM C 1293, 2008).

ASTM C 1293 is considered more reliable than ASTM C 1260 because 1293 uses an actual concrete mix and larger specimens, and is not immersed into a harsh alkali environment.

9.4.3 Outdoor Exposure Blocks

The University of Texas at Austin has an outdoor exposure site with concrete block specimens created to provide realistic ASR expansion results to real world cases. The blocks measure 28 x 15 x 15 in. nominally, are mixed with the same ASTM C 1293 proportions, and are wet cured for 7 days prior to outdoor exposure. Measurements are taken with two different length digital comparators at the top and all sides of the concrete block. There is no formal failure expansion measurement but cracking is noticed at 0.04% (Ideker et al., 2012).

This test method is thought be better than both ASTM C 1260 and 1293 because neither of the other two methods account for the effects of outdoor exposure. Outdoor exposure provides variations in temperature, moisture availability, and loading. Ideker et al. (2012) stated that the ideal test method does not exist. ASTM C 1260 is an aggressive test that can fail specimens while they would not fail in ASTM C 1293. Also, it has been noticed that the opposite can occur; specimens can pass 1260 but show deleterious expansion in the field. ASTM C 1293 is more reliable but if SCMs are used then the test is extended to 2 years, while 1260 is only a 16-day test. 1293 may relate expansions closer to field conditions but 2 years is a long period of time to access ASR. The same goes for the outdoor exposure block—too much time and effort goes into these blocks, which prohibits widespread acceptance and use.

Chapter 10. Materials and Testing Methods

This chapter will discuss the materials and testing methods used throughout the duration of the project. The majority of the materials used were already on hand at The University of Texas at Austin and some had to be brought in from other locations. The testing methods were mostly executed at the CMRG laboratory, as well as at additional university locations and at TxDOT materials division.

10.1 Materials

The materials used for this project were selected because they fit a certain criteria. The fly ashes selected covered a wide range of chemical and mineralogical compositions. We wanted to make sure that the both the short and long-term testing of this project would accurately reflect the many different sources of fly ashes. Also, many of the fly ashes selected have been used before in different projects at The University of Texas at Austin. This was convenient for us because we could could compare and relate our short-term data to the long-term data previously gathered. Because this project was sponsored by TxDOT, most of the fly ashes are from Texas sources. Eleven of the original fourteen fly ashes are from Texas while three were brought in to extend the ranges of chemical properties. In addition to these fourteen, TxDOT provided us with four more fly ashes to test.

Table 10.1 has the original fourteen fly ashes that were introduced in the proposal. This table also lists the experiments previously conducted on the fly ashes. The chemical compositions of these fly ashes are also located on the table but may differ from the values used for calculations because these values may be from older or different samples. Please note that this report will have the number system located on the left column of this table. Table 10.2 provides the mineralogy of the two cements used during this project; because this report focuses mainly on ASR, only cement 1 was used because of its high alkali content.

Table 10.1: Original Proposal Fly Ashes

Fly Ash	Chemical Composition						Physical Property	ASR			External Sulfate Attack Test Methods			DEF	AEA* demand
ID	CaO	Al_2O_3	SiO_2	Fe_2O_3	MgO	Na_2O_{eq}	LOI	ASTM 1567	ASTM 1293	Exposure Block	ASTM 1012	Exposure site		Kelham / Fu	
												UT	W. Texas		
FA-1	1.1	30.6	55.8	5.1	0.7	1.78	1.99	X	X	X	X				X
FA-2	9.9	20.4	56.2	6.8	2.6	1.2	0.19								X
FA-3	12.8	23.7	52.1	4.6	2.0	0.84	0.95	X	X	X	X	X	X	X	X
FA-4	14.4	18.9	51.0	7.9	2.91	1.19	0.46				X				X
FA-5	14.6	22.8	47.2	4.6	3.5	2.2	0.51		X	X	X				X
FA-6	15.8	21.2	40.7	4.5	3.5	8.46	0.53	X	X	X					
FA-7	18.9	19	32.7	5.8	4.3	8.7	1.2	X	X	X					
FA-8	21.6	19.3	41.3	6.5	4.4	1.94	0.16				X				
FA-9	23.5	18.8	38.6	6.7	4.8	2.1	0.28				X	X	X		
FA-10	25.3	21.4	36.5	5.2	4.5	1.78	0.15		X	X					
FA-11	25.4	21.2	34.6	5.7	4.6	2.1	0.55	X	X	X	X				X
FA-12	25.8	20.6	37.2	6.1	4.3	1.93	0.13		X	X	X				
FA-13	27.5	18.1	33.1	6.6	5.5	2.1	0.4	X	X	X	X			X	X
FA-14	28.9	17.8	30.7	5.9	6.6	2.35	0.44		X	X	X		X		

Table 10.2: Cement Mineralogy

Cement ID	SiO2	Al2O3	Fe2O3	CaO	MgO	SO3	Na2O	K2O	TiO2	Mn2O3	P2O5	Cl	ZnO	Cr2O3	LOI	CO2	C3S	C2S	C3A	C4AF
C-1	18.95	5.35	2.57	63.87	1.14	3.27	0.113	0.9	0.23	0.049	0.34	0.007	0.0108	0.0122	2.99	1.806	58	11	10	8
C-2	20.04	4.49	3.63	63.8	0.72	3.02	0.037	0.62	0.21	0.096	0.305	0.0063	0.007	0.0149	2.75	1.759	54	16	6	11

10.2 Testing Methods

This chapter describes the experiments conducted on the fly ashes. Many of the procedures were followed in accordance with ASTM and others followed procedures from previous work done by researchers.

10.2.1 X-Ray Fluorescence

All eighteen fly ashes and the two cements were sent to the TxDOT materials laboratory to be analyzed using their XRF instrument (as the CMRG laboratory does not currently have an XRF instrument). We did assist with a few sample preparations.

The use of XRF helped us determine the chemical compositions of our samples. XRF analysis involved an x-ray beam aimed at the sample; some of these beams cause more beams to form in the sample and escape. An x-ray detector collects the x-rays and measures the different amounts of energy that escaped. The energies are a function of the atomic number of the atom so we then can determine the element it was from (Wirth, Barth 2012).

The samples were analyzed on a 1kW Wavelength Dispersive S4 Explorer manufactured by Bruker-AXS. Our samples were prepared for XRF analysis using the fused bead method. This method consisted of heating a mixture of the sample with a flux to 800°C to 1200°C. The flux then melts and the sample dissolves, creating a homogeneous glass. Figure 10.1 shows the apparatus used for the XRF sample preparation. This image was taken after the heating process and during the pouring process, when the homogeneous sample is allowed to cool to become glass.

Figure 10.1: XRF Sample Preparation

The XRF procedure and analysis was conducted in accordance with ASTM C114, The Chemical Analysis of Hydraulic Cement.

10.2.2 Particle Size Distribution

This section discusses the two methods used to analyze the particle size distribution of the samples. The particle size distributions of the samples were analyzed with the laser diffraction technique and the wet No. 325 sieve technique.

ASTM C 430 Residue Retained on No. 325 Sieve

This experiment is to assist determine the fineness of the samples. The standard calls for a 1.000 g sample placed on a clean and dry No. 325 sieve. We used an all-brass 3-inch diameter Humboldt sieve. Then wet the sample with a gentle stream of water and remove to adjust the pressure of the water. Place the sample under the stream of water once again and rotate the sample for 1 minute so that it is evenly wet. Next, rinse the sample with 50 ml of deionized water and dry in an oven. Allow the sieve to cool and weigh sample. Figure 10.2 explains how the fineness of the sample is to be determined. F is fineness of the sample expressed as percentage passing the No. 325 sieve, R_c is the corrected residue, R_s is the residue retained on sieve, and C is a correction factor for the sieve used (ASTM C 430).

$$R_c = R_s \times (100 + C)$$
$$F = 100 - R_c$$

Figure 10.2: Calculation of Fineness (ASTM C 430)

Laser Diffraction

Laser diffraction involves a light from a laser passed into a group of particles suspended in air. The particles scatter the light while different size particles scatter the light at different angles. The instrument has several photo detectors at different angles to measure the light. The light patterns can then be converted to particle size using scattering theory (Malvern 2012).

The laser diffraction machine used for this project was a Spraytec by Malvern Instruments, Inc. with Spraytec software. The material refractive index was 2.5 with an imaginary index of 0.1 and the instrument used isopropyl alcohol as the dispersive agent. The instrument calculated the diameter of 10%, 50%, and 90% numerically and produced a particle size distribution plot.

10.2.3 Total Alkalis (Acid-Soluble)

The total alkalis of our samples were determined using the XRF method. We also determined the total alkali percentage in accordance with ASTM C 114/311. This standard has a section that covers the determination of sodium oxide and potassium oxide of our samples.

The procedure calls for 1.000 g of sample placed in a 150-mL beaker and dispersed with 20 mL of water while swirling. Then add 5.0 mL of concentrated HCl and then dilute to 50 mL. Next, digest and stir on a hot plate for 15 minutes and filter into a 100-mL volumetric flask. Allow to cool and then dilute to the 100-mL line with water (ASTM C114). The concentrations of sodium oxide and potassium oxide are then determined using the flame photometry method discussed in section 3.2.8.

10.2.4 Available Alkalis

The available alkali experiment followed the procedure from ASTM C 311. This experiment was conducted on all eighteen fly ashes as well as C-1. The purpose of this test is to determine the available alkalis rather than the total alkalis within the sample.

ASTM C 311 specifies weighing 5.0 g of the sample along with 2.0 g of hydrated lime and mixing with 10 mL of water in a 25-mL vial. Shake, seal, and store in an oven at 35°C for 28 days. Then, open the vial and grind while added a small amount of water. Bring total volume to

200 mL and let stand at room temperature for one hour. Filter into a 500-mL volumetric flask and neutralize with dilute HCl while using phenolphthalein as the pH indicator. Dilute the remaining volume with water and then measure alkali concentrations using the flame photometer.

10.2.5 Pore Solution Extraction

This experiment involves the extraction of pore solution from a cement paste. The procedure followed is one conducted by students and researchers at The University of Texas at Austin. They have their own steel apparatus to place in a compression machine and extraction pore solution from concrete, mortar, and paste. Figure 10.3 shows a diagram with two views of the pore press apparatus.

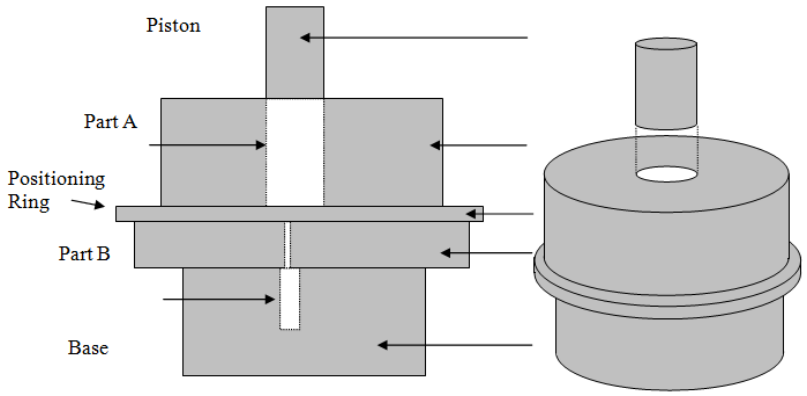

Figure 10.3: Pore Press Apparatus

The following procedure was used for this experiment for the use of cement paste. The procedure varies slightly for mortar and concrete. First, place the sample in a heavy duty plastic bag and crush with a hammer roughly to fragments of less than 0.375 inches. Place approximately 250 g of material and a Teflon disc in a 200-mL beaker and record the weight. Now, the steel apparatus must be assembled as in Figure 10.3 and placed inside of the compression machine. A plastic vial is place inside of the base part to collect the pore solution. The sample is placed in 3 layers and compacted inside of part A. The Teflon disc is place above the sample and the piston above that. Next, apply load at a rate of about 35,000 lbs/min to a maximum of 500,000 lbs depending on the sample size. Our sample sizes were small so we typically had a maximum load of roughly 250,000 lbs because the piston would become almost flush with part A. Remove the sample, along with the Teflon disc and weight out. Then, place in an oven for 24 hours and weigh again. The plastic vial within the base should contain pore solution from the sample. Measure the alkali concentration using the flame photometer.

10.2.6 ASTM C 1260, 1567

ASTM C 1260 and 1567 permit the detection of the potential alkali-silica reactivity of aggregate and combinations of cementious materials. Our goal using these experiments was to not test the reactivity of an aggregate but the usefulness of fly ash additions. Because of this, we used one of our most reactive fine aggregate for all the mixes.

The first step of this procedure is to batch the materials and place at room temperature for 24 hours prior to mixing. The standard calls for batching material for three prisms but we batched for four prisms because of the possibility of one breaking during demolding. 586.7 g of cementious material and 1320 g of graded fine aggregate were used with a w/cm of 0.47. Next, mix the materials in accordance with ASTM C 305 for mortar mixes and place in assembled prism molds. Then, demold prisms after 24 hours, take initial comparator readings, and place in 80°C oven. The following day take readings again and then place in an 80°C 1 M NaOH solution. The standard then calls for at least three intermediate measurements before 14 days. We measured at 3, 7, 10, 14, 21, and 28 days. Expansion beyond 0.1% at 14 days is considered a failure (ASTM C 1260).

10.2.7 Leeching Test

This leeching experiment was conducted to determine the amount of available alkalis in a cementious binder. Similar experiments have been performed by many researchers but we followed the procedure created by Dr. M. Thomas of the University of New Brunswick.

This test involved the use of the fourteen original fly ashes proposed and C-1 yielding 15 samples. A 25% cement replacement was used for all mixes except the control at a w/cm. Paste samples were created using a high shear mixer at 40 RPM with a mix sequence of 1 min mixing and a 1 min rest period repeated twice for three total minutes mixing. Each sample was placed in a polyethylene cylinder. The samples were rotated for the first 24 hours to prevent segregation. Next, the samples were placed in an enclosed bucket over water in a 100°F oven for 90 days. The samples were removed and crushed. Large samples were saved for pore solution and others to determine evaporable and non-evaporable water contents. The remainder was grinded and sieved between a No.16 and No. 80 sieve (.180mm-1.18mm).

Some time before removing the samples from the oven, simulated pore solutions were created using NaOH and KOH. The pore solutions were created to have the same Na_2O to K_2O ratios as the cementing materials used in each sample. This was done at OH^- concentrations of 0.0, 0.1, 0.2, 0.3, and 0.6 mol/L. Then 1.5 g of the sieved paste sample was place into 15 mL of its corresponding simulated pore solution in a 20-mL vial, sealed with silicone, and weighed. Fifteen paste samples were used at 5 different concentrations, yielding 75 samples, but we did this twice to yield 150 samples. The samples were allowed to rest in solution for 90 days and then weighed again. This was done to check for any evaporation that might factor into concentration calculations. The samples were vacuumed filtered and alkali concentrations were produced using the flame photometer. We would now know the difference in alkali concentrations before and after the paste was place in the simulated pore solutions to determine how much was bound or released by the paste.

10.2.8 Flame Photometer

The flame photometer test was not an experiment on its own but rather assisted with other experiments such as total alkali, available alkali, pore solution extraction, and leeching. The flame photometer apparatus allowed us to determine the concentrations of sodium and potassium ions in solution.

The flame photometer used for our experiments was the Cole Parmer Dual-Channel Flame Photometer, Figure 10.4, which allowed us to obtain Na^+ and K^+ results simultaneously. Figure 10.5 describes the process involved during flame photometry. A solution is aspirated into a low temperature flame where the water evaporates leaving solid residue of evaporation. The

solid breaks down to form atomic species where the atoms are excited by the flame and its electrons move to a higher energy state. The electrons eventually return to ground state and the loss of energy creates a discrete wavelength of light. The amount of light is proportional to the number of atoms in the flame and the concentration in the original solution. This light is measured by a photo detector and the concentrations are displayed in a digital readout (Parmer 2008).

Figure 10.4: Dual Flame Photometer (Cole Parmer)

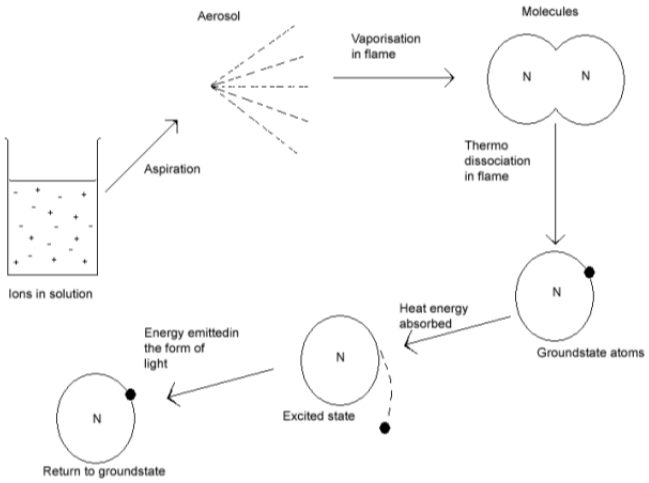

Figure 10.5: The Process Involved in Flame Photometry (Sherwood Scientific)

Chapter 11. Results and Analysis

This section will cover the results and analysis of the experiments conducted on the raw materials. These tests involved only the different fly ashes and cements and did not involve their hydration into paste, mortar, or concrete.

11.1 Particle Size Distribution

Fineness of fly ash is thought to be one important characteristic that determines its efficiency in preventing ASR. Finer pozzolans are more efficient AT reducing ASR expansion because fineness affects the pozzolanic activity. It has been shown that the use of ultra-fine fly ash (UFFA), even with a CaO of 11.8%, is very effective in terms of ASR (Malver, Lenke, 2006). Particle size distribution was evaluated using the wet No. 325 sieve method and the laser diffraction methods.

11.1.1 Wet No. 325 Sieve

This test was conducted with accordance with ASTM C 430 Residue Retained on No. 325 Sieve. ASTM C 618 requires all fly ashes to have a maximum of 34% retained when wet-sieved on a No. 325 sieve. Figure 11.1 illustrates the results from our testing. Clearly, the entire group of fly ashes was well above 34% retained or 66% passing mark. The fly ashes were arranged throughout the x-axis from low to high CaO contents. A general trend is noticeable, as CaO content increases so does the percent passing the #325 sieve, except for FA-5 and FA-8. These two fly ashes are distinct from the group because of their extremely high alkali content (Na_2O_e>8%).

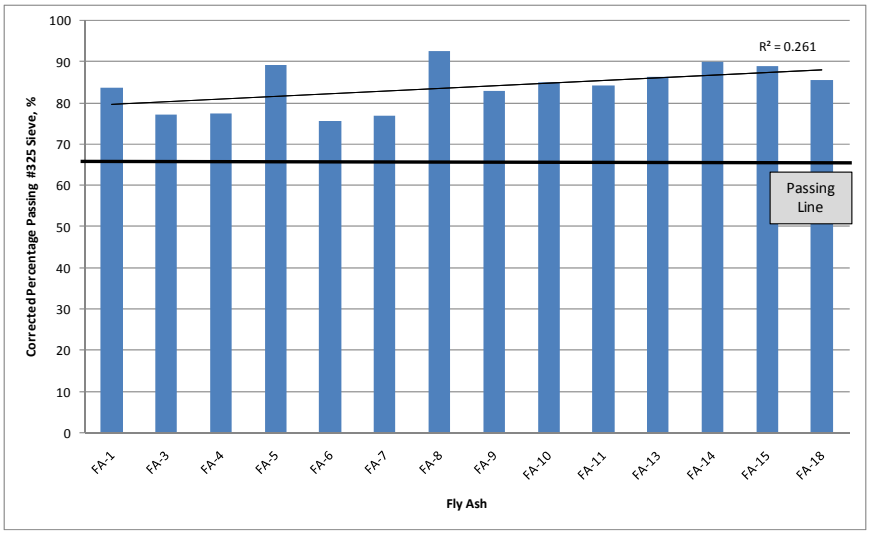

Figure 11.1: Percent Passing No. 325 Sieve

We can notice that the higher CaO fly ashes are finer in size and might conclude that they would be more effective for reducing ASR expansion. This is not the case for several reasons. The lower CaO fly ashes are already more pozzolanic because of their chemistry, not their particle size. When interpreting the results from particle size and relating them to ASR, only fly

ashes with similar chemical compositions and different particle sizes should be compared. For example, when comparing two fly ashes with similar CaO and Na_2O_e contents and different particle sizes, the one with finer particles would be expected to perform better.

11.1.2 Laser Diffraction

Figure 11.2 shows the particle size distribution for all 18 fly ashes. The curves show a relatively even distribution of all sizes without any gaps. Figure 11.2 is divided into two groups, between Figure 11.3 and Figure 11.4, because of the large number of samples. In order to more accurately understand the results, the figures were divided by CaO content.

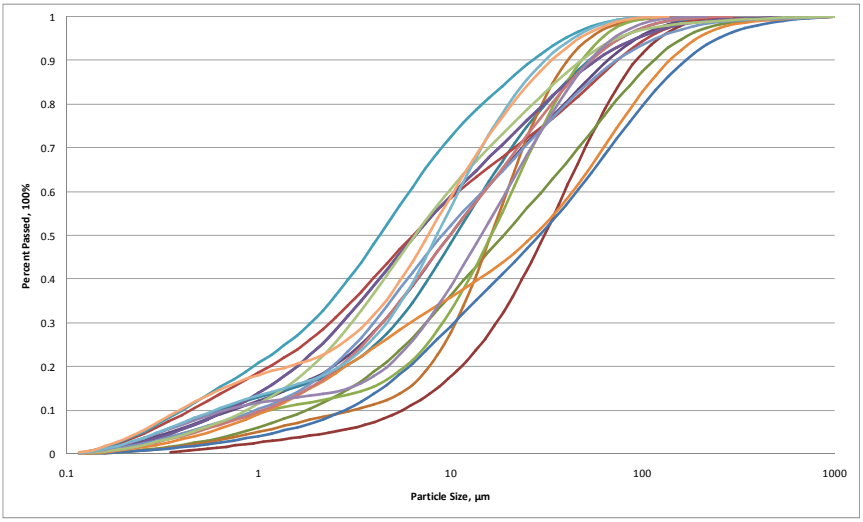

Figure 11.2: Fly Ash Particle Size Distribution

In studying the three figures, the higher CaO fly ashes again seem to have the smaller particle sizes. According to Roy et al. (1985), high calcium fly ashes have few cenospheres, generally have specific gravities of 2.3 to 2.8, and usually have finer particle sizes than low calcium fly ashes.

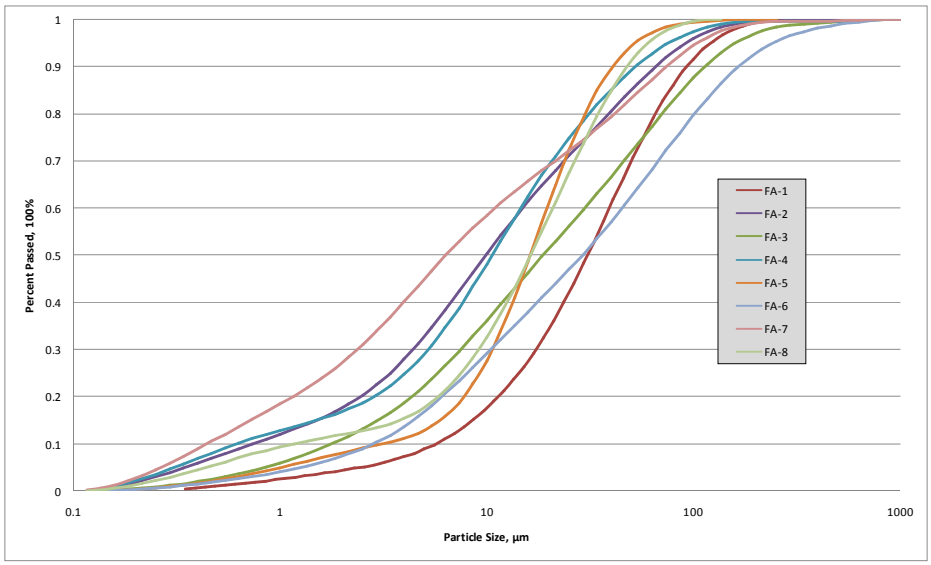

Figure 11.3: Particle Size Distribution (CaO<20%)

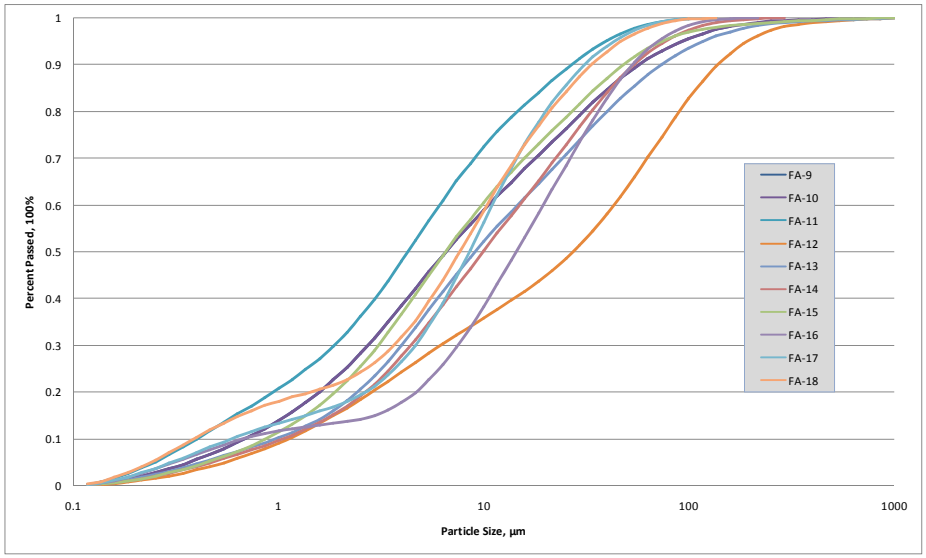

Figure 11.4: Particle Size Distribution (CaO>20%)

Figure 11.5 shows the particle size comprised of 50% by weight. Again we can see that the higher CaO fly ashes appear to have smaller diameters. The average diameter (composed of 50% by weight for Class F fly ashes) is 15.5 µm; the average diameter for Class C fly ashes is 11.5 µm.

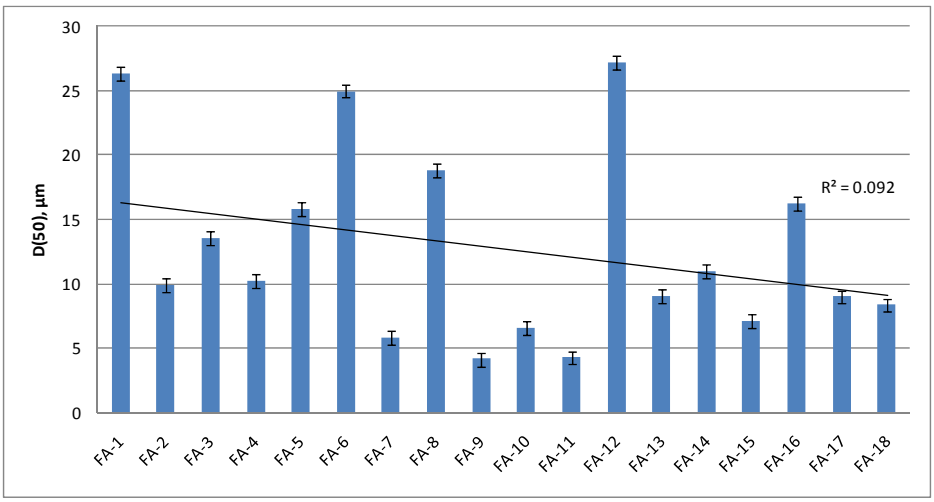

Figure 11.5: Average Particle Diameter by Mass

Lorenzo et al. (1994) conducted a study on two fly ashes with very similar calcium and alkali contents but different particle sizes. They studied alkali concentrations of pore solution of paste samples of these two fly ashes. They determined that the fly ash with the finer particles also had the paste samples with lower alkali concentrations in the pore solution.

If we closely study Figure 11.4, we can see the particles of FA-15 are considerably smaller than those of FA-13. We can also see these two fly ashes have similar calcium and alkali contents with FA-15 having a slightly higher CaO of 25.5 to 24.7 and higher Na_2O_e of 1.4 to 1.3. From just looking at the chemistry, we would expect FA-13 to perform better in ASR but that is not the case. According to ASTM C 1293 results with 40% fly ash replacement, FA-15 had a 2-year expansion measurement of 0.009% while FA-13 had a measurement of .033%. We believe the difference is mainly due to the particle size difference between the two. The fineness increases the pozzolanic activity—even though both fly ashes are high in calcium, they still display pozzolanic characteristics as well.

11.1.3 X-Ray Fluorescence

The XRF results gave us the chemical compositions of the different fly ashes and cements used throughout the research. Figure 11.6 displays the results for our fly ashes and cements, respectively, from the testing conducted by TxDOT. The fly ashes were labeled and organized according to CaO percentage. The fly ashes are organized in an ascending manor with respect to the CaO percentage. Figure 11.6 shows the large ranges of CaO contents of the fly ashes chosen for this research along with the Na_2O_e percentages. The CaO contents range from 1 to almost 30%; while most of the Na_2O_e percentages are similar, two are much higher at around 8%.

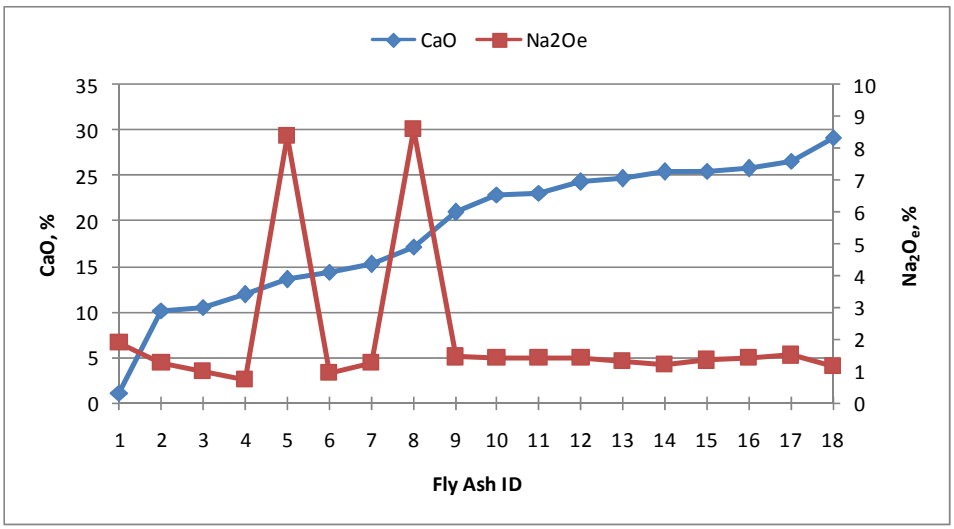

Figure 11.6: CaO and Na2Oe Percentages

As mentioned previously, the classification of fly ashes according to ASTM depends on the sum of three of the oxides. Any sum above 70% is a Class F fly ash and above 50% is a Class C ash. This attempt at classification is confusing since a sum above 70% is also above 50%, which means a Class F fly ash is also a Class C fly ash. The Canadian Standards Association (CSA) classifies fly ashes into three categories solely dependent on CaO content. Type F has CaO < 8%, Type CI has CaO 8–20%, and Type CH has CaO > 20%.

Table 11.1: Fly Ash XRF Results

Fly Ash	Chemical Composition										
ID	SiO_2	Al_2O_3	Fe_2O_3	Sum of Oxides	CaO	MgO	SO_3	Na_2O	K_20	Na_2O_e	LOI
FA-1	53.8	29.5	4.6	87.9	1.1	0.7	0.1	0.4	2.2	1.9	1.8
FA-2	51.4	20.7	7.1	79.2	10.2	3.0	0.3	0.4	1.3	1.3	
FA-3	55.3	17.8	7.6	80.7	10.6	2.3	0.4	0.3	1.1	1.0	0.2
FA-4	51.6	22.8	3.8	78.2	11.9	2.0	0.5	0.2	0.8	0.7	1.1
FA-5	42.9	21.6	4.3	68.8	13.6	2.5	0.9	8.1	0.4	8.4	0.4
FA-6	49.9	18.1	7.8	75.8	14.5	2.8	0.7	0.3	0.9	0.9	0.4
FA-7	45.7	21.0	5.1	71.9	15.3	3.6	0.5	0.8	0.8	1.3	0.5
FA-8	34.9	19.2	5.5	59.6	17.2	3.5	2.8	8.4	0.4	8.6	0.7
FA-9	37.4	18.9	6.5	62.9	21.0	4.3	1.1	1.2	0.4	1.4	0.1
FA-10	33.9	19.3	6.4	59.5	22.9	4.6	0.8	1.2	0.3	1.4	0.2
FA-11	34.4	18.4	6.6	59.4	23.1	4.6	1.3	1.2	0.4	1.4	0.3
FA-12	33.5	19.4	6.0	58.9	24.3	5.4	1.1	1.2	0.3	1.4	
FA-13	31.8	18.6	6.4	56.8	24.7	4.4	2.4	1.1	0.3	1.3	0.3
FA-14	32.5	19.3	6.0	57.7	25.4	4.4	1.2	1.1	0.2	1.2	0.5
FA-15	30.8	19.5	5.6	56.0	25.5	4.5	1.4	1.2	0.3	1.4	0.3
FA-16	32.0	17.2	5.8	55.0	25.8	6.1	1.9	1.3	0.3	1.4	
FA-17	30.9	17.3	5.8	53.9	26.6	7.8	2.3	1.4	0.2	1.5	
FA-18	27.1	17.1	5.8	50.0	29.2	6.2	3.5	1.1	0.2	1.2	0.6

Table 11.2: Cement XRF

Cement ID	C-1	C-2
SiO_2	18.95	20.04
Al_2O_3	5.35	4.49
Fe_2O_3	2.57	3.63
CaO	63.87	63.8
MgO	1.14	0.72
SO_3	3.27	3.02
Na_2O	0.113	0.037
K_2O	0.9	0.62
TiO_2	0.23	0.21
Mn_2O_3	0.049	0.096
P_2O_5	0.34	0.305
Cl	0.007	0.0063
ZnO	0.0108	0.007
Cr_2O_3	0.0122	0.0149
LOI	2.99	2.75
CO_2	1.806	1.759
C_3S	58	54
C_2S	11	16
C_3A	10	6
C_4AF	8	11

Determining the chemical compositions and classification was important in order to somewhat predict its behavior towards ASR resistance in concrete. Higher CaO fly ashes are less effective in controlling ASR and require more replacement than Class F fly ashes to mitigate expansion. Figure 11.7 shows the sum of oxides percentage on the left axis and the CaO percentage on the right axis. According to ASTM, FA 1-4 and FA 6-7 are Class F fly ashes and FA-5 and FA 8-18 are Class C fly ashes. According to CSA, FA-1 would be Type F, FA 2-8 would be a Type CI, and FA 9-18 would be Type CH.

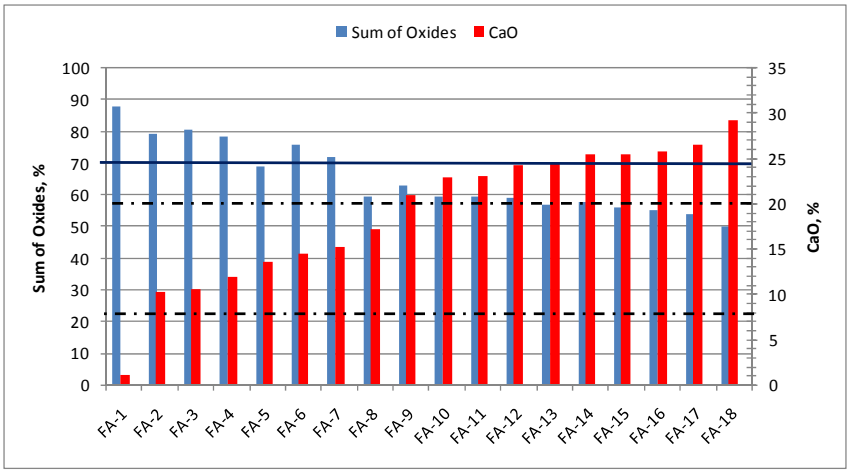

Figure 11.7: Sum of Oxides, CaO Percentages

Class C fly ashes are known to be less effective in reducing pore solution pH and require large dosages to control ASR induced expansion. Higher CaO fly ashes are less pozzolanic in nature, which allows more CH to remain in the system, helping maintain a high pH. This promotes dissolution of silica. The hydrates that are produced when using a Class C fly ash—such as C-S-H—tend to have a higher C/S ratio and lower potential for binding alkalis. The hydration products in Class F fly ashes tend to have a lower C/S ratio and bind alkalis within thus removing them from availability for reaction.

11.1.4 Total Alkalis (Acid-Soluble)

This section refers to the results and analysis of the Total Alkali test method from ASTM C 311 and ASTM C 114. The procedure is described in detail in Section 10.2.3. The standard states that this test method does not determine total alkalis of materials with large amount of acid-insoluble materials. In other words, this test method will determine only the acid-soluble alkalis in fly ash.

This procedure was implemented on 14 of the fly ashes. Figures 11.8–11.10 display the results of the acid-soluble experiment. Figure 11.8 displays the results for the 14 fly ashes in a column chart with the Na_2O_e percentage by mass on the y-axis. Because the fly ashes are numbered from low to high calcium, from this figure it is already noticeable that the lower calcium fly ashes had considerably fewer acid-soluble alkalis. FA-5 and FA-8 are the high alkali fly ashes and they had more acid-soluble alkalis than others of similar calcium content. FA18 had the highest amount of acid-soluble alkalis, even higher than FA-5 and FA-8. In fact the majority of Class C fly ashes had higher amounts of acid-soluble alkalis than the fly ashes with high alkali contents.

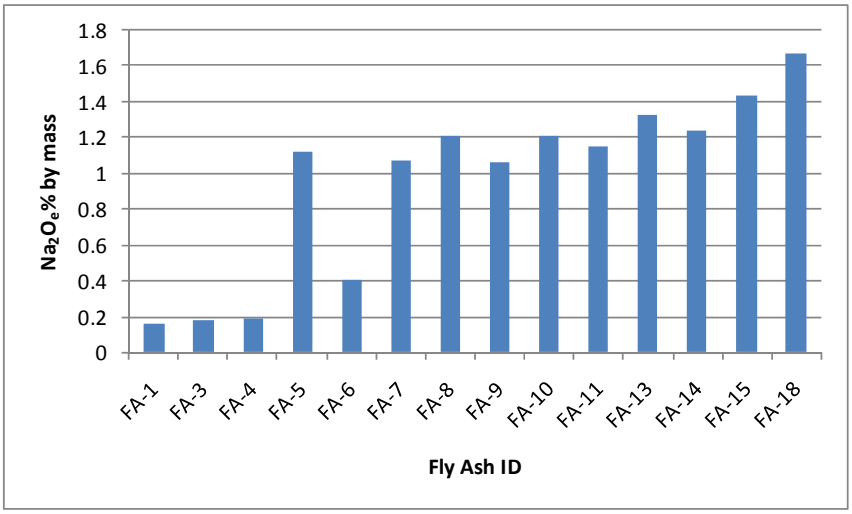

Figure 11.8: Acid-Soluble Results

Figure 11.9 has the same acid-soluble alkali results but plotted as CaO content increases. A strong trend shows that, as CaO content increases in the fly ash, so does the amount of acid-soluble alkalis. The r-squared value of 0.751 confirms a trend. The data points seem to be separated into groups and it is distinct which the Class C and Class F fly ashes are. The lower group of data points includes Class F fly ashes and the higher group the Class C fly ashes. In the

middle of the chart is a group of points: two of them are the high alkali fly ashes and the other is FA-7. FA-7 is Class F fly ash but has a rather high calcium content of 15.3%.

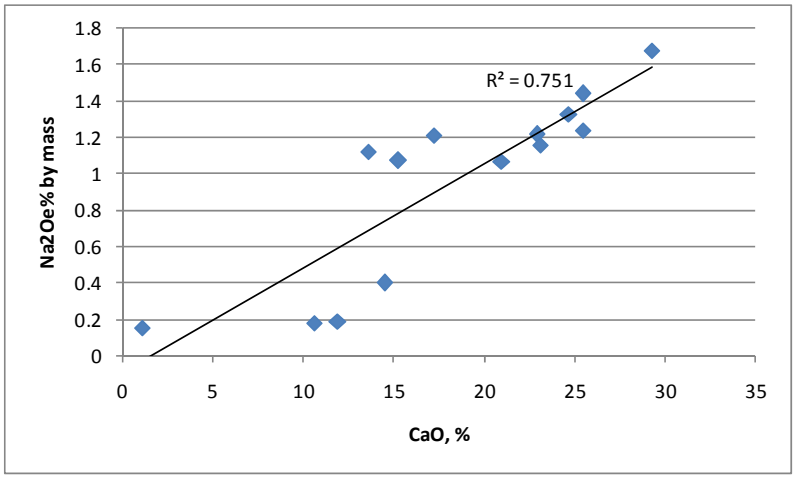

Figure 11.9: Acid-Soluble Alkalis (CaO)

Figure 11.10 displays the acid-soluble alkalis as a percentage of the amount of total amount of alkalis present in the fly ash. This again is plotted as CaO content increases. The trend line again fits the set data well and the r-squared value is higher than before at 0.763. What is noticeable here is that the two high alkali fly ashes only had a very small percentage of their alkalis acid-soluble. The only fly ash with a lower percentage was FA-1, the fly ash with the by far the lowest calcium content. From this figure, the two classes of fly ashes are again separated into two groups. The two groups are separated by the 60% line off of the y-axis. All of the Class C fly ashes have more than 60% of their alkalis acid-soluble and all the Class F fly ashes have less than 60%. The only exception was FA-7.

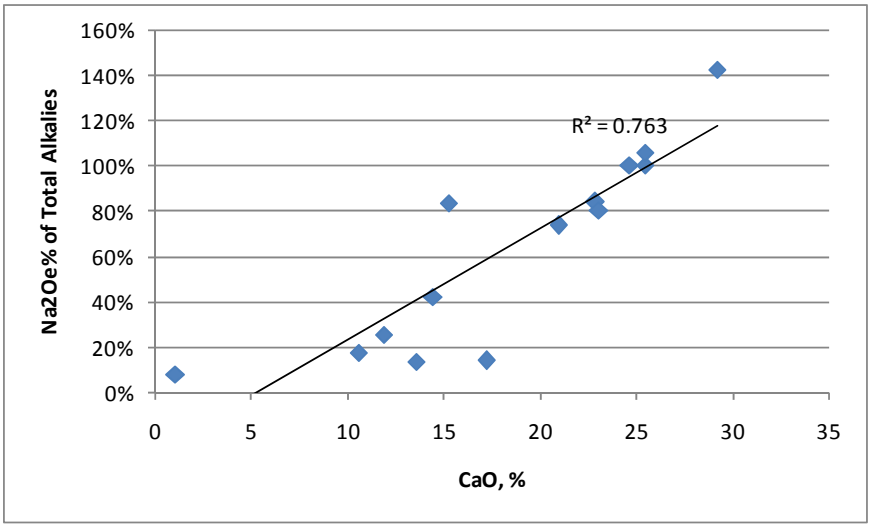

Figure 11.10: Acid-Soluble/Total Alkalis (CaO)

Figure 11.11 shows the acid-soluble alkalis plotted with the total Na_2O_e on the x-axis. One would think that the amount of acid-soluble alkalis would relate to the amount of total alkalis. In fact, it seems that the CaO content of the fly ash has more effect on the amount of acid-soluble alkalis. Appendix C has more figures relating acid-soluble alkalis to the SiO_2 content and other parameters. The SiO_2 content of the fly ash appears to play a big role in acid-soluble alkalis, with the trend line having a r-squared value of 0.90.

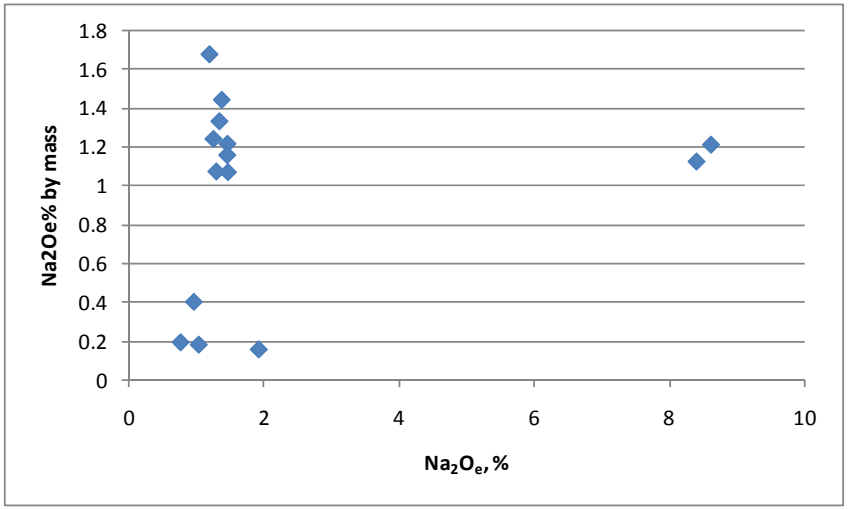

Figure 11.11: Acid-Soluble Alkalis (Na_2O_e)

Figure 11.11 shows a trend relating total alkalis to acid-soluble but the two high alkali fly ashes do not correspond greatly with the rest of the group. Also, a trend line was put on this set of data points but even with the exclusion of FA-5 and FA-8 the r-squared value was low.

Figure 11.12 plots the set of data against a compositional parameter that Professor M. Thomas of the University of New Brunswick has published on several of his papers. The x-axis is based off the chemical composition of the fly ashes $[(Na_2O_e)^{0.33}xCaO]/SiO_2^2$ is what Dr. Thomas used to relate the chemical composition of a concrete binder to ASR induced expansion (Thomas, 2011). He has also concluded similar relationships with the OH^- concentration in pore solutions.

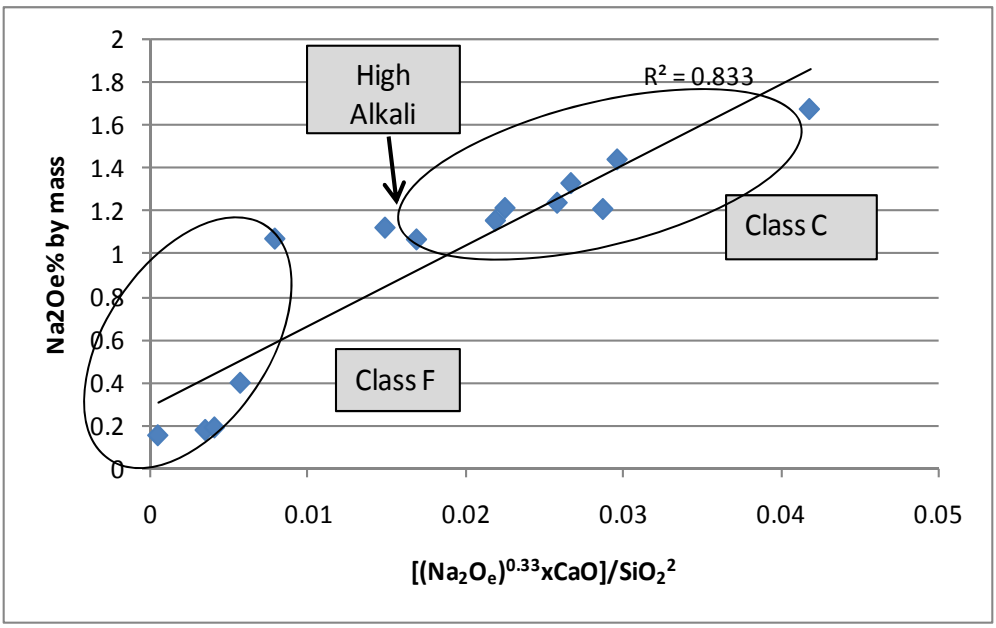

Figure 11.12: Acid-Soluble Compositional Parameter

$[(Na_2O_e)^{0.33}xCaO]/SiO_2^2$ can also be used to relate the acid-soluble alkalis of fly ash. Figure 11.12 shows that as the chemical ratio increases so does the amount of acid-soluble alkalis. This chemical index shows that acid-soluble alkalis are not just function of the amounts of Na_2O_e, CaO, or SiO_2 individually but a function of the three combined. All three factors into the amounts of acid-soluble alkalis that fly ash have.

11.2 ASTM C 1260, 1567

ASTM C 1260 is the accelerated mortar bar test for reactive aggregates and ASTM C 1567 is the experiment for testing the effectiveness of pozzolans on preventing deleterious ASR expansion. As previously mentioned, expansion above 0.10% at 14-day measurements are indicative of potentially deleterious expansion. Expansions below 0.10% are likely to produce acceptable expansions when tested in concrete.

A large number of fly ashes were chosen to be tested under ASTM C 1567 and the expansion results are located in Appendix A. The same reactive aggregate was used for all mixes. For the fly ashes chosen, testing was conducted at cement replacements of fly ash of 20, 30, and 40%. Further testing was conducted on FA-8 because of its failure to mitigate expansion and will be discussed later.

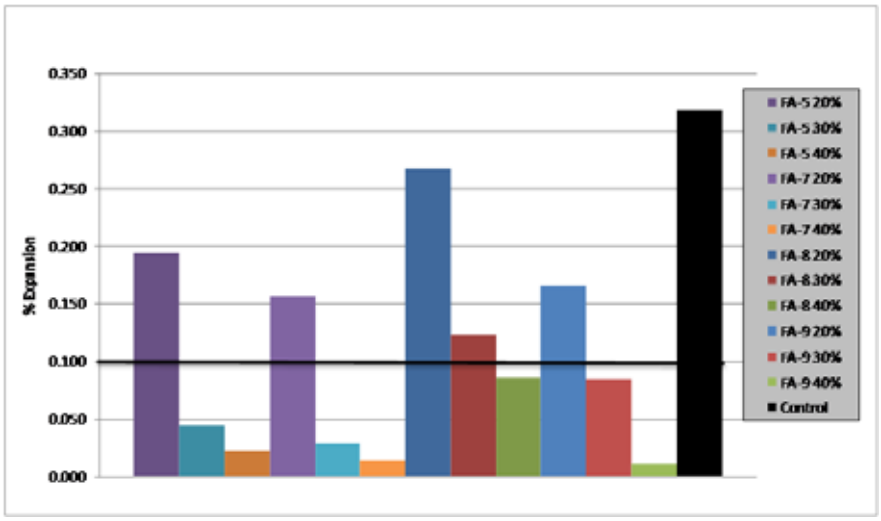

Figure 11.13: ASTM C 1260 14-Day Expansions with Similar Chemical Compositions

ASTM C displays the 14-day expansion measurements for FA-5, 7, 8, and 9 for 20, 30, and 40% replacement levels. The black column is the control using C-1, the high alkali cement, and the black line coming across 0.1% expansion is the failure requirement. These four fly ashes were chosen because FA-5 and FA-8 have high alkali contents and the other two have similar chemical compositions to these two. We wanted to determine if the high alkali contents of the fly ashes affected the testing even though these mortar bars are exposed to harsh conditions of 1 M NaOH. By studying the results of FA-8, it appears the alkalis in the fly ash do play a role in the expansion. From Figure 11.13 we can see that expansion increases as the CaO of the mortar binder increases. Knowing this we would expect FA-9 to have higher expansions than FA-8 but the alkalis within the FA-8 affected the expansion of the mortar bars. In addition, FA-5 has slightly higher expansions than FA-7 with higher a CaO. Also, notice how all the fly ash samples performed better than the control using C-1. The control had a 14-day expansion greater than 0.30%, which is three times the limit for deleterious expansion. In this case, the replacement of high alkali cement with high alkali fly ash was an improvement and continued to improve as fly ash dosages increased. The same conclusions can be reached with Figure 11.14, the 28-day results. Also, from Figure 11.14, we can conclude that the rate of expansion after 14 days of FA-8 continued to increase.

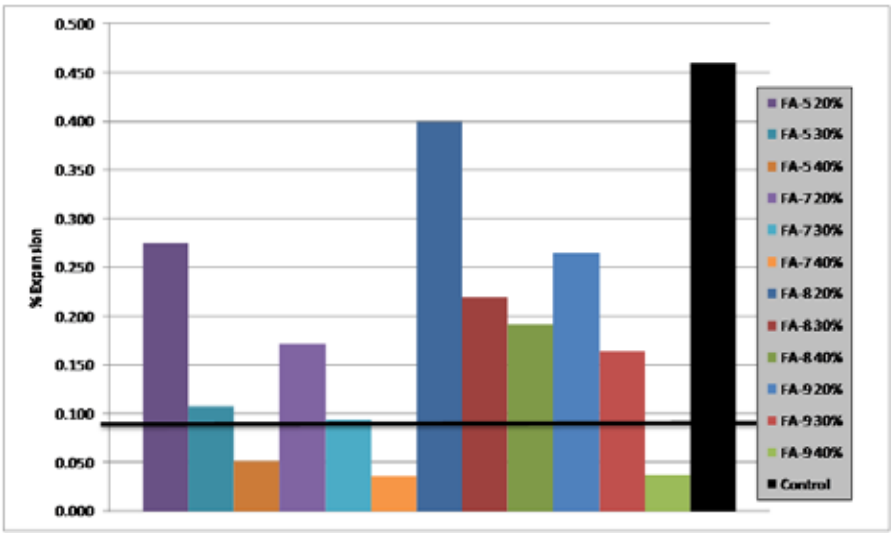

Figure 11.14: ASTM C 1260 28-Day Similar Chemical Compositions

Further testing was conducted on FA-8 because of its unusual behavior. Expansions close to 0.1% at 14 days and 0.2% at 28 days for 40% were noticed. Because of this, additional testing was conducted with higher replacement dosages. Results are located on Figure 11.15. From here we can see that increased dosages have adverse effect to some level. Expansions increase at dosages of 45 and 50%. The expansions at 45 and 50% are greater than those of 40%. Samples of replacement levels of 40, 45, and 50% were tested twice because of this behavior. The expansion began to decrease once again at a replacement of 55%.

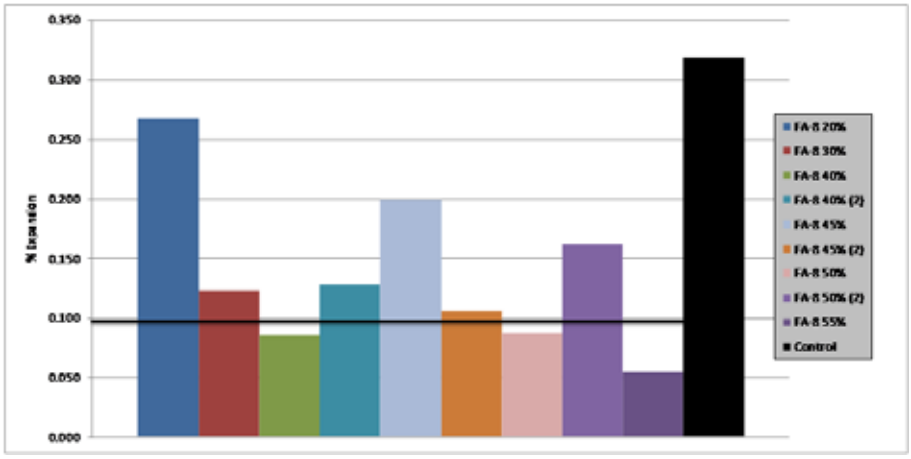

Figure 11.15: ASTM C1567 14-Day Expansions for FA-8

Figure 11.16 shows the results of FA-2, 8, and 17 at 14 days using different replacement levels. FA-2 performed far better than FA-17, and even FA-8 performed better than FA-17. A replacement level of 20% percent of FA-2 was enough to keep expansions below 0.1% and 40% showed very small expansion. FA-17 is the fly ash with the second highest calcium content and showed very deleterious expansions at all replacement levels. It even performed worse than the high alkali fly ash. The expansion with 40% replacement was still 0.20% at 14 days—not even close to the limit. A mix would require very large replacement levels to have the possibility of

having acceptable expansions. FA-17 did, however, improve the performance over the control especially at 40% replacement.

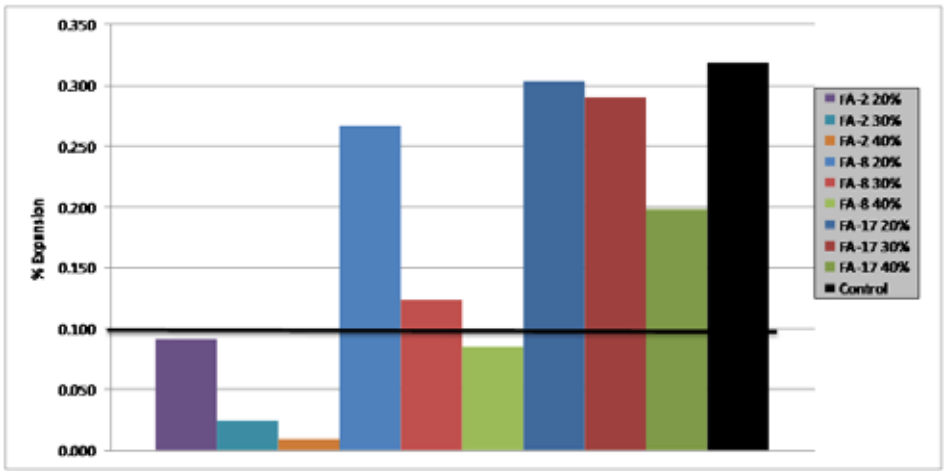

Figure 11.16: ASTM C 1260 14-Day Expansion - Wide Range of CaO

Figure 11.17 through Figure 11.20 contain the entire set of 1260 14-day expansion measurements conducted for this report. It contains readings from FA-2 to FA-17 with several in between and including the control. The exact fly ashes used are shown in the plots in Appendix A.

The relationship between the acid-soluble alkalis to the chemical composition of the fly ash can be related to the expansion results to the chemical composition of the mortar binder. For example, the CaO content of the binder for the 20% FA-2 mix would be $20\%xCaO_{FA\text{-}2}+80\%CaO_{C\text{-}1}$. Figure 11.17 shows us the CaO content of the binder increases so ASR induced expansion. The trend line fits the set of data good enough for a r-squared value of 0.709. None of the data points veer off the trend line including the high alkali and control mixes.

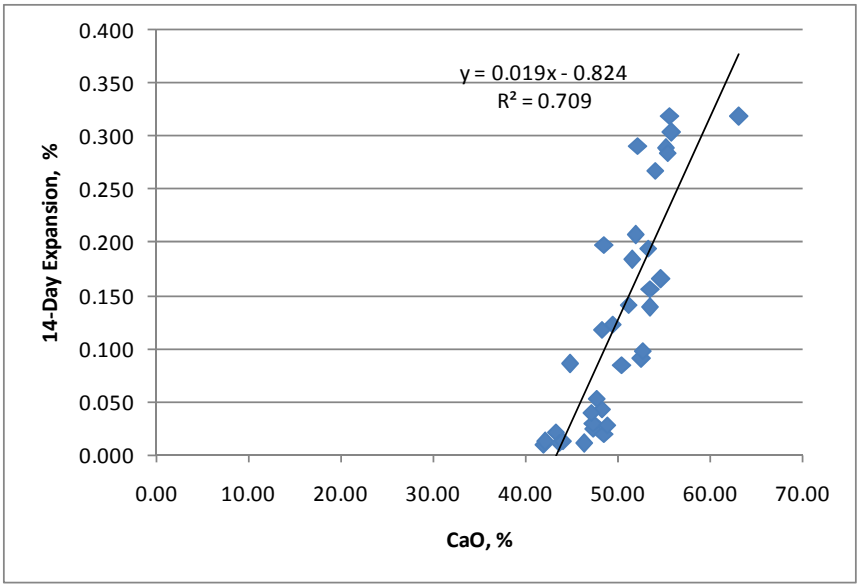

Figure 11.17: ASTM 1260 14-Day Expansion - CaO Relationship

Figure 11.18 relates expansion to the alkali content of the binder. The set of points far off to the right are the mixes involving high alkali fly ashes. Ignoring these points and adding a trend line to the rest of the set of data did not result in a high r-squared value. Although there was some correlation, it was not nearly as good as with CaO in Figure 11.17.

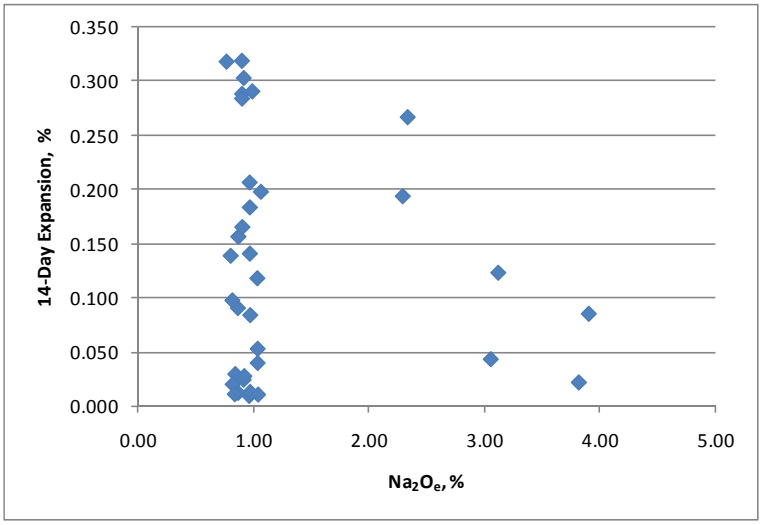

Figure 11.18: ASTM 1260 14-Day Expansion - Na_2O_e Relationship

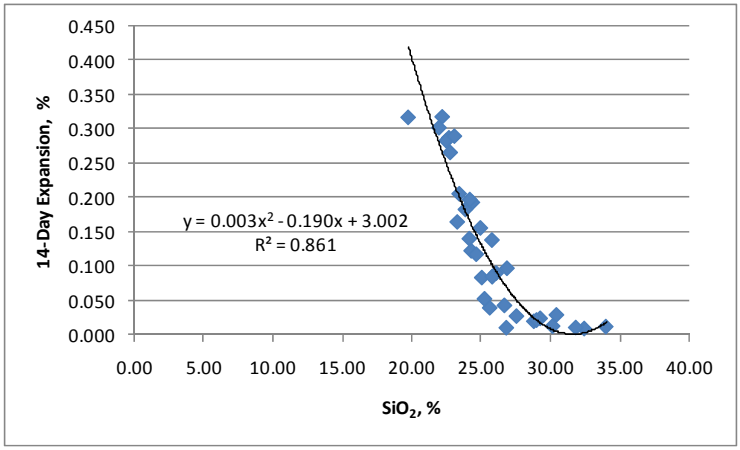

Figure 11.19: ASTM 1260 14-Day Expansion - SiO_2 Relationship

Figure 11.19 illustrates the relationship between expansion and SiO_2 content of the binder. What is interesting about this set of data is that it follows the curve of a second order polynomial. It appears that as the SiO_2 content of the binder increase the expansion decreases linearly to about roughly 28% SiO_2. After this point, there is hardly any expansion at all.

In Figure 11.20, the expansion data is related to the same chemical index used before. We can see that there is a trend, but it is not as strong as with the CaO and the SiO_2. Despite this we can still see that all three chemical parameters of the binder are affecting the expansion during the ASTM C 1260 experiment.

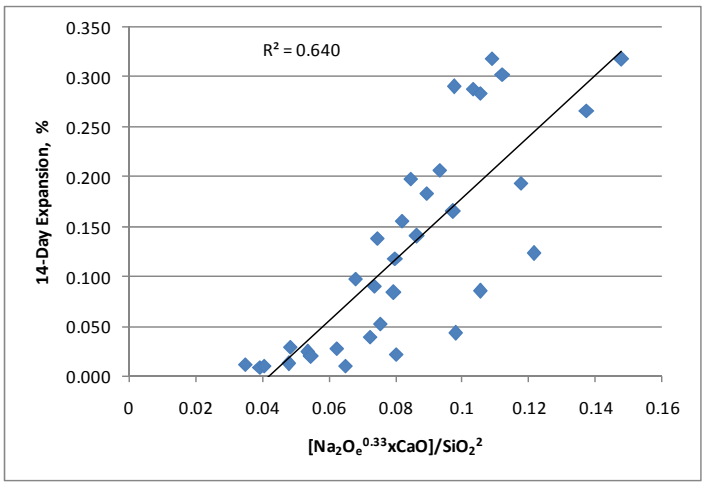

Figure 11.20: ASTM 1260 14-Day Expansion - Chemical Index

The same correlations were performed for 28-day expansion result and the plots are located in Appendix A. They again show strong trends relating the chemical parameters of the binder to the expansion results.

11.3 Paste

This section discusses the results and analysis for the experiments involving paste samples. The pore solution extraction, available alkalis, and leeching experiments involved testing on paste samples with fly ash.

11.3.1 Pore Solution Extraction

The pore solution chemistry study was conducted on 15 mixes that were also used for the leeching experiment in the following section. The procedure for this experiment is described in Section 10.2.5. A total of 15 paste samples were created with 25% fly ashes replacement and a w/cm = 0.5. These sealed samples were allowed to cure over water at 100°F for 90 days.

Figure 11.21 displays the sum of the alkali concentrations in the pore solution after 90 days of curing. Hydroxide concentrations were not tested because of the small amount of pore solution extracted. Paste samples were only large enough to extract enough solution for alkali readings in the flame photometer. $[Na^{+}+K^{+}]$ should be very close to $[OH^{-}]$ unless there are large amounts of other anions such as sulfate.

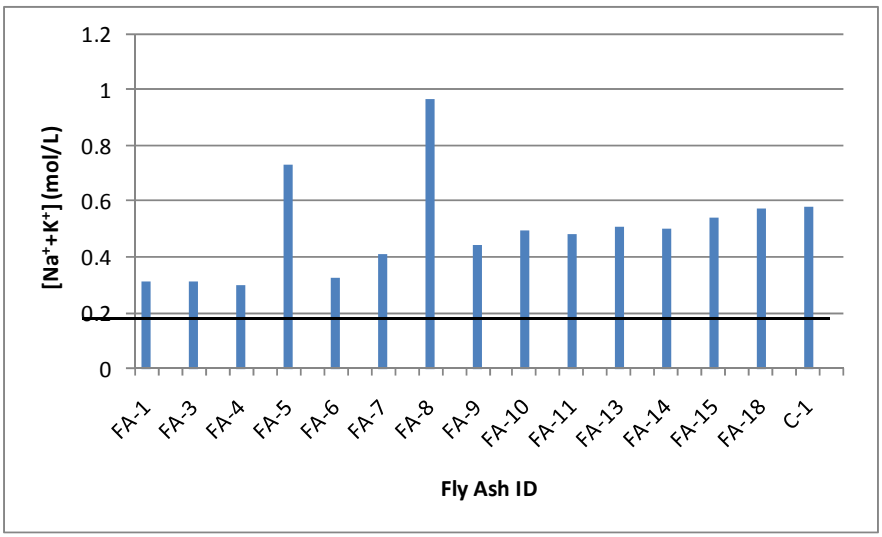

Figure 11.21: Pore Solution Alkali Concentrations

FA-5 and FA-8 have alkali concentrations way above anything else, even the control mix with high alkali cement. Clearly, these two fly ashes had a large amount of their alkalis released into the pore solution contributing to the alkalis present from the cement. The black line going across and intersecting the y-axis at 0.44 what the theoretical pore solution concentration would be with a 25% inert diluent. All samples had a 25% cement replacement with fly ash except the control. Figure 11.21 shows that FA-9 acted as a diluent while the other Class F fly ashes (except FA-5 & FA-8) showed reduced the alkali concentration even more. This shows that these fly ashes are acting more than just a diluent but their hydration products are binding alkalis from the pore solution released by the cement.

By study the Class C fly ashes, one can notice that their concentrations are above that of theoretical inert diluent concentration. These fly ashes did not act as an inert dilute and did contribute alkalis into the pore solution. There fly ashes had no effect of binding alkalis like the Class F fly ashes. More of their alkalis were available and went into solution.

Figures 11.22–11.24 relate the chemical composition of the paste binder to the alkali concentration in the pore solution. All but three samples followed the same trend, the high alkali fly ashes (HA FA) and control (C-1). Figure 11.22 illustrates that as the CaO content of the binder increases so does the alkali concentration of the pore solution. Figure 11.23 shows that as the SiO_2 content of the binder increases the pore solution concentration decreases. The trend lines fit the data very well with r-squared values of 0.839 and 0.958. Figure 11.24 shows the relationship with the amount of alkalis in the binder to the alkali pore solution concentration. There is noticeable but weak trend showing that as the alkali content in the binder increases so does the alkali pore solution concentration. The trend is not as strong here because many of the Class F and C fly ashes have similar alkali contents but it is clear that lower calcium fly ashes have more affect at reducing alkali pore solution concentrations.

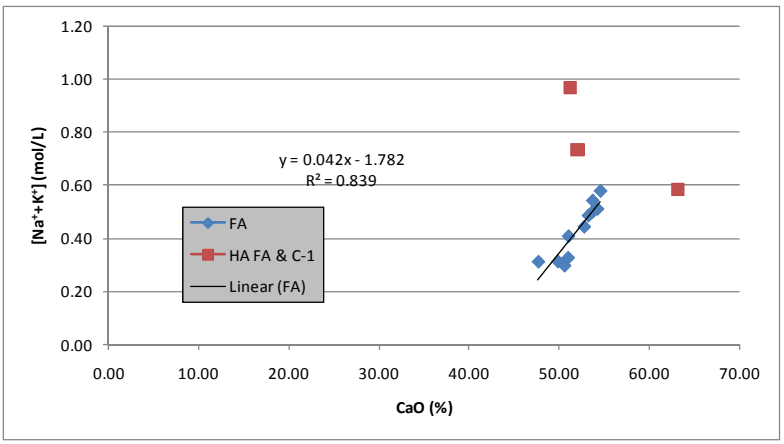

Figure 11.22: Pore Solution Concentration (CaO)

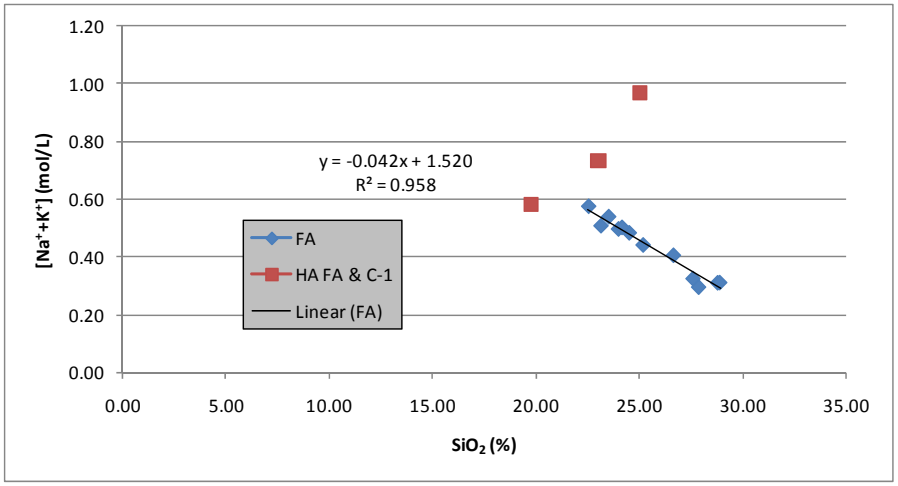

Figure 11.23: Pore Solution Concentration (SiO_2)

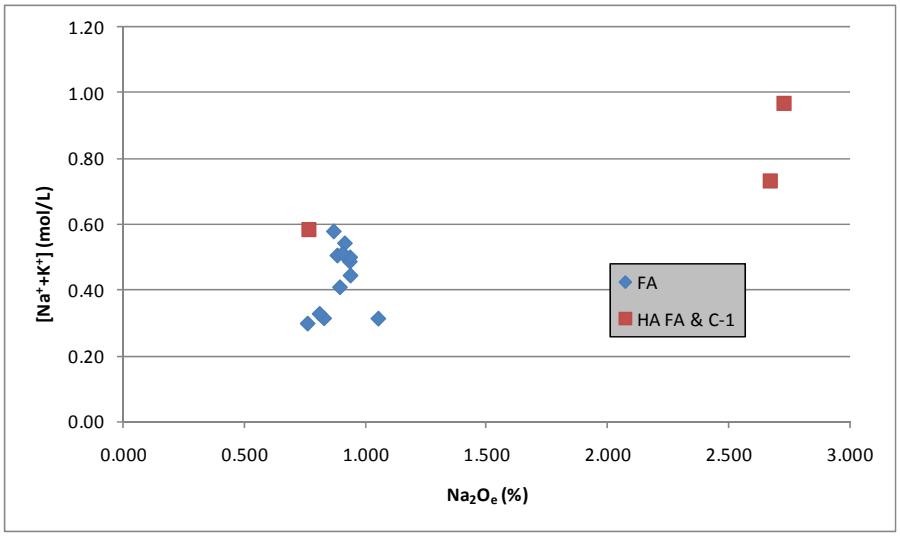

Figure 11.24: Pore Solution Concentration (Na_2O_e)

Many researchers believe that the CaO/SiO_2 of the binder greatly factors into the amount of alkalis present in the pore solution. This can be seen in Figure 11.25. Others (such as Thomas and Shehata, 2006) state that the Na_2O_e of the binder also plays a role. Figure 11.26 shows the contribution of all three being factored in. The trend for Figure 11.27 is slightly stronger but both are still great.

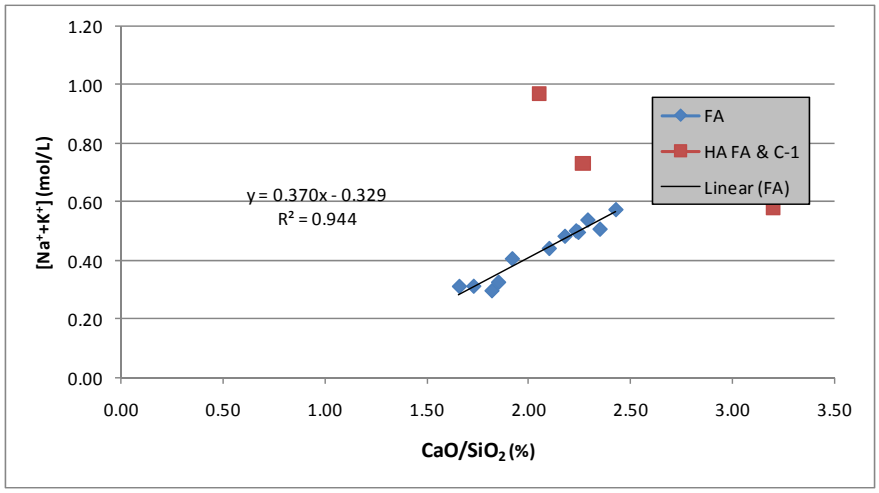

Figure 11.25: Pore Solution Concentration (CaO/SiO_2)

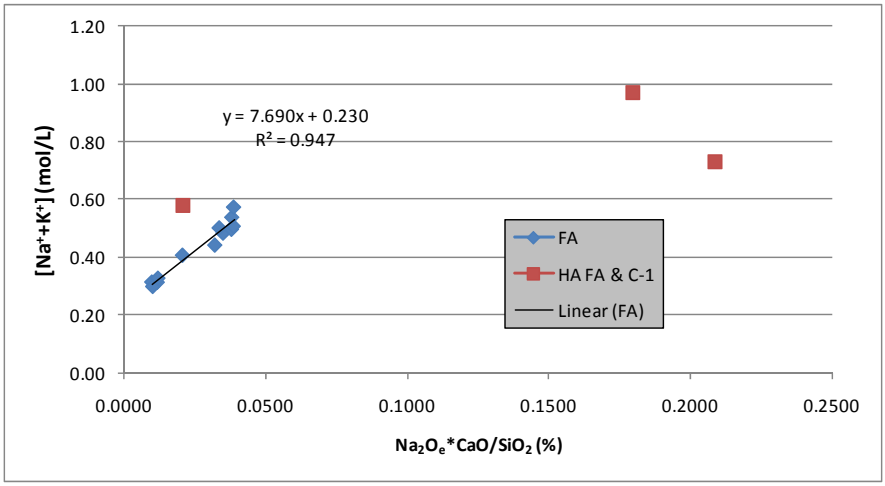

Figure 11.26: Pore Solution Concentration (Na_2O_exCaO/SiO_2)

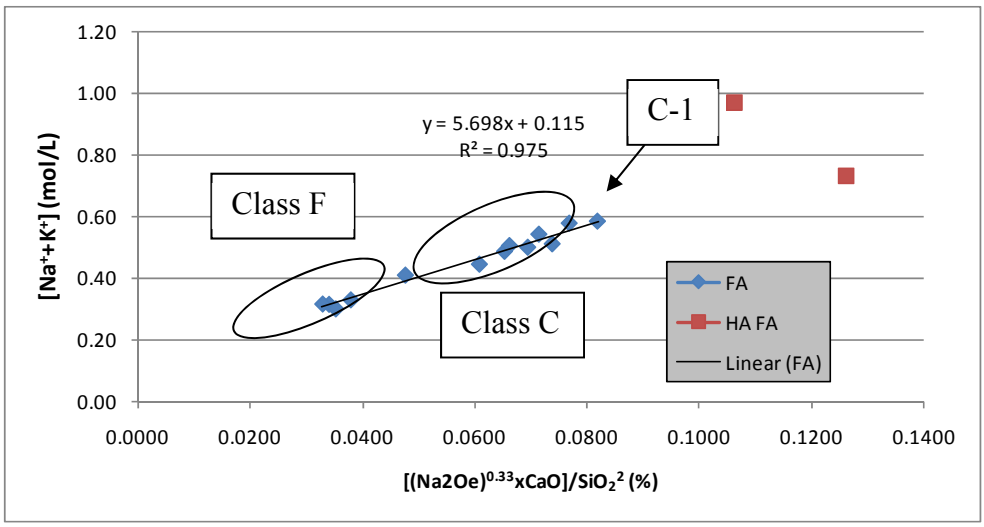

Figure 11.27: Pore Solution Concentration (Chemical Index)

None of the previous figures accounted for the absence of fly ash or the high alkali mixes. Using the chemical index in Figure 11.27, produced by Dr. Thomas, the control mix is included in the trend line. As this chemical index of the binder increases so does the alkali pore solution concentration and the figure also distinguishes the two classes of fly ashes. The r-squared value here is the highest of all the previous figures. Unfortunately, this chemical index still does not relate the two high alkali fly ash mixes.

11.3.2 Leeching

The leeching experiment was conducted to investigate the amounts of alkali that can be leached from paste samples into simulated pores solutions of different alkali concentrations. The solutions were created with the same K_20/Na_20 ratio as the paste binder to be placed in it. The procedure is described in detail in section 3.2.7. The same paste samples used for the pore solution extraction were used for this experiment.

Figure 11.28 displays the results of the leeching experiment at 0 M OH- with the available alkalis expressed on the y-axis. The term *available alkalis* refers to the amount of alkalis that were released from the paste into the simulated pore solutions. They are expressed as Na2Oe% of the mass of the binder of the cementing materials. The mass of the cementing materials were corrected for evaporable and bound water with a correction for LOI. The concentrations of the alkalis were also corrected for the small amounts of pore fluid contributed by the paste when soaked into the solution.

Figure 11.28 illustrates that the higher calcium and higher alkali fly ashes released more alkalis into solution than the low calcium fly ashes. Similar relationships appear in the figures of different OH- concentrations in Appendix C. The two classes of fly ashes appear to be separated by the 1% available Na_2O_e line off of the y-axis.

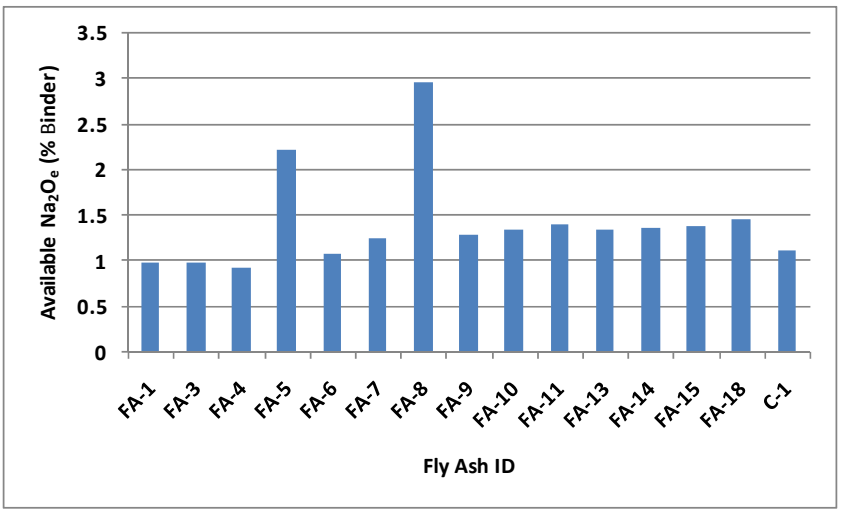

Figure 11.28: Leeching at 0 M OH-

Figures 11.29 through 11.32 show how the chemical compositions of the paste binder factor into the amount of available alkalis when placed in distilled water. Again we notice a positive correlation as CaO increases and a negative correlation as SiO_2 increases. The two high alkali fly ashes and C-1 do not fit the trend that the others follow. Figure 11.31 illustrates that the amount of alkalis present in the binder does not affect the amount of available alkalis as much as CaO and SiO_2 do. The trend for this set of data is not as strong.

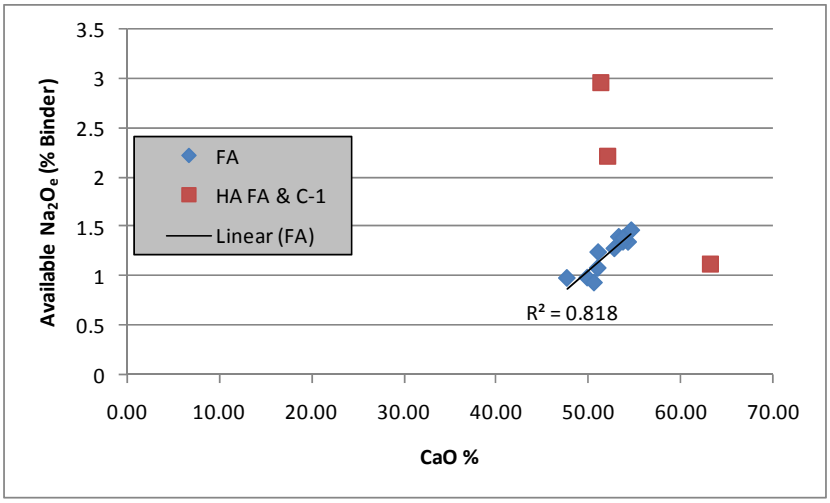

Figure 11.29: Leeching at 0 M OH- (CaO)

When combing the three chemical parameters into the chemical index described before, we again see a positive correlation. Figure 11.32 shows that as this chemical index increases, so does the amount of available alkalis. This figure is displaying only the results from the paste placed in distilled water.

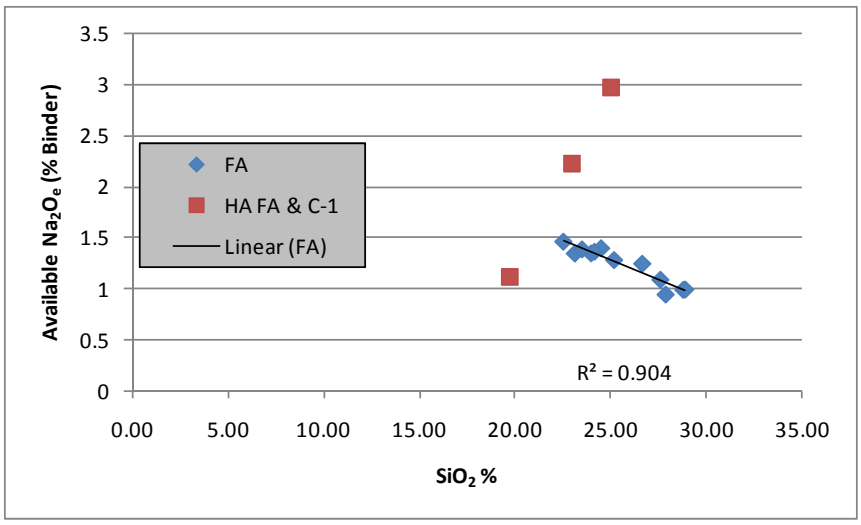

Figure 11.30: Leeching at 0 M OH- (SiO_2)

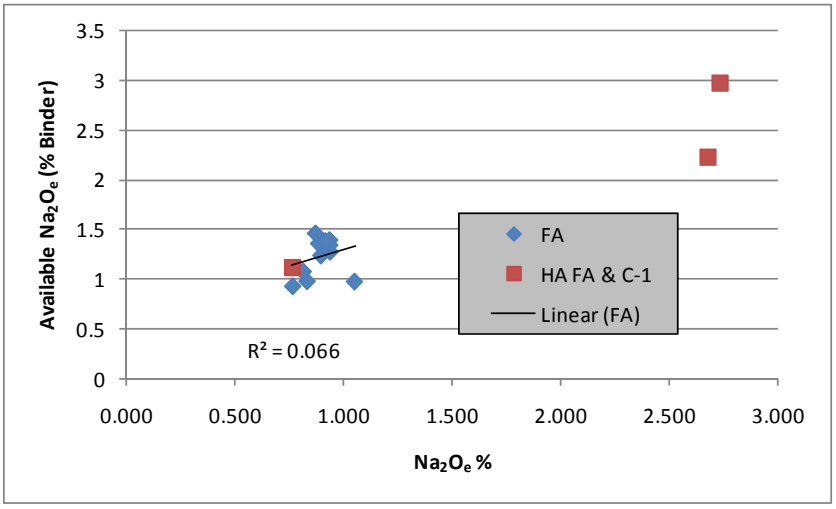

Figure 11.31: Leeching at 0 M OH- (Na_2O_e)

Figures 11.32–11.36 show the chemical index being linked to the available alkalis when the paste was place in solutions of different alkalinity. Notice in Figure 11.32 how the majority of the data set is between 1.5% and 1.0% alkalis except for FA-5 and FA-8. Now, in Figure 11.33 we can see this same group migrated between roughly 1.5% and 0.5%. This figure is displaying the results for a simulated pore solution of 0.1 M OH-. Figure 11.34 displays the results of concentrations at 0.2 M OH-. The same thing occurs as the concentration increased. The data set moved the available alkali range of 1.0 to 0%. In this figure we can see a data point in the negative region. This means that the paste did not release any alkalis but it instead absorbed or bound alkalis.

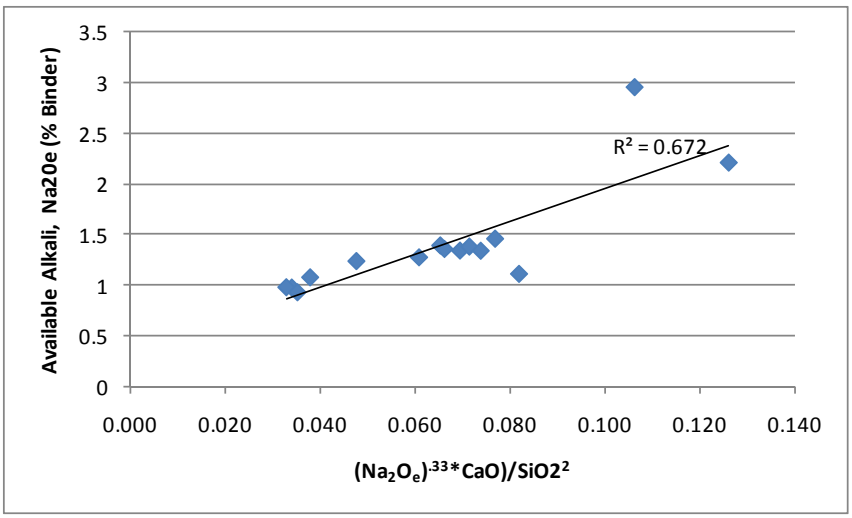

Figure 11.32: Leeching at 0 M OH- (Chemical Index)

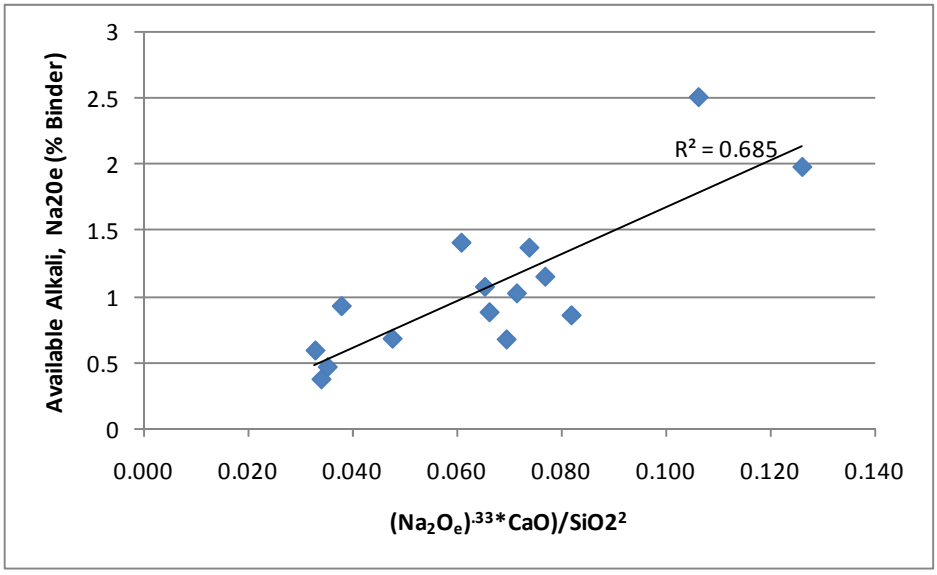

Figure 11.33: Leeching at 0.1 M OH- (Chemical Index)

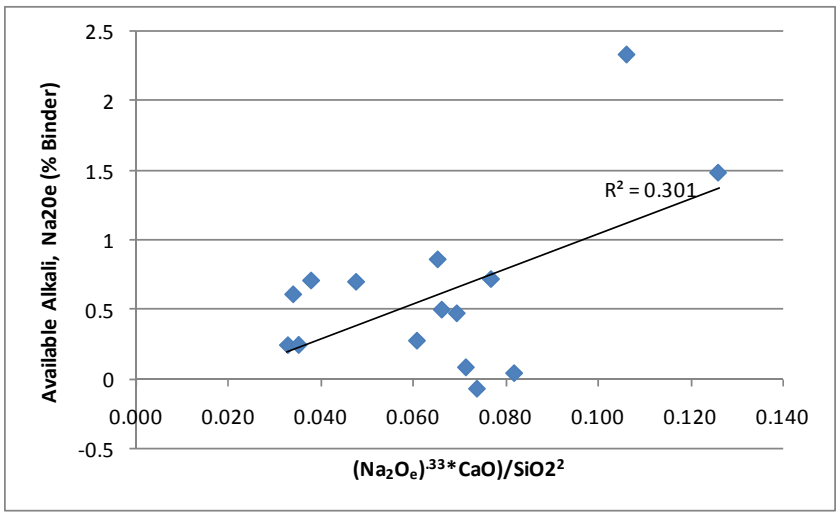

Figure 11.34: Leeching at 0.2 M OH - (Chemical Index)

This trend discontinues in Figure 11.35 as the concentration is increased to 0.3 M OH-. The set of data is spread out linearly between 0.5 and 2.5%. The slope of the trend line is greater; it also fits the data set well. In this figure we can make the distinction between the two fly ashes as the upper right group are Class C and the lower left group are Class F. This figure, however, did not accommodate the results for the high alkali fly ashes as the previous figures did.

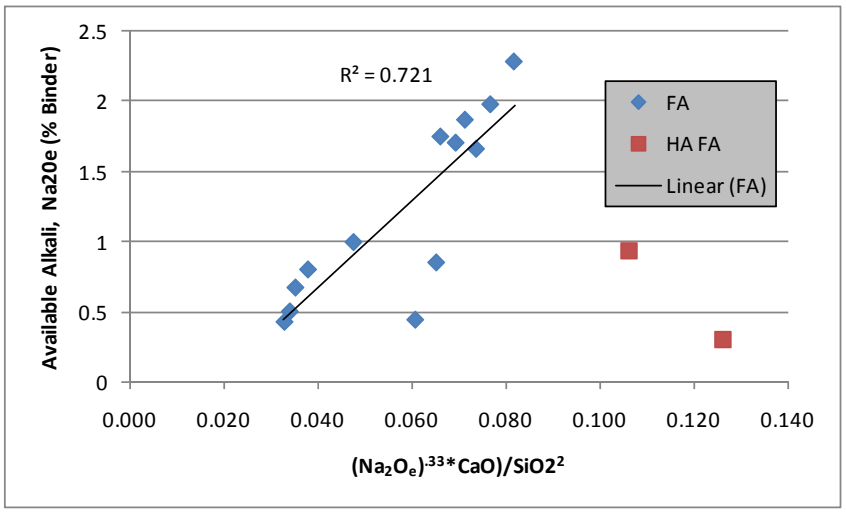

Figure 11.35: Leeching at 0.3 M OH- (Chemical Index)

Figure 11.36 shows the results for the paste samples placed in 0.6 M OH- solutions. The results for this test were completely different from the others. At this concentration the data set displayed a negative correlation as the chemical index increased. Several of the data points are in the negative range meaning the samples absorbed alkalis. This is unusual because the points that absorbed alkalis are the fly ashes with high alkalis.

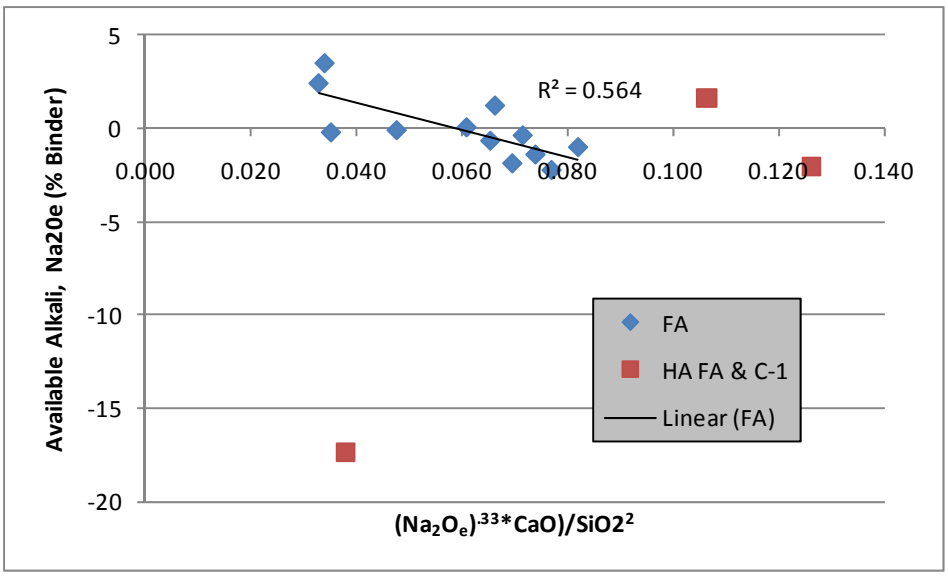

Figure 11.36: Leeching at 0.6 M OH- (Chemical Index)

Figure 11.37 illustrates the entire data set for this leeching experiment. The plot is congested with the large amount of data but the overall trend can be seen. The majority of the fly ashes follow this trend. The amount of available alkalis decrease as the simulated pore solution concentration goes from 0 to 0.2 M. From 0.2 to 0.3 M there is a significant increase in the available alkalis but it goes down again from 0.3 M to 0.6 M.

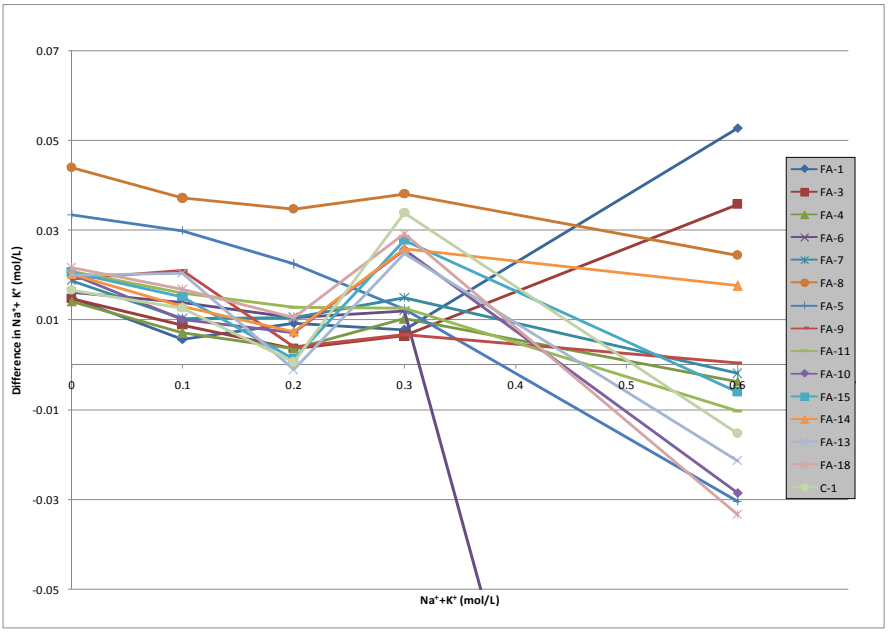

Figure 11.37: Overall Data Set for Leeching Experiment

11.3.3 Available Alkalis

This section discusses the results of the available alkali experiment from ASTM C 311. The procedure is explained in detail in section 10.2.4. The purpose of this experiment is to

determine the amount of alkalis that are available from fly ashes for reaction with aggregates. Because some of the fly ash alkalis can be tied up in crystalline phases, this experiment attempts to determine how much are not.

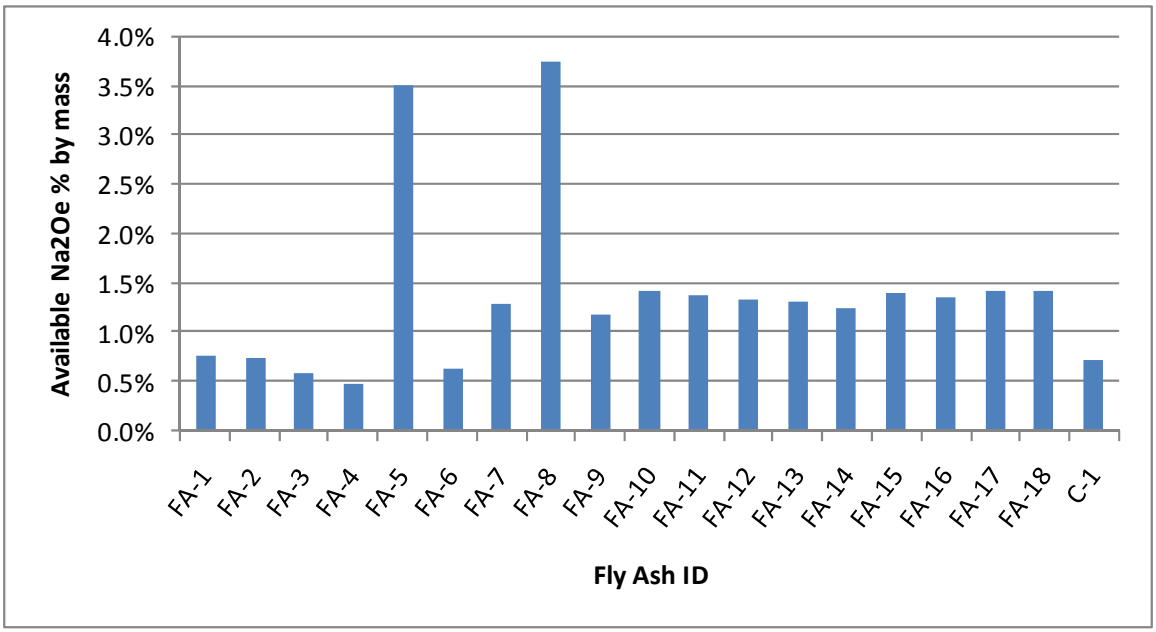

Figure 11.38: Available Alkalis

Figure 11.38 shows the results for this experiment performed on all 18 fly ashes. The two high alkalis clearly had a large amount of alkalis available. The Class F fly ashes had significantly fewer alkalis available than the Class C fly ashes. FA-7 had a large amount of its alkalis present especially for a Class F ash but it does have a high amount of CaO relatively speaking. It appears as if the 1.0% available alkalis is the distinction between Class C and F fly ashes. All Class C fly ashes have above 1.0% available alkalis and Class F fly ashes are below.

Figures 11.39–11.41 relate the available alkalis to the chemical composition of the fly ash to the amount of available alkalis. Relationships between CaO and available alkalis were not performed because of the addition of hydrated lime to the fly ashes during the experiment.

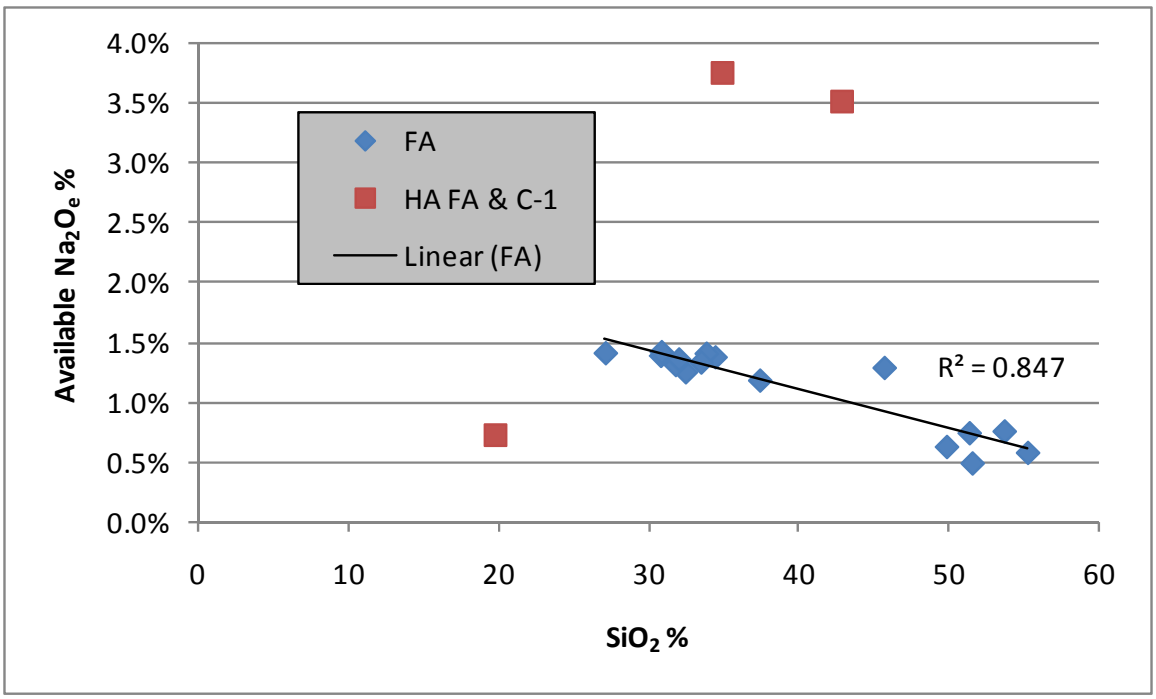

Figure 11.39: Available Alkalis (SiO_2)

Figure 11.39 relates the available alkalis to the SiO_2 content of the fly ash. As SiO_2 increases, the amount of available alkalis decreases. The high alkali fly ashes and cement again did not fit the trend but the rest of the group had a r-squared value of 0.847. Here we can also see the distinction between both classes of fly ash with Class F being cluster on the right and Class C being the group on the left.

Figure 11.40 shows this relationship with SiO_2 but the y-axis expresses the available alkalis as a percentage of the total alkalis. Now here we can see that some fly ashes showed over a hundred percent of their alkalis being available. This is probably due to some error but what can still be noticed here is that the higher SiO_2 fly ashes had significantly less percentages of their alkalis available.

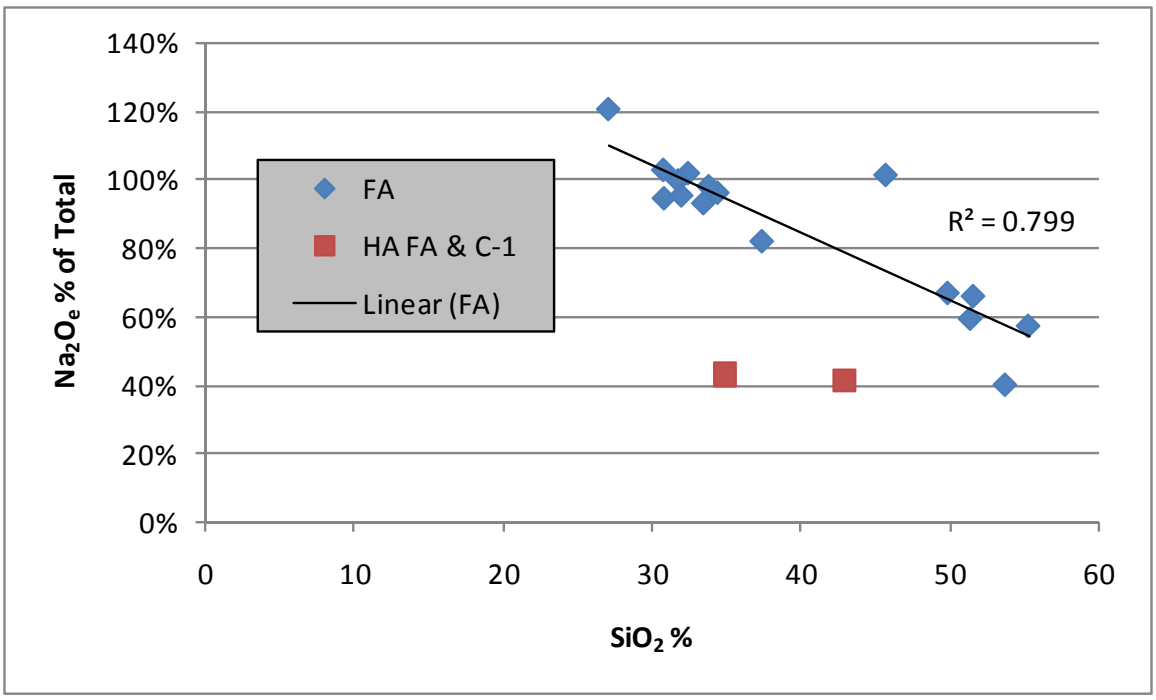

Figure 11.40: Available Alkalis/Total (SiO_2)

Figure 11.41 shows the relationship between available alkalis and alkali contents of the fly ashes. A weak trend can be noticed, as alkali content increase so does the amount of available alkalis for ASR reaction. The high alkali fly ashes followed this trend as well with their large Na_2O_e percent resulting in high amounts of available alkalis.

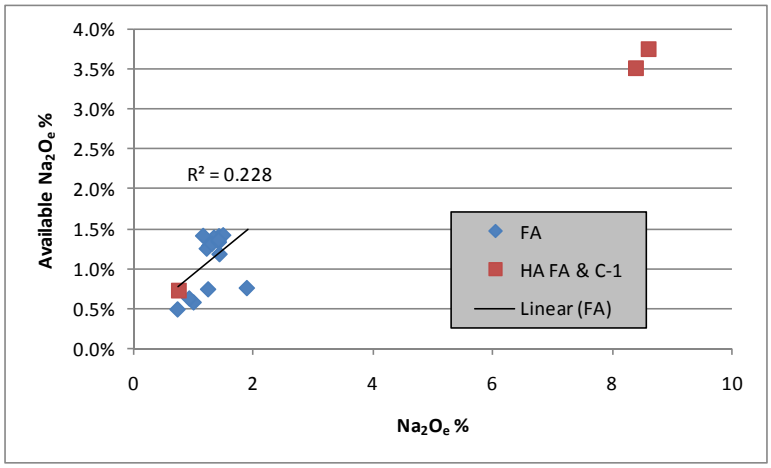

Figure 11.41: Available Alkalis (Na_2O_e)

Chapter 12. Discussion

The experiments conducted for this report were performed because of the importance to be able to characterize fly ash in a way that best predicts how it will perform in concrete with an emphasis on ASR. The data resulting from these experiments were determined using a series of short-term test discussed previously. In this section, some of this data will be compared and implemented with long-term data.

The following three figures contain expansion results from ASTM C 1260 & 1293, and outdoor exposure blocks. Figure 12.1 has 2-year expansion data from ASTM C 1293 concrete prisms with 35% fly ash replacement. The x-axis has the corresponding results from the paste pore solution study with 25% fly ash replacement. There had not been any 1293 testing performed with 25% fly ash replacement so the data for 5% was used. Despite this fact, there appears to be a linear relationship between the paste pore solution alkali concentration and concrete expansion. As the pore solution increases, the ASR expansion percentage increases. This figure illustrates how the pozzolanic activity of fly ash reduces pore solution alkalis thus reducing ASR induced expansion. Notice the differences between FA-7 and FA-10. This fly ash changed from a Class F to Class C fly ash. This difference in the chemical composition resulted in these differences on the plot. FA-10 had an increase 0.1 M in the pore solution and this also resulted in an increase of expansion by more than 0.025%. The highest data point on the plot is FA-18. This fly ash with the highest calcium content also had the highest pore solution concentration corresponding to the highest concrete expansion.

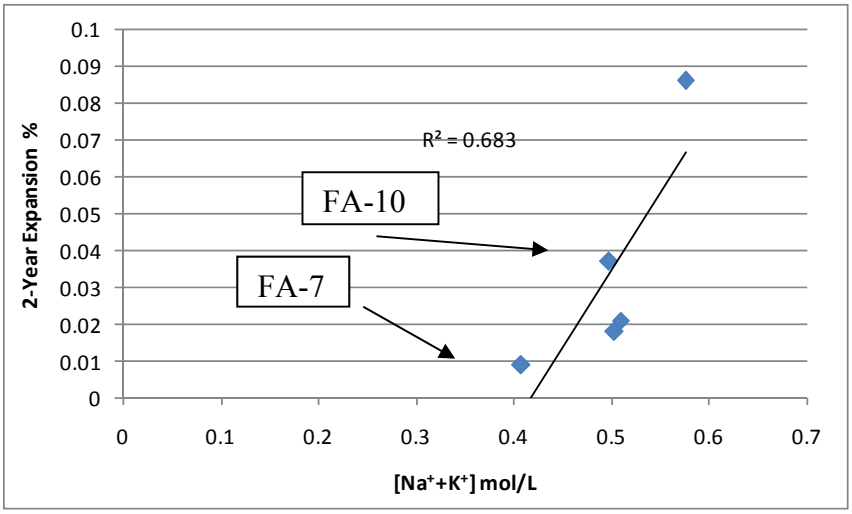

Figure 12.1: ASTM C 1293 35% Fly Ash Expansion with Pore Solution Study

Figure 12.2 illustrates similar relationships but with ASTM C1260 results with 30% fly ash replacement. There is a linear relationship between the paste pore solution and mortar expansion. As the pore solution increases, so does the expansion of the mortar bar. The lowest data point is FA-3 and the highest point is FA-11. The points in between also have calcium contents that are in between FA-3 & 11. There are significant differences in pore solution concentrations and expansion.

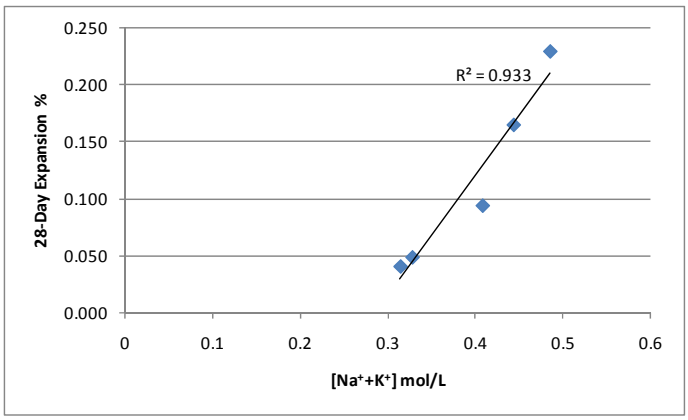

Figure 12.2: ASTM C 1260 Expansion with Pore Solution Study

Figure 12.3 illustrates between the chemical index and the outdoor exposure block expansion. This figure has four different sets of plots because of the differences of age and aggregate type. This set of data consists of three different aggregates but aggregate WR has two sets because they are of different ages. This set of data consists of several different fly ashes used at different replacement levels. The chemical index corresponds greatly with the expansion data. This index creates a great trend but it is high dependent on the aggregate used and age of the specimen. Notice the high r-squared value of aggregate WR. This fine aggregate has an almost perfect relationship between the data points and the trend line. The other aggregates showed similar trends but not nearly as strong. The points that are on the far right of each set are the control mixes. These mixes have no fly ash in them and have large differences in chemical index and expansion data. For example, the red squares represent FA-13 at 30, 35, and 40% replacement and its control mix. Notice the large difference between 30% replacement and its control mix. The difference is large even with the use of a high calcium fly ash. The PL mixes had Class F fly ashes used and notice how almost the entire located on the bottom left corner of the chart. The only data point on the right side is the control. These mixes have replacement levels between 20 and 30% while the Class C mixes had higher replacement levels and did not perform as well. Lower replacement levels of Class F fly ash outperformed the higher replacement levels of Class C mixes.

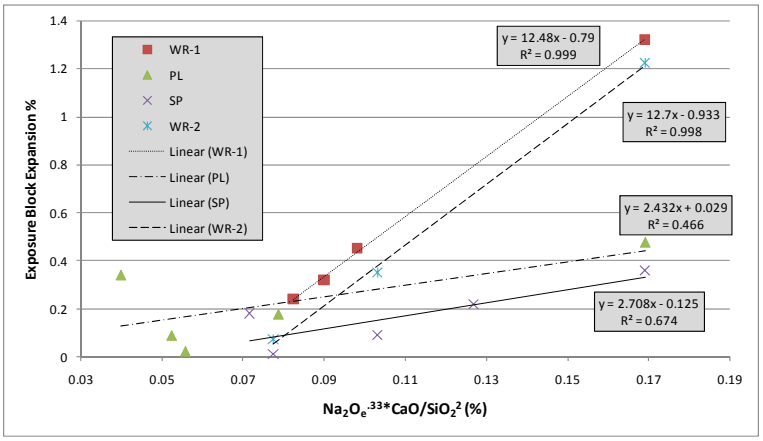

Figure 12.3: Exposure Block Data with Chemical Index

Figure 12.4 is the same as the figure in the pore solution section but illustrates the difference between FA-7 and FA-10. Recently this fly ash underwent a change in its chemical composition. The chemical compositions for these two fly ashes are located in Table 12.1. This change from Class F to Class C resulted in an increase of the paste pore solution concentration from 0.40 to 0.50 with a 25% replacement level. The chemical index relates the change in chemical composition to the change in pore solution alkali content. The alkali content did not change very much but the CaO and SiO_2 did and this result in the fly ash not being as effective in lowering pore solution alkalis.

Table 12.1: Chemical Composition of FA-7 & 10

ID	CaO	SiO_2	Na_2O_e
FA-7	15.3	45.7	1.3
FA-10	22.9	33.9	1.4

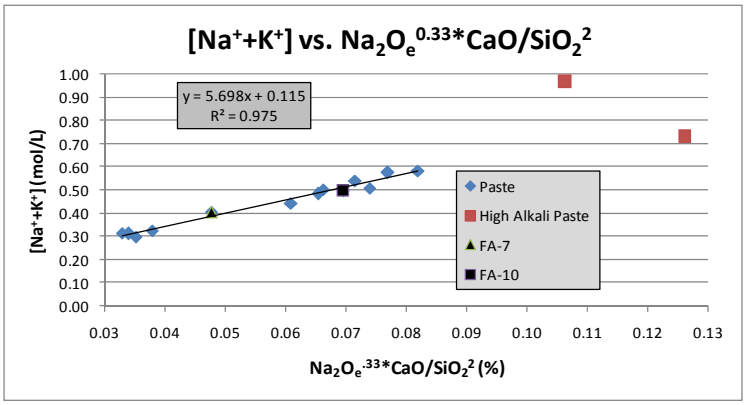

Figure 12.4: Pore Solution Study with Chemical Composition Change of Fly Ash

The chemical index will not work completely in predicting pore solution alkali concentration because the pore solution is dependent on many parameters other than the chemical composition of the binder. Aggregates and fineness of the fly ash can also effect pore solution concentrations. The chemical index can, however, be used to roughly estimate what the pore solution can be. The equation from the trend line from the pore solution data using the chemical index was used on ASTM C 1293 specimens. Figure 12.5 used the equation y = 5.698x + 0.115 to estimate the pore solution concentration of concrete prisms with four different fly ashes with different alkali dosages. This plot shows how the Class F fly ash is predicted to have a lower pore solution than the Class C fly ashes according to the chemical index.

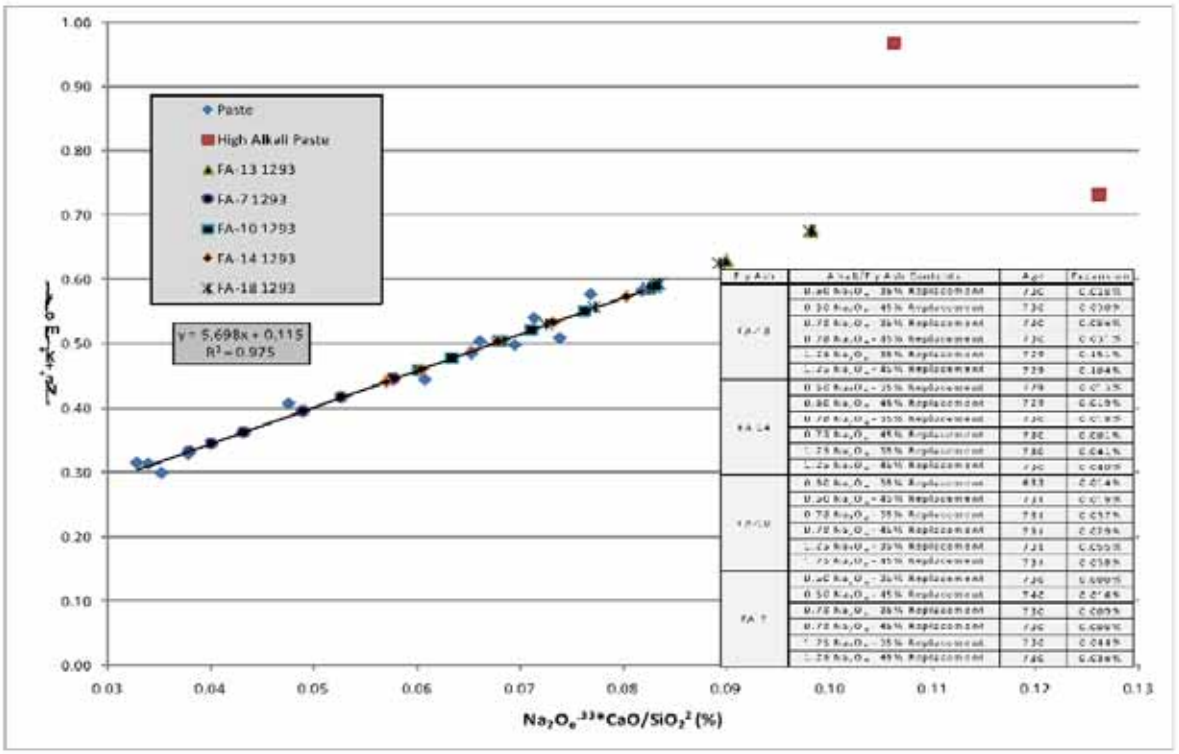

Figure 12.5: Comparison of ASTM C 1293 Pore Solution

Chapter 13. Conclusion

13.1 Summary of Project

In this study, various characteristics/properties of a wide range of fly ashes were evaluated and correlated to the various fly ashes ability to reduce ASR-induced expansion in laboratory bars/prisms and in some cases, outdoor exposure sites.

13.2 Conclusions

Although all the fly ashes studied reduced expansion to some extent, the efficacy of prevention is strongly linked to fly ash chemistry and mineralogy. Through correlating fly ash characteristics to short- and long-term ASR test results, insight was gained in better understanding what fly ash traits most impact the efficacy of reducing expansion due to ASR. The calcium oxide (CaO) content was found to be a strong indicator of fly ash performance, as expected from many past studies. Strong correlations were found between the effects of pore solution composition on expansion, and predictive models were applied, based on previous research by Thomas, providing a useful tool for practitioners to estimate the effectiveness of a given fly ash, based on its chemical and mineralogical composition (including alkalis).

13.3 Future Work

Future work related to the characterization of fly ash and its relation to ASR includes the following:

- Development of standardized test method for rapidly determining the contribution of fly ash alkalis to the pore solution in concrete.
- Validation of model aimed at predicting pore solution of concrete based on chemical/mineralogical composition of binder system (including fly ash).
- Evaluation of additional fly ashes to enhance the database developed under this project.

References

ASTM Standard, C114. *Standard Test Methods for Chemical Analysis of Hydraulic Cement*. West Conshohocken, PA: ASTM International, 2011. Print. www.astm.org.

ASTM Standard, C1260. *Standard Test Method for Potential Alkali Reactivity of Aggregates (Mortar-Bar Method)*. West Conshohocken, PA: ASTM International, 2007. Print. www.astm.org.

ASTM Standard, C1293. *Standard Test Method for Determination of Length Change of Concrete Due to Alkali-Silica Reaction.* West Conshohocken, PA: ASTM International, 2008. Print. www.astm.org.

ASTM Standard, C1567. *Standard Test Method for Determining the Potential Alkali-Silica Reactivity of Combinations of Cementitious Materials and Aggregate (Accelerated Mortar-Bar Method)*. West Conshohocken, PA: ASTM International, 2011. Print. www.astm.org.

ASTM Standard, C305. *Standard Practice for Mechanical Mixing of Hydraulic Cement Pastes and Mortars of Plastic Consistency*. West Conshohocken, PA: ASTM International, 2012. Print. www.astm.org.

ASTM Standard, C311. *Standard Test Methods for Sampling and Testing Fly Ash or Natural Pozzolans for Use in Portland-Cement Concrete*. West Conshohocken, PA: ASTM International, 2011. Print. www.astm.org.

ASTM Standard, C430. *Standard Test Method for Fineness of Hydraulic Cement by the 45-Mm (No. 325) Sieve*. West Conshohocken, PA: ASTM International, 2003. Print. www.astm.org.

ASTM Standard, C618. *Standard Specification for Coal Fly Ash and Raw or Calcined Natural Pozzolan for Use in Concrete*. West Conshohocken, PA: ASTM International, 2012. Print. www.astm.org.

Baert, G., et al. "Interaction between the Pozzolanic Reaction of Fly Ash and the Hydration of Cement." *Ghent University*: n. page. Print.

Barlow, Donald F., and Peter J. Jackson. "The Release of Alkalis from Pulverized-Fuel Ashes and Ground Granulated Blast furnace Slags in the Presence of Portland Cements." *Cement and Concrete Research* (1988): n. page. Print.

Berube, M. A., et al. "Influence of Particle Size Distribution on the Effectiveness of Type-F Fly Ash in Suppressing Expansion Due to Alkali-Silica Reactivity." *SP 153-10 Milwaukee Conference*: n. page. Print.

Chancey, Ryan Thomas. "Characterization of Crystalline and Amorphous Phases and Respective Reactivities in a Class F Fly Ash." Diss. 2008. Print.

Diamond, Sidney. "Effects of Two Danish Flyashes on Alkali Contents of Pore Solutions of Cement-Flyash Pastes." *Cement and Concrete Research* (1981): n. page. Print.

Duchesne, J., and M. A. Berube. "The Effectiveness of Supplementary Cementing Materials in Suppressing Expansion Due to ASR: Another Look at the Reaction Mechanisms Part 2: Pore Solution Chemistry." *Cement and Concrete Research* (1994a): n. page. Print.

Duchesne, Josee, and Marc-Andre Berube. "Available Alkalies from Supplementary Cementing Materials." *ACI Materials Journal* (1994b): n. page. Print.

"The Effectiveness of Supplementary Cementing Materials in Suppressing Expansion Due to ASR: Another Look at the Reaction Mechanisms Part 1: Concrete Expansion and Portlandite Depletion." *Cement and Concrete Research* (1993): n. page. Print.

Farbriarz, Josef, and Ramon L. Carrasquillo. *Effectiveness of Fly Ash Replacement in the Reduction of Damage Due to Alkali-Aggregate Reaction in Concrete*. N.p.: n.p., 1986. Print.

Fernandez-Jimenez, A., and A. Palomo. "Characterisation of Fly Ashes. Potential Reactivity as Alkaline Cements." *FUEL* (2003): n. page. Print.

Ferraris, Chiara F. *Alkali-Silica Reaction and High Performance Concrete*. N.p.: n.p., 1995. Print.

FHWA. N.p., 2011. Web. <http://www.fhwa.dot.gov/pavement/concrete/asr/history.cfm>.

Fournier, Benoit, and Marc-Andre Berube. "Alkali–Aggregate Reaction in Concrete: A Review of Basic Concepts and Engineering Implications." *Canadian Journal of Civil Engineering* (2000): n. page. Print.

Fraay, A. L., J. M. Bijen, and Y. M. Haan. "The Reaction of Fly Ash in Concrete. A Critical Examination." *Cement and Concrete Research* (1989): n. page. Print.

Garcia-Diaz, E., et al. "Mechanism of Damage for the Alkali-Silica Reaction." *Cement and Concrete Research* (2006): n. page. Print.

Geochemical Instrumentation and Analysis. N.p., 2012. Web. <http://serc.carleton.edu/research_education/geochemsheets/techniques/XRF.html>.

Glasser, F. P., and J. Marr. "The Alkali Binding Potential of OPC and Blended Cements." *Cemento* (1985): n. page. Print.

Helmuth, Richard, comp. *Alkali-Silica Reactivity: A Overview of Research*. N.p.: n.p., 1993. Print. SHRP-C-342.

Hemmings, R. T., and E. E. Berry. "On the Glass in Coal Fly Ashes: Recent Advances." *Materials Research Society* (1988): n. page. Print.

Hong, Sung, and F. P. Glasser. "Alkali Binding in Cement Pastes Part I. The C-S-H Phase." *Cement and Concrete Research* (1999): n. page. Print.

Hooton, R. D., and M. D. Thomas. "Pore Solution Analysis as a Tool for Studying Early –Age Hydration & Predicting Future Durability." Cement Hydration Summit. 2009. Print.

Huffman, Morris, and Michael D. Thomas, comps. *Use of Fly Ash in Concrete*. N.p.: ACI Committee 232, 2003. Print. ACI Committee 232.

Ideker, Jason H., et al. "Do Current Laboratory Test Methods Accurately Predict Alkali-Silica Reactivity?" *ACI Materials Journal* (2012): n. page. Print.

Junsomboon, Jaroon, and Jaroon Jamunee. "Determination of Potassium, Sodium, and Total Alkalies in Portland Cement, Fly Ash, Admixtures, and Water of Concrete by a Simple Flow Ime Photometric Systemnjection Fla." *Journal of Automated Methods and Management in Chemistry* (2011): n. page. Print.

Kutchko, Barbara G., and Ann G. Kim. "Fly Ash Characterization by SEM-EDS." *FUEL*: n. page. Print.

Lee, C. "Effects of Alkalies in Class C Fly Ash on Alkali-Aggregate Reaction." *Trondheim Conference* (1989): n. page. Print.

Lee, Chau. "Available Alkalis in Fly Ash and Their Effects on Alkali-Aggregate Rection." Diss. 1986. Print.

Lee, Chau, Scott Schlorholtz, and Turgut Demirel. "Available Alkalis in Fly Ash." *Materials Research Society* (1986): n. page. Print.

Lorenzo, P., et al. "Effect of Fly Ashes with High Total Alkalinity of the Pore Solution of Hydrated Portland Cement Paste." *Journal of the American Ceramic Society* (1996): n. page. Print.

Malvar, L. J., and L. R. Lenke. "Efficiency of Fly Ash in Mitigating Alkali Silica Reaction Based on Chemical Composition." *ACI Materials Journal* (2006): n. page. Print.

- - -. "Minimum Fly Ash Cement Replacement to Mitigate Alkali Silica Reaction." *U.S. Navy*: n. page. Print.

Malvern. N.p., 2012. Web. <http://www.malvern.com/processeng/systems/laser_diffraction/technology/technology.htm>.

Mings, M. L., et al. "Characterization of Fly Ash by X-Ray Analysis Methods." *Transportation Research Record*: n. page. Print.

Mitchell, L. D., et al. *The Mechanistic Differences between Alkali Silica and Alkali Carbonate Reactions as Studied by X-ray Diffraction*. N.p.: n.p., 2004. Print. NRCC.

Nixon, P. J., et al. "The Effect of a Pfa with a High Total Alkali Content on Pore Solution Composition and Alkali Silica Reaction." *Magazine of Concrete Research* (1986): n. page. Print.

Pepper, Leonard, comp. *Influence of Alkali Content of Fly Ash on Effectiveness in Preventing Expansion of Concrete*. N.p.: n.p., 1963. Print.

Rahhal, V., and R. Talero. "Fast Physics-Chemical Characterization of Fly Ash." *Journal of Thermal Analysis and Calorimetry* (2009): n. page. Print.

Ravina, Dan. "Optimized Determination of PFA (Fly Ash) Fineness with Reference to Pozzolanic Activity." *Cement and Concrete Research* (1980): n. page. Print.

Roy, Della, Karen Luke, and Sidney Diamond. "Characterization of Fly Ash and Its Reactions in Concrete." *Materials Research Society* (1985): n. page. Print.

Sakai, Etsuo, et al. "Hydration of Fly Ash Cement." *Cement and Concrete Research* (2005): n. page. Print.

Schulz, N. F. "Measurement of Surface Areas by Permeametry." *International Journal of Mineral Processing* (1974): n. page. Print.

Schure, Mark R., et al. "Surface Area and Porosity of Coal Fly Ash." *Environmental Science & Technology* (1985): n. page. Print.

Shehata, Medhat H. "The Effects of Fly Ash and Silica Fume on Alkali Silica Reaction in Concrete." Diss. 2001. Print.

Shehata, Medhat H., and Michael Thomas. "The Effect of Fly Ash Composition on the Expansion of Concrete Due to Alkali-Silica Reaction." *Cement and Concrete Research* (2000): n. page. Print.

Shehata, Medhat H., and Michael D. Thomas. "Alkali Release Characteristics of Blended Cements." *Cement and Concrete Research* (2006): n. page. Print.

Shehata, Medhat H., Michael D. Thomas, and Roland F. Bleszynski. "The Effects of Fly Ash Composition on the Chemistry of Pore Solution in Hydrated Cement Pastes." *Cement and Concrete Research* (1999): n. page. Print.

Taylor, H. F. "A Method for Predicting Alkali Ion Concentrations in Cement Pore Solutions." *Advances in Cement Reseach* (1987): n. page. Print.

Thomas, Michael. "The Effect of Supplementary Cementing Materials on Alkali-Silica Reaction: A Review." *Cement and Concrete Research* (2010): n. page. Print.

Touma, Wissam Elias. "Alkali-Silica Reaction in Portland Cement Concrete: Testing Methods and Mitigation Alternatives." Diss. 2000. Print.

Wang, Aiqin, Chengzhi Zhang, and Wei Sun. "Fly Ash Effects II. The Active Effect of Fly Ash." *Cement and Concrete Research* (2004): n. page. Print.

Wesche, K. "Test Methods for Determining the Properties of Fly Ash and of Fly Ash for Use in Buiilding Materials." *Materials and Structures* (1989): n. page. Print.

Wesche, Karlhans. *Fly Ash in Concrete: Properties and Performance: Report of Technical Committee 67-FAB Use of Fly Ash in Builiding*. London: E & FN Spon, 1991. Print.

Appendix A: ASTM C 1260 Testing Results

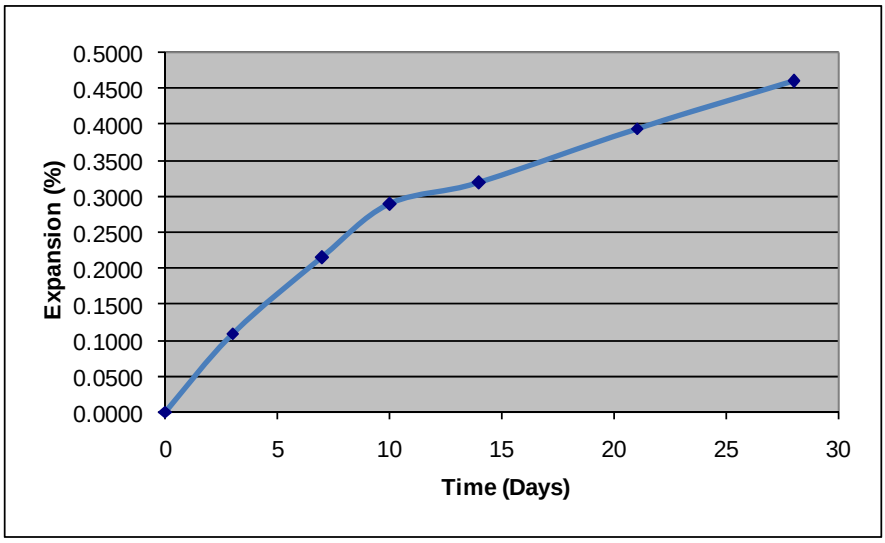

Figure A-1: C-1 (Control)

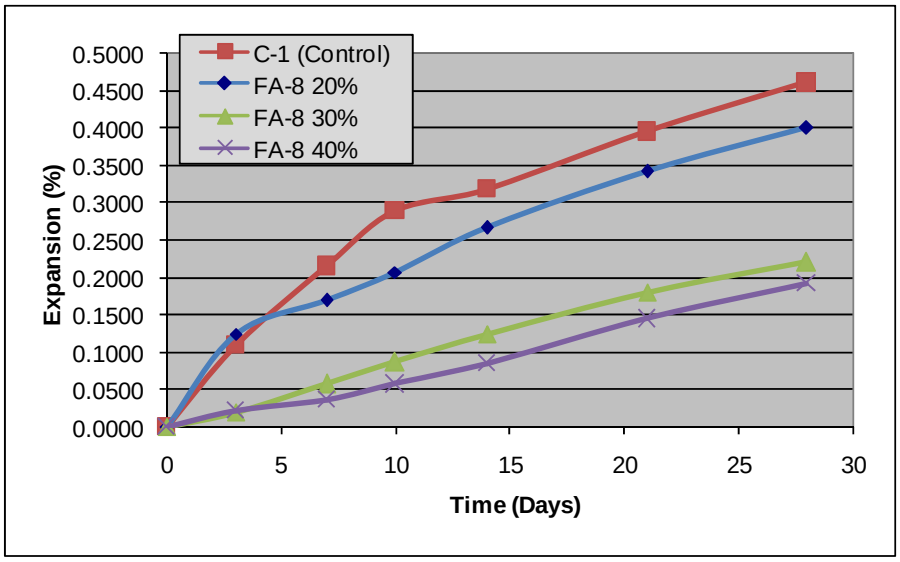

Figure A-2: FA-8 (1)

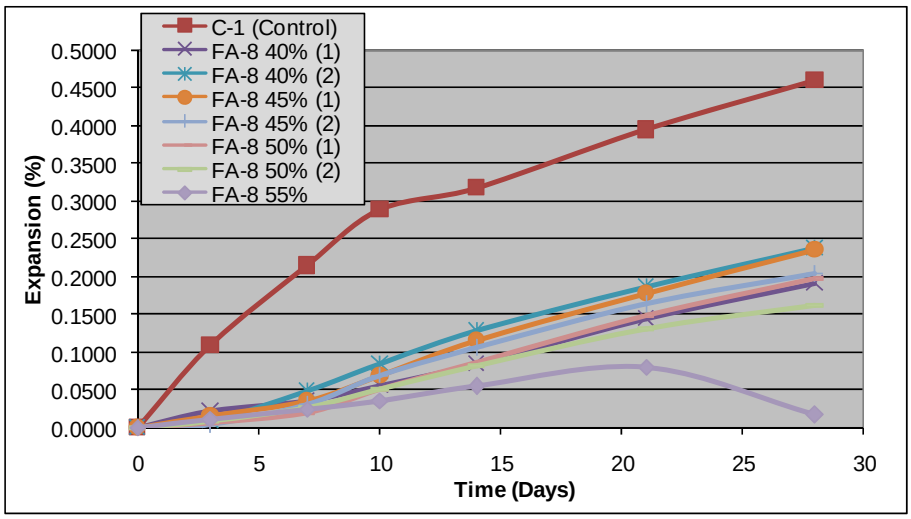

Figure A-3: FA-8 (2)

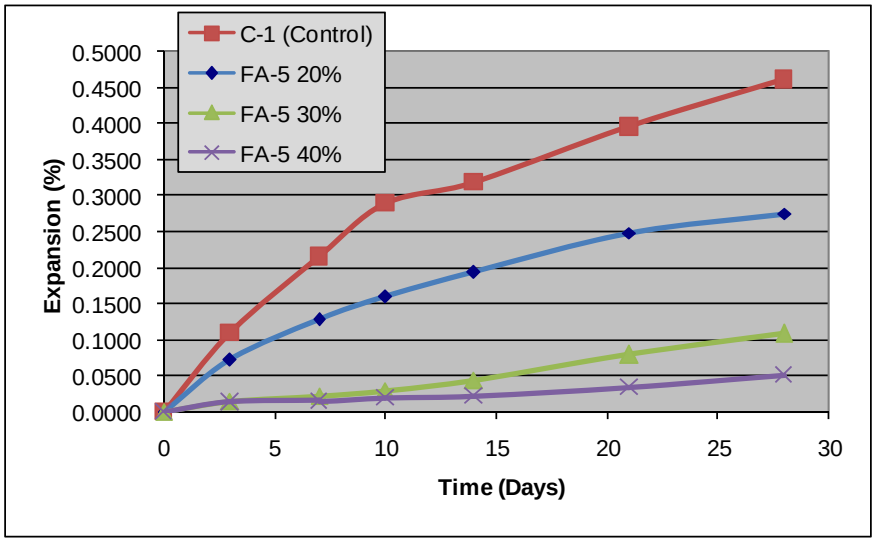

Figure A-4: FA-5

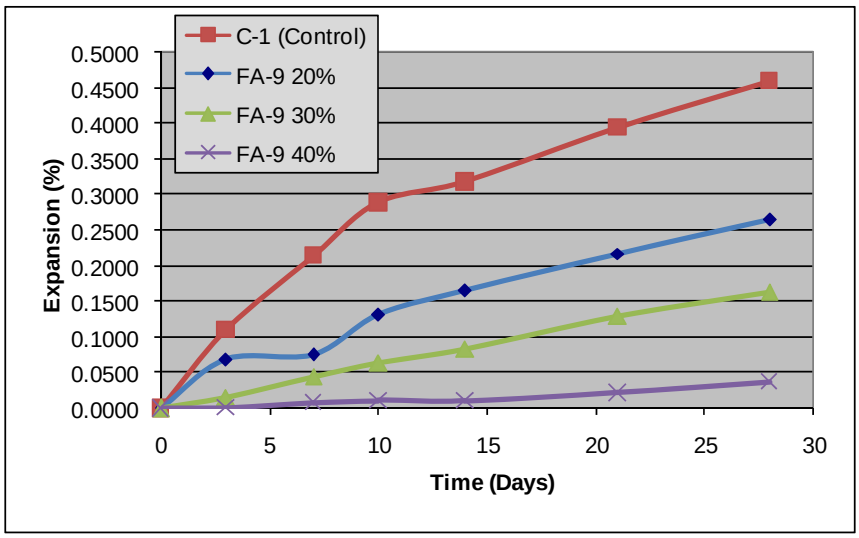

Figure A-5: FA-9

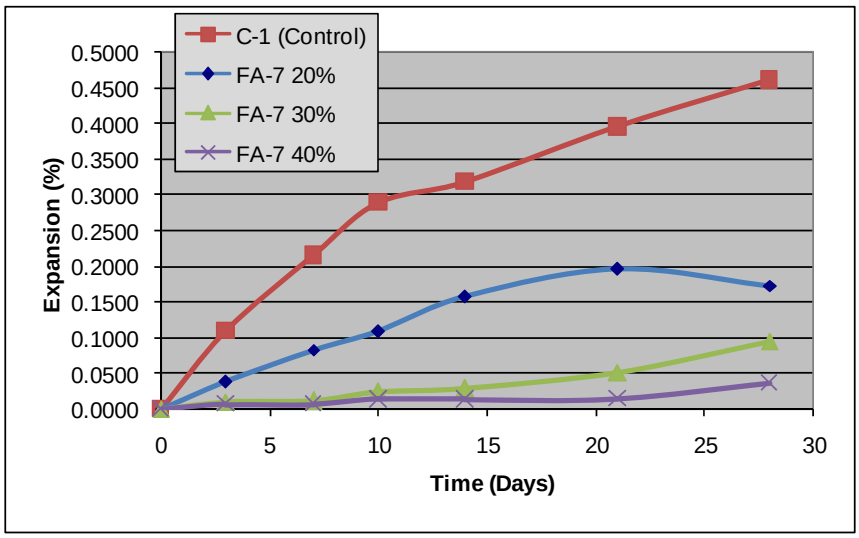

Figure A-6: FA-7

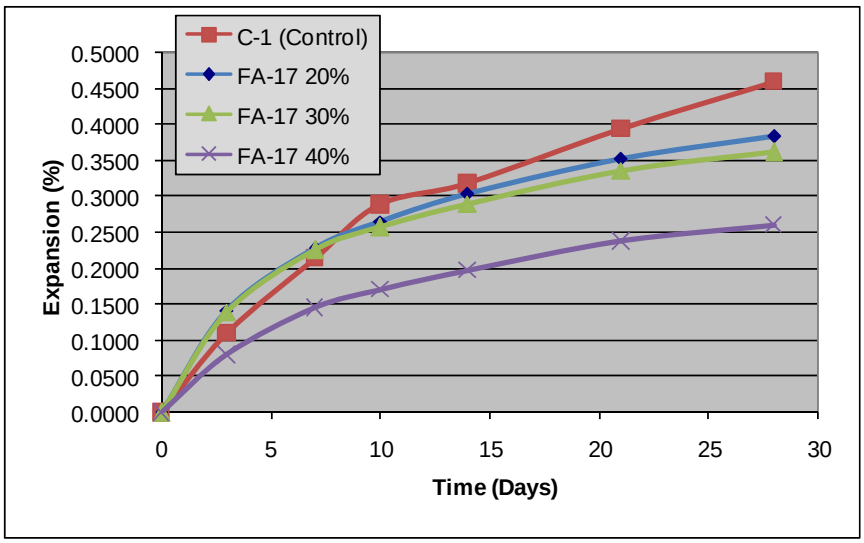

Figure A-7: FA-17

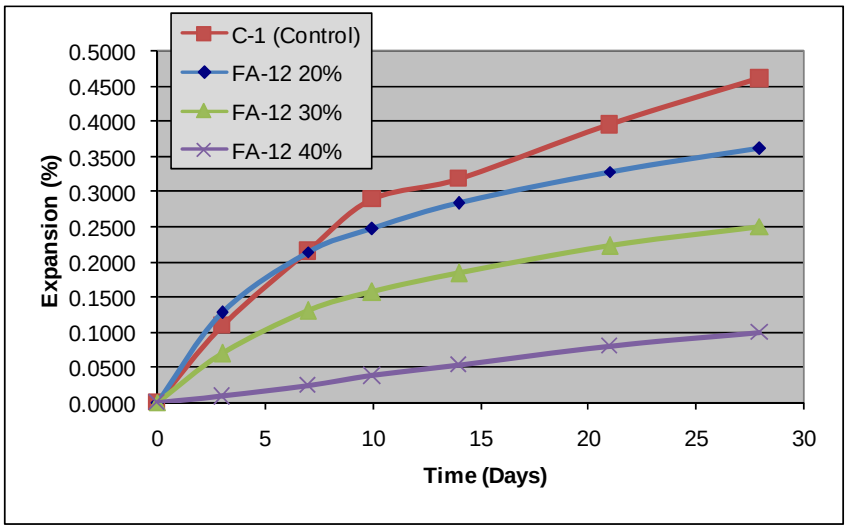

Figure A-8: FA-12

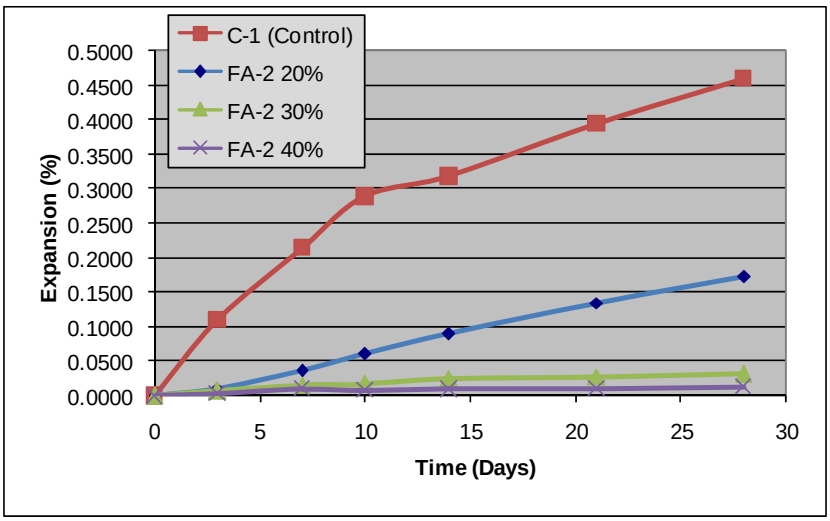

Figure A-9: FA-2

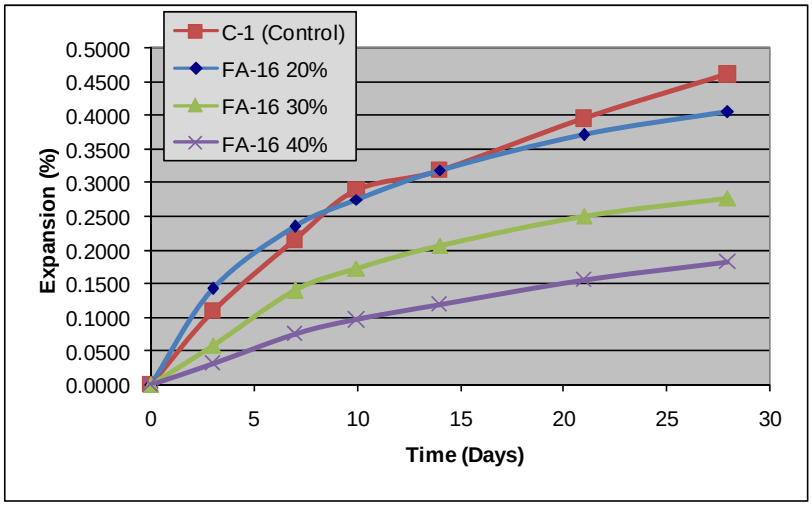

Figure A-10: FA-16

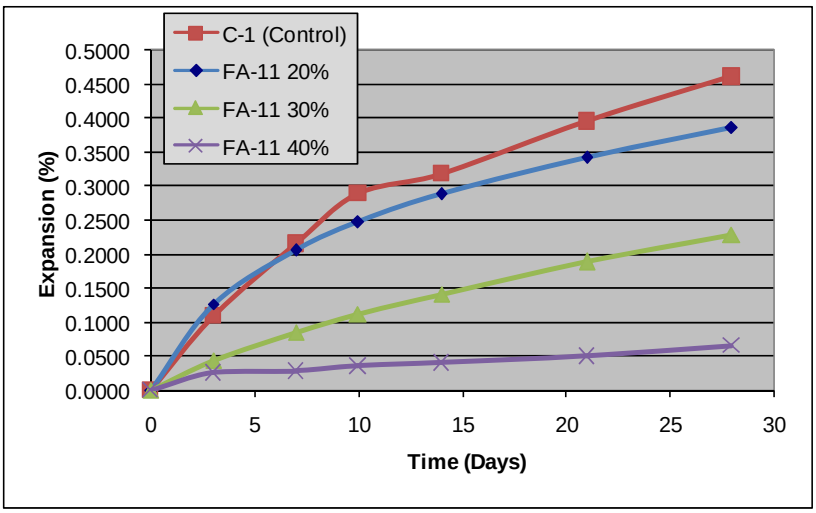

Figure A-11: FA-11

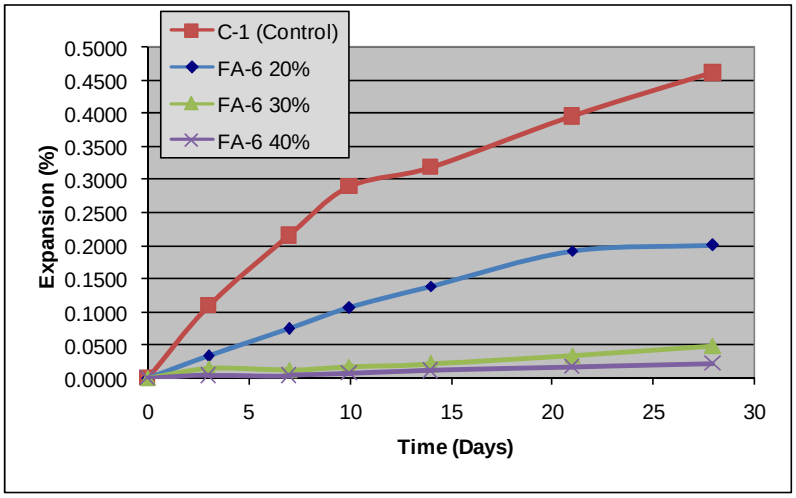

Figure A-12: FA-6

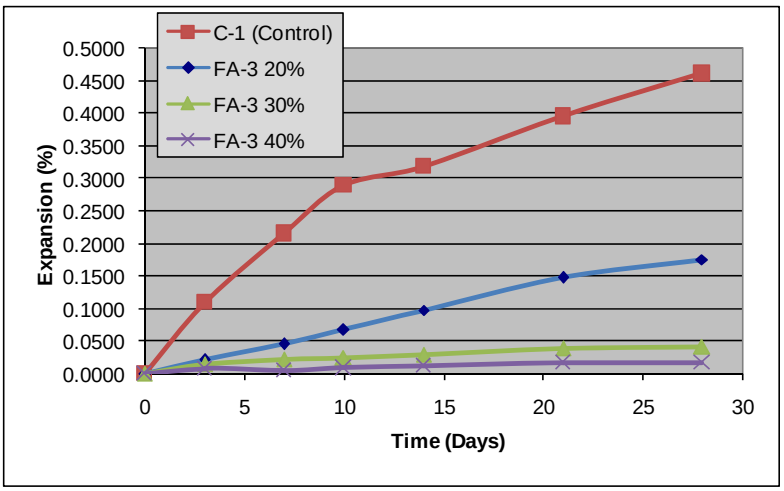

Figure A-13: FA-3

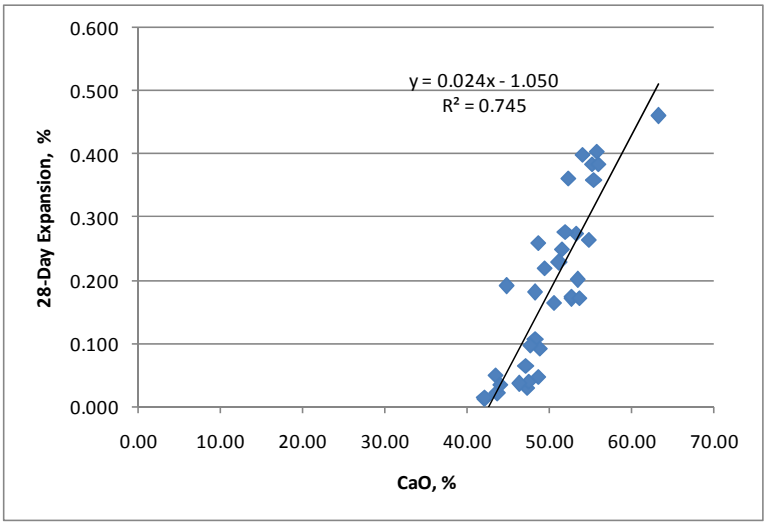

Figure A-14: ASTM C 1260 28 Days (CaO)

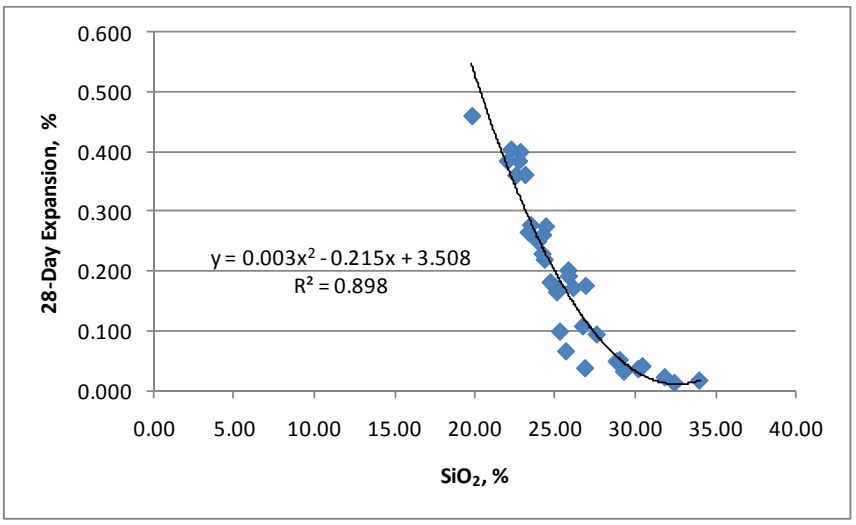

Figure A-15: ASTM C 1260 28 Days (SiO_2)

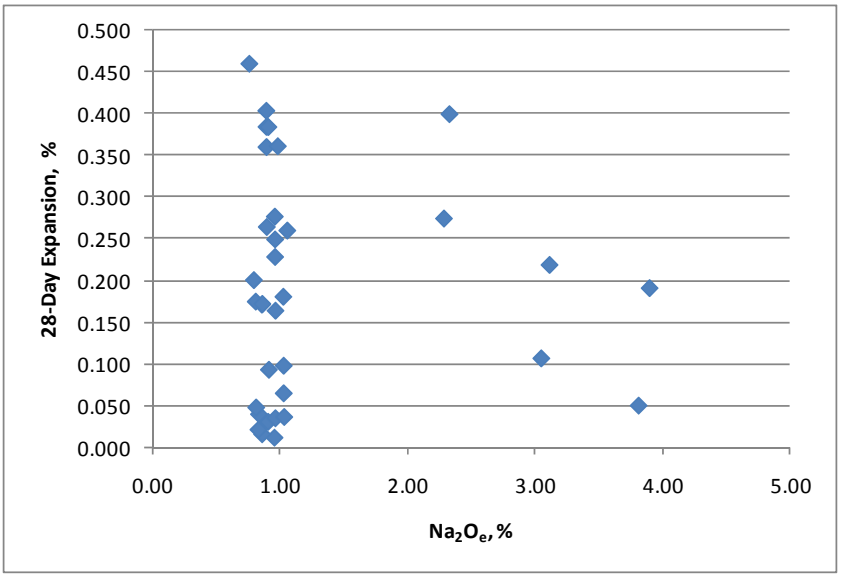

Figure A-16: ASTM C 1260 28 Days (Na_2O_e)

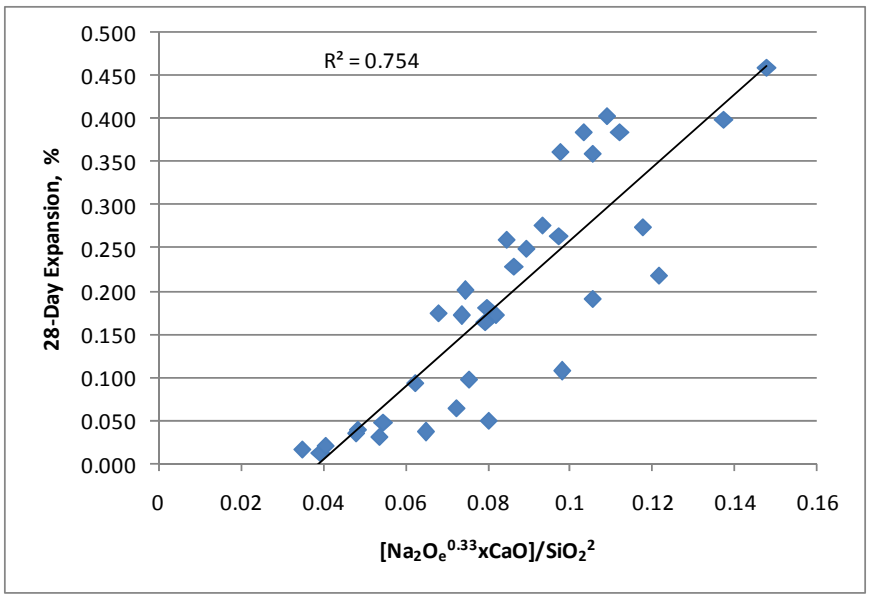

Figure A-17: ASTM C 1260 28-Day Chemical Index

Appendix B: XRF Trends

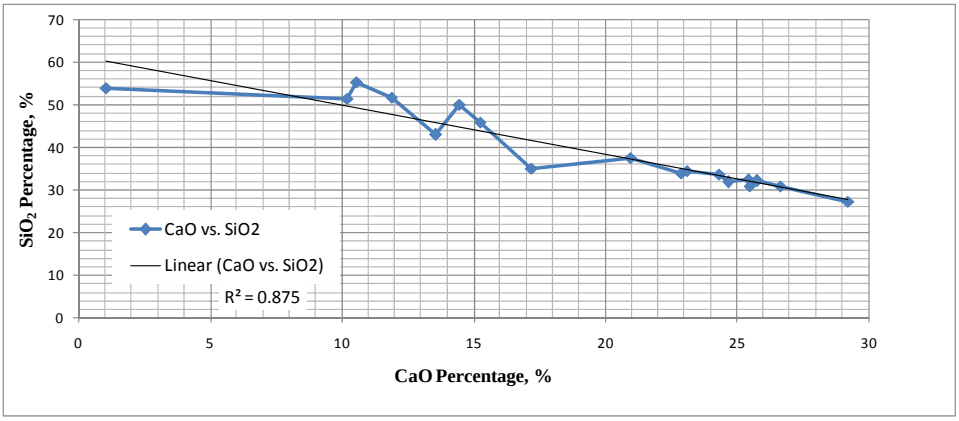

Figure B-1: CaO vs. SiO_2

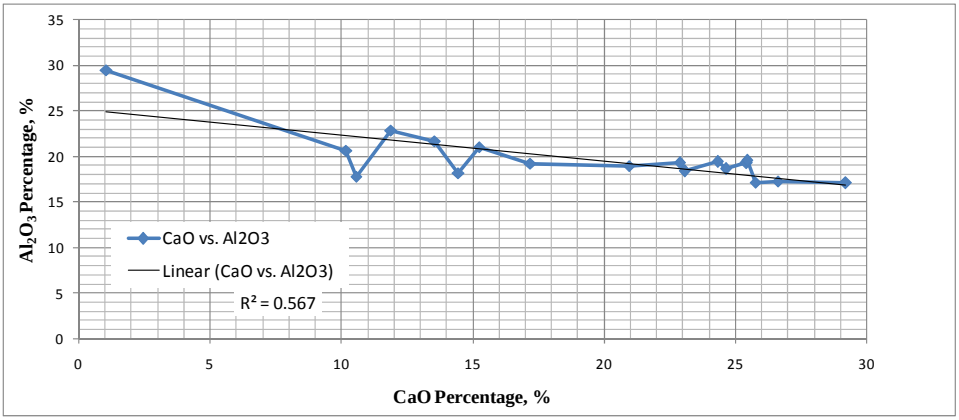

Figure B-2: CaO vs. Al_2O_3

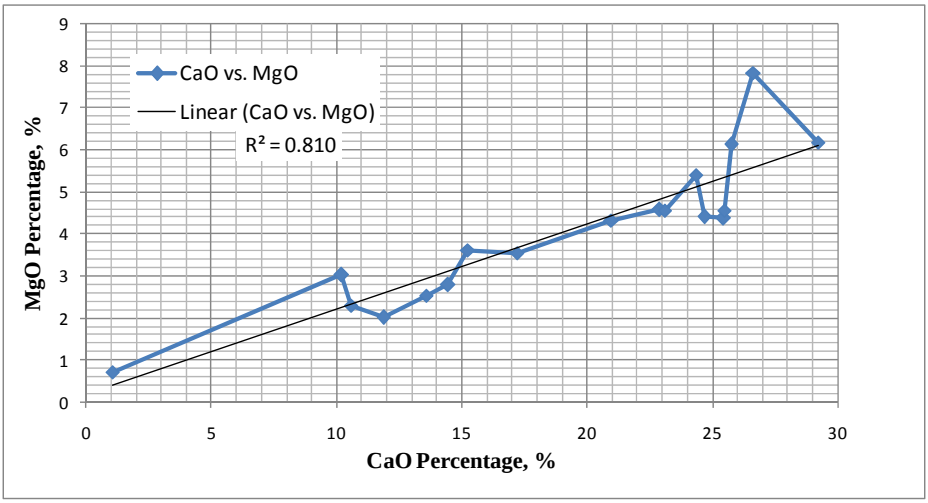

Figure B-3: CaO vs. MgO

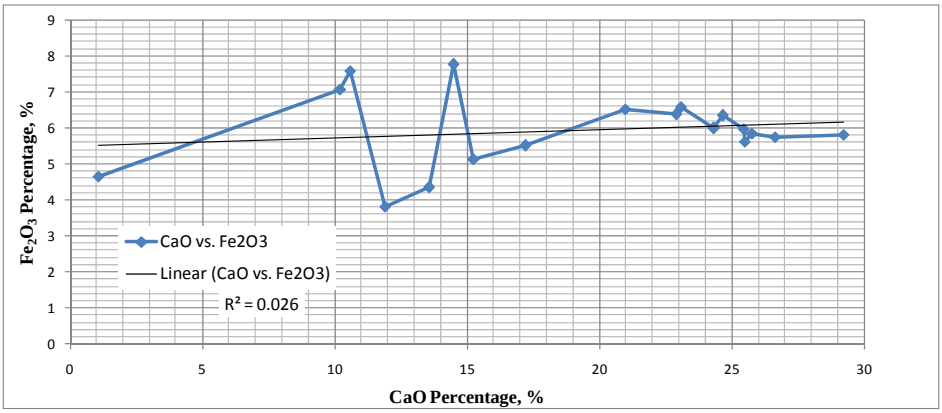

Figure B-4: CaO vs. Fe_2O_3

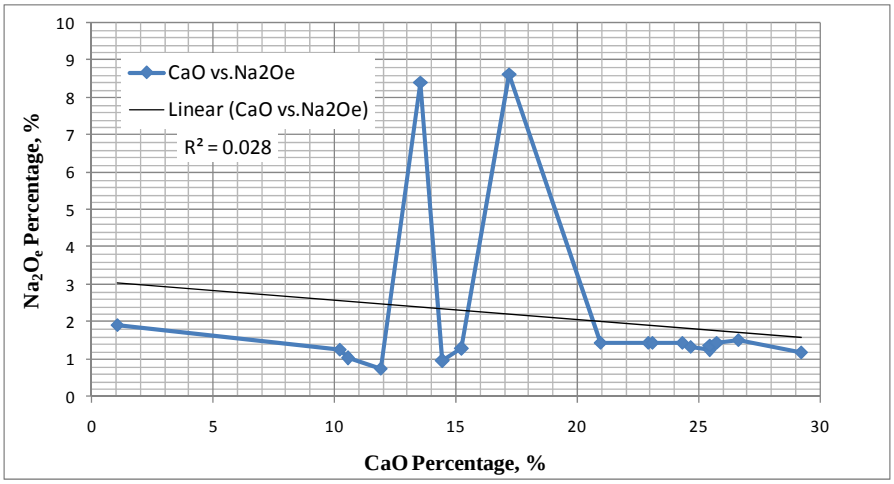

Figure B- 5: CaO vs. Na_2Oe

Appendix C: Trends for Total Alkalis, Available Alkalis, Pore Solution, and Leeching

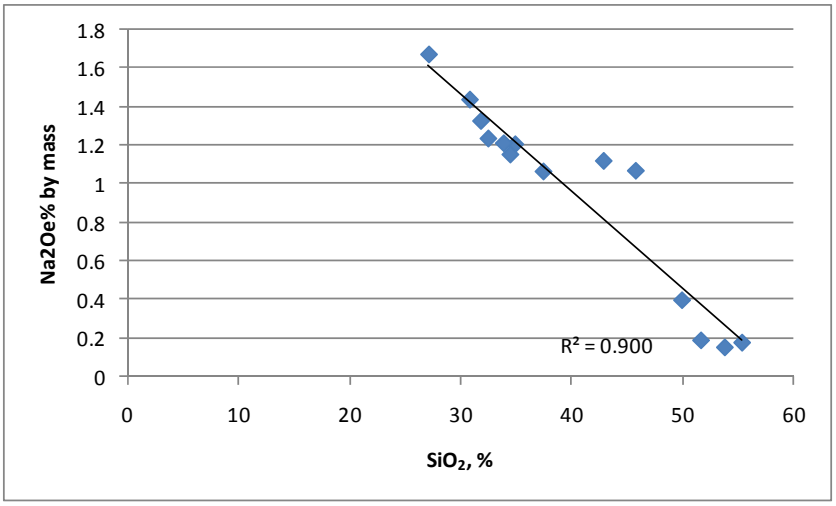

Figure C-1: Acid-Soluble Alkalis (SiO_2)

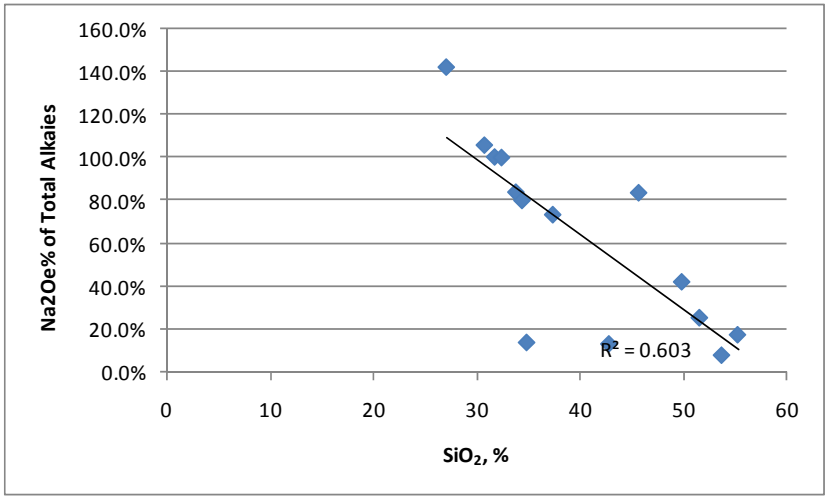

Figure C-2: Acid-Soluble/Total Alkalis (SiO_2)

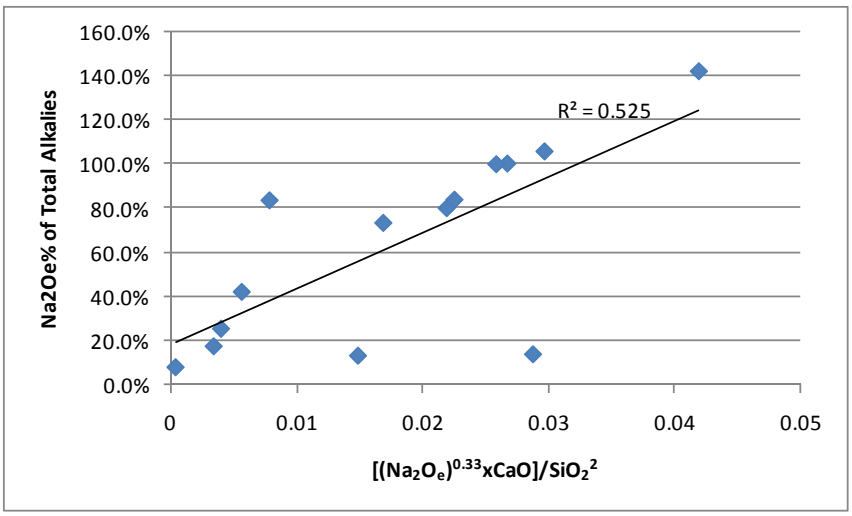

Figure C-3: Acid-Soluble/Total Alkalis (Chemical Index)

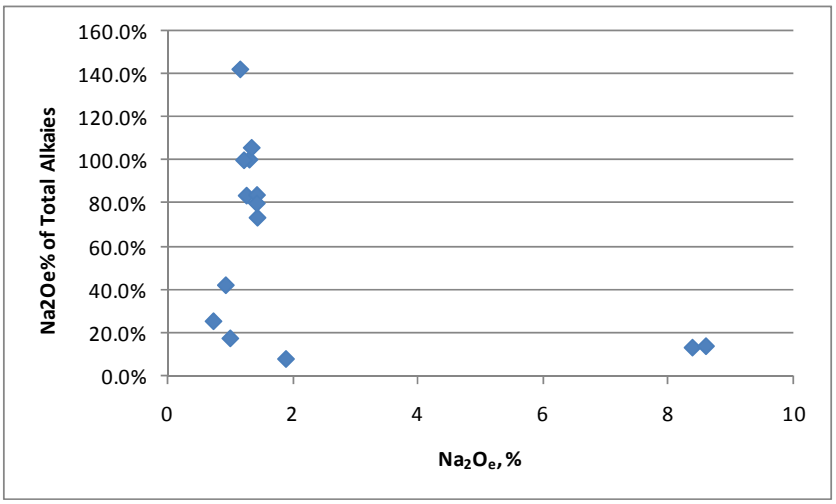

Figure C-4: Acid-Soluble/Total Alkalis (Na_2O_e)

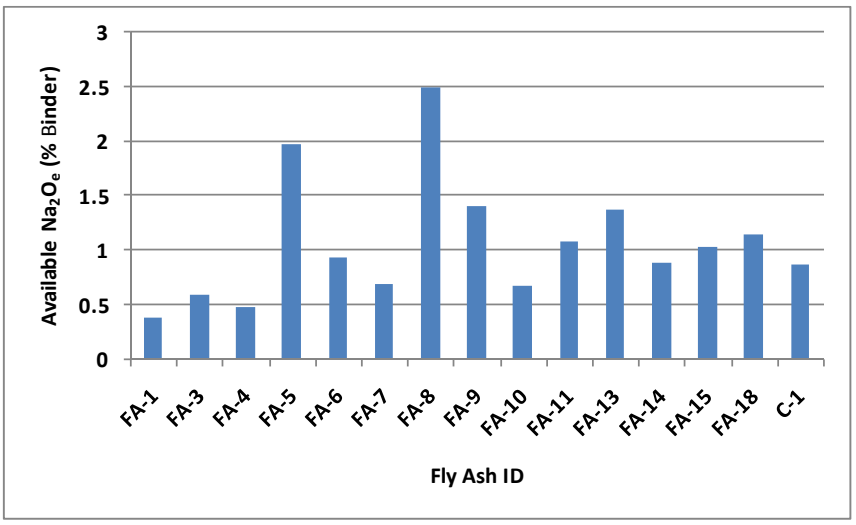

Figure C-5: Leeching at 0.1 M OH-

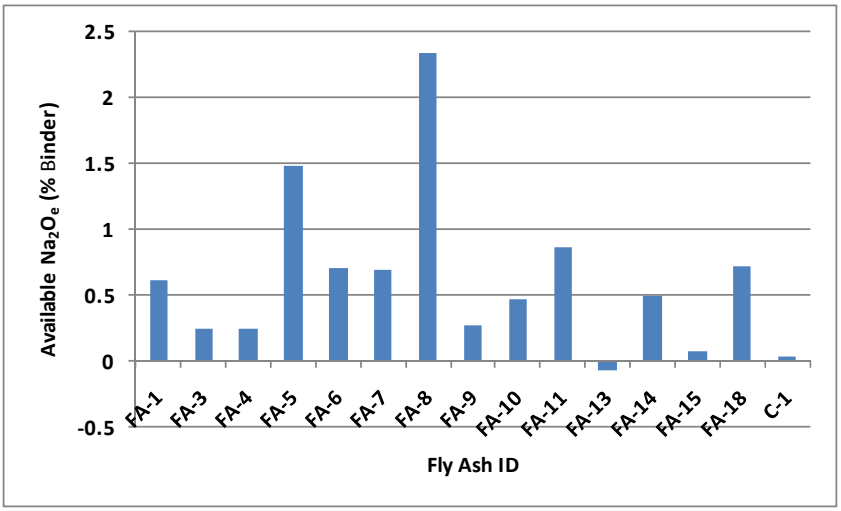

Figure C-6: Leeching at 0.2 M OH-

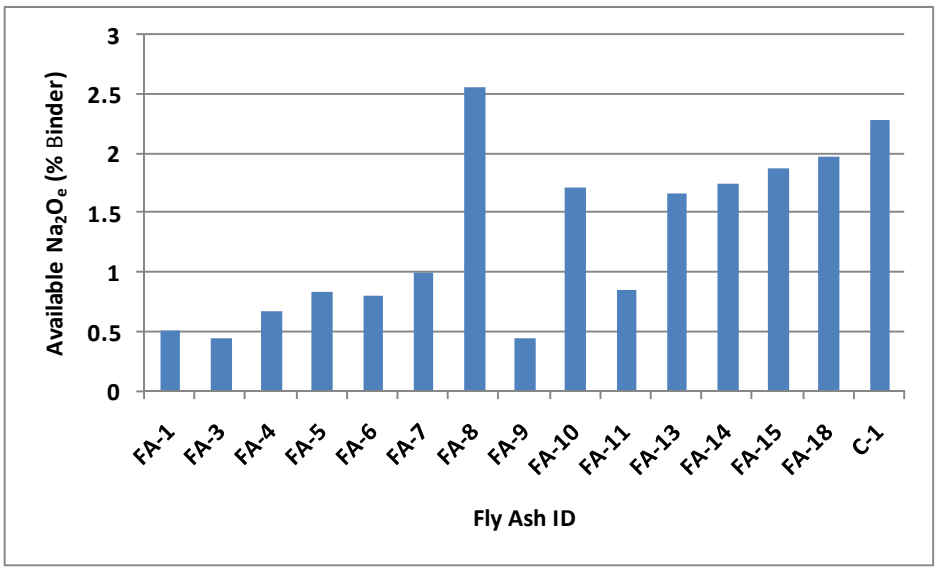

Figure C-7: Leeching at 0.3 M OH-

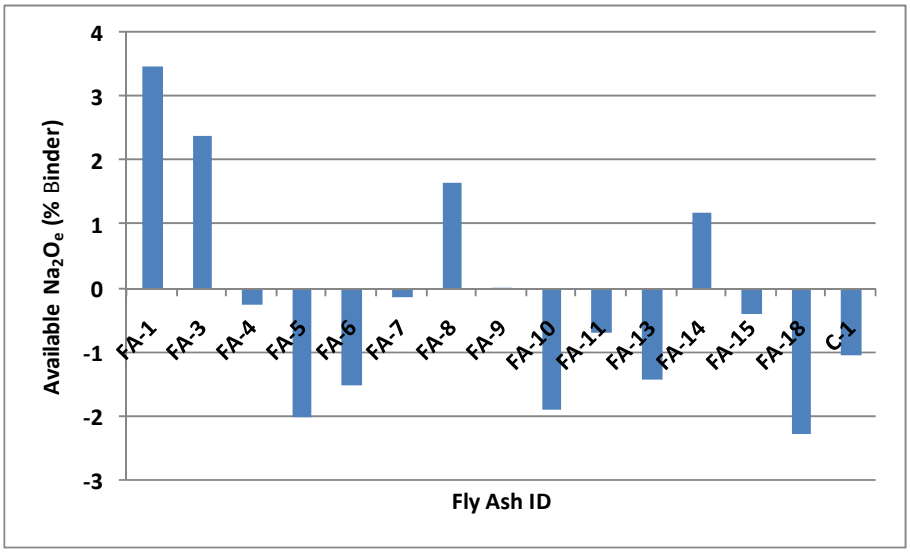

Figure C-8: Leeching at 0.6 M OH-